UNIVERSIDAD NACIONAL AUTÓNOMA DE MÉXICO

DOCTORADO EN CIENCIAS BIOMÉDICAS

INSTITUTO DE NEUROBIOLOGÍA

EFECTO DE LA OXITOCINA SOBRE LA ACTIVIDAD DEPENDIENTE DE CALCIO INTRACELULAR DE NEURONAS DEL ASTA DORSAL DE LA MÉDULA ESPINAL

T E S I S

QUE PARA OPTAR POR EL GRADO DE:

DOCTORA EN CIENCIAS

PRESENTA:

IBT. IRMA ALEJANDRA TELLO GARCÍA

DIRECTOR DE TESIS

DR. MIGUEL CONDÉS LARA
INSTITUTO DE NEUROBIOLOGÍA

COMITÉ TUTOR

DRA. MARTHA LEÓN OLEA
INSTITUTO NACIONAL DE PSIQUIATRIA "RAMÓN DE LA FUENTE MUÑIZ"

DR. GERARDO ROJAS PILONI
INSTITUTO DE NEUROBIOLOGÍA

JURIQUILLA, QUERÉTARO. ABRIL, 2021

A mis abuelos, **MANUEL TELLO GUZMAN** y **ROSA GARCÍA JAVIER**,
el ombligo y la raíz de todo mi mundo. Quienes trabajaron duro para darle a sus 7 hijos
una sola herencia: la formación académica que ellos no pudieron tener.

En memoria de mi amiga, hermana y compañera
de sueños **ADRIANA RAMÍREZ COSMES**. Este sueño era
también tuyo y hoy yo lo cumplo por las dos.

AGRADECIMIENTOS

A mi madre **SOLEDAD TELLO** por creer siempre en mí, por su amor y su apoyo incondicional. Tu gran fortaleza y determinación me inspira cada día a luchar por mis sueños. Eres la mujer más fuerte y dulce que conozco, jamás me alcanzará la vida para agradecerte lo que has hecho por mí. Te amo con todo mi ser.

A mi hermano **DIEGO TELLO** que, sin saberlo, desde que llego a mi vida y siendo tan pequeño me enseñó tantas cosas. Con el paso de los años su amor y entrega por lo que hace me han inspirado a convertirme en una mejor persona y a luchar para llegar muy lejos y muy alto. Te adoro con el alma.

A mi padre **ANGEL TELLO** por alimentar mi curiosidad con su infinito ingenio, eres el hombre más inteligente que conozco. A ti te debo el soñar algún día ser científica y estudiar en la UNAM. Me has enseñado y dado tanto en la vida, mi amor por ti es infinito.

A toda mi familia de sangre y a mi familia por elección, en Oaxaca y Querétaro, por su amor, compañía y apoyo. Son una parte muy importante de mí y los llevo conmigo siempre a donde quiera que voy.

A **ARTURO GONZALEZ ISLA** por sus porras, su apoyo, sus consejos y su guía durante los momentos más difíciles del doctorado. Fuiste sin duda una pieza clave durante los últimos años para ver mi sueño cumplirse. Gracias por siempre.

A mi mentor, el **DR. MIGUEL CONDÉS LARA** por su guía y apoyo durante estos años. Por darme la confianza y la libertad de contribuir en este proyecto y enseñarme con el ejemplo la pasión por la investigación científica.

A mis tutores, la **DRA. MARTHA LEÓN OLEA** y el **DR. GERARDO ROJAS PILONI** por sus comentarios y recomendaciones a lo largo del doctorado.

A la **DRA. GUADALUPE MARTÍNEZ LORENZANA** por el apoyo y enseñanza brindados en técnicas de histología, inmunofluorescencia, trazado y marcado neuronal, y microscopía. Al **DR. ABIMAEL GONZÁLEZ HERNÁNDEZ** por su asesoría y retroalimentación en el desarrollo del proyecto. Al **DR. BENITO ORDAZ SÁNCHEZ** por el apoyo brindado en técnicas de

imagenología de calcio intracelular. Al **DR. JESÚS PÉREZ ORTEGA** por el apoyo brindado en técnicas de análisis de datos obtenidos de imagenología de calcio intracelular. A mi amigo el **DR. ALFREDO MANZANO GARCÍA** por su retroalimentación e invaluable apoyo durante su paso por el laboratorio. A mis compañeros **HÉCTOR, ENRIQUE, ANTONIO, MOHAMMED, GUSTAVO Y MARÍA JOSÉ** por las pláticas, las risas, los pasteles y el apoyo brindado.

Al jurado de examen de grado por su retroalimentación y recomendaciones.

Al Consejo Nacional de Ciencia y Tecnología (**CONACyT**) por la beca número 582491.

A la **UNIVERSIDAD NACIONAL AUTÓNOMA DE MÉXICO** por brindarme educación superior gratuita y de calidad, y por el apoyo brindado al desarrollo de mi carrera científica a través de sus diferentes programas y becas, siguiendo fielmente su ideal de servicio al país y la humanidad. De hoy en adelante y para siempre…

POR MI RAZA HABLARÁ EL ESPÍRITU.

El presente proyecto fue realizado en el laboratorio B16 de Dolor y Epilepsia del Instituto de Neurobiología, UNAM Juriquilla, a cargo del Dr. Miguel Condés Lara y fue financiado por el Programa de Apoyo a Proyectos de Investigación e Innovación Tecnológica (PAPIIT) con los proyectos IN200415 para el Dr. Miguel Condés Lara y IA203117 para el Dr. Abimael González Hernández.

RESUMEN

Los circuitos que transmiten la información nociceptiva en la médula espinal se componen principalmente de neuronas de proyección y de interneuronas excitatorias e inhibitorias. Estos circuitos reciben entradas de la periferia y de núcleos supraespinales, y envían salidas a núcleos supraespinales también. La oxitocina (OT) se ha estudiado como un modulador potencial de la analgesia endógena actuando sobre circuitos nociceptivos a nivel de la médula espinal. Hasta ahora, los mecanismos no se conocen detalladamente. Algunos estudios sugieren que tal modulación implica la activación del receptor de oxitocina (OTR) dado que éste se expresa en varios elementos de los circuitos nociceptivos del asta dorsal de la médula espinal. Como la mayoría de los estudios de la OT como modulador potencial de analgesia endógena se centran en el efecto unicelular de este péptido, en el presente trabajo nos centramos en la acción global de la OT en poblaciones de células del asta dorsal utilizando imagenología de calcio. El objetivo del presente estudio fue evaluar la acción predominante de OT en las células del asta dorsal de la médula espinal bajo condiciones similares a las inducidas por el dolor neuropático como son la sensibilización central a través de la activación receptores de N-Metil-D-aspartato (NMDA) y el modelo de dolor neuropático de inyección de formalina al 5%. Se utilizó imagenología de $[Ca^{2+}]i$ en rebanadas de médula espinal (500-550 µm de espesor) de ratas Wistar de 8-12 días de edad (P8-P12). Las rebanadas de médula espinal se incubaron con Fluo-8 AM y luego se registró la actividad dependiente de calcio en videos de 4 minutos con un microscopio de fluorescencia, con el fin de evaluar los cambios en la actividad dependiente del calcio en diferentes condiciones experimentales: actividad espontánea (Control), NMDA (8 µM), OT(5 µM), NMDA+OT, OT+NMDA y formalina 5% (15 µl formalina inyectada s.c. en el dorso de la pata trasera, 48 horas antes del experimento). El análisis de datos se llevó a cabo con algoritmos escritos en LabView® y MatLab® donde los cambios en la fluorescencia de las regiones de interés (ROI), correspondientes a las células, se midieron, normalizaron y contaron para evaluar los cambios en la actividad de las neuronas bajo diferentes condiciones experimentales. Además, se realizó un análisis de coactividad para estimar los cambios en los patrones de activación de las poblaciones celulares medidos como el número de picos de coactivación. La actividad celular espontánea dependiente de calcio (control) del asta dorsal fue escasa y la actividad sincronizada estuvo ausente. La preincubación con NMDA aumentó la actividad, y la cantidad de neuronas activas y también promovió la sincronización de la

actividad celular. En presencia de NMDA, la aplicación de OT aumentó la actividad neuronal global, pero en comparación con el grupo NMDA, la OT redujo la sincronización de las células del asta dorsal de la médula espinal. Sin la presencia de NMDA, la OT no afectó la actividad global de las neuronas en comparación con el control. Finalmente, cuando se aplicó antes del NMDA, la OT aumentó la actividad global, lo que implica un mayor número de neuronas activas. Sin embargo, su aplicación no tuvo un efecto significativo en la tasa de sincronización. Cuando se analizó la coactividad de las células, se encontró una correlación entre la actividad global y los picos de coactividad en presencia de NMDA y OT+NMDA, pero no en presencia de NMDA+OT. Finalmente, se evaluó la dinámica de actividad en células del asta dorsal de la médula espinal bajo una condición de dolor neuropático crónico (inyección de formalina 5%). Los resultados mostraron que la actividad dependiente del calcio evocada por la inyección de formalina es similar a la actividad evocada por la aplicación NMDA medida como: i) número de células activas, ii) actividad global, iii) tasa de actividad acumulada y, v) picos de coactividad. Los resultados demostraron que: 1) las acciones globales de NMDA en los circuitos del asta dorsal de la médula espinal, promoviendo altas tasas de actividad y sincronización de células; 2) en presencia de NMDA, la OT aumentó las tasas de actividad, pero curiosamente disminuyó la actividad coordinada; 3) el tratamiento preventivo de OT no afectó la actividad global de los efectos del NMDA en las células del asta dorsal de la médula espinal; y 4) la aplicación de NMDA imita la dinámica de actividad en las células del asta dorsal evocada por un modelo de dolor neuropático crónico. Los resultados sugieren que la OT tiene un efecto global en la actividad de las células del asta dorsal de la médula espinal al disminuir los patrones de actividad generados previamente por condiciones de sensibilización central. Este efecto de OT podría ser responsable de las funciones antinociceptivas atribuidas a este péptido. Sin embargo, es necesario un análisis más profundo para evaluar e identificar específicamente cómo cambia la dinámica de actividad de poblaciones celulares específicas.

ABSTRACT

Spinal cord nociceptive circuits are composed mainly of projection neurons and excitatory and inhibitory interneurons. These circuits receive inputs from the periphery and supraspinal nuclei and, send outputs to supraspinal nuclei as well. Oxytocin (OT) has been studied as a potential modulator of endogenous analgesia by acting upon nociceptive circuits at the spinal cord level. Until now, the detailed mechanisms remain still undetermined. Some studies suggest that such modulation involves the activation of oxytocin receptor (OTR) given that the OTR is expressed by several elements of the spinal dorsal horn (SDH) spinal cord circuit. As the majority of the studies of OT, as a potential modulator of endogenous analgesia, are focused on the single-cell effect of this peptide, in the present work we focused on the global action of OT along with the dorsal horn cell populations without losing single-cell resolution using calcium imaging. The present study aimed to evaluate the predominant action of OT in the SDH network under spinal conditions similar to those induced by the central sensitization via activation of N-Methyl-D-aspartate (NMDA) receptors and a well-described model of neuropathic pain-like formalin 5% injection. Ca^{2+} imaging was used on spinal cord slices (500-550 µm thick) of 8-12 days old (P8-P12) Wistar rats. Spinal cord slices were incubated with Fluo-8 AM and then calcium-dependent activity was recorded for 4 minutes with a fluorescence microscope to evaluate changes in calcium-dependent activity under different conditions: spontaneous activity (Control), NMDA (8 µM), OT(5 µM), NMDA+OT, OT+NMDA and formalin 5% (15 µl formalin injected s.c. into the dorsal surface of the hind paw, 48 h prior experiment). Data analysis was carried out with algorithms written in LabView® and MatLab® where changes in fluorescence of regions of interest (ROI's), corresponding to cells, were measured, normalized, and counted to evaluate differences in slice activity changes under different conditions. Also, coactivity analysis was performed to estimate the changes in activation patterns of cell populations measured in the number of coactivation peaks. Spontaneous calcium-dependent cellular activity (control) of the dorsal horn was scarce and, synchronized activity was absent. Preincubation with NMDA increased activity involving a higher number of neurons and synchronization of cell activity was also induced. In the presence of NMDA, the addition of OT increased global neuronal activity, but when compared with the NMDA group, OT reduced the synchronization of SDH cells. Without the presence of NMDA, OT did not present a significant change in global neuron activity compared with control. Finally, when

applied before NMDA, OT increased the activity involving a higher number of neurons but does not have a significant effect on the synchronization rate of cell activity. When the coactivity of cells was analyzed, a correlation between global activity and coactivation peaks was found with the presence of NMDA and OT+NMDA but not in the presence of NMDA+OT. Finally, we tested the activity dynamics on SDH cells under a chronic neuropathic pain condition (5% formalin injection), results showed that calcium-dependent activity evoked by formalin injection is similar to that evoked activity by NMDA application measured as i) the number of active cells, ii) global activity, iii) Cumulative activity rate and, v) peaks of coactivity. Results demonstrate that 1) the global actions of NMDA in the SDH circuitry by promoting high rates of activity and the synchronization of cells; 2) in NMDA presence, OT increased activity rates but interestingly prevented the conformation of coordinated activity, 3) preventive treatment of OT did not show to have an effect on the global actions of NMDA at SDH cells, and 4) NMDA application mimicked the activity dynamics on dorsal horn cells evoked by a chronic neuropathic pain model. Results suggest that OT has a global effect on the activity of spinal dorsal horn cells by decreasing activity patterns previously generated by central sensitization conditions. This effect of OT could be responsible for the antinociceptive functions attributed to this peptide. However, deeper analysis is needed to specifically evaluate and identify how the activity dynamics of specific cell populations change.

ABREVIACIONES

$[Ca^{2+}]i$	Concentración de calcio Intracelular
Ca^{2+}	Iones de calcio
DAG	Diacilglicerol
DRG	Ganglios de la raíz dorsal
GABA	Ácido γ-aminobutírico
GECIs	Indicadores de calcio genéticamente modificados
IP_3	Inositol trifosfato
IP_3R	Receptor(es) de inositol trifosfato
LTP	Potenciación a largo plazo
MRGPRD+	Fibras C no mielínicas
nAChR	Receptores nicotínicos de acetilcolina
NCX	Intercambiador de sodio-potasio
NMDA	N-Metil-D-aspartato
NMDAr	Receptor(es) de NMDA
ns	No significativo
OT	Oxitocina
OTR	Receptor(es) de oxitocina
PI	Fosfatidilinositol
PLC	Fosfolipasa C
PMCA	ATPasa de calcio de la membrana plasmática
RE	Retículo endoplásmico
ROI	Área de interés, por sus siglas en inglés
RyR	Receptor(es) de rianodina
s.c.	Subcutánea
SEM	Error estándar de la media, por sus siglas en ingles
SERCA	ATPasa de calcio del retículo sarco-endoplásmico
WDRn	Neuronas de amplio rango dinámico

CONCEPTOS BASICOS

Coactivación

Actividad conjunta o casi conjunta de grupos de neuronas en un tiempo corto y que se encuentran dispersas en un área pequeña de tejido (Carrillo-Reid et al., 2008, 2009; Pérez-Ortega et al., 2016).

Sincronización/Coordinación

Grupos de neuronas que tienen actividad conjunta (coactividad) configurando eventos de red o estados que se alternan y conforman secuencias recurrentes a lo largo del tiempo (Carrillo-Reid et al., 2008, 2009).

Ensamble neuronal

Grupos de neuronas con actividad conjunta (coactividad) y secuencial. Las neuronas pertenecientes a un ensamble presentan coactividad repetida en una ventana de tiempo corta, esta actividad repetida puede representar diferentes estímulos sensoriales o conductas motoras o cognitivas. Un ensamble neuronal representa la unidad básica de constitución de la actividad de un circuito neuronal (Carrillo-Reid & Yuste, 2020).

NOTA DE LECTURA

El presente documento cuenta con hipervínculos que le permitirán navegar rápidamente hacia secciones, figuras y tablas mencionadas en el texto. Los hipervínculos están resaltados a lo largo del documento con letras en **negritas** para su fácil identificación.

CONTENIDO

1. INTRODUCCIÓN

En la médula espinal converge la información sensorial, motora y autonómica entre diferentes partes del cuerpo y el cerebro. En el asta ventral de la médula espinal se procesa la información motora. Por otro lado, en el asta dorsal se procesa la información sensorial tanto a estímulos nocivos como no-nocivos. La importancia del asta dorsal en el procesamiento de la información nociceptiva es evidente y los circuitos que contribuyen a la transmisión de la información nociceptiva en esta estructura son de particular importancia en este proyecto el cual estudió los efectos antinociceptivos de la oxitocina (OT) sobre las poblaciones celulares del asta dorsal de la médula espinal ya que la evidencia reciente ha descrito a la OT como un inhibidor de la actividad nociceptiva en el sistema nervioso central (SNC) (Condés-Lara et al., 1994; García-Boll et al., 2018; González-Hernández et al., 2019; Juif & Poisbeau, 2013; Miranda-Cardenas et al., 2006; Robinson et al., 2002) y en las terminales nerviosas periféricas, tanto en experimentos electrofisiológicos como conductuales (González-Hernández et al., 2017). También, se ha reportado el uso de la OT como una alternativa exitosa para el manejo del dolor en seres humanos (Miguel Condés-Lara et al., 2016; Zayas-González et al., 2019). En estudios realizados previamente en ratas se demostró que la administración de OT produce un efecto antinociceptivo al reducir las señales relacionadas con la nocicepción. En particular, la evidencia muestra que la OT es capaz de disminuir la actividad eléctrica de aferentes primarias que transmiten información nociceptiva a neuronas del asta dorsal de la médula espinal y, por lo tanto, inhibir la transmisión de dicha información (Miranda-Cardenas et al., 2006). Sin embargo, la participación intrínseca de la OT y su efecto en la inhibición de la transmisión de información nociceptiva en los circuitos funcionales de procesamiento sensorial del asta dorsal aún no se ha estudiado ampliamente.

Desde la descripción de las láminas del asta dorsal por Rexed en 1954, la mayoría de los trabajos de investigación de diversos grupos han perseguido un mejor y más profundo conocimiento de los aspectos histológicos de esta región (Rexed, 1954). Adicional a esto, la electrofisiología se ha utilizado durante varios años como la técnica estándar para estudiar la fisiología de los componentes neuronales del asta dorsal debido a su excelente sensibilidad y resolución temporal. Sin embargo, las redes funcionales de procesamiento sensorial no eran completamente accesibles con las técnicas utilizadas en el siglo pasado.

Los avances recientes de técnicas como la imagenología de calcio intracelular ($[Ca^{2+}]i$) con microscopía epifluorescente o de uno o dos fotones realizadas tanto en tejido intacto de la médula espinal (in vivo) o en rebanadas y/o cultivos (in vitro) han sido benéficas para entender cómo se transmite la información sensitiva en el asta dorsal y cómo esta responde a diferentes estímulos nocivos. Una de las ventajas de utilizar imagenología de calcio es que permite la observación y análisis de grandes áreas con varias neuronas. Además, a través del desarrollo de indicadores de calcio altamente sensibles o indicadores de calcio genéticamente codificados, esta técnica permite estudiar la correlación y la interacción entre los diferentes tipos de neuronas de la médula espinal y su papel en la transmisión de información sensorial para entender cómo funcionan los circuitos sensoriales del asta dorsal. Algunos estudios de imagenología de calcio realizados en tejido intacto de la médula espinal (in vivo) (Cirillo et al., 2012; Davalos et al., 2008; Emery et al., 2016; Farrar et al., 2012; Fenrich et al., 2012; Johannssen & Helmchen, 2010; Sekiguchi et al., 2016; Vrontou et al., 2013) y en rebanadas o cultivos (in vitro) han sido esenciales para entender cómo funcionan grupos de células y cómo responden a diferentes estímulos (Luo et al., 2008; Ruscheweyh & Sandkühler, 2005).

En el presente trabajo, utilizamos imagenología de $[Ca^{2+}]i$ en rebanadas del asta dorsal de la médula espinal para evaluar la actividad espontánea dependiente de calcio de neuronas del asta dorsal de la médula espinal, recrearemos una situación de sensibilización central en la médula espinal inducida por la activación de los receptores NMDA y posteriormente evaluamos los cambios producidos por la OT antes y después de la activación de NMDAr. También, evaluamos el efecto de la OT sobre la actividad espontanea dependiente de calcio de neuronas del asta dorsal y, finalmente, utilizamos un modelo de dolor neuropático para evaluar cómo es la actividad dependiente de calcio de neuronas del asta dorsal de la médula espinal. Con el análisis de los datos experimentales obtenidos, evaluamos parámetros como el número de células activas, actividad global, picos de coactividad y actividad acumulada para determinar diferencias significativas en la actividad celular correspondiente a cada condición.

2. ANTECEDENTES

2.1. Dolor y nocicepción

La asociación internacional para el estudio del dolor (IASP) define el dolor como “Una experiencia sensorial y emocional desagradable asociada con, o similar a la asociada con, daño tisular real o potencial” (Raja et al., 2020). Dada esta definición podemos interpretar que aun cuando hay bases fisiológicas para detectar e interpretar un estímulo como doloroso, lo que conforma en sí la experiencia de dolor es siempre la experiencia emocional asociada a este estimulo. Dado que lo anterior convierte al dolor en algo subjetivo, se vuelve difícil de estudiar. Es por esto por lo que se ha optado por usar el término nocicepción, para la IASP este término se define como “Los procesos neuronales de codificado y procesamiento de un estímulo nocivo” (Loeser & Treede, 2008) y hace referencia a los procesos moleculares y celulares que se llevan a cabo durante la transducción, transmisión, procesamiento y modulación de los estímulos nocivos. Es decir, el dolor conlleva siempre en su procesamiento la nocicepción (Sneddon, 2018). La activación de nociceptores y las vías y procesos encargados de transmitir la información nociceptiva también estimula los sistemas descendentes de analgesia endógena como un mecanismo homeostático.

2.2. Mecanismos centrales de la nocicepción

La transmisión de la información nociceptiva comienza con la activación de diferentes tipos de receptores expresados en el cuerpo. El tipo de estímulo detectado por cada neurona depende del tipo de receptor expresado en la terminal nerviosa. Una vez transducido el estímulo, las fibras aferentes primarias conducen la información nociceptiva a la médula espinal (Burgess & Perl, 1967; Gardner & Johnson, 2000).

Las fibras aferentes primarias de los ganglios de la raíz dorsal se separan al llegar a la médula espinal de acuerdo con su modalidad sensorial y su campo receptivo periférico. En relación con estas características, las fibras hacen sinapsis con diferentes tipos de neuronas en láminas específicas de la médula espinal (Basbaum et al., 2009). Se sabe que las láminas superficiales I y II, también conocidas como sustantia gelatinosa de Rolando, comprenden neuronas de proyección e interneuronas inhibitorias (GABAérgicas o glicinérgicas) y excitatorias (glutamatérgicas) que se ramifican localmente. Estas láminas reciben información predominantemente nociceptiva a partir de pequeñas fibras mielínicas

(Aδ) y fibras no mielínicas (C). Mientras que las láminas III-V, también conocidas como el núcleo propio, incluyen interneuronas locales excitatorias e inhibitorias y reciben información no nociceptiva de fibras mielínicas (Aβ), aunque algunas neuronas de la lámina V, llamadas células de amplio rango dinámico (WDR), también responden a estímulos nociceptivos (fibras C) y proyectan a núcleos supraespinales (Ribeiro-da-Silva & de Koninck, 2009; Todd, 2010).

El asta dorsal de la médula espinal es un sitio importante para la modulación endógena de la nocicepción, por representar el sitio de primer relevo en el paso de la información sensorial y nociceptiva. Además de recibir información nociceptiva de la periferia, el asta dorsal de la médula espinal también está regulada por sistemas moduladores descendentes que comprenden axones originados en núcleos supraespinales entre los cuales se encuentran la sustancia gris periacueductal, médula rostroventromedial, núcleos del rafe, en particular el rafe magno, locus coeruleous y el hipotálamo. También, en el asta dorsal hay circuitos locales como aquellos que desencadenan los reflejos nocifensivos mediados por la médula espinal y que comprenden proyecciones de neuronas del asta dorsal al asta ventral (Millan, 2002).

Después de su primer relevo en el asta dorsal, la información nociceptiva se transmite hacia núcleos supraespinales a través de seis tractos: espinotalámico, espinorreticular, espinomesencefálico, cervicotalámico, espinohipotalámico y espinoparabraquial. Por último, la información nociceptiva arribará a la corteza cerebral, el tallo cerebral o el diencéfalo donde se codificarán los componentes emocionales y sensitivos del dolor, las respuestas autonómicas a éste y se iniciará la modulación endógena descendente, respectivamente (Basbaum & Bushnell, 2009).

Por su organización y la complejidad de las interacciones entre sus diferentes componentes celulares, los circuitos neuronales involucrados en el procesamiento de la información nociceptiva en el asta dorsal de la médula espinal no han sido totalmente descritos.

2.3. Oxitocina

La oxitocina (OT) es un neuropéptido de estructura molecular conformada por una cadena de 9 aminoácidos (cisteína – tirosina – isoleucina – glutamina – asparagina – cisteína – prolina – leucina – glicina). La OT se sintetiza y secreta en el SNC por neuronas

magnocelulares y parvocelulares de los núcleos paraventricular (NPV) y supraóptico (NSO) del hipotálamo. Desde ambos núcleos, el NPV y el NSO, la OT se transporta a través de los axones de neuronas magnocelulares a la hipófisis posterior por el tracto supraóptico–hipófisial donde se secreta al torrente sanguíneo para efectuar sus funciones como neurohormona sobre órganos específicos (Gimpl & Fahrenholz, 2001; Kandel et al., 2012; von Bohlen und Halbach & Dermietzel, 2006). Por otro lado, la OT a través de terminales axónicas de neuronas parvocelulares del NPV, se transporta y libera a distintos núcleos del SNC (médula espinal, amígdala, bulbo olfatorio y núcleo del tracto solitario, entre otros) donde actúa como neuromodulador (von Bohlen und Halbach & Dermietzel, 2006). En específico, la OT llega a la médula espinal por medio de proyecciones hipotalámico-espinales desde el NPV del hipotálamo (Condés-Lara et al., 2007; Jo et al., 1998; Sawchenko & Swanson, 1982; Shiraishi et al., 1995; Swanson, 1977; Swanson & McKellar, 1979).

La OT tiene funciones conocidas y bien descritas como su participación en la facilitación de las contracciones uterinas durante el parto y por ser la molécula principal que desencadena la producción y la secreción de leche materna durante la lactancia (Gimpl & Fahrenholz, 2001; Zigmond et al., 1999). La producción de OT en machos sugiere que esta molécula tiene otras funciones, no ligadas al sexo, como el comportamiento afectivo y la memoria social (Benarroch, 2013; von Bohlen und Halbach & Dermietzel, 2006). Recientemente, a la OT se le ha atribuido una función en los procesos de analgesia endógenos (Breton et al., 2009; Condés-Lara et al., 2006; Juif & Poisbeau, 2013; Miranda-Cardenas et al., 2006; Robinson et al., 2002).

La OT se une a su receptor Para realizar sus funciones como neuromodulador. El receptor a OT (OTR) es un receptor metabotrópico (ligado a proteínas G) cuya estructura está conformada por siete dominios transmembranales unidos por asas intracelulares y extracelulares, una secuencia amino terminal extracelular que sirve como sitio de unión al ligando y una secuencia carboxilo terminal intracelular que está en contacto con la proteína G (Gimpl & Fahrenholz, 2001; Nestler et al., 2009; von Bohlen und Halbach & Dermietzel, 2006). El OTR está acoplado principalmente a proteínas $G_{q/11}$ por lo que activan el sistema de segundo mensajero de la fosfolipasa C para inducir un incremento en la concentración de calcio intracelular (Busnelli et al., 2012; Gimpl & Fahrenholz, 2001). El acoplamiento del OTR a otras proteínas G como la Gαi también ha sido reportado en la literatura, en este

caso, la OT disminuye la actividad de la adenilato ciclasa y por consecuencia no hay liberación de Ca^{2+} al citoplasma (Busnelli et al., 2012).

2.3.1. Acciones antinociceptivas de la OT en la médula espinal

Como se mencionó anteriormente, la OT participa en mecanismos endógenos de antinocicepción. En estudios recientes se han descrito funciones antinociceptivas de la OT en el SNC (García-Boll et al., 2018; González-Hernández et al., 2019; Juif & Poisbeau, 2013; Miranda-Cardenas et al., 2006; Robinson et al., 2002) y en el sistema nervioso periférico (González-Hernández et al., 2017; Qiu et al., 2014). También, nuestro grupo reportó el uso de la OT en el manejo del dolor en seres humanos (Miguel Condés-Lara et al., 2016; Zayas-González et al., 2019). La administración de OT ha demostrado un efecto antinociceptivo sorprendente al disminuir la actividad celular relacionada con la nocicepción y a su vez, disminuir las conductas relacionadas a la percepción del dolor.

En primer lugar, el PVN del hipotálamo, que envía axones oxitocinérgicos al asta dorsal de la médula espinal, es capaz de regular la transmisión de la información nociceptiva (Condés-Lara et al., 2007, 2008, 2009; Millan, 2002; Sawchenko & Swanson, 1982; Shiraishi et al., 1995; Swanson & McKellar, 1979). Estudios previos han demostrado que la estimulación eléctrica del PVN produce un aumento en la concentración de OT en plasma, líquido cefalorraquídeo y médula espinal y, también, que esta estimulación eléctrica inhibe la actividad nociceptiva por la liberación de OT en el asta dorsal (Miguel Condés-Lara et al., 2006, 2008; Martínez-Lorenzana et al., 2008; Miranda-Cardenas et al., 2006; Rojas-Piloni et al., 2008).

En particular, la aplicación espinal de OT inhibe la actividad eléctrica de fibras aferentes Aδ y C sin afectar la actividad de fibras aferentes no nociceptivas (Aβ) (Miranda-Cardenas et al., 2006; Rojas-Piloni et al., 2007, 2010). Así mismo, la OT tiene una acción antinociceptiva sobre las neuronas de las láminas I y II del asta dorsal de la médula espinal (Jo et al., 1998) y en láminas más profundas IV, V y VI (Condés-Lara et al., 2006; González-Hernández et al., 2017; Rojas-Piloni et al., 2010). Además, se reportó en la literatura que la OT puede activar interneuronas GABAérgicas que a su vez disminuyen de manera presináptica la actividad de fibras aferentes primarias de neuronas de primer orden y que el efecto de la OT sobre estas interneuronas GABAérgicas se previene utilizando un antagonista a OTR.

Por otro lado, la coadministración de OT con glutamato en el asta dorsal inhibe la activación mediada por glutamato de neuronas (Condés-Lara et al., 2003), incluso se sugiere que la actividad antinociceptiva mediada por la OT está regulada por poblaciones de células glutamatérgicas que inducen inhibición GABAérgica dando como resultado un decremento en la excitabilidad de las neuronas del asta dorsal (Breton et al., 2009; Rojas-Piloni et al., 2008).

Los mecanismos de acción de la OT sobre las diferentes poblaciones celulares de la médula espinal y el efecto global de la OT en la médula espinal no han sido del todo estudiado. Al ejercer efecto sobre diferentes poblaciones celulares en la médula espinal, es de suma importancia estudiar los efectos globales de la OT e ir difiriendo poblaciones celulares. De esta manera se obtendría una aproximación de participación de cada uno en el efecto antinociceptivo total de la OT.

2.4. Generalidades de la señalización de calcio en neuronas

Dentro de los diferentes tipos de células que existen en los organismos biológicos, los iones de calcio (Ca^{2+}) generan señales intracelulares que desencadenan una gran variedad de funciones: desde una contracción muscular en células musculares, hasta el control de la proliferación celular o incluso la muerte celular (Berridge et al., 2000). En el SNC, las señales de calcio intracelular pueden regular procesos que van desde la liberación de neurotransmisores en una escala de tiempo tan pequeña como microsegundos hasta la transcripción de genes en una escala de tiempo que puede durar desde varios minutos hasta algunas horas (Grienberger & Konnerth, 2012).

El calcio es un mensajero intracelular esencial en las neuronas; en estado de reposo la concentración de calcio intracelular ($[Ca^{2+}]i$) se encuentra entre 50-100 nM, esta concentración puede aumentar hasta 1000 nM durante la actividad eléctrica (Grienberger & Konnerth, 2012). La $[Ca^{2+}]i$ de una célula estará determinada por el balance entre iones entrantes, iones salientes, y el intercambio de iones de los compartimentos internos de calcio, principalmente del retículo endoplásmico (RE) (Grienberger & Konnerth, 2012).

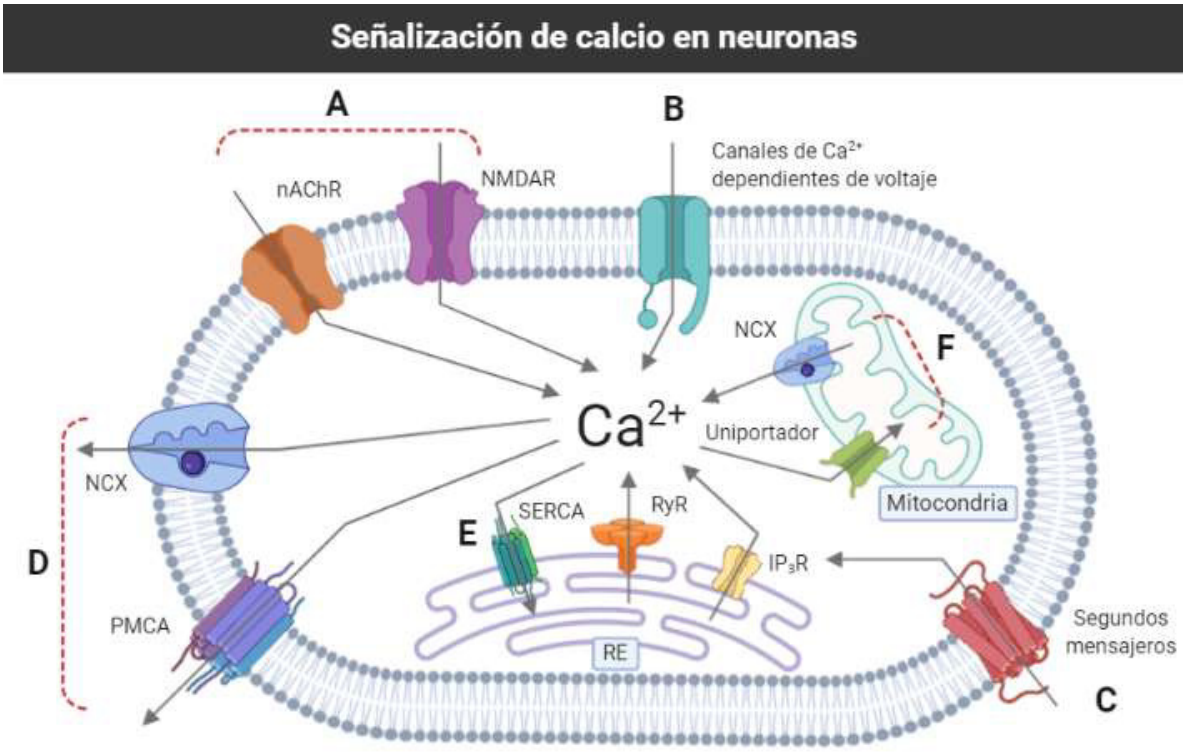

Figura 1. Señalización de calcio en neuronas. Mecanismos de entrada de iones de calcio al citoplasma: **(A)** canales activados por ligandos, como los receptores ionotrópicos a glutamato (NMDAR) y receptores nicotínicos de acetilcolina (nAChR), **(B)** canales de calcio dependientes de voltaje **(C)** activación de sistemas de segundos mensajeros como el sistema del fosfatidilinositol (PI) que desencadena la liberación de Ca^{2+} de compartimentos intracelulares y está mediada por los receptores a inositol trifosfato (IP3R) y los receptores a rianodina (RyR) del retículo endoplásmico (RE) (Berridge, 1993; Nestler et al., 2009). Mecanismos de salida de calcio del citoplasma: **(D)** por el intercambiador de sodio-calcio (NCX) y por la ATPasa de calcio de la membrana plasmática (PMCA), **(E)** por la ATPasa de calcio del retículo sarco-encoplásmico (SERCA) y **(F)** las mitocondrias regulan los niveles de calcio durante la actividad celular al introducir Ca^{2+} por medio del uniportador de calcio mitocondrial para después liberarlo lentamente al citoplasma por medio del NCX (Berridge et al., 2000; Grienberger & Konnerth, 2012). Creado por la autora de esta tesis con BioRender.com.

La entrada de Ca^{2+} extracelular al interior de la célula puede darse por distintos mecanismos, los más importantes son: i) por medio de canales activados por ligandos como son los receptores ionotrópicos a glutamato (NMDAR) y receptores nicotínicos de acetilcolina (nAChR) **(Figura 1 A)**, ii) por canales de calcio dependientes de voltaje activados por la depolarización de las neuronas **(Figura 1 B)**, y iii) por la activación de sistemas de segundos mensajeros como el sistema del fosfatidilinositol (PI) **(Figura 1 C)** que desencadena la liberación de Ca^{2+} de compartimentos intracelulares y está mediada

por los receptores a inositol trifosfato (IP_3R) y los receptores a rianodina (RyR) del RE (Berridge, 1993; Nestler et al., 2009).

Para mantener la homeostasis de calcio dentro de la célula, los Ca^{2+} son removidos del citoplasma por diferentes mecanismos: iv) el intercambiador de sodio-calcio (NCX) y la ATPasa de calcio de la membrana plasmática (PMCA) remueven el calcio del citoplasma hacia el medio extracelular **(Figura 1 D)**, v) la ATPasa de calcio del retículo sarco-encoplásmico (SERCA) remueve el calcio del citoplasma hacia el RE **(Figura 1 E)**, y vi) las mitocondrias también regulan la homeostasis de Ca^{2+} durante la actividad celular al introducir Ca^{2+} por medio del uniportador de calcio mitocondrial para después liberarlo lentamente al citoplasma por medio del NCX **(Figura 1 F)** (Berridge et al., 2000; Grienberger & Konnerth, 2012).

Para este proyecto, es importante conocer los mecanismos de movilización de la $[Ca^{2+}]i$ por dos mecanismos principales. El primero de ellos es por la activación de los NMDAR **(Figura 1 A)**, ya que usaremos el NMDA como potenciador de la actividad celular dependiente de calcio en la médula espinal. Los receptores a NMDA son canales iónicos a glutamato. Estos receptores son catiónicos inespecíficos y son permeables a los iones sodio, potasio y calcio (Nestler et al., 2009). Se ha estudiado que la fracción de Ca^{2+} que contribuye a la corriente catiónica a través de los NMDAR es aproximadamente del 6% al 12% (Grienberger & Konnerth, 2012). Estos receptores son los encargados de regular en su mayoría el flujo entrante de calcio en la post sinapsis, un aumento en la $[Ca^{2+}]i$ postsináptico es importante en procesos como las modificaciones a largo plazo de las sinapsis neuronales, como lo que sucede en procesos de sensibilización central y la potenciación a largo plazo (LTP) (Grienberger & Konnerth, 2012; Kandel et al., 2012). Es importante mencionar que un modulador importante de la función de los NMDAR es el potencial de membrana, ya que este es capaz de determinar la eficacia del bloqueo de magnesio dependiente de voltaje. Por lo anterior, las corrientes de iones entrantes del NMDAR aumentan en función de un incremento en la depolarización de la neurona, como ocurre durante los disparos de potenciales de acción en las neuronas (Berridge et al., 2000; Kandel et al., 2012; Nestler et al., 2009).

El segundo mecanismo de movilización de Ca^{2+} de interés en este proyecto es por la activación de segundos mensajeros **(Figura 1 C)**. Las proteínas G tienen una función importante en los procesos de señalización transmembranal en el SNC. Estas proteínas se

encuentran unidas a diferentes tipos de receptores transmembranales en el sistema nervioso, con agonistas específicos y diferentes de acuerdo con el tipo de receptor (un ejemplo de estos receptores es el OTR). Hay tres tipos de proteína G principales involucradas en la transmisión de señales producidas por la unión de un agonista a su receptor: G_s, $G_{i/o}$ y G_q (Nestler et al., 2009). Como se ha descrito anteriormente, el OTR es un receptor que está ligado a proteínas G, principalmente a proteínas G_q. Para este receptor en específico, la unión de la OT desencadena la activación de la proteína G, que actúa como factor de acoplamiento capaz de regular la fosfolipasa C (PLC) (Gimpl & Fahrenholz, 2001). La PLC, a su vez, metaboliza el PI para formar inositol trifosfato (IP_3) y diacilglicerol (DAG). El IP_3 desencadena la liberación de Ca^{2+} del RE y este aumento en los niveles citoplasmáticos de calcio activa a su vez los receptores RyR, propiciando la liberación de calcio mediada por calcio al citoplasma (Berridge, 1993, 1998; Gimpl & Fahrenholz, 2001). La liberación de Ca^{2+} por medio de IP_3R es principalmente desencadenada por neurotransmisores como el glutamato y también por la unión de un ligando a receptores acoplados a proteínas G_q. Por otro lado, la liberación de Ca^{2+} por RyR es un proceso mediado por los mismos iones de calcio. Es decir, este proceso puede desencadenarse por incrementos en la $[Ca^{2+}]i$, como sucede con el incremento en el flujo de Ca^{2+} después de un potencial de acción o por acción de sistemas de segundos mensajeros (Grienberger & Konnerth, 2012; Nestler et al., 2009).

2.5. Imagenología de calcio para el estudio de procesos sensoriales y nocicepción en la médula espinal

Para estudiar el efecto global de la OT se requieren de técnicas experimentales que permitan la observación de varias células al mismo tiempo y además poder conservar la resolución individual de las células. Para esto, en el presente proyecto hemos decidido utilizar la imagenología de calcio intracelular en el asta dorsal de la médula espinal para estudiar mecanismos de nocicepción y antinocicepción asociados a la OT. La imagenología de calcio ha sido poco usada para estudiar los mecanismos sensoriales y nociceptivos en la médula espinal. A continuación, se hace un recuento de las diferentes aproximaciones usadas (**Figura 2**). Las imágenes de calcio de la médula espinal se pueden realizar a través de preparaciones in vivo o in vitro.

Figura 2. Imagenología de calcio en la médula espinal. En el diagrama se muestra un resumen de las aplicaciones de la imagenología de calcio intracelular en el estudio de los mecanismos sensoriales y nociceptivos a nivel de la médula espinal. Creado por la autora de esta tesis con BioRender.com

2.5.1. Imagenología de calcio in vivo

La imagenología de calcio in vivo se utiliza para estudiar las funciones de la médula espinal en una configuración de animales enteros y se pueden llevar a cabo mediante una observación única o continua. En imagenología de calcio de una sola observación, se expone previamente la médula espinal en animales anestesiados. Su principal ventaja es que la fijación de la médula espinal mediante un estereotáxico reduce los movimientos respiratorios que podrían afectar a la estabilidad de los registros (Davalos et al., 2008). Sin embargo, dado que la exposición a la médula espinal puede causar daño e inflamación tisular, esta técnica es útil para una sola sesión de registro (Davalos et al., 2008). Para esta breve observación, los indicadores de calcio micro inyectados, o su electroporación en la célula, y los indicadores de calcio codificados genéticamente son las herramientas más utilizadas para este tipo de imágenes de calcio (Paredes et al., 2008). La imagenología de calcio in vivo a largo plazo es relevante para estudiar la fisiología celular, así como para la progresión de la enfermedad o lesión. Las preparaciones in vivo a largo plazo se pueden utilizar para tomar imágenes de la médula espinal durante varios meses. A través de una ventana de vidrio o la implantación de una cámara de registro para preservar el acceso al tejido y minimizar los movimientos no deseados, los investigadores pueden examinar la actividad de la médula espinal varias veces después de una sola cirugía (Farrar et al., 2012).

La ventaja más significativa de esta técnica es que el tejido se puede conservar para sesiones de registro posteriores. Los estudios de viabilidad realizados varios días después de la implantación de una ventana de vidrio o una cámara de registro han tenido resultados prometedores, como el registrar la actividad dependiente del calcio de las células durante varias semanas (Farrar et al., 2012). Estos estudios han medido la respuesta inflamatoria al dispositivo implantado en la médula espinal y no han detectado ningún daño en los vasos sanguíneos y el tejido circundante (Farrar et al., 2012; Fenrich et al., 2012). Los indicadores de calcio genéticamente modificados (GECIs) se utilizan principalmente para registros crónicos porque pueden dirigirse selectivamente a tipos celulares específicos (Schultz et al., 2017). Brevemente, los GECIs utilizan proteínas fluorescentes genéticamente modificadas en conjunto con proteínas sensibles a Ca^{2+} para evaluar cambios en las $[Ca^{2+}]i$ en una o varias poblaciones celulares específicas a la vez. Una de las ventajas de utilizar estos indicadores de calcio es que evaluan cambios en las $[Ca^{2+}]i$ tanto a nivel celular, como a nivel de organelos (Rochefort et al., 2008). También, los GECIs se expresan de manera estable durante meses en subtipos celulares específicos, por lo que facilitan el estudio de procesos como memoria y aprendizaje, y son útiles para el estudio de la evolución de diferentes circuitos neuronales tanto en animales anestesiados como despiertos (Looger & Griesbeck, 2012). Por lo tanto, las preparaciones in vivo permiten a los investigadores estudiar todo el sistema implicado en la transmisión de información sensorial desde el campo receptivo periférico hasta las láminas superficiales (500 µm) de la médula espinal tanto en animales anestesiados como despiertos.

En cuanto a la transmisión de la información sensorial, la imagenología de calcio in vivo realizada en animales despiertos es útil para estudiar la respuesta de las neuronas del asta dorsal a diferentes estímulos cutáneos (Cirillo et al., 2012; Sekiguchi et al., 2016; Vrontou et al., 2013). Usando microscopía de dos fotones y microscopios miniaturizados de un fotón, Sekiguchi y colaboradores (2016) mostraron que diferentes estímulos cutáneos (pulsos de aire, pellizcos y acicalamiento) activan conjuntos superpuestos de neuronas del asta dorsal en ratones despiertos. Además, los resultados mostraron que cada célula que responde a estímulos cutáneos puede codificar el tipo y la intensidad del estímulo en sus transitorios de calcio (Sekiguchi et al., 2016). La imagenología de calcio in vivo también ha sido valiosa para estudiar las respuestas primarias de las fibras aferentes sensoriales en el asta dorsal de la médula espinal tras la estimulación cutánea (Vrontou et al., 2013). Por ejemplo, en su estudio pionero utilizando indicadores de calcio genéticamente codificados (GECI) , Vrontou

y colaboradores (2013) identificaron un grupo de fibras C no mielínicas que responden al tacto suave de la pata trasera. Adicionalmente, los autores aplicaron los resultados obtenidos de los experimentos de imagenología de calcio a un modelo conductual de preferencia de lugar condicionado y demostraron que la activación de las fibras C, que respondían al tacto suave en los experimentos de imagenología de calcio, podía modificar la actividad conductual en ratones (Vrontou et al., 2013). Además, el papel de los astrocitos en las redes de la médula espinal también se ha estudiado con técnicas como la imagenología de calcio in vivo usando dos marcadores celulares específicos para astrocitos como la sulforodamina 101 y el Oregon-Green BAPTA-1 (Cirillo et al., 2012). Los resultados mostraron que la actividad dependiente de calcio de los astrocitos en el asta dorsal de la médula espinal aumenta durante la estimulación sensorial en comparación con las condiciones de reposo, demostrando que los astrocitos tienen un papel durante la transmisión de información sensorial en el asta dorsal (Cirillo et al., 2012). Sin embargo, se requieren más estudios para comprender completamente el papel de los astrocitos en este proceso.

En cuanto a la transmisión de estímulos nociceptivos, los estímulos nocivos alteran la actividad dependiente de calcio en la médula espinal en condiciones de dolor agudo o crónico (Johannssen & Helmchen, 2010; Vrontou et al., 2013). Algunos grupos han estudiado la respuesta a la estimulación mecánica nociva mediante imágenes de la actividad dependiente del calcio de las neuronas y fibras C aferentes al asta dorsal de la médula espinal (Vrontou et al., 2013). Usando imagenología de calcio in vivo y microscopía de dos fotones, un estudio mostró que las fibras C no mielínicas (descritas como fibras MRGPRD+) se activaron fuertemente al utilizar un estímulo de pellizco en la pata trasera ipsilateral, y no se activaron mediante estímulos de cepillado (Vrontou et al., 2013). Estos resultados sugieren la especificidad de las fibras MRGPRD+ en la transmisión de información de estímulos nocivos en el asta dorsal de la médula espinal. Otro estudio midió la respuesta de las neuronas del asta dorsal a los estímulos periféricos de pellizco (Johannssen & Helmchen, 2010) mostrando que las células superficiales del asta dorsal que estaban silentes en ausencia de estímulos, se activaban después de estimular con un pellizco, y que la amplitud de estos transitorios de calcio evocados era proporcional a la fuerza del estímulo periférico (Johannssen & Helmchen, 2010).

El papel de los astrocitos en la transmisión nociceptiva a nivel del asta dorsal también ha sido estudiado por imagenología de calcio in vivo. Los astrocitos contribuyen a la

nocicepción interactuando con las neuronas en el asta dorsal, pero se desconoce la relación entre la actividad astrocítica y la actividad de la neuronas. La imagenología de calcio in vivo se utilizó para estudiar la respuesta de los astrocitos a estímulos de pellizco en la periferia en ratones despiertos y anestesiados; los resultados mostraron que los astrocitos responden a intensos estímulos nocivos. Los estímulos débiles no evocaban una respuesta dependiente del calcio (Sekiguchi et al., 2016).

El asta dorsal de la médula espinal es uno de los sitios más importantes para estudiar los cambios debidos a la sensibilización central inducida por los procesos nociceptivos. Sin embargo, los estudios de imágenes de calcio in vivo también se realizaron en otras estructuras involucradas en el procesamiento de la nocicepción, por ejemplo, el núcleo trigémino, las terminales nerviosas y los ganglios de raíz dorsal (DRG). Los resultados de diferentes estudios demostraron que la actividad dependiente del calcio, de diferentes estructuras involucradas en la transmisión de estímulos tanto sensitivos como nociceptivos, cambia en presencia de estímulos mecánicos o térmicos nocivos (Emery et al., 2016; Kim et al., 2014; Yarmolinsky et al., 2016).

2.5.2. Imagenología de calcio in vitro

Las rebanadas de médula espinal se utilizan regularmente para los registros de imagenología de calcio in vitro para estudiar la actividad dependiente del calcio de las neuronas y las células gliales en las láminas profundas de la médula espinal. Los indicadores de calcio son comunes para este tipo de preparación porque se cargan rápidamente en las células y no necesitan ser transferidos o expresados, por lo que las rebanadas están listas para la toma de imágenes después de algunos minutos (Luo et al., 2008; Paredes et al., 2008; Ruscheweyh & Sandkühler, 2005). La principal ventaja de las preparaciones in vitro es que se puede acceder fácilmente a láminas profundas de la médula espinal que aún no están disponibles con imagenología de dos fotones. Sin embargo, las imágenes in vitro de calcio no se han utilizado ampliamente para estudios sensoriales y nociceptivos. Esta observación es notable ya que esta técnica se puede utilizar para estudiar los cambios relacionados con los procesos nociceptivos en la médula espinal. El asta dorsal de la médula espinal es uno de los sitios más importantes para estudiar los mecanismos de plasticidad involucrados en el dolor y mecanismos relacionados con los cambios dependientes de la actividad en la señalización de calcio, que es útil para entender el desarrollo de los procesos nociceptivos (Luo et al., 2008).

En cuanto al uso de la imagenología de calcio en preparaciones in vitro para estudiar los mecanismos referentes a la nocicepción en el asta dorsal de la médula espinal se ha reportado que la actividad dependiente de calcio de células en las láminas superficiales se altera en presencia de dolor inflamatorio (Luo et al., 2008; Ruscheweyh & Sandkühler, 2005). Estudios en rebanadas de médula espinal mostraron un aumento en la amplitud de los transitorios de calcio en las neuronas de la lámina I y II que se correlaciona con la respuesta inflamatoria (Luo et al., 2008). Además, bajo condiciones similares al dolor crónico, las neuronas de las láminas I y II del asta dorsal exhibieron actividad dependiente de calcio sincrónica y repetitiva, correspondiente a la potenciación a largo plazo (LTP) asociada con el dolor neuropático (Ruscheweyh & Sandkühler, 2005), efecto que atribuyen a la activación de los receptores NMDA (Luo et al., 2008; Ruscheweyh & Sandkühler, 2005; Woolf & Salter, 2000). Como se mencionó anteriormente, la imagenología de calcio intracelular en rebanadas de médula espinal proporciona acceso a láminas más profundas (III-VI). Sin embargo, la mayoría de los estudios sólo han reportado la actividad de las células en las láminas I y II.

2.6. Perspectivas de las técnicas de imagenología de calcio en el estudio de procesos sensoriales y nocicepción

Dado que diferentes células se pueden registrar simultáneamente a través de imagenología de calcio, esta técnica podría ser eficaz para analizar la actividad de las poblaciones celulares, incluidas las neuronas y la glía. Además, la presencia de varios marcadores de calcio facilita la diferenciación completa entre la actividad neuronal y glial (incluyendo diferentes tipos de células gliales) (Paredes et al., 2008). Registrar diferentes patrones de actividad dentro de las poblaciones neuronales podría revelar información valiosa sobre la codificación de estímulos de intensidades variables dentro de la misma población celular. La imagenología de calcio también ofrece un campo más amplio de registro de actividad, esta es una gran ventaja ya que se pueden registrar diferentes células dentro de una línea de tiempo específica. Esto señala el uso potencial de imágenes de calcio en el análisis de la correlación de la actividad de grupos de neuronas no sólo dentro de la misma población, sino también entre diferentes poblaciones celulares. Esto proporcionará datos sobre los patrones de actividad de diferentes poblaciones neuronales y cómo se afectan en el procesamiento de la información sensorial.

Por otro lado, las técnicas de registro de la actividad neuronal por imágenes de calcio son candidatos relevantes en el campo de la optogenética, especialmente en animales que se mueven libremente, para superar muchas limitaciones como el registro de estructuras profundas, la biodisponibilidad de acceso a la columna vertebral y los movimientos no deseados. Por lo tanto, podría ser el puente para explicar los cambios en los transitorios de calcio y su correlación con ciertos elementos conductuales.

Por último, la imagenología de calcio in vivo a largo plazo proporciona un método prolongado y limitadamente invasivo para el registro de la actividad celular. La observación secuencial en el mismo animal puede ayudar a entender diferentes fenómenos fisiológicos sensoriales y relacionados con el dolor; además, se podría realizar una línea temporal de evolución de la enfermedad con el fin de describir cómo las condiciones patológicas, como el dolor neuropático, modifican los patrones de actividad neuronal.

3. PREGUNTAS DE INVESTIGACIÓN

Tomando en cuenta lo anterior, se plantearon las siguientes preguntas de investigación:

- ¿Cómo es la actividad espontánea dependiente de calcio de células del asta dorsal de la médula espinal?
- ¿Se ve esta actividad afectada por la sensibilización central inducida por una condición de dolor neuropático?
- ¿Tiene la OT un efecto sobre las células del asta dorsal de la médula espinal? ¿Qué pasa con la actividad celular derivada de una condición de sensibilización central cuando aplicamos OT?

4. HIPÓTESIS

Con base a los hallazgos previos se postula que:

Si los patrones de actividad dependiente de calcio intracelular del asta dorsal de la médula espinal se ven afectados por condiciones de sensibilización central como el dolor neuropático, entonces la aplicación de OT modificara estos patrones de actividad.

Para responder a las preguntas de investigación previamente descritas y probar nuestra hipótesis, desarrollamos el siguiente objetivo general y los siguientes objetivos específicos.

5. OBJETIVOS

5.1. General

Evaluar la actividad espontánea dependiente de calcio en el asta dorsal de la medula espinal y como se ve afectada bajo condiciones de dolor neuropático.

5.2. Específicos

- Evaluar la actividad espontánea dependiente de calcio de células del asta dorsal de la médula espinal.
- Evaluar la actividad dependiente de calcio evocada con un modelo de sensibilización central por activación de receptores NMDA
- Evaluar el efecto de la OT sobre la actividad dependiente de calcio en las dos condiciones anteriormente mencionadas.
- Evaluar y comparar la actividad evocada con NMDA y la actividad dependiente de calcio evocada por un modelo de dolor neuropático previamente descrito, como es la inyección de formalina 5%.

Para cumplir con los objetivos aquí descritos, se eligió usar la imagenología de calcio intracelular en rebanadas de médula espinal, ya que nos permite evaluar la actividad de un número grande de células, además podemos tener acceso a láminas profundas del asta dorsal de la médula espinal. También se utilizaron diferentes condiciones experimentales para evaluar el efecto de diferentes fármacos sobre la actividad dependiente de calcio de neuronas del asta dorsal. Por último, con el análisis de los datos obtenidos se realizó una comparación entre las diferentes condiciones experimentales. Un resumen del diseño experimental y de los grupos experimentales evaluados se presenta en la **Figura 3**.

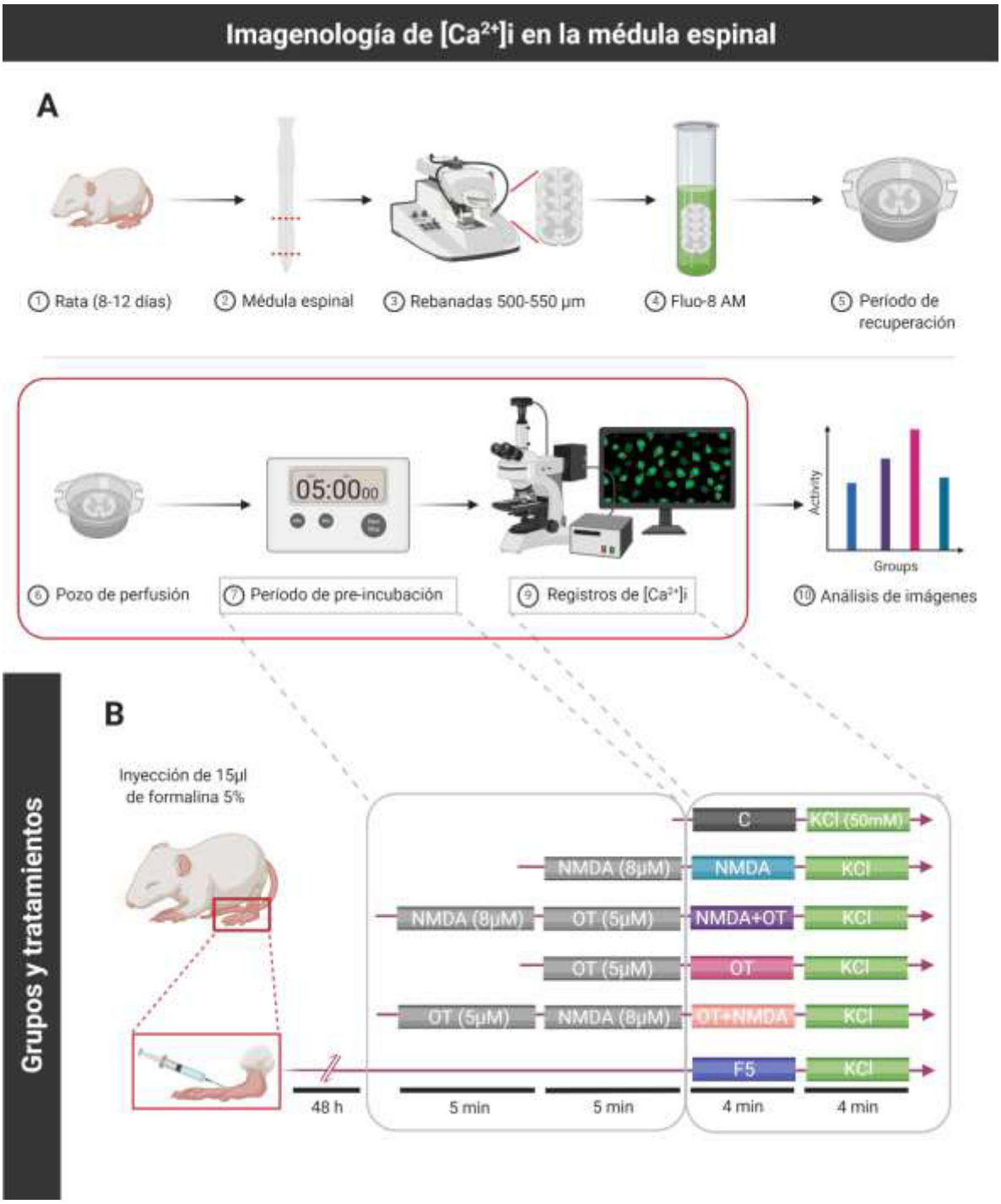

Figura 3. Imagenología de [Ca^{2+}]i en la médula espinal. (A) Línea temporal de los experimentos correspondientes a imagenología de [Ca^{2+}]i, desde la extracción de la médula espinal hasta el registro de la actividad dependiente de [Ca^{2+}]i en neuronas del asta dorsal de la médula espinal. **(B) Grupos y tratamientos.** Esquema y línea temporal de los diferentes grupos, tratamientos y su aplicación. Creado por la autora de esta tesis con BioRender.com

6. MATERIALES Y MÉTODOS

6.1. Animales experimentales y normas éticas

Para este proyecto se utilizaron ratas Wistar neonatas de 8 a 12 días de edad (P8-P12) de ambos sexos en los experimentos. Los animales se alojaron en cajas de plástico transparente y se mantuvieron en un ciclo de luz-oscuridad de 12:12 horas (luces encendidas a las 07:00 horas) a temperatura ambiente (22°C ± 2°C), con alimento y agua ad libitum. Todos los experimentos siguieron las Guías de los Institutos Nacionales de Salud para el Cuidado y Uso de Animales de Laboratorio (publicación NIH no 80-23, revisada en 1996) y las Guías de la Asociación Internacional para el Estudio del Dolor (IASP) para el Uso de Animales en Investigación (Zimmermann, 1983), y se llevaron a cabo con la aprobación del Comité de Bioética en el Instituto de Neurobiología (Protocolos Bioéticos números 008 - 010). Se hicieron todos los esfuerzos para evitar el sufrimiento y utilizar sólo el número de animales necesarios para producir datos científicos fiables.

6.2. Trazado de neuronas de proyección en la médula espinal

6.2.1. Inyección de dextrán tetrametil-rodamina (DTMR)

Con la finalidad de identificar las poblaciones de neuronas de proyección del asta dorsal de la médula espinal en ratas neonatas, se realizaron inyecciones de DTMR en el núcleo gracilis (GRA) izquierdo de ratas Wistar de 6 días de edad. Las ratas fueron anestesiadas con sevofluorano al 4%, control de temperatura a 38°C por medio de un sistema de agua circulante y ventilación asistida (2/3 N_2O y 1/3 O_2). Una vez colocadas en el estereotáxico, se realizó una incisión en la parte posterior del cuello y se disecaron los músculos de la nuca para permitir el acceso por el foramen atlanto-occipital. Las inyecciones de trazador neuronal se realizaron utilizando pipetas de vidrio con una punta de 5-8 µm, las cuales se llenaron con DTMR que fue inyectado por presión. El volumen inyectado oscila entre 30-50 nl, aproximadamente. Por último, los animales fueron suturados y al salir de la anestesia se les colocó en una caja con el resto de la camada.

6.2.2. Histología de los sitios de inyección y de la médula espinal

Se esperaron 48 horas después de la inyección, para que se llevara a cabo el transporte del trazador hasta la porción lumbar de la médula espinal. Las ratas se anestesiaron

profundamente con pentobarbital (50 mg/kg) y perfundidas transcardialmente con solución salina 0.9%, seguido por una solución de paraformaldehído 4% en buffer de fosfatos (0.1 M, pH 7.4). El SNC se disectó y colocó en la misma solución de paraformaldehído al 4% en buffer de fosfatos (0.1 M, pH 7.4) para su post-fijación durante 2 horas. Posteriormente, el tejido se colocó en una solución de sacarosa al 30% para ser crio protegido y almacenado hasta su procesamiento como se describe a continuación.

6.2.2.1. Sitio de inyección

Se realizaron cortes continuos de 40 µm con el micrótomo (Leica Instruments) del sitio de inyección. Los cortes se montaron en un portaobjetos de manera consecutiva, deshidratados y conservados en DPX para su análisis posterior.

6.2.2.2. Médula espinal

Para determinar la distribución de las neuronas del asta dorsal que proyectan al GRA, se realizó una seriación de cortes de la porción lumbar de la médula espinal. Se realizaron cortes de 40 µm de toda la porción lumbar en el micrótomo (Leica instruments) y los cortes se dividieron en 5 series que se utilizaron de la siguiente manera: 1) se montó en portaobjetos, se deshidrato y se conservó en DPX para el análisis de las células marcadas con trazador, 2) se realizó una tinción de Nissl y posteriormente se montó y deshidrató, 3) se realizó inmunofluorescencia a NeuN (marcador nuclear de neuronas). Las últimas dos series se almacenaron en buffer de fosfatos para su posterior análisis.

6.3. Inmunofluorescencia

Los cortes de médula espinal se preincubaron con una solución de PBS (0.1 M, pH 7.4) y Triton-X-100 1% por 20 minutos a temperatura ambiente y después incubados con el anticuerpo primario: Mouse anti-NeuN (1:1000, Chemicon) o Nissl stain por 24 horas a 4°C. Después, los cortes fueron lavados por 5 minutos con una solución PBS 0.1 M para ser incubados con el anticuerpo secundario correspondiente: Goat-anti mouse IgG Alexa fluor 488 (1:300, Invitrogen, cat. # A32723) por 2 horas a 4°C. Finalmente, los cortes de médula espinal se lavaron por 5 minutos con PBS, montaron en portaobjetos, y fijaron en DPX.

6.4. Microscopía confocal y toma de imágenes

Los cortes del sitio de inyección y el hasta dorsal de la médula espinal se observaron en el microscopio confocal LSM 510 o LSM 780 (Zeiss, México). Se obtuvieron imágenes representativas tanto del sitio de inyección como de las regiones del asta dorsal donde se encontraron neuronas de proyección (**Figura 4**, **Figura 5**).

6.5. Imagenología de calcio intracelular

6.5.1. Preparación de rebanadas de médula espinal

Las ratas (P8-P12) se anestesiaron con pentobarbital (50 mg/kg) y perfundieron transcardialmente con una solución salina con sacarosa helada (4°C) (sacarosa, 238 mM; glucosa, 30 mM; $NaHCO_3$, 25 mM; KCl, 3 mM; $MgCl_2$, 2.5 mM; oxigenada con 95% O_2, 5% CO_2; pH 7.4). Después, se extrajo y montó la sección lumbosacra de la médula espinal en un vibrotomo NVSL Vibroslice™ (World Precision Instruments Inc., Sarasota, FL, EE.UU.) y se obtuvieron rebanadas transversales de 500-550 µm de espesor. Las rebanadas permanecieron a temperatura ambiente (22-24 °C) durante al menos 1 hora antes de los experimentos en solución salina que contiene (en mM): 119 NaCl, 30 Glucosa, 25 $NaHCO_3$, 6 KCl, 2.5 $MgCl_2$, 1.5 $CaCl_2$, oxigenado con 95% O_2, 5% CO_2, pH 7.4.

6.5.2. Registros de calcio intracelular y tratamientos

Las rebanadas se incubaron en condiciones de oscuridad de 30-60 minutos a temperatura ambiente en una solución con 1 ml de solución salina más 1.8 % de D-manitol (Sigma-Aldrich Co., St. Louis, MO, EE. UU.; CAS No. 69-65-8) y 20 µl de una solución que contiene 5 µg de Fluo-8® AM (AAT Bioquest Inc., Sunnyvale, CA, EE. UU.; CAS No. 1345980-40-6) diluido en 50 µl dimetilsulfoxido (DMSO), y equilibrado con 95% O_2 y 5% CO_2. Para obtener las señales de fluorescencia de $[Ca^{2+}]i$ se utilizó un microscopio de fluorescencia Olympus IX81 invertido y motorizado equipado con un objetivo UPlanSApo 10x/0.40na (Olympus Latin America, Inc, Florida, FL, EE. UU.). Para registrar las señales fluorescentes de los transitorios de $[Ca^{2+}]i$, se dieron pulsos de luz a 488 nm (35 -100 ms de exposición) a la rebanada de médula espinal utilizando una lámpara de xenón (módulo Cell-R DSU, Olympus) conectada al microscopio por medio de fibra óptica. Los cambios en la fluorescencia de las señales de $[Ca^{2+}]i$ se registraron con una cámara CCD digital ORCA®-R2 (Hamamatsu Photonics K.K. Japan) que da un campo de imagen de 866 x 660 µm

(**Figura 7 A, B**). Se utilizó el software de adquisición de imágenes xCellence-RT, v1.2 (Olympus Soft Imaging Solution GmbH, Alemania) para adquirir vídeos cortos de 240 segundos (240 seg = 1 epoch; 4-5 fps) a intervalos de tiempo de 200-250 ms con un tiempo de exposición de entre 35-60 ms. Un esquema ilustrativo del protocolo experimental correspondiente a la imagenología de $[Ca^{2+}]i$ puede observarse a detalle en la **Figura 3 A**.

Al final de cada experimento, se aplicó solución de cloruro de potasio a la cámara de registro como control positivo (concentración final KCl 50 mM). Las neuronas activas (de 15 a 124 dependiendo de cada condición experimental) durante el experimento se identificaron debido a sus transitorios de $[Ca^{2+}]i$ (**6.6.1. Detección de actividad neuronal**) y registraron bajo diferentes tratamientos (**Figura 4 B**):

i. Control: no se aplicó ningún tratamiento a la rebanada. Registros de la actividad basal de las células del asta dorsal, el objetivo fue observar cómo es la actividad espontánea en el asta dorsal de la médula espinal.
ii. NMDA: NMDA (8 µM) fue añadido a la preparación y preincubado durante 5 minutos antes de cada registro, con el objetivo de evaluar los cambios en la actividad dependiente del calcio de las células del asta dorsal espinal bajo una entrada excitatoria, similar a una sensibilización central por la activación del NMDAr, como la que ocurre bajo condiciones de dolor neuropático.
iii. NMDA+OT: OT (5 µM) se agregó a la preparación después de la previa incubación con NMDA (8 µM), con el objetivo de evaluar si la OT tiene efecto sobre la actividad previamente evocada por el tratamiento con NMDA.
iv. OT: se agregó OT (5 µM) a la rebanada para evaluar su efecto en la actividad espontánea.
v. OT+NMDA: al invertir el orden de los fármacos se buscó evaluar si la OT producía un efecto protector al ser aplicada antes que el NMDA.
vi. Formalina 5%: la inyección de formalina (5%) se realizó 48 horas antes de los registros de $[Ca^{2+}]i$, con el fin de evaluar la actividad dependiente del calcio de las células del asta dorsal bajo una condición de dolor neuropático y comparar si la aplicación de NMDA podría reproducir este patrón de actividad como un modelo de dolor neuropático in vitro.

Los experimentos con NMDA se preincubaron 5 minutos antes de los registros. Los experimentos para el grupo NMDA+OT se preincubaron durante 5 minutos con NMDA,

después se agregó OT y se preincubó por 5 minutos más (10 minutos en total). Los experimentos de OT se preincubaron 5 minutos antes de los registros. No se añadió NMDA a la preparación. Para el grupo OT+NMDA, se agregó y preincubó la OT durante 5 minutos y después se agregó el NMDA para una segunda incubación de 5 minutos (10 minutos en total). Un diagrama de los grupos experimentales y una línea temporal de los tratamientos y su aplicación puede observarse a detalle en la **Figura 3 B**.

6.6. Análisis de imágenes

El procesamiento inicial de imágenes se llevó a cabo utilizando Im-Patch© (http://impatch.ifc.unam.mx/), un software de acceso abierto para analizar los cambios en las señales fluorescentes dependientes de $[Ca^{2+}]i$. Este programa fue escrito en el entorno de programación LabVIEW (National Instruments™, EE.UU.) por el Dr. Jesús Pérez Ortega y ha sido ampliamente utilizado en otros trabajos analizando señales fluorescentes dependientes de $[Ca^{2+}]i$ (Aparicio-Juárez et al., 2019; Pérez-Ortega et al., 2016; Rendón-Ochoa et al., 2018). En breve, este programa nos permite extraer una imagen resumen, que se obtiene de la desviación estándar de la fluorescencia de cada vídeo. Después, las coordenadas de localización de las neuronas activas durante el experimento se detectan automáticamente mediante el reconocimiento de patrones utilizando plantillas circulares con un diámetro de 3 píxeles (4 µm) (**Figura 7 B y C**). Los transitorios de calcio, representados como cambios en la fluorescencia (Fi-Fo)/Fo (donde Fi es la intensidad de fluorescencia y F0 la fluorescencia basal de cada neurona), de cada región de interés se extraen a lo largo del tiempo (**Figura 7 D**). El fotoblanqueo, el ruido y los fenómenos de airy disk se corrigen como se ha descrito anteriormente.

6.6.1. Detección de actividad neuronal

Se ha reportado que la primera derivada de un transitorio de $[Ca^{2+}]i$ refleja la descarga eléctrica de las neuronas. Específicamente, la parte positiva de la primera derivada a lo largo del tiempo de un transitorio de $[Ca^{2+}]i$ es similar a la duración de los trenes de disparo en las neuronas (Carrillo-Reid et al., 2008; Pérez-Ortega et al., 2016; Plata et al., 2013). Por lo tanto, los frames con neuronas activas (vistos con su derivada) se tomaron como una medida indirecta de la actividad eléctrica de las neuronas a lo largo del tiempo (actividad global). En todos los casos, sólo se consideraron transitorios con amplitudes 2.5 veces superiores a la desviación estándar del valor de ruido para el análisis. Todos los registros

se examinaron manualmente para eliminar los transitorios de calcio atribuidos a las células gliales, que se han descrito como más lentos que las señales de las neuronas (minutos de duración) (Carrillo-Reid et al., 2008; Pérez-Ortega et al., 2016; Plata et al., 2013). La detección de la actividad neuronal se llevó a cabo como se describió anteriormente (Carrillo-Reid et al., 2008; Pérez-Ortega et al., 2016; Plata et al., 2013). Brevemente, se construyó una matriz binaria (N x F) con los datos que representa la actividad de las neuronas registradas simultáneamente a lo largo del tiempo (una matriz por epoch), donde 1 representa una neurona activa y 0 una inactiva. Esta matriz binaria se llamó matriz experimental, donde cada fila corresponde a una neurona activa (N), mientras que las columnas representan el número de frames (F) en el vídeo, de la siguiente manera: 1 columna es igual a 1 frame. Al graficar la matriz experimental, obtenemos una representación gráfica de la actividad celular como se muestra en el raster plot de la **Figura 7 E**. La suma de cada columna en la matriz experimental es un vector de coactividad (1xF) que representa la coactividad de varias neuronas a lo largo del tiempo. Al graficar estos vectores de coactividad, obtenemos una representación gráfica como se muestra en el histograma de coactividad de la **Figura 7 F**.

6.6.2. Análisis de coactividad

Después de construir la matriz experimental, el análisis de coactividad se realizó en un programa hecho a medida, escrito en MATLAB (MathWorks, Inc. MA, EE. UU.) por el Dr. Jesús Pérez Ortega (https://github.com/PerezOrtegaJ/Neural_Ensemble_Analysis), que incluye algunos algoritmos del Brain Connectivity Toolbox de MATLAB (https://sites.google.com/site/bctnet/). En este programa, se obtuvieron vectores de coactividad de cada matriz experimental y la probabilidad de que un pico de coactividad dado apareciera por casualidad se evaluó determinando un umbral de significancia utilizando permutaciones de Monte Carlo (1000 veces) como se describió anteriormente (Carrillo-Reid et al., 2008; Pérez-Ortega et al., 2016; Plata et al., 2013). El umbral de significancia se estableció como $p < 0.05$, y se marcó como una línea punteada en cada histograma de coactividad (Carrillo-Reid et al., 2008; Pérez-Ortega et al., 2016; Plata et al., 2013). También, todos los picos que superaron el nivel de significancia se denotan en rojo (**Figura 9**). Para el análisis, se almacenaron picos significativos de coactividad neuronal en una matriz de picos de coactividad (A x P), donde A es el número de células activas en cada pico, y P es el número de picos de coactividad. El coeficiente de similitud de Jaccard se midió para evaluar si los vectores de coactividad eran diferentes entre sí (Carrillo-Reid

et al., 2008; Pérez-Ortega et al., 2016; Plata et al., 2013). Además, para evaluar un aumento o disminución en la sincronización de la actividad, se contaron vectores de coactividad en cada epoch. Un esquema ilustrativo del proceso de análisis de imágenes puede observarse en la **Figura 4**.

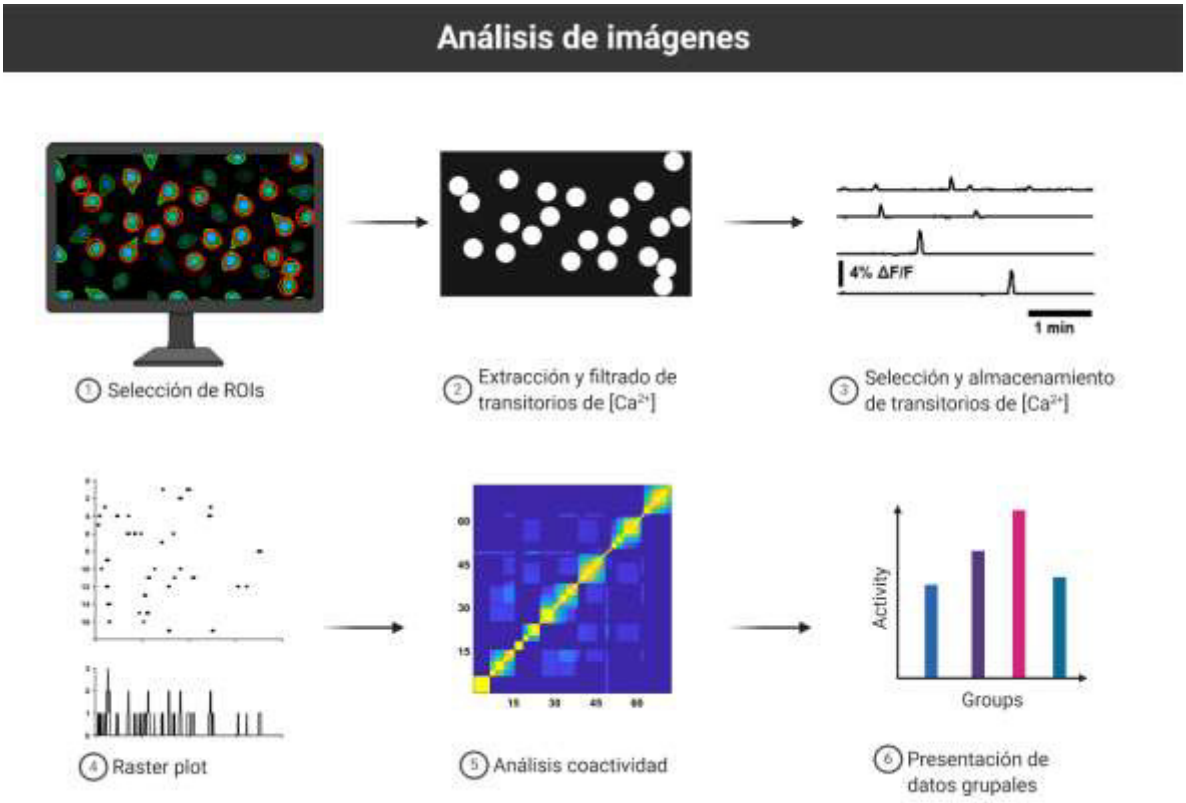

Figura 4. Análisis de imágenes. Diagrama general del procesamiento de imágenes, desde la extracción de los transitorios de calcio hasta la presentación por grupos y análisis estadístico. Creado por la autora de esta tesis con BioRender.com

6.7. Fármacos

Aparte del anestésico (pentobarbital sódico; PiSA®, México) y otros reactivos mencionados anteriormente, este estudio también utilizó los siguientes compuestos (obtenidos de las fuentes indicadas): ácido N-metil-D-aspártico (NMDA; CAS No 6384-92-5) y sal de acetato de oxitocina hidratado (OT; CAS No. 50-56-6) comprado a Sigma-Aldrich Co. (St. Louis, MO, USA). Las soluciones de stock de OT y NMDA se prepararon antes de los experimentos y se agregaron a la cámara de registro a la concentración final de 5 µM de

OT y 8 µM de NMDA. Para algunos experimentos, la formalina 5% (15 µl, diluida en solución salina) se inyectó por vía subcutánea (s.c.) en la superficie dorsal de la pata trasera 48 horas antes de la extracción de la médula espinal. El NMDA y la OT se disolvieron en solución salina isotónica (0.9 % NaCl).

6.8. Datos y análisis estadístico

La mayoría de los métodos estadísticos utilizados para el análisis de datos se han descrito previamente (Carrillo-Reid et al., 2008; Pérez-Ortega et al., 2016; Plata et al., 2013). Brevemente, se analizó el número de células activas, se consideró la actividad total durante cada epoch, se detectó y contabilizó el número de picos de coactividad para cada condición experimental in vitro y se graficaron estos datos como la media ± error estándar de la media (SEM). Se utilizó una prueba de Kruskal-Wallis no pareada con la prueba post hoc de Dunn para analizar las diferencias entre cada grupo en comparación con la condición de control y dentro de los grupos. Se graficó la actividad total con respecto a los picos de coactividad para comparar la relación entre ambas variables. También, se realizó un análisis de regresión lineal para obtener los valores de pendiente y la importancia de la correlación entre las variables. Finalmente, la actividad global de cada condición a lo largo del tiempo estuvo representada por una gráfica de actividad acumulada y las tasas de incremento de la actividad se aproximaron con regresiones lineales ad hoc (Carrillo-Reid et al., 2008; Pérez-Ortega et al., 2016; Plata et al., 2013). Consideramos los valores de diferencia estadística como $p<0.05$.

7. RESULTADOS

7.1. Poblaciones de neuronas de proyección en el asta dorsal de la médula espinal

Con la finalidad de analizar la distribución de neuronas de proyección de la médula espinal que proyectan al GRA, se utilizaron inyecciones de trazador neuronal e inmunofluorescencia. Se verificó la localización del sitio de inyección (**Figura 5**) y se analizó la distribución de las células de proyección al núcleo GRA a nivel lumbar de la médula espinal. Se observó un marcaje principalmente en tres áreas diferentes a lo largo del asta dorsal (**Figura 6**), una en las láminas superficiales I y II (**Figura 6 A**), la segunda cercana a la parte más lateral de las láminas III y IV (**Figura 6 B**) y la última en la lámina 6 cerca del canal central (**Figura 6 C**).

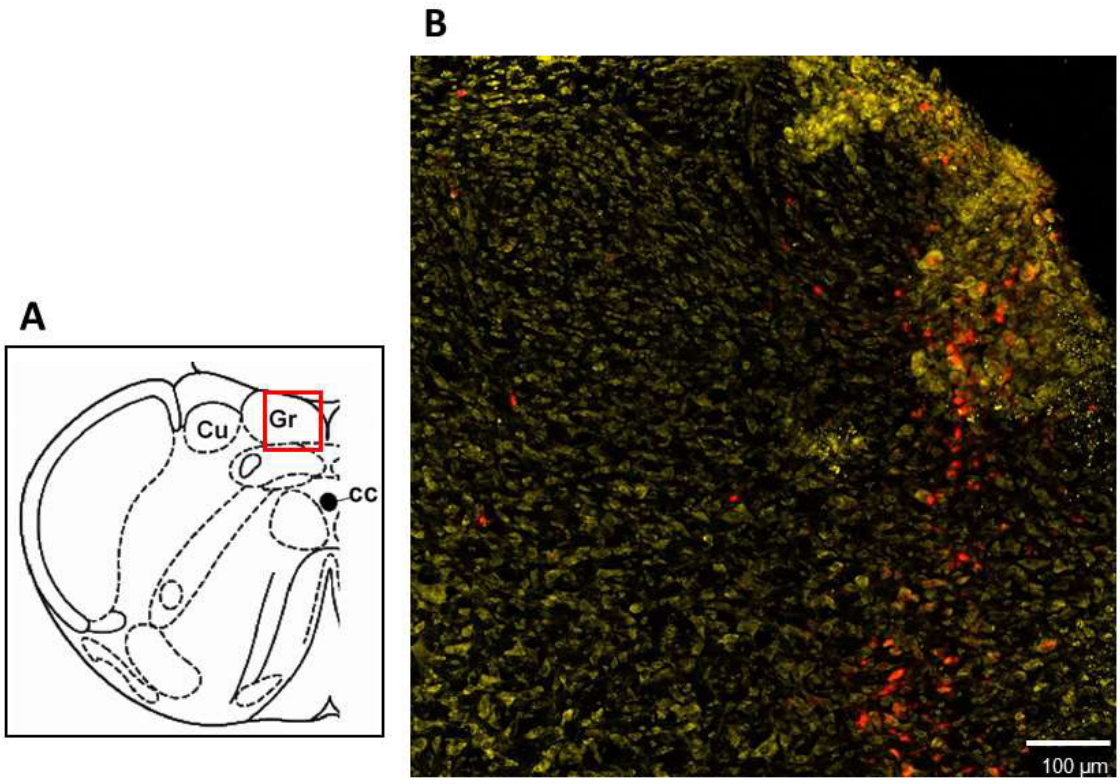

Figura 5. Sitio de inyección de dextrán tetrametil rodamina (DTMR). (A) Diagrama del núcleo GRA donde se inyectó el DTMR, obtenido de (Paxinos & Watson, 2007) **(B)** Imagen obtenida del microscopio confocal que muestra el sitio de inyección (rojo) y cuerpos neuronales (amarillo) con una tinción de Nissl (amarillo). Barra de escala = 100 *µm.*

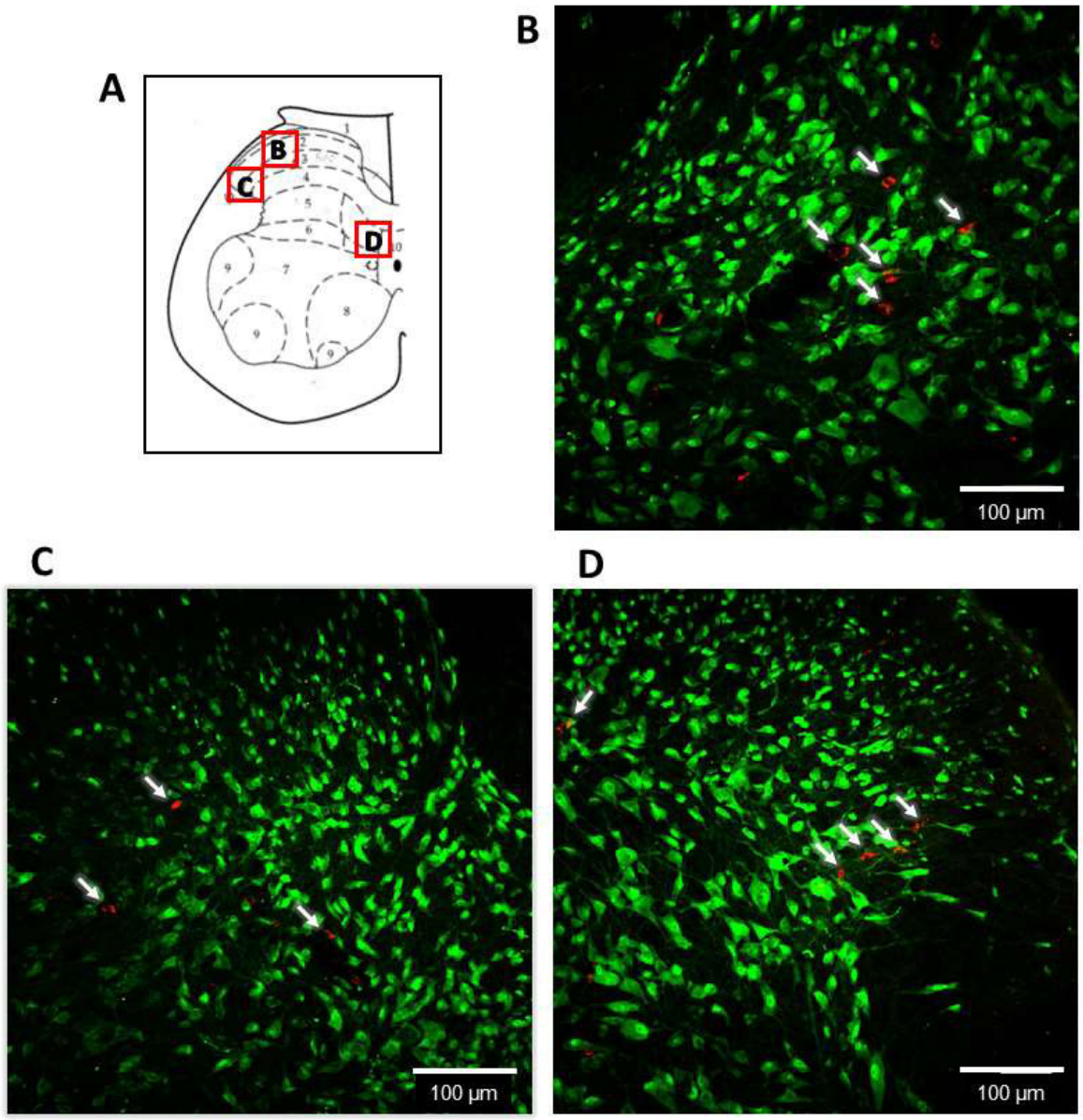

Figura 6. Células de proyección al GRA en el asta dorsal de la médula espinal. (A) Diagrama de la médula espinal obtenido de (Paxinos & Watson, 2007), donde se marcan las 3 áreas donde se encontraron neuronas de proyección al GRA. Se observaron tres poblaciones de neuronas de proyección en el asta dorsal: **(B)** láminas superficiales I y II; **(C)** parte lateral de las láminas III y IV; y **(D)** lámina 6 cerca del canal central. Las flechas blancas señalan células de proyección al GRA marcadas con DTMR (rojo) y cuerpos neuronales con una inmunofluorescencia a NeuN (verde), *barra de escala 100 µm.*

7.2. Actividad dependiente de calcio del asta dorsal de la médula espinal

Con el objetivo de analizar la actividad espontánea dependiente de calcio en el asta dorsal de la médula espinal, se realizaron registros de imagenología de $[Ca^{2+}]i$ en rebanadas de

médula espinal. Se registró un área de 866 x 660 µm del asta dorsal de la médula espinal. Esta área cubre las láminas de Rexed I a la V del asta dorsal (**Figura 7 A**). Los videos de los registros del área visualizada se analizaron como se describió en la sección **6.6 Análisis de imágenes** y se obtuvo una imagen de resumen. A partir de esta, se realizó la selección automática de las neuronas activas. Las coordenadas de cada neurona se utilizaron para identificar la localización de cada célula en el área registrada, como se muestra en la **Figura 7 C**. La **Figura 7 D** ejemplifica transitorios de $[Ca^{2+}]i$ representativos de cuatro neuronas activas de manera espontánea del asta dorsal durante 4 minutos de grabación (epoch). Por cada epoch se realizó un raster plot para visualizar la actividad de varias neuronas activas, donde los puntos representan la actividad neuronal, el número de cada célula activa en el eje Y (organizado de la lámina más superficial a la más profunda, I a V, en orden ascendente) y la línea temporal del experimento en el eje X (**Figura 7 E**). Un histograma de actividad se muestra debajo de cada raster plot, y esto representa la coactividad de las neuronas a lo largo del tiempo. En este caso, cada pico es un vector de coactividad extraído del raster plot (**Figura 7 F**). En términos generales, tal como se ha validado en otros tejidos neuronales (Carrillo-Reid et al., 2008; Jáidar et al., 2010; Pérez-Ortega et al., 2016; Plata et al., 2013), la secuencia de picos de coactividad podría denotar la secuencia de actividad de diferentes grupos de varias neuronas alternando su actividad durante los registros. Por lo anterior, para analizar el papel de la OT sobre la dinámica de actividad de células del asta dorsal de la médula espinal, analizamos los transitorios $[Ca^{2+}]i$ de las células bajo diferentes condiciones.

7.2.1. El NMDA aumenta la actividad dependiente de calcio de las células en el asta dorsal

Para evaluar los cambios en la actividad dependiente de calcio intracelular del asta dorsal de la médula espinal, aplicamos un promotor de la actividad celular in vitro, que además se correlaciona con condiciones de sensibilización central in vivo. En primer lugar, se caracterizó la actividad espontánea dependiente de $[Ca^{2+}]i$ en las células del asta dorsal (**Figura 8 B; Control**). Como se muestra en la **Figura 8 D**, la actividad basal (es decir, el número de frames con neuronas activas) de rebanadas de médula espinal fue escasa (365.30 ± 37.18, n=7), y el número de células involucradas también fue bajo (**Figura 8 C**, 25.14 ± 2.54, n=7 rebanadas) durante los 4 minutos de registro. Esta escasez de actividad

espontánea dependiente de $[Ca^{2+}]i$ en las células del asta dorsal ya fue reportado en estudios previos (Luo et al., 2008; Ruscheweyh & Sandkühler, 2005).

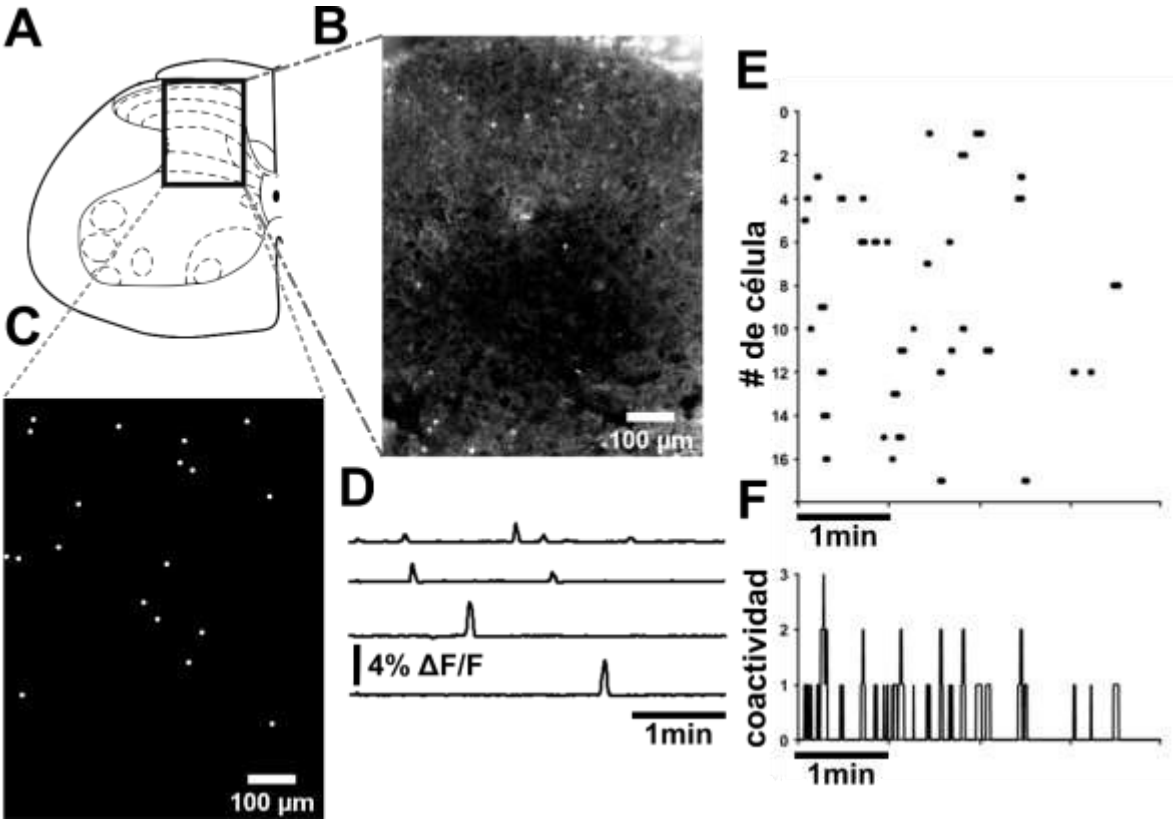

Figura 7. Registro de la actividad dependiente de $[Ca^{2+}]i$ de células del asta dorsal de la médula espinal. (A) Esquema de la zona de la médula espinal donde se realizaron los registros, obtenido de (Paxinos & Watson, 2007). **(B)** Área del tejido de la médula espinal registrada durante 4 minutos. Las rebanadas de médula espinal se cargaron con Fluo-8 AM; se registró la actividad espontánea *(barra de escala de 100 µm).* **(C)** Selección automática de neuronas activas y su localización en el área de tejido registrada durante el experimento. **(D)** Ejemplos de transitorios de calcio de 4 *neuronas durante los registros de actividad (ΔF/F).* **(E)** Raster plot que muestra la actividad espontánea de >15 neuronas en el asta dorsal de la médula espinal. Cada fila representa la actividad de una sola neurona a lo largo del tiempo; las células se ordenan y numeran de superficial a profunda (de arriba a abajo, eje Y) y las columnas representan el número de frames en los registros convertidos a escala de minutos (eje X, barra de escala de 1 minuto). **(F)** El histograma de coactividad muestra la suma de la actividad neuronal del raster plot a lo largo del tiempo y representa el número de neuronas coactivas durante los registros (barra de escala de 1 minuto).

Puesto que nuestro interés era analizar el efecto de OT bajo una condición excitatoria, utilizamos NMDA como un promotor de la actividad para aumentar la actividad del circuito del asta dorsal. Se sabe, que los receptores sensibles a NMDA son los principales

mediadores de los cambios en la actividad neuronal mediados por la movilización de $[Ca^{2+}]i$ asociados al dolor neuropático en la médula espinal (Luo et al., 2008; Ruscheweyh & Sandkühler, 2005). Además, se ha utilizado y validado un enfoque similar en otras estructuras del sistema nervioso (Carrillo-Reid et al., 2008; Jáidar et al., 2010; Plata et al., 2013). Bajo estas consideraciones, evaluamos si la aplicación de NMDA en rebanas de médula espinal puede aumentar el número de eventos de transitorios de $[Ca^{2+}]i$. Los resultados mostraron que la aplicación de NMDA (8 µM) en las rebanadas de médula espinal aumenta el número de células activas (**Figura 8 C**, 58.00 ± 6.32, n=7 rebanadas, p=0.0219, Kruskal-Wallis, post-test de Dunn) y produce un aumento parcial en la actividad global que sin ser estadísticamente significativo, en comparación con el grupo control marca una tendencia al aumento (**Figura 8 D**, 729.00 ± 106.80, n=7 rebanadas, p=0.0658, Kruskal-Wallis, post-test de Dunn).

Teniendo en cuenta que la OT puede actuar como un inhibidor de la actividad nociceptiva en animales (García-Boll et al., 2018; González-Hernández et al., 2019) y seres humanos (Miguel Condés-Lara et al., 2016; Zayas-González et al., 2019) a nivel espinal, aplicamos NMDA (8 µM) + OT (5 µM) y evaluamos si la OT modifica la actividad dependiente de $[Ca^{2+}]i$ evocada en primer lugar por la aplicación de NMDA. El tratamiento con NMDA+OT aumentó el número de células activas aumenta de manera similar al grupo NMDA, en comparación con el grupo control (**Figura 8 C**, 72.43 ± 13.56, n=7 rebanadas, p=0.0061, Kruskal-Wallis, post-test de Dunn). Además, la aplicación de NMDA+OT aumentó no sólo el número de células activas, sino también la actividad global (**Figura 8 D**, 928.70 ± 210.40, n=7 rebanadas, p=0.0229, Kruskal-Wallis, post-test de Dunn) en comparación con el grupo control. También, aplicamos sólo OT (5 µM) a la preparación. La OT no produjo un efecto significativo ni en el número de células activas (**Figura 8 C**, 34.29 ± 5.02 células activas, p>0.9999, Kruskal-Wallis, post-test de Dunn), ni en la actividad global en comparación con el grupo control (**Figura 8 D**, 428.70 ± 77.49, n=7 rebanadas, p>0.9999, Kruskal-Wallis, post-test de Dunn).

Teniendo en cuenta el efecto de la OT al ser aplicada después del NMDA, nos preguntamos si esta tendría un efecto diferente al ser aplicada de manera preventiva, es decir antes de que ocurra un evento similar al de sensibilización central. Por esto, aplicamos OT (5 µM) antes de aplicar NMDA (8 µM) a la preparación (OT+NMDA). De acuerdo con los registros obtenidos, los resultados sugieren que invertir el orden de aplicación de los tratamientos, si bien genera un cambio significativo en el número de células activas (**Figura 8 C**, 89.14 ±

8.78, n=7 rebanadas, p=0.001, Kruskal-Wallis, post-test de Dunn) y en la actividad global (**Figura 8 D**, 1160.00 ± 118.90, n=7 rebanadas, p=0.0003, Kruskal-Wallis, post-test de Dunn) cuando se compara con el control; cuando se compara con el grupo NMDA + OT, no se genera un cambio en la respuesta de las células del asta dorsal de la médula espinal ni en el número de células activas (**Figura 8 C**, 89.14 ± 8.78, n=7 rebanadas, ns, Kruskal-Wallis, post-test de Dunn), ni en la actividad global (**Figura 8 D**, 1160.00 ± 118.90 , n=7 rebanadas, ns, Kruskal-Wallis, post-test de Dunn). Los datos referentes al número de células activas y la actividad global pueden observarse en la **Tabla 1 A y Tabla 1 B** respectivamente.

7.2.2. La oxitocina modifica la dinámica de actividad de las células evocada previamente por NMDA en el asta dorsal

Con la finalidad de evaluar modificaciones en la dinámica de actividad de las células, se realizó un análisis de coactividad. Por esto, se caracterizó si el aumento en el número de células activas inducido por NMDA produce cambios en la dinámica de actividad del circuito del asta dorsal. Basándonos en estudios similares de otras estructuras, donde la aplicación de NMDA produce cambios en la dinámica de actividad de las células (Carrillo-Reid et al., 2008; Pérez-Ortega et al., 2016; Plata et al., 2013), analizamos la coactivación de las neuronas como se describió anteriormente (Plata et al., 2013).

Tabla 1. Datos estadísticos. Tabla con los datos estadísticos usados para comparar cada una de la variables en los diferentes grupos.

A. Número de células (Figura 8C)

Grupo	n	MEDIA	SEM	p	Prueba	Post Hoc
Control	7	25.14	2.54			
NMDA	7	58.00	6.32	0.0219	Kruskal-Wallis	Dunn
NMDA+OT	7	72.43	13.56	0.0061		
OT	7	34.29	5.02	> 0.9999		
OT+NMDA	7	89.14	8.78	0.0001		

B. Actividad/epoch (Figura 8D)

Grupo	n	MEDIA	SEM	p	Prueba	Post Hoc
Control	7	365.30	37.18			
NMDA	7	729.00	106.80	0.0658	Kruskal-Wallis	Dunn
NMDA+OT	7	928.70	210.40	0.0229		
OT	7	428.70	77.49	> 0.9999		
OT+NMDA	7	1160.00	118.90	0.0003		

C. Picos de coactividad (Figura 10B)

Grupo	n	MEDIA	SEM	p	Prueba	Post Hoc
Control	7	5.43	1.11			
NMDA	7	19.14	3.91	0.0065	Kruskal-Wallis	Dunn
NMDA+OT	7	12.14	2.73	0.2754		
OT	7	7.86	2.49	> 0.9999		
OT+NMDA	7	15.14	3.38	0.0397		

D. Correlación actividad-coactividad (Figura 10C)

Grupo	n	SLOPE	SEM	p	Prueba
Control	7	-0.5901	1.445	0.7	
NMDA	7	3.954	1.444	0.0409	
NMDA+OT	7	5.401	6.45	0.4406	Regresión lineal
OT	7	3.334	2.511	0.2416	
OT+NMDA	7	6.591	2.325	0.0365	

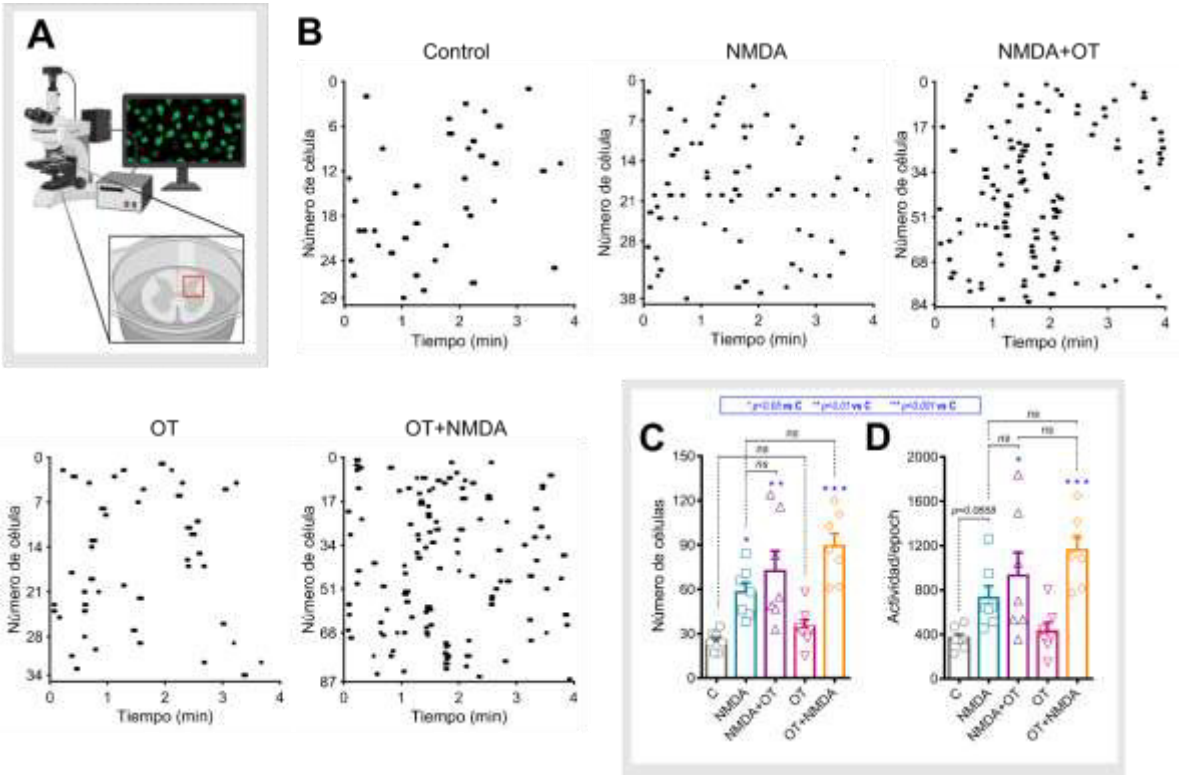

Figura 8. El NMDA aumenta la actividad de las neuronas del asta dorsal de la médula espinal. **(A)** Área de la médula espinal que fue registrada durante los experimentos, correspondiente a las láminas I a V del asta dorsal. Creado con BioRender.com. **(B)** Raster plots representativos de los diferentes grupos: Control, NMDA, NMDA+OT, OT y OT+NMDA (concentraciones: NMDA *8 µM* y OT *5 µM*); cada raster plot muestra 4 minutos actividad de las neuronas del asta dorsal. Nótese la escasa actividad espontanea (control) y bajo el tratamiento con OT; la actividad dependiente de $[Ca^{2+}]i$ presenta cambios bajo las condiciones restantes (NMDA, NMDA+OT, OT+NMDA). **(C)** Número de células activas. La gráfica compara el número de células activas durante el registro de cada condición experimental; es claro que los tratamientos NMDA, NMDA+OT y OT+NMDA aumentan el número de células activas en comparación con el control, no ocurre esto con el tratamiento con OT. **(D)** Actividad global. La gráfica compara la actividad total de cada registro bajo los diferentes tratamientos. El grupo NMDA aumenta el número de células activas y se aprecia una tendencia a aumentar parcialmente la actividad global en comparación con la condición de control. Además, la aplicación de NMDA+OT aumentó significativamente no sólo el número de células, sino también la actividad global en comparación con la condición de control, lo que indica que la OT recluta elementos celulares extra a los reclutados por el grupo NMDA, lo mismo ocurrió cuando se aplicó la OT y posteriormente el NMDA (OT+NMDA). Finalmente, el tratamiento con OT no generó cambios significativos ni en el número de células activas, ni en la actividad global. Los datos se representan como la media ± SEM, n=7 por grupo, $p<0.05$(*), $p<0.01$(**) o $p>0.001$(***) comparados con el grupo Control, Kruskal-Wallis con post hoc de Dunn. OT: oxitocina

Una vez más, en la **Figura 9** los raster plots muestran la actividad de las células del asta dorsal a lo largo del tiempo bajo diferentes condiciones (**Figura 9 A, B, C, D y E**). Los puntos resaltados en color rojo representan la actividad de neuronas con significancia estadística

para la coactividad. Los histogramas de coactividad, debajo de cada uno de los raster plots, representan la suma de la actividad neuronal de cada epoch (**Figura 9, histograma de coactividad**). Cada pico de coactividad representa un grupo de células activas al mismo tiempo. Después de las permutaciones de Monte Carlo (véase **6.6.2 Análisis de coactividad**), todos los picos de coactividad indicados en rojo superaron el umbral de significancia representado en los histogramas de coactividad como una línea horizontal discontinua (**Figura 9, histograma de coactividad**). Se comparó el número de picos de coactividad de cada condición experimental (ver **Tabla 1 C**), encontramos pocos picos de coactividad espontáneos en el grupo control (**Figura 10 B**, 5.43 ± 1.11, n=7 rebanadas). Por el contrario, la aplicación de NMDA (8 µM) promueve cambios en la dinámica de actividad de los circuitos de la médula espinal caracterizados por un aumento en el número de células coactivas, contado como el número de picos de coactividad (**Figura 10 B**,19.14 ± 3.91, n=7 rebanadas, p=0.0065, Kruskal-Wallis, post-test de Dunn), lo que indica que los grupos de neuronas coordinan su actividad y se alternan con otras agrupaciones de neuronas a lo largo del tiempo. Curiosamente, la aplicación de NMDA+OT revierte los cambios en la dinámica de la coactividad, reduciendo el número de picos coactivos a niveles no estadísticamente significativos en comparación con el grupo de control (**Figura 10 B**, 12.14 ± 2.73, n=7 rebanadas, p=0.2754, Kruskal-Wallis, post-test de Dunn). Además, la aplicación OT no produjo ningún cambio en el número de picos de coactividad en comparación con el grupo de control (**Figura 10 B**, 7.86 ± 2.49, n=7 rebanadas, p>0.9999, Kruskal-Wallis, post-test de Dunn). Curiosamente, el tratamiento con OT+NMDA incrementó la actividad coordinada de neuronas del asta dorsal de la médula espinal comparada con el control (**Figura 10 B**, 15.14 ± 3.38, n=7 rebanadas, p=0.0397, Kruskal-Wallis, post-test de Dunn). Este aumento en el número de picos de coactividad fue similar al ocasionado por la aplicación de NMDA (**Figura 10 B**, 19.14 ± 3.91, n=7 rebanadas, ns, Kruskal-Wallis, post-test de Dunn).

Con el objetivo de analizar si la coactividad observada implicaba los mismos grupos de células en una actividad sincrónica, medimos el índice de similitud de Jaccard de todos los vectores (picos) de coactividad significativos y comparamos todos los pares posibles para evaluar si estos tienen los mismos componentes (neuronas) o no. Luego, los coeficientes de similitud entre dos vectores se graficaron como una matriz de correlación cruzada en una escala de pseudo-color (**Figura 10 A**). En esta representación, una apariencia de parches denota que grupos similares de varias neuronas se sincronizaron a lo largo del

tiempo, es decir, las mismas neuronas repiten su actividad a lo largo del tempo (Carrillo-Reid et al., 2008; Jáidar et al., 2010; Pérez-Ortega et al., 2016; Plata et al., 2013). Como se ve en la **Figura 10 A**, la aplicación de NMDA produce un alto nivel de sincronización marcado como una apariencia de parches.

Para evaluar si la actividad global y la coactividad de las células estaban correlacionadas o no, realizamos un análisis de regresión lineal comparando la actividad total de cada experimento con la coactividad (ver **Tabla 1 D**). Encontramos que sólo el grupo NMDA y OT+NMDA mostraron una correlación significativa entre la actividad global y la coactividad que no está presente las otras condiciones experimentales (**Figura 10 C**, NMDA y OT+NMDA, $p<0.05$, n=7 rebanadas, regresión lineal). Estos resultados sugieren que la aplicación de NMDA induce la sincronización en la actividad dependiente de $[Ca^{2+}]i$ de las neuronas del asta dorsal de la médula espinal y que la OT, cuando se aplica después del NMDA, actúa interrumpiendo este nivel de sincronización. No pasa esto cuando se aplica OT de manera preventiva a la preparación experimental, ya que la OT antes del NMDA no es suficiente para evitar ni la coactividad, ni la coordinación de los grupos de neuronas del asta dorsal de la médula espinal.

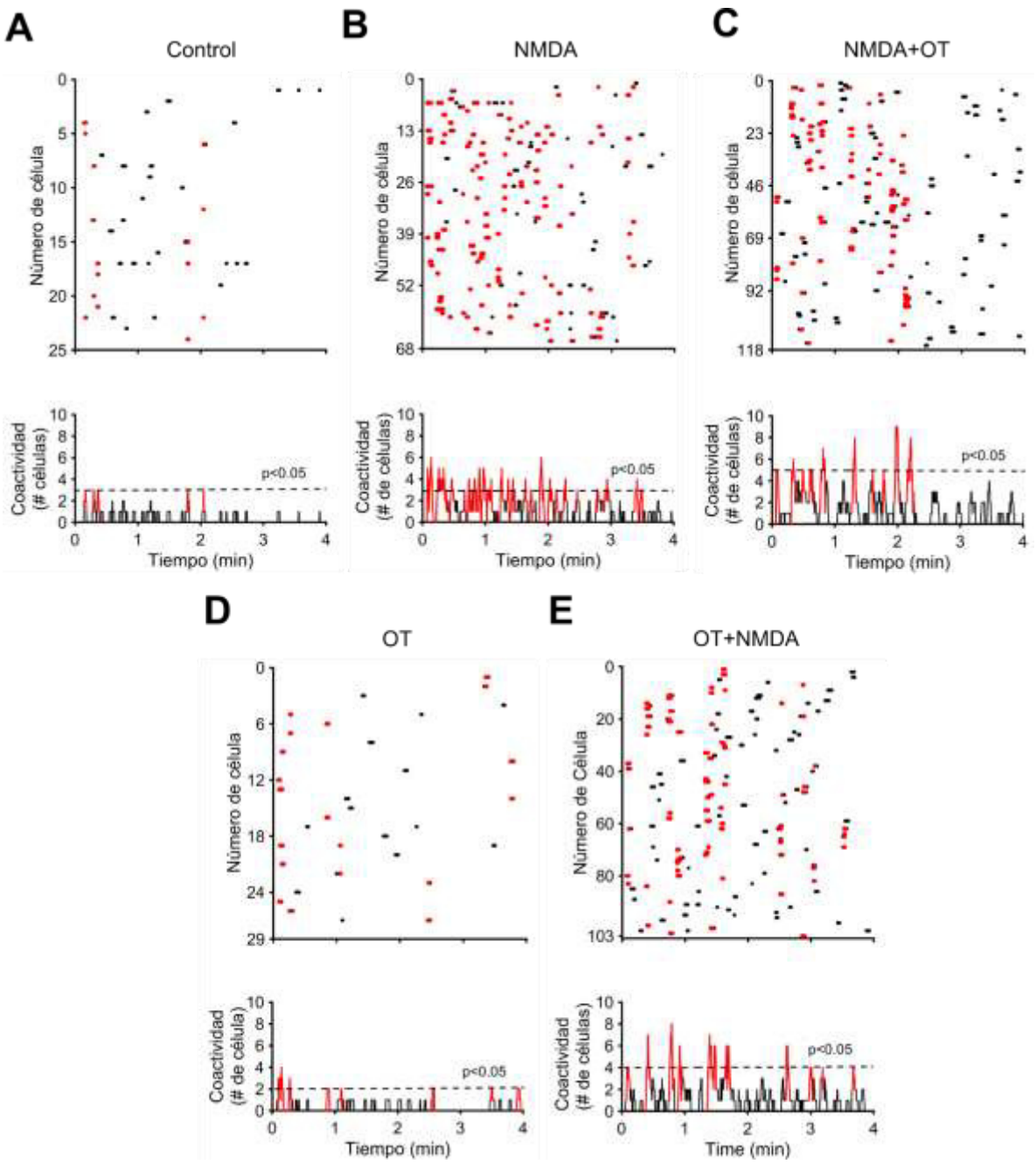

Figura 9. Efecto de la oxitocina en la coactividad en poblaciones de células del asta dorsal de la médula espinal. (A) Raster plots representativos de cada uno de los diferentes tratamientos: Control, NMDA, NMDA+OT, OT y OT+NMDA; los puntos rojos en cada raster plot representan la actividad simultánea de conjuntos de neuronas con actividad recurrente ($p<0.05$). Debajo de cada raster plot, se graficó un histograma de coactividad, el cual representa la suma del número de células coactivas a lo largo del tiempo. Los picos de coactividad significativos fueron resaltados en rojo y el umbral de significancia está representado como una línea horizontal discontinua. OT: oxitocina.

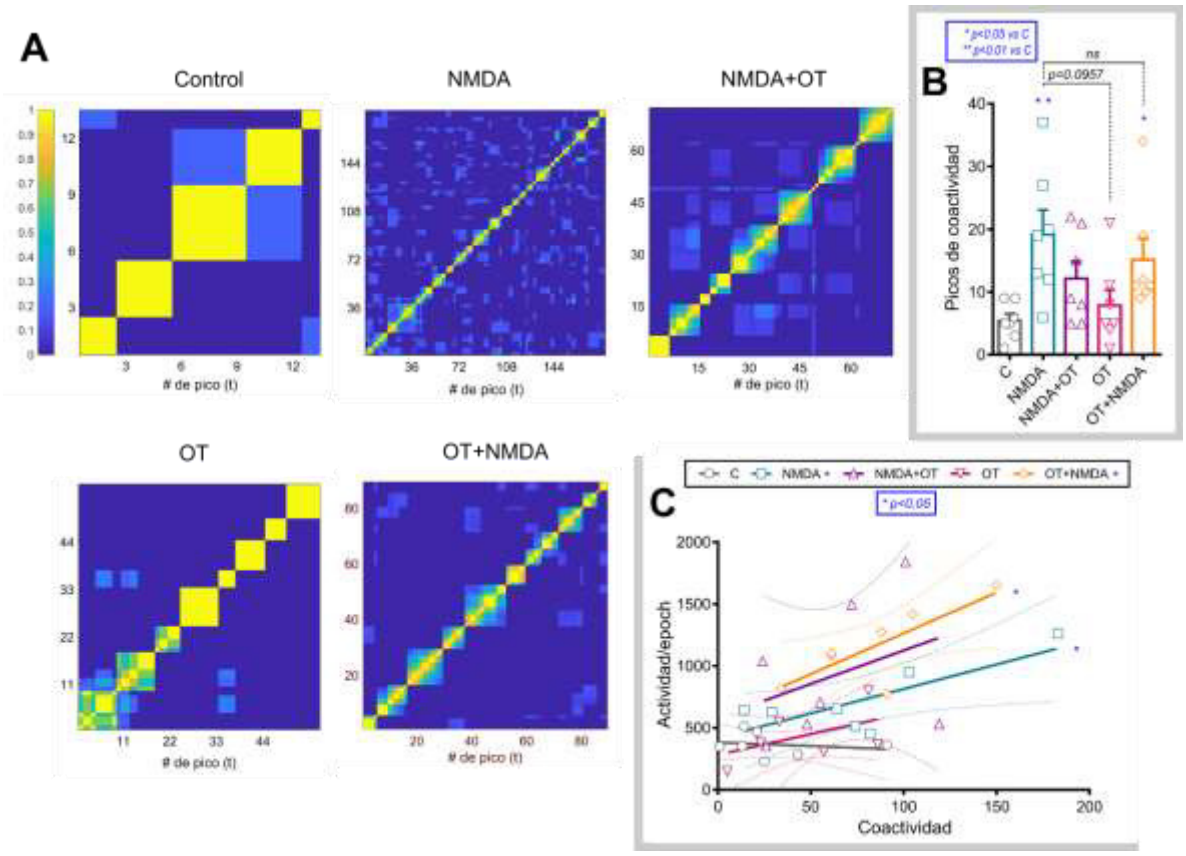

Figura 10. La oxitocina modifica la dinámica de actividad de las células previamente evocada por NMDA en el asta dorsal. (A) Matriz de correlación cruzada del índice de similitud de Jaccard; compara todos los posibles pares de vectores de coactividad a lo largo del tiempo para cada tratamiento: Control, NMDA, NMDA+OT, OT y OT+NMDA. Nótese una alta coordinación de células con el tratamiento de NMDA. **(B)** Número de picos de coactivación; el gráfico representa la presencia de picos de sincronización para cada grupo. La actividad coordinada de las células se ve incrementada significativamente con el grupo NMDA, así como para el grupo OT+NMDA. El tratamiento con OT reduce el número de picos de coactividad producidos por la aplicación previa de NMDA. **(C)** Correlación entre la actividad global de los epoch (eje Y) y la coactividad (eje X) para cada condición. Al graficar ambas variables y realizar una regresión lineal, solo los grupos NMDA y OT+NMDA mostraron una correlación significativa entre ambas variables, $p<0.05$. Los resultados sugieren que el tratamiento con OT reduce la coordinación de la actividad cuando es aplicada después del tratamiento de NMDA (NMDA+OT), esto no sucede si se pretrata con OT (OT+NMDA). La barra de escala de color en A representa la correlación entre los vectores de coactividad presentados en cada matriz de correlación. Los datos en B se presentan como media ± SEM. En C las líneas sólidas representan la regresión lineal y las líneas punteadas representan el 95% del intervalo de confianza, n=7, $p<0.05$(*) en comparación con el control. Para B: Kruskal-Wallis con la prueba post hoc de Dunn; para C: pendiente diferente de cero. OT: oxitocina, ns: no significativo.

7.2.3. La inyección de formalina in vivo produce cambios en la actividad neuronal a nivel espinal in vitro asociados al dolor neuropático

Otros estudios han mostrado evidencia que sugiere que la inyección de formalina 5% en la pata trasera de ratas produce cambios en el asta dorsal de la médula espinal a largo plazo relacionados con el dolor neuropático (Fu et al., 2001; Salinas-Abarca et al., 2017; Zhang et al., 2007). Estos cambios a nivel espinal se han reportado entre 24-72 horas después de la inyección de formalina. Por lo tanto, para evaluar si los cambios en la dinámica de actividad neuronal producidos por la aplicación in vitro de NMDA son similares a los cambios producidos por una sensibilización central desarrollada por un modelo de dolor neuropático, inyectamos formalina al 5% en la pata trasera de las ratas y 48 horas más tarde evaluamos si la inyección causó cambios ex vivo en la actividad neuronal de la médula espinal. Por último, evaluamos y comparamos los cambios producidos por la inyección de formalina al 5% con respecto al grupo control y al grupo NMDA. Un ejemplo de la actividad evocada por la inyección de formalina al 5% se representa como un raster plot en la **Figura 11 A**, acompañado por los rasters plot característicos de los grupos control y NMDA. La primera variable evaluada fue el número de células activas en cada condición **(ver Tabla 2 A)**. En este caso, la formalina aumentó el número de células activas durante el registro (54.00 ± 8.29, n=7 rebanadas, p=0.0501, Kruskal-Wallis, post-test de Dunn). Este aumento fue similar al generado por la aplicación de NMDA (55.86 ± 4.49, n=7 rebanadas, p=0.0183, Kruskal-Wallis, post-test de Dunn) como puede observarse en la **Figura 11 B.** Después, se comparó la actividad global de las tres diferentes condiciones experimentarles **(ver Tabla 2 B)**. La inyección de formalina presentó una tendencia al aumento de la actividad global comparada con el control (**Figura 11 C**, 701.30 ± 112.3, n=7 rebanadas, p=0.0775, Kruskal-Wallis, post-test de Dunn) y a su vez no aumentó la actividad producido por la aplicación de NMDA (**Figura 11 C,** 758.40 ± 82.12, n=7 rebanadas, p=0.0196, Kruskal-Wallis, post-test de Dunn). Cuando evaluamos la coactividad de las tres condiciones experimentales **(ver Tabla 2 C)**, identificamos que la formalina aumentó el número de picos de coactividad cuando es comparada con el control (**Figura 11 D**, 8.71 ± 2.36, n=7 rebanadas, p=0.0408, Kruskal-Wallis, post-test de Dunn). A su vez, este aumento es similar al producido por la aplicación de NMDA (**Figura 11 D**, 11.00 ± 2.31, n=7 rebanadas, p=0.0052, Kruskal-Wallis, post-test de Dunn). Al sumar la actividad a lo largo del tiempo, se obtuvo un gráfico de la actividad acumulada (**Figura 11 E**). Este gráfico muestra la actividad global total para cada condición a lo largo del tiempo (se realizó un ajuste ad hoc de línea recta, donde el valor de

la pendiente se convirtió en la tasa de incremento de la actividad a lo largo del tiempo (Plata et al., 2013). El promedio de los experimentos del grupo de control mostró una tasa de incremento de 98.38 ± 1.06 act/min, que aumenta a 184.10 ± 1.70 act/min para el grupo NMDA, y a 176.60 ± 1.83 act/min para el grupo de formalina **(ver Tabla 2 D)**.

Los resultados obtenidos sugieren que la inyección de formalina in vivo produce cambios a largo plazo a nivel espinal en la actividad neuronal mediados por la movilización de $[Ca^{2+}]i$ asociados al dolor neuropático y que estos cambios son visibles 48 horas después de la inyección. Por otro lado, los resultados sugieren que los cambios producidos por un modelo de dolor neuropático in vivo pueden ser evocados de igual manera in vitro con la aplicación de NMDA.

Tabla 2. Datos estadísticos para el grupo con formalina. Tabla con los datos estadísticos usados para comparar cada una de la variables en los grupos Control, NMDA y Formalina 5%.

A. Número de células (Figura 11B)

Grupo	n	MEDIA	SEM	p	Prueba	Post Hoc
Control	7	30.43	3.64			
NMDA	7	55.86	4.49	0.0183	Kruskal-Wallis	Dunn
Formalina	7	54.00	8.29	0.0501		

B. Actividad/epoch (Figura 11C)

Grupo	n	MEDIA	SEM	p	Prueba	Post Hoc
Control	7	386.40	59.95			
NMDA	7	758.40	82.12	0.0196	Kruskal-Wallis	Dunn
Formalina	7	701.30	112.30	0.0775		

C. Picos de coactividad (Figura 11D)

Grupo	n	MEDIA	SEM	p	Prueba	Post Hoc
Control	7	2.00	1.00			
NMDA	7	11.00	2.31	0.0052	Kruskal-Wallis	Dunn
Formalina	7	8.71	2.36	0.0408		

D. Actividad acumulada (Figura 11E)

Grupo	n	(act/min)	SEM
Control	7	98.38	1.06
NMDA	7	184.10	1.70
Formalina	7	176.60	1.83

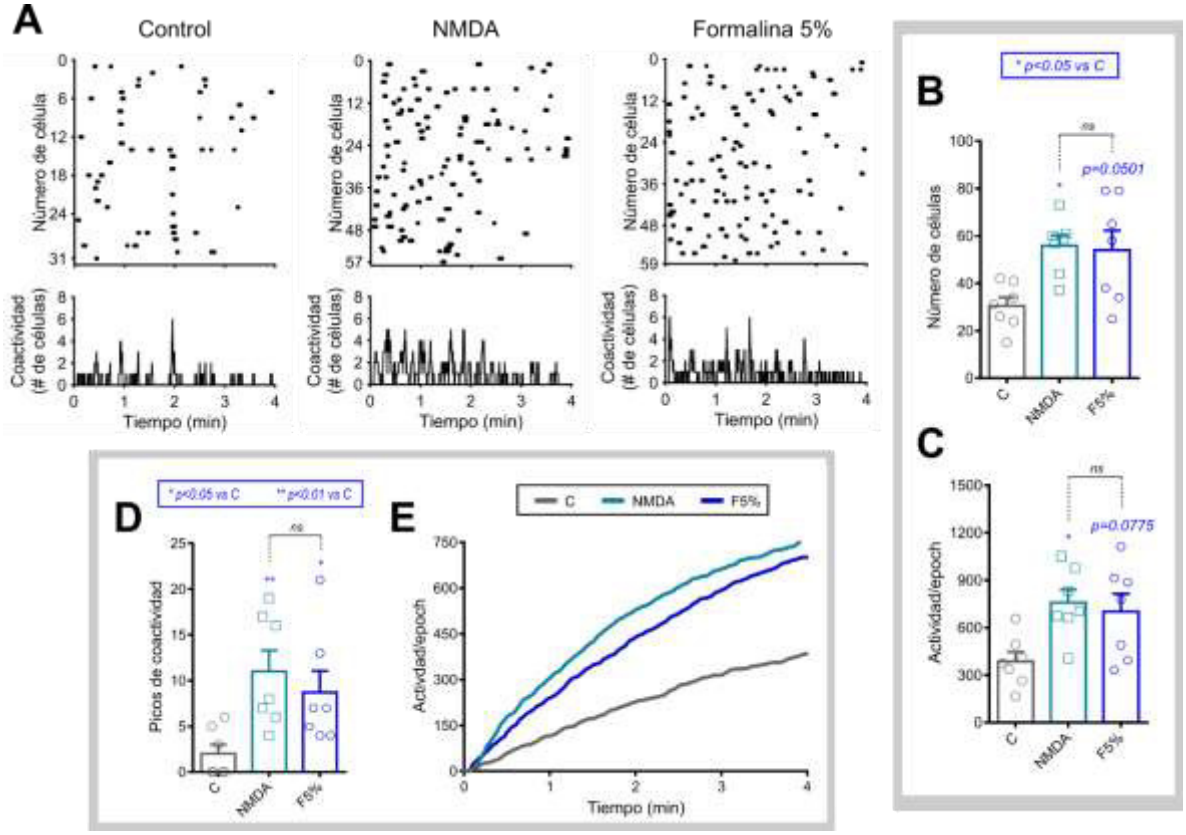

Figura 11. El NMDA induce cambios en la dinámica de actividad celular del asta dorsal de la médula espinal similares a los evocados por la inyección de Formalina 5%. (A) Raster plots representativos de la actividad de las neuronas del asta dorsal en condiciones: Control, NMDA y Formalina 5% (F5%). **(B)** Número de células activas. Es claro que los tratamientos NMDA y F5% aumentan el número de células activas en comparación con el control. **(C)** Actividad global. El grupo NMDA aumenta el número de células activas y la actividad global como se describió anteriormente; además, con la inyección de formalina 5% se observan los mismos aumentos generados por NMDA sin que estos resulten estadísticamente significativos. **(D)** Número de picos de coactividad; el gráfico representa la presencia de picos de sincronización para cada grupo. La actividad coordinada de las células se ve incrementada significativamente con el grupo NMDA, así como para el grupo F5%. **(E)** Actividad acumulada a lo largo del tiempo de diferentes condiciones: Se observa que la inyección in vivo de formalina 5% ,48 horas antes del experimento de imagenología de calcio ex vivo, produce cambios en la dinámica de actividad de los circuitos neuronales del asta dorsal de la médula espinal, esta misma dinámica es evocada por la aplicación NMDA. Los datos en B, C y D se representan como la media ± SEM, n=7 por grupo, $p<0.05$(*), $p<0.01$(**) comparados con el grupo Control, Kruskal-Wallis con post hoc de Dunn. En E los datos se muestran como la media, n=7 por grupo, las tasas de incremento de la actividad fueron: Control: 98.37 ± 1.05 act/min, NMDA: 184.10 ± 1.70 act/min y F5%: 176.60 ± 1.82 act/min.

8. DISCUSIÓN Y CONCLUSIONES

En conjunto, los resultados mostraron lo siguiente: (i) La naturaleza silente de los circuitos neuronales del asta dorsal en condiciones basales. (ii) Los circuitos del asta dorsal se pueden activar con la aplicación de NMDA, el cual aumenta el número de células activas y la actividad global de las células del asta dorsal de la médula espinal. También, el NMDA produce un aumento en las tasas de actividad coordinada de los microcircuitos del asta dorsal. (iii) La OT puede alterar los patrones de actividad coordinada de conjuntos de neuronas en el asta dorsal de la médula espinal; y (iv) después de 48 horas, la inyección de formalina in vivo produce cambios a largo plazo mediados por la movilización de $[Ca^{2+}]i$ a nivel espinal en la actividad neuronal asociados al dolor neuropático y estos cambios pueden ser evocados in vitro con la aplicación de NMDA.

En condiciones normales, los circuitos del asta dorsal se han descrito como silentes, tanto en rebanadas de médula espinal (in vitro) (Luo et al., 2008; Ruscheweyh & Sandkühler, 2005) como en preparaciones in vivo (Johannssen & Helmchen, 2013). Esto se confirma con nuestros resultados, en los cuales a pesar de que se observan transitorios de calcio espontáneos de neuronas en condiciones control, existe una escasa actividad sincronizada en las neuronas (**Figura 8**, **Figura 9**, **Figura 10**). Debido a la naturaleza silenciosa de los circuitos del asta dorsal de la médula espinal, utilizamos NMDA como un promotor de la actividad neuronal, de acuerdo con reportes anteriores que demuestran que la aplicación de NMDA puede inducir un aumento de la actividad dependiente del calcio en redes silenciosas de otras estructuras cerebrales (Carrillo-Reid et al., 2008; Pérez-Ortega et al., 2016; Plata et al., 2013). Además, se ha documentado ampliamente que la activación del NMDAr es crucial para la amplificación de la señalización nociceptiva en la médula espinal que conduce a mecanismos de plasticidad como la sensibilización central, que es el componente principal del dolor inflamatorio y neuropático (Hong-mei et al., 2004; Ikeda et al., 2006; Keefer et al., 2001; Woolf & Salter, 2000; Xie et al., 2016). Además, la activación del sistema glutamatérgico, y particularmente la activación del NMDAr, se ha implicado en mecanismos de facilitación de señalización nociceptiva en la médula espinal como la alodinia y la hiperalgesia.

En el presente trabajo, reportamos que la aplicación de NMDA en rebanadas de médula espinal puede promover la actividad de un circuito silente por naturaleza incrementando la

actividad total dependiente del calcio y el número de células activas. Este es el primer estudio que reporta los efectos de la activación del NMDAr en un gran número de células (entre 38 y 84 por rebanada) que cubren las láminas I-V del asta dorsal (**Figura 8**). Además, nuestros hallazgos se correlacionan con evidencia complementaria que describe que los estímulos nociceptivos periféricos y la estimulación eléctrica de las raíces dorsales aumentan el número y la amplitud de los transitorios de calcio de las neuronas en las láminas superficiales (I-II) del asta dorsal y que estos cambios están mediados por la activación del NMDAr (Ikeda et al., 2006; Johannssen & Helmchen, 2013; Luo et al., 2008; Vrontou et al., 2013).

El NMDA también produjo cambios en la dinámica de actividad dependiente del calcio del asta dorsal promoviendo la actividad coordinada de las neuronas (**Figura 9**,**Figura 10**). De acuerdo con este hallazgo, otros grupos de investigación reportaron que la aplicación de NMDA en cultivos de células de la médula espinal puede generar actividad coordinada que dura varias horas (Keefer et al., 2001). Además, al registrar la actividad de los circuitos neuronales en la médula espinal durante una condición nociceptiva in vivo, los resultados mostraron evidencia de actividad coordinada en la médula espinal (ver revisión: Nelson et al., 2019). Esta actividad sincrónica dependiente del calcio mediada por la activación del NMDAr se reportó previamente en rebanadas de médula espinal, específicamente en las láminas superficiales (I-III) del asta dorsal, pero sólo bajo la condición de una eliminación total de la inhibición sináptica mediante el bloqueo de receptores a $GABA_A$ y glicina (Ruscheweyh & Sandkühler, 2005). Nuestros resultados demostraron que la aplicación de NMDA por sí sola puede evocar altas tasas de actividad coordinada en grupos de neuronas del asta dorsal (láminas I-V) incluso cuando la inhibición sináptica permaneció intacta.

Para dilucidar si la OT puede modificar la facilitación de la actividad coordinada producida por la activación NMDAr en las neuronas del asta dorsal, aplicamos OT a las rebanadas previamente incubadas con NMDA. Constatamos que la aplicación de OT no reduce la actividad global producida previamente por NMDA, por el contrario, la aumenta parcialmente (**Figura 8**). Sin embargo, la OT es capaz de reducir la actividad coordinada asociada con la señalización de calcio nociceptiva, medida como número de picos de coactividad (**Figura 9**). En estudios previos, se reportó que la OT modula la respuesta excitatoria glutamatérgica en la médula espinal mediante la reducción de la tasa de disparo previamente incrementada por la señalización nociceptiva (Condés-Lara et al., 2005; Jo et al., 1998; Miranda-Cardenas et al., 2006; Robinson et al., 2002). Aunque la reducción de la

actividad dependiente de NMDAr por OT se ha descrito en cultivos neuronales (Caruso et al., 1993), estudios previos muestran que la principal fuente de acción inhibitoria por OT en la red neuronal del asta dorsal de la médula espinal se debe al aumento general de la transmisión GABAérgica por medios directos e indirectos (Jiang et al., 2014; Mazzuca et al., 2011; Rojas-Piloni et al., 2007). En primer lugar, los datos indican que la OT aumenta directamente los niveles basales de la transmisión GABAérgica extracelular (González-Hernández et al., 2014; Qi et al., 2012). En segundo lugar, la OT disminuye simultáneamente la actividad glutamatérgica regulando la expresión de la subunidad NR1 de receptores glutamatérgicos y los niveles de glutamato en el espacio extracelular mediante la regulación del transportador glutamatérgico 1 (Qi et al., 2012). Además, se ha descrito una inhibición indirecta de los circuitos del asta dorsal de la médula espinal por la acción de OT que surge de la activación de una subpoblación de neuronas glutamatérgicas que promueve la inhibición local mediante el reclutamiento de interneuronas GABAérgicas (Breton et al., 2008).

En resultados obtenidos por otros grupos de investigación se ha sugerido que el efecto inhibitorio de la OT en el asta dorsal de la médula espinal es eficaz sólo después de la activación previa de la señalización glutamatérgica relacionada con la nocicepción (Nersesyan et al., 2017; Sun et al., 2018). Por ejemplo, la OT contrarresta la potenciación de la actividad excitatoria, caracterizada como un aumento en la frecuencia y amplitud de las corrientes postsinápticas excitatorias, producida por la activación de receptores TRPV1 por capsaicina en un modelo de dolor sin mostrar ningún efecto por sí misma en el sistema intacto (Sun et al., 2018). Lo anterior se observa no sólo a nivel espinal, sino también a nivel periférico donde la evidencia previa sugiere que la OT interactúa directa o indirectamente con el receptor TRPV1 y atenúa la nocicepción inducida por la capsaicina a través de la desensibilización de los receptores TRPV1 sin mostrar un efecto sobre las células intactas (Nersesyan et al., 2017). Los resultados obtenidos por Sun y sus colaboradores en 2018 y Nersesyan y sus colaboradores en 2017 se relacionan con nuestros resultados, que mostraron que el tratamiento con OT reduce la coordinación de la actividad neuronal después de la aplicación NMDA, pero esto no ocurre al aplicar la OT antes de activar los circuitos espinales con NMDA y que la OT aplicada sobre el sistema experimental intacto no tiene ningún efecto significativo (**Figura 9**, **Figura 10**)

Una limitación sobre la acción inhibidora de la OT en modelos nociceptivos es el uso de enfoques single-cell, debido a los efectos que la OT puede tener en diferentes poblaciones

celulares dependiendo del contexto, lo cual denota la importancia de estudiar las acciones globales de la OT sobre el circuito en conjunto. Nuestros resultados complementan los datos obtenidos de aproximaciones single-cell ya que evalúan el asta dorsal de la médula espinal como un circuito completo, mostrando que, a pesar del aumento de la actividad global dependiente del calcio y el reclutamiento de células antes no activas, la OT interrumpe la coordinación de la actividad neuronal en el asta dorsal, lo cual podría sugerir una posible inhibición de la señalización nociceptiva dependiente de calcio (**Figura 10**), que pudiera ser la responsable de su acción antinociceptiva.

Anteriormente se reportó que la inyección de formalina al 5% en la pata trasera de la rata puede producir: i) alodinia térmica y mecánica secundaria de larga duración e hiperalgesia de 1 a 3 días después de su inyección y que estos efectos pueden durar de 3 a 4 semanas (Fu et al., 2001; Zhang et al., 2007). También, se reportaron efectos como ii) hipersensibilidad y cambios moleculares en los ganglios de la raíz dorsal y el asta dorsal de la médula espinal que se asemejan a los inducidos por lesión al nervio, alcanzando sus efectos máximos entre 1 a 3 días después de la inyección de formalina (5%), estos efectos permanecieron durante al menos 14 días (Salinas-Abarca et al., 2017). Basándonos en esta evidencia, usamos formalina al 5% para inducir cambios similares a aquellos que ocurren en la actividad de las células del asta dorsal espinal bajo condiciones de dolor neuropático. Como los efectos máximos de la formalina se reportaron entre las 24 y 72 horas después de la inyección, evaluamos la actividad dependiente del calcio a las 24 horas y también a las 48 horas después de la inyección de formalina y los cambios en la actividad dependiente del calcio se observaron principalmente después de 48 horas de inyección de formalina. Con el fin de dilucidar si la activación del NMDAr en las neuronas del asta dorsal de la médula espinal observada en nuestros experimentos está relacionada con la señalización nociceptiva por dolor neuropático, inyectamos formalina al 5% en la superficie dorsal de la pata trasera de las ratas 48 horas antes de los registros de $[Ca^{2+}]i$. Después de comparar 4 diferentes parámetros entre estos dos grupos, como son: i) el número de células activas, ii) la actividad global, iii) la tasa de acumulación de actividad neuronal y iv) el número de picos de coactividad, encontramos que la actividad dependiente de calcio evocada por la aplicación de NMDA in vitro es similar a la evocada en el asta dorsal por un modelo de dolor neuropático como lo es la inyección de formalina al 5% en la que se han descrito cambios duraderos en la movilización de calcio de neuronas del asta dorsal, como los observados en nuestros resultados (**Figura 11**). Nuestros resultados se relacionan con la

evidencia presentada anteriormente por otro grupo de investigación, que mostró que después de 24 horas, la lesión periférica puede desencadenar cambios duraderos en los patrones de señalización de calcio en las neuronas del asta dorsal (Luo et al., 2008), lo que apoya así la idea de que la actividad coordinada producida por la activación de los NMDAr's potencializa los cambios relacionados con la nocicepción en la dinámica de actividad del asta dorsal de la médula espinal, similar a un modelo de dolor neuropático. Si bien estas similitudes no se relacionan a mecanismos de acción o vías de señalización, el efecto global causado por ambas condiciones sobre la actividad dependiente de calcio está relacionada. Estos resultados nos permiten considerar que la aplicación de NMDA puede utilizarse como un modelo in vitro para evocar la actividad dependiente de calcio que se observa en condiciones de dolor neuropático en las células del asta dorsal de la médula espinal. Esto mismo se ha observado, por ejemplo, en estudios realizados en el núcleo estriado in vitro donde la aplicación de NMDA evoca actividad excitatoria de los microcircuitos neuronales que es similar y está correlacionada a aquella producida durante actividades motoras in vivo (Carrillo-Reid et al., 2008; Plata et al., 2013; Vautrelle et al., 2009).

En resumen, los resultados presentados aquí, combinados con evidencias previas de nuestro grupo y otros grupos, indican que la aplicación de OT podría representar un tratamiento potencial para prevenir los cambios duraderos en la movilización de calcio en el asta dorsal con respecto a la sensibilización central en condiciones de dolor neuropático. El asta dorsal de la médula espinal es el sitio de la primera sinapsis en la vía del dolor y es crucial para estudiar los mecanismos de plasticidad que conducen al dolor crónico. Estudiar los cambios globales en la dinámica de actividad de la red subyacente a la sensibilización central y cómo el tratamiento con OT contrarresta estos cambios resultará útil para comprender el desarrollo y el posible tratamiento del dolor crónico.

9. CONSIDERACIONES FINALES

Los cambios en la actividad neuronal dependiente del calcio en el procesamiento somatosensorial y del dolor no han sido ampliamente estudiados, lo que representa una excelente oportunidad de investigación para obtener más datos relacionados con estos fenómenos fisiológicos. En la médula espinal, la imagenología de calcio se utiliza para realizar el registro simultáneo de las poblaciones neuronales y representa una poderosa herramienta que contribuirá a obtener datos relevantes sobre la dinámica de actividad de las redes neuronales de la médula espinal. En consecuencia, esto permitiría a los investigadores entender cómo se procesa la información en el asta dorsal de la médula espinal como respuesta a un estímulo sensorial dado o en condiciones patológicas como dolor neuropático. En este contexto, en nuestro laboratorio, mostramos cómo la oxitocina puede modificar la actividad neuronal relacionada con el dolor en el asta dorsal de la médula espinal utilizando imagenología de calcio in vitro. Creemos que las técnicas de diagnóstico por imágenes de calcio pueden ser extremadamente valiosas para estudiar fenómenos relacionados con el dolor, así como procesos de codificación somatosensorial a niveles espinales y supraespinales. Los estudios futuros confirmarán la eficacia de esta herramienta en los campos del procesamiento sensorial y la nocicepción. Mientras tanto, los avances y mejoras en las técnicas de registro de la actividad celular por imagenología de calcio podrían disminuir sus limitaciones y potenciar su uso para comprender mejor la interacción entre las poblaciones celulares en el asta dorsal en condiciones fisiológicas y patológicas.

10. REFERENCIAS

Aparicio-Juárez, A., Duhne, M., Lara-González, E., Ávila-Cascajares, F., Calderón, V., Galarraga, E., & Bargas, J. (2019). Cortical stimulation relieves parkinsonian pathological activity in vitro. European Journal of Neuroscience, 49(6), 834–848. https://doi.org/10.1111/ejn.13806

Basbaum, A. I., Bautista, D. M., Scherrer, G., & Julius, D. (2009). Cellular and molecular mechanisms of pain. Cell, 139(2), 267–284. https://doi.org/10.1016/j.cell.2009.09.028

Basbaum, A. I., & Bushnell, C. M. (2009). Science of Pain (1st ed., Vol. 51, Issue 1). Elsevier Inc.

Benarroch, E. E. (2013). Oxytocin and vasopressin: Social neuropeptides with complex neuromodulatory functions. Neurology, 80(16), 1521–1528. https://doi.org/10.1212/WNL.0b013e31828cfb15

Berridge, M. J. (1993). Inositol trisphosphate and calcium signaling. In Nature (Vol. 361, Issue 6410, pp. 315–325). Nature. https://doi.org/10.1038/361315a0

Berridge, M. J. (1998). Neuronal calcium signaling. In Neuron (Vol. 21, Issue 1, pp. 13–26). Cell Press. https://doi.org/10.1016/S0896-6273(00)80510-3

Berridge, M. J., Lipp, P., & Bootman, M. D. (2000). The versatility and universality of calcium signalling. Nature Reviews Molecular Cell Biology, 1(1), 11–21. https://doi.org/10.1038/35036035

Breton, Jean D., Poisbeau, P., & Darbon, P. (2009). Antinociceptive action of oxytocin involves inhibition of potassium channel currents in lamina II neurons of the rat spinal cord. Molecular Pain, 5, 1744-8069-5–63. https://doi.org/10.1186/1744-8069-5-63

Breton, Jean Didier, Veinante, P., Uhl-Bronner, S., Vergnano, A. M., Freund-Mercier, M. J., Schlichter, R., & Poisbeau, P. (2008). Oxytocin-induced antinociception in the spinal cord is mediated by a subpopulation of glutamatergic neurons in lamina I-II which amplify GABAergic inhibition. Molecular Pain, 4(1), 1744-8069-4–19. https://doi.org/10.1186/1744-8069-4-19

Burgess, P. R., & Perl, E. R. (1967). Myelinated afferent fibers responding specifically to noxious stimulation of the skin. The Journal of Physiology, 190(3), 541–562. https://doi.org/10.1113/jphysiol.1967.sp008227

Busnelli, M., Saulière, A., Manning, M., Bouvier, M., Galés, C., & Chini, B. (2012). Functional selective oxytocin-derived agonists discriminate between individual G protein family subtypes. Journal of Biological Chemistry, 287(6), 3617–3629. https://doi.org/10.1074/jbc.M111.277178

Carrillo-Reid, L., Tecuapetla, F., Ibáñez-Sandoval, O., Hernández-Cruz, A., Galarraga, E., & Bargas, J. (2009). Activation of the cholinergic system endows compositional properties to striatal cell assemblies. Journal of Neurophysiology, 101(2), 737–749. https://doi.org/10.1152/jn.90975.2008

Carrillo-Reid, L., Tecuapetla, F., Tapia, D., Hernández-Cruz, A., Galarraga, E., Drucker-Colin, R., & Bargas, J. (2008). Encoding network states by striatal cell assemblies. Journal of Neurophysiology, 99, 1435–1450. https://doi.org/10.1152/jn.01131.2007

Carrillo-Reid, L., & Yuste, R. (2020). What Is a Neuronal Ensemble? In Oxford Research Encyclopedia of Neuroscience. Oxford University Press. https://doi.org/10.1093/acrefore/9780190264086.013.298

Caruso, S., Agnello, C., Campo, M. G., & Nicoletti, F. (1993). Oxytocin reduces the activity of N-methyl — D — aspartate receptors in cultured neurons. Journal of Endocrinological Investigation, 16(11), 921–924. https://doi.org/10.1007/BF03348959

Cirillo, G., de Luca, D., & Papa, M. (2012). Calcium imaging of living astrocytes in the mouse spinal cord following sensory stimulation. Neural Plasticity, 2012, 1–7. https://doi.org/10.1155/2012/425818

Condés-Lara, M., Veinante, P., Rabai, M., & Freund-Mercier, M. J. (1994). Correlation between oxytocin neuronal sensitivity and oxytocin-binding sites in the amygdala of the rat: electrophysiological and histoautoradiographic study. Brain Research, 637(1–2), 277–286. https://doi.org/10.1016/0006-8993(94)91245-9

Condés-Lara, Miguel, González, N. M., Martínez-Lorenzana, G., Delgado, O. L., & Freund-Mercier, M. J. (2003). Actions of oxytocin and interactions with glutamate on spontaneous and evoked dorsal spinal cord neuronal activities. Brain Research, 976(1), 75–81. https://doi.org/10.1016/S0006-8993(03)02690-8

Condés-Lara, Miguel, Maie, I. A. S., & Dickenson, A. H. (2005). Oxytocin actions on afferent evoked spinal cord neuronal activities in neuropathic but not in normal rats. Brain Research, 1045(1–2), 124–133. https://doi.org/10.1016/j.brainres.2005.03.020

Condés-Lara, Miguel, Martínez-Lorenzana, G., Rodríguez-Jiménez, J., & Rojas-Piloni, G. (2008). Paraventricular hypothalamic nucleus stimulation modulates nociceptive responses in dorsal horn wide dynamic range neurons. Neuroscience Letters, 444(2), 199–202. https://doi.org/10.1016/j.neulet.2008.08.027

Condés-Lara, Miguel, Martínez-Lorenzana, G., Rojas-Piloni, G., & Rodríguez-Jiménez, J. (2007). Branched oxytocinergic innervations from the paraventricular hypothalamic nuclei to superficial layers in the spinal cord. Brain Research, 1160(1), 20–29. https://doi.org/10.1016/j.brainres.2007.05.031

Condés-Lara, Miguel, Rojas-Piloni, G., Martínez-Lorenzana, G., López-Hidalgo, M., & Rodríguez-Jiménez, J. (2009). Hypothalamospinal oxytocinergic antinociception is mediated by GABAergic and opiate neurons that reduce A-delta and C fiber primary afferent excitation of spinal cord cells. Brain Research, 1247, 38–49. https://doi.org/10.1016/j.brainres.2008.10.030

Condés-Lara, Miguel, Rojas-Piloni, G., Martínez-Lorenzana, G., Rodríguez-Jiménez, J., López Hidalgo, M., & Freund-Mercier, M. J. (2006). Paraventricular hypothalamic influences on spinal nociceptive processing. Brain Research, 1081(1), 126–137. https://doi.org/10.1016/j.brainres.2006.01.050

Condés-Lara, Miguel, Zayas-González, H., Manzano-García, A., Córdova-Quiroz, E., Granados-Mortera, J., García-Cuevas, M., Morales-Gómez, J., & González-Hernández, A. (2016). Successful pain management with epidural oxytocin. CNS Neuroscience and Therapeutics, 22(6), 532–534. https://doi.org/10.1111/cns.12551

Davalos, D., Lee, J. K., Smith, W. B., Brinkman, B., Ellisman, M. H., Zheng, B., & Akassoglou, K. (2008). Stable in vivo imaging of densely populated glia, axons and blood vessels in the mouse spinal cord using two-photon microscopy. Journal of Neuroscience Methods, 169(1), 1–7. https://doi.org/10.1016/j.jneumeth.2007.11.011

Emery, E. C., Luiz, A. P., Sikandar, S., Magnúsdóttir, R., Dong, X., & Wood, J. N. (2016). In vivo characterization of distinct modality-specific subsets of somatosensory neurons using GCaMP. Science Advances, 2(11), e1600990. https://doi.org/10.1126/sciadv.1600990

Farrar, M. J., Bernstein, I. M., Schlafer, D. H., Cleland, T. A., Fetcho, J. R., & Schaffer, C. B. (2012). Chronic in vivo imaging in the mouse spinal cord using an implanted chamber. Nature Methods, 9(3), 297–302. https://doi.org/10.1038/nmeth.1856

Fenrich, K. K., Weber, P., Hocine, M., Zalc, M., Rougon, G., & Debarbieux, F. (2012). Long-term in vivo imaging of normal and pathological mouse spinal cord with subcellular resolution using implanted glass windows. Journal of Physiology, 590(16), 3665–3675. https://doi.org/10.1113/jphysiol.2012.230532

Fu, K. Y., Light, A. R., & Maixner, W. (2001). Long-lasting inflammation and long-term hyperalgesia after subcutaneous formalin injection into the rat hindpaw. Journal of Pain, 2(1), 2–11. https://doi.org/10.1054/jpai.2001.9804

García-Boll, E., Martínez-Lorenzana, G., Condés-Lara, M., & González-Hernández, A. (2018). Oxytocin inhibits the rat medullary dorsal horn Sp5c/C1 nociceptive transmission through OT but not V1A receptors. Neuropharmacology, 129, 109–117. https://doi.org/10.1016/j.neuropharm.2017.11.031

Gardner, E. P., & Johnson, K. O. (2000). The Somatosensory System: Receptors and Central Pathways. In Principles of Neural Science (5th ed., pp. 431–437). Mc Graw Hill.

Gimpl, G., & Fahrenholz, F. (2001). The Oxytocin receptor system: Structure, function, and regulation. Physiological Reviews, 81(2), 629–683. https://doi.org/10.1152/physrev.2001.81.2.629

González-Hernández, A., Espinosa De Los Monteros-Zuñiga, A., Martínez-Lorenzana, G., & Condés-Lara, M. (2019). Recurrent antinociception induced by intrathecal or peripheral oxytocin in a neuropathic pain rat model. Experimental Brain Research, 237(11), 2995–3010. https://doi.org/10.1007/s00221-019-05651-7

González-Hernández, A., Manzano-García, A., Martínez-Lorenzana, G., Tello-García, I. A., Carranza, M., Arámburo, C., & Condés-Lara, M. (2017). Peripheral oxytocin receptors inhibit the nociceptive input signal to spinal dorsal horn wide-dynamic-range neurons. Pain, 158(11), 2117–2128. https://doi.org/10.1097/j.pain.0000000000001024

González-Hernández, A., Rojas-Piloni, G., & Condés-Lara, M. (2014). Oxytocin and analgesia: Future trends. In Trends in Pharmacological Sciences (Vol. 35, Issue 11, pp. 549–551). Elsevier Ltd. https://doi.org/10.1016/j.tips.2014.09.004

Grienberger, C., & Konnerth, A. (2012). Imaging calcium in neurons. In Neuron. https://doi.org/10.1016/j.neuron.2012.02.011

Hong-mei, Z., Li-jun, Z., Xiao-dong, H. U., Neng-wei, H. U., Tong, Z., Xian-guo, L. I. U., Zhang, H.-M., Zhou, L.-J., Hu, X.-D., Hu, N.-W., Zhang, T., & Liu, X.-G. (2004). Acute nerve injury induces long-term potentiation of C-fiber evoked field potentials in spinal dorsal horn of intact rat. *Sheng Li Xue Bao : Acta Physiologica Sinica*, 56(5), 591–596. http://www.ncbi.nlm.nih.gov/pubmed/15497039

Ikeda, H., Stark, J., Fischer, H., Wagner, M., Drdla, R., Jäger, T., & Sandkühler, J. (2006). Synaptic amplifier of inflammatory pain in the spinal dorsal horn. Science, 312(5780), 1659–1662. https://doi.org/10.1126/science.1127233

Jáidar, O., Carrillo-Reid, L., Hernández, A., Drucker-Colín, R., Bargas, J., & Hernández-Cruz, A. (2010). Dynamics of the Parkinsonian striatal microcircuit: Entrainment into a dominant network state. Journal of Neuroscience, 30(34), 11326–11336. https://doi.org/10.1523/JNEUROSCI.1380-10.2010

Jiang, C.-Y., Fujita, T., & Kumamoto, E. (2014). Synaptic modulation and inward current produced by oxytocin in substantia gelatinosa neurons of adult rat spinal cord slices. Journal of Neurophysiology, 111(5), 991–1007. https://doi.org/10.1152/jn.00609.2013

Jo, Y. H., Stoeckel, M. E., Freund-Mercier, M. J., & Schlichter, R. (1998). Oxytocin modulates glutamatergic synaptic transmission between cultured neonatal spinal cord dorsal horn neurons. Journal of Neuroscience, 18(7), 2377–2386. https://doi.org/10.1523/jneurosci.18-07-02377.1998

Johannssen, H. C., & Helmchen, F. (2010). In vivo Ca^{2+} imaging of dorsal horn neuronal populations in mouse spinal cord. Journal of Physiology, 588(18), 3397–3402. https://doi.org/10.1113/jphysiol.2010.191833

Johannssen, H. C., & Helmchen, F. (2013). Two-photon imaging of spinal cord cellular networks. In Experimental Neurology (Vol. 242, pp. 18–26). https://doi.org/10.1016/j.expneurol.2012.07.014

Juif, P., & Poisbeau, P. (2013). Neurohormonal effects of oxytocin and vasopressin receptor agonists on spinal pain processing in male rats. Pain, 154(8), 1449–1456. https://doi.org/10.1016/j.pain.2013.05.003

Kandel, E. R., Schwartz, J. H., Jessell, T. M., Siegelbaum, S. A., & Hudspeth, A. J. (2012). Principles of Neural Science (5th ed.). https://neurology.mhmedical.com/book.aspx?bookID=1049

Keefer, E. W., Gramowski, A., & Gross, G. W. (2001). NMDA receptor-dependent periodic oscillations in cultured spinal cord networks. Journal of Neurophysiology, 86(6), 3030–3042. https://doi.org/10.1152/jn.2001.86.6.3030

Kim, Y. S., Chu, Y., Han, L., Li, M., Li, Z., LaVinka, P. C., Sun, S., Tang, Z., Park, K., Caterina, M. J., Ren, K., Dubner, R., Wei, F., & Dong, X. (2014). Central terminal sensitization of TRPV1 by descending serotonergic facilitation modulates chronic pain. Neuron, 81(4), 873–887. https://doi.org/10.1016/j.neuron.2013.12.011

Loeser, J. D., & Treede, R.-D. (2008). The Kyoto protocol of IASP Basic Pain Terminology☆. Pain, 137(3), 473–477. https://doi.org/10.1016/j.pain.2008.04.025

Looger, L. L., & Griesbeck, O. (2012). Genetically encoded neural activity indicators. In Current Opinion in Neurobiology (Vol. 22, Issue 1, pp. 18–23). Elsevier Current Trends. https://doi.org/10.1016/j.conb.2011.10.024

Luo, C., Seeburg, P. H., Sprengel, R., & Kuner, R. (2008). Activity-dependent potentiation of calcium signals in spinal sensory networks in inflammatory pain states. Pain, 140(2), 358–367. https://doi.org/10.1016/j.pain.2008.09.008

Martínez-Lorenzana, G., Espinosa-López, L., Carranza, M., Aramburo, C., Paz-Tres, C., Rojas-Piloni, G., & Condés-Lara, M. (2008). PVN electrical stimulation prolongs withdrawal latencies and releases oxytocin in cerebrospinal fluid, plasma, and spinal cord tissue in intact and neuropathic rats. Pain, 140(2), 265–273. https://doi.org/10.1016/j.pain.2008.08.015

Mazzuca, M., Minlebaev, M., Shakirzyanova, A., Tyzio, R., Taccola, G., Janackova, S., Gataullina, S., Ben-Ari, Y., Giniatullin, R., & Khazipov, R. (2011). Newborn analgesia mediated by oxytocin during delivery. Frontiers in Cellular Neuroscience, 5, 1–9. https://doi.org/10.3389/fncel.2011.00003

Millan, M. J. (2002). Descending control of pain. Progress in Neurobiology, 66(6), 355–474. https://doi.org/https://doi.org/10.1016/S0301-0082(02)00009-6

Miranda-Cardenas, Y., Rojas-Piloni, G., Martínez-Lorenzana, G., Rodríguez-Jiménez, J., López-Hidalgo, M., Freund-Mercier, M. J., & Condés-Lara, M. (2006). Oxytocin and electrical stimulation of the paraventricular hypothalamic nucleus produce antinociceptive effects that are reversed by an oxytocin antagonist. Pain, 122(1–2), 182–189. https://doi.org/10.1016/j.pain.2006.01.029

Nelson, N. A., Wang, X., Cook, D., Carey, E. M., & Nimmerjahn, A. (2019). Imaging spinal cord activity in behaving animals. In Experimental Neurology (Vol. 320, p. 112974). Academic Press Inc. https://doi.org/10.1016/j.expneurol.2019.112974

Nersesyan, Y., Demirkhanyan, L., Cabezas-Bratesco, D., Oakes, V., Kusuda, R., Dawson, T., Sun, X., Cao, C., Cohen, A. M., Chelluboina, B., Veeravalli, K. K., Zimmermann, K., Domene, C., Brauchi, S., & Zakharian, E. (2017). Oxytocin modulates nociception as an agonist of pain-sensing TRPV1. Cell Reports, 21(6), 1681–1691. https://doi.org/10.1016/j.celrep.2017.10.063

Nestler, E. J., Hyman, S. E., & Malenka, R. C. (2009). Molecular Neuropharmacology. A Foundation for Clinical Neuroscience (2nd ed.). Mc Graw Hill.

Paredes, R. M., Etzler, J. C., Watts, L. T., Zheng, W., & Lechleiter, J. D. (2008). Chemical calcium indicators. Methods, 46(3), 143–151. https://doi.org/10.1016/j.ymeth.2008.09.025

Paxinos, G., & Watson, C. (2007). The Rat Brain in Stereotaxic Coordinates (6th ed.). Academic Press. https://www.elsevier.com/books/the-rat-brain-in-stereotaxic-coordinates/paxinos/978-0-12-374121-9

Pérez-Ortega, J., Duhne, M., Lara-González, E., Plata, V., Gasca, D., Galarraga, E., Hernández-Cruz, A., & Bargas, J. (2016). Pathophysiological signatures of functional connectomics in parkinsonian and dyskinetic striatal microcircuits. Neurobiology of Disease, 91, 347–361. https://doi.org/10.1016/J.NBD.2016.02.023

Plata, V., Duhne, M., Pérez-Ortega, J., Hernández-Martinez, R., Rueda-Orozco, P., Galarraga, E., Drucker-Colín, R., & Bargas, J. (2013). Global actions of nicotine on the striatal microcircuit. Frontiers in Systems Neuroscience, 7, 78. https://doi.org/10.3389/fnsys.2013.00078

Qi, J., Han, W. Y., Yang, J. Y., Wang, L. H., Dong, Y. X., Wang, F., Song, M., & Wu, C. F. (2012). Oxytocin regulates changes of extracellular glutamate and GABA levels induced by

methamphetamine in the mouse brain. Addiction Biology, 17(4), 758–769. https://doi.org/10.1111/j.1369-1600.2012.00439.x

Qiu, F., Qiu, C., Cai, H., Liu, T., Qu, Z., Yang, Z., Li, J.-D., Zhou, Q.-Y., & Hu, W.-P. (2014). Oxytocin inhibits the activity of acid-sensing ion channels through the vasopressin, V1A receptor in primary sensory neurons. British Journal of Pharmacology, 171, 3065–3076. https://doi.org/10.1111/bph.12635

Raja, S. N., Carr, D. B., Cohen, M., Finnerup, N. B., Flor, H., Gibson, S., Keefe, F. J., Mogil, J. S., Ringkamp, M., Sluka, K. A., Song, X.-J., Stevens, B., Sullivan, M. D., Tutelman, P. R., Ushida, T., & Vader, K. (2020). The revised International Association for the Study of Pain definition of pain: concepts, challenges, and compromises. Pain, 161(9), 1976–1982. https://doi.org/10.1097/j.pain.0000000000001939

Rendón-Ochoa, E. A., Hernández-Flores, T., Avilés-Rosas, V. H., Cáceres-Chávez, V. A., Duhne, M., Laville, A., Tapia, D., Galarraga, E., & Bargas, J. (2018). Calcium currents in striatal fast-spiking interneurons: Dopaminergic modulation of Ca V 1 channels. BMC Neuroscience, 19(1), 42. https://doi.org/10.1186/s12868-018-0441-0

Rexed, B. (1954). A cytoaRexed, B. (1954). A cytoarchitectonic atlas of the spinal cord in the cat. Journal of Comparative Neurology, 100(2), 297–379. https://doi.org/10.1002/cne.901000205

Ribeiro-da-Silva, A., & de Koninck, Y. (2009). Morphological and Neurochemical Organization of the Spinal Dorsal Horn. In Science of Pain (Vol. 5, pp. 279–310). Elsevier. https://doi.org/10.1016/B978-012370880-9.00163-8

Robinson, D. a, Wei, F., Wang, G. D., Li, P., Kim, S. J., Vogt, S. K., Muglia, L. J., & Zhuo, M. (2002). Oxytocin mediates stress-induced analgesia in adult mice. The Journal of Physiology, 540(Pt 2), 593–606. https://doi.org/10.1113/jphysiol.2001.013492

Rochefort, N. L., Jia, H., & Konnerth, A. (2008). Calcium imaging in the living brain: prospects for molecular medicine. In Trends in Molecular Medicine (Vol. 14, Issue 9, pp. 389–399). Elsevier. https://doi.org/10.1016/j.molmed.2008.07.005

Rojas-Piloni, G., López-Hidalgo, M., Martínez-Lorenzana, G., Rodríguez-Jiménez, J., & Condés-Lara, M. (2007). GABA-mediated oxytocinergic inhibition in dorsal horn neurons by hypothalamic paraventricular nucleus stimulation. Brain Research, 1137(1), 69–77. https://doi.org/10.1016/j.brainres.2006.12.045

Rojas-Piloni, G., Martínez-Lorenzana, G., Delatorre, S., & Condés-Lara, M. (2008). Nociceptive spinothalamic tract and postsynaptic dorsal column neurons are modulated by paraventricular hypothalamic activation. European Journal of Neuroscience, 28(April), 546–558. https://doi.org/10.1111/j.1460-9568.2008.06366.x

Rojas-Piloni, G., Mejía Rodríguez, R., Martínez Lorenzana, G., & Condés Lara, M. (2010). Oxytocin, but not vassopressin, modulates nociceptive responses in dorsal horn neurons. Neuroscience Letters, 476(1), 32–35. https://doi.org/10.1016/j.neulet.2010.03.076

Ruscheweyh, R., & Sandkühler, J. (2005). Long-range oscillatory Ca^{2+} waves in rat spinal dorsal horn. European Journal of Neuroscience, 22(8), 1967–1976. https://doi.org/10.1111/j.1460-9568.2005.04393.x

Salinas-Abarca, A. B., Avila-Rojas, S. H., Barragán-Iglesias, P., Pineda-Farias, J. B., & Granados-Soto, V. (2017). Formalin injection produces long-lasting hypersensitivity with characteristics of neuropathic pain. European Journal of Pharmacology, 797, 83–93. https://doi.org/10.1016/j.ejphar.2017.01.018

Sawchenko, P. E., & Swanson, L. W. (1982). Immunohistochemical identification of neurons in the paraventricular nucleus of the hypothalamus that project to the medulla or to the spinal cord in the rat. Journal of Comparative Neurology, 205(3), 260–272. https://doi.org/10.1002/cne.902050306

Schultz, S. R., Copeland, C. S., Foust, A. J., Quicke, P., & Schuck, R. (2017). Advances in two-photon scanning and scanless microscopy technologies for functional neural circuit imaging. Proceedings of the IEEE, 105(1), 139–157. https://doi.org/10.1109/JPROC.2016.2577380

Sekiguchi, K. J., Shekhtmeyster, P., Merten, K., Arena, A., Cook, D., Hoffman, E., Ngo, A., & Nimmerjahn, A. (2016). Imaging large-scale cellular activity in spinal cord of freely behaving mice. Nature Communications, 7, 11450. https://doi.org/10.1038/ncomms11450

Shiraishi, T., Onoe, M., Kojima, T., Sameshima, Y., & Kageyama, T. (1995). Effects of hypothalamic paraventricular nucleus: Electrical stimulation produce marked analgesia in rats. Neurobiology, 3(3–4), 393–403. https://europepmc.org/article/med/8696307

Sneddon, L. U. (2018). Comparative physiology of nociception and pain. In Physiology (Vol. 33, Issue 1, pp. 63–73). American Physiological Society. https://doi.org/10.1152/physiol.00022.2017

Sun, W., Zhou, Q., Ba, X., Feng, X., Hu, X., Cheng, X., Liu, T., Guo, J., Xiao, L., Jiang, J., Xiong, D., Hao, Y., Chen, Z., & Jiang, C. (2018). Oxytocin relieves neuropathic pain through GABA release and presynaptic TRPV1 inhibition in spinal cord. Frontiers in Molecular Neuroscience, 11, 248. https://doi.org/10.3389/fnmol.2018.00248

Swanson, L. W. (1977). Immunohistochemical evidence for a neurophysin-containing autonomic pathway arising in the paraventricular nucleus of the hypothalamus. Brain Research, 128(2), 346–353. https://doi.org/10.1016/0006-8993(77)91000-9

Swanson, L. W., & McKellar, S. (1979). The distribution of oxytocin- and neurophysin-stained fibers in the spinal cord of the rat and monkey. Journal of Comparative Neurology, 188(1), 87–106. https://doi.org/10.1002/cne.901880108

Todd, A. J. (2010). Neuronal circuitry for pain processing in the dorsal horn. Nature Reviews Neuroscience, 11(12), 823–836. https://doi.org/10.1038/nrn2947

Vautrelle, N., Carrillo-Reid, L., & Bargas, J. (2009). Diversity of Up-State Voltage Transitions During Different Network States. In Cortico-Subcortical Dynamics in Parkinson's Disease (pp. 1–13). Humana Press. https://doi.org/10.1007/978-1-60327-252-0_5

von Bohlen und Halbach, O., & Dermietzel, R. (2006). Neurotransmitters and Neuromodulators: Handbook of Receptors and Biological Effects (2nd ed.). WILEY-VCH. https://www.wiley.com/en-mx/Neurotransmitters+and+Neuromodulators:+Handbook+of+Receptors+and+Biological+Effects,+2nd,+Completely+Revised+and+Enlarged+Edition-p-9783527609079

Vrontou, S., Wong, A. M., Rau, K. K., Koerber, H. R., & Anderson, D. J. (2013). Genetic identification of C fibres that detect massage-like stroking of hairy skin in vivo. Nature, 493(7434), 669–673. https://doi.org/10.1038/nature11810

Woolf, C. J., & Salter, M. W. (2000). Neuronal plasticity: Increasing the gain in pain. Science 288 (5472) 1765–1768) https://doi.org/10.1126/science.288.5472.1765

Xie, J. D., Chen, S. R., Chen, H., Zeng, W. A., & Pan, H. L. (2016). Presynaptic N-methyl-D-aspartate (NMDA) receptor activity is increased through protein kinase C in paclitaxel-induced neuropathic pain. Journal of Biological Chemistry, 291(37), 19364–19373. https://doi.org/10.1074/jbc.M116.732347

Yarmolinsky, D. A., Peng, Y., Pogorzala, L. A., Rutlin, M., Hoon, M. A., & Zuker, C. S. (2016). Coding and plasticity in the mammalian thermosensory system. Neuron, 92(5), 1079–1092. https://doi.org/10.1016/j.neuron.2016.10.021

Zayas-González, H., González-Hernández, A., Manzano-García, A., Hernández-Rivero, D., García-Cuevas, M. A., Granados-Mortera, J. C., Vaca-Aguirre, L., Flores-Fierro, S., Martínez-Lorenzana, G., & Condés-Lara, M. (2019). Effect of local infiltration with oxytocin on hemodynamic response to surgical incision and postoperative pain in patients having open laparoscopic surgery under general anesthesia. European Journal of Pain, 23(8), 1519–1526. https://doi.org/10.1002/ejp.1427

Zhang, F. Y., Wan, Y., Zhang, Z. K., Light, A. R., & Fu, K. Y. (2007). Peripheral formalin injection induces long-lasting increases in cyclooxygenase 1 expression by microglia in the spinal cord. Journal of Pain, 8(2), 110–117. https://doi.org/10.1016/j.jpain.2006.06.006

Zigmond, M. J., Bloom, F. E., Landis, S. C., Roberts, J. L. ., & Squire, R. L. (1999). Fundamental Neuroscience (1st ed.). Academic Press. https://www.em-consulte.com/article/23698/fundamental-neuroscience-zigmond-bloom-landis-robe

Zimmermann, M. (1983). Ethical guidelines for investigations of experimental pain in conscious animals. Pain, 16(2), 109–110. https://doi.org/10.1016/0304-3959(83)90201-4

11. ÍNDICE DE FIGURAS

tratamiento con OT; la actividad dependiente de $[Ca^{2+}]i$ presenta cambios bajo las condiciones restantes (NMDA, NMDA+OT, OT+NMDA). **(C)** Número de células activas. La gráfica compara el número de células activas durante el registro de cada condición experimental; es claro que los tratamientos NMDA, NMDA+OT y OT+NMDA aumentan el número de células activas en comparación con el control, no ocurre esto con el tratamiento con OT. **(D)** Actividad global. La gráfica compara la actividad total de cada registro bajo los diferentes tratamientos. El grupo NMDA aumenta el número de células activas y se aprecia una tendencia a aumentar parcialmente la actividad global en comparación con la condición de control. Además, la aplicación de NMDA+OT aumentó significativamente no sólo el número de células, sino también la actividad global en comparación con la condición de control, lo que indica que la OT recluta elementos celulares extra a los reclutados por el grupo NMDA, lo mismo ocurrió cuando se aplicó la OT y posteriormente el NMDA (OT+NMDA). Finalmente, el tratamiento con OT no generó cambios significativos ni en el número de células activas, ni en la actividad global. Los datos se representan como la media ± SEM, n=7 por grupo, $p<0.05$(*), $p<0.01$(**) o $p>0.001$(***) comparados con el grupo Control, Kruskal-Wallis con post hoc de Dunn. OT: oxitocina..... 36

Figura 9. Efecto de la oxitocina en la coactividad en poblaciones de células del asta dorsal de la médula espinal. (A) Raster plots representativos de cada uno de los diferentes tratamientos: Control, NMDA, NMDA+OT, OT y OT+NMDA; los puntos rojos en cada raster plot representan la actividad simultánea de conjuntos de neuronas con actividad recurrente ($p<0.05$). Debajo de cada raster plot, se graficó un histograma de coactividad, el cual representa la suma del número de células coactivas a lo largo del tiempo. Los picos de coactividad significativos fueron resaltados en rojo y el umbral de significancia está representado como una línea horizontal discontinua. OT: oxitocina..... 39

Figura 10. La oxitocina modifica la dinámica de actividad de las células previamente evocada por NMDA en el asta dorsal. (A) Matriz de correlación cruzada del índice de similitud de Jaccard; compara todos los posibles pares de vectores de coactividad a lo largo del tiempo para cada tratamiento: Control, NMDA, NMDA+OT, OT y OT+NMDA. Nótese una alta coordinación de células con el tratamiento de NMDA. **(B)** Número de picos de coactivación; el gráfico representa la presencia de picos de sincronización para cada grupo. La actividad coordinada de las células se ve incrementada significativamente con el grupo NMDA, así como para el grupo OT+NMDA. El tratamiento con OT reduce el número de

12. PUBLICACIONES DURANTE EL DOCTORADO

12.1. Publicaciones derivadas de esta tesis

Tello-García, I. A., Pérez-Ortega, J., Martínez-Lorenzana, G., González-Hernández, A., & Condés-Lara, M. (2020). **Oxytocin prevents neuronal network pain-related changes on spinal cord dorsal horn in vitro.** Cell Calcium, 90, 102246. https://doi.org/10.1016/j.ceca.2020.102246 (Ver apéndice 1)

12.2. Publicaciones derivadas de colaboraciones con otros proyectos

Martínez-Lorenzana, G., Gamal-Eltrabily, M., **Tello-García, I. A.**, Martínez-Torres, A., Becerra-González, M., González-Hernández, A., & Condés-Lara, M. (2021). **CLARITY with neuronal tracing and immunofluorescence to study the somatosensory system in rats**. Journal of Neuroscience Methods, 350, 109048. https://doi.org/10.1016/j.jneumeth.2020.109048 (Ver apéndice 1)

Condés-Lara, M., Martínez-Lorenzana, G., Rojas-Piloni, G., **Tello-García, I. A.**, Manzano-García, A., Rubio-Beltran, E., & González-Hernández, A. (2018). **Axons of Individual Dorsal Horn Neurons Bifurcated to Project in Both the Anterolateral and the Postsynaptic Dorsal Column Systems.** Neuroscience, 371, 178–190. https://doi.org/10.1016/j.neuroscience.2017.11.050 (Ver apéndice 1)

Manzano-García, A., González-Hernández, A., **Tello-García, I. A.**, Martínez-Lorenzana, G., & Condés-Lara, M. (2018). **The role of peripheral vasopressin 1A and oxytocin receptors on the subcutaneous vasopressin antinociceptive effects.** European Journal of Pain, 22(3), 511–526. https://doi.org/10.1002/ejp.1134 (Ver apéndice 1)

González-Hernández, A., Manzano-García, A., Martínez-Lorenzana, G., **Tello-García, I. A.**, Carranza, M., Arámburo, C., & Condés-Lara, M. (2017). **Peripheral oxytocin receptors inhibit the nociceptive input signal to spinal dorsal horn wide-dynamic-range neurons.** Pain, 158(11), 2117–2128. https://doi.org/10.1097/j.pain.0000000000001024 (Ver apendice 1)

13. PARTICIPACIÓN EN CURSOS Y CONGRESOS

13.1. Congresos nacionales

Efecto de la administración local de oxitocina o vasopresina sobre la nocicepción inducida por formalina (presentación oral). **Irma A. Tello-García**, Abimael González-Hernández, Alfredo de Jesús Manzano-García, Guadalupe Martínez-Lorenzana, Javier Rodríguez-Jiménez, Miguel Condés-Lara; LVIII Congreso Nacional Sociedad Mexicana de Ciencias Fisiológicas, A. C. San Miguel de Allende, Guanajuato, México del 6 al 10 de septiembre de 2015.

13.2. Congresos internacionales

Changes of intracellular calcium concentrations induced by oxytocin and vasopressin on dorsal horn cells from spinal cord slices: implications in nociception modulation (poster). **Irma A. Tello-García**, Guadalupe Martínez-Lorenzana, Abimael González-Hernández, Jesús Pérez-Ortega, José Bargas, Miguel Condés-Lara. Neuroscience 2017. Washington D.C., EUA del 10 al 15 de noviembre de 2017.

Electrophysiological, behavioral and molecular identification of peripheral oxytocin receptors modulating nociception (poster). **Irma A. Tello-García**, Abimael González-Hernández, Alfredo Manzano-García, Guadalupe Martínez-Lorenzana, Miguel Condés-Lara, M. Carranza, Carlos Arámburo. 16th World Congress on Pain. Yokohama, Japón del 26 al 30 de septiembre de 2016.

13.3. Cursos

Neural Engineering Methods and Applications (curso). University of Texas at Dallas & Universidad Nacional Autónoma de México. Instituto de Neurobiología, Querétaro, México. Del 6 al 10 de agosto de 2018.

APENDICE 1. ARTICULOS PUBLICADOS DURANTE EL DOCTORADO

Cell Calcium 90 (2020) 102246

Contents lists available at ScienceDirect

Cell Calcium

journal homepage: www.elsevier.com/locate/ceca

Oxytocin prevents neuronal network pain-related changes on spinal cord dorsal horn *in vitro*

Irma A. Tello-García[a], Jesús Pérez-Ortega[b], Guadalupe Martínez-Lorenzana[a], Abimael González-Hernández[a], Miguel Condés-Lara[a,*,1]

[a] Departamento de Neurobiología del Desarrollo y Neurofisiología, Instituto de Neurobiología, Universidad Nacional Autónoma de México, Campus Juriquilla, Boulevard Juriquilla, No. 3001, C.P. 76230, Querétaro, Mexico
[b] The NeuroTechnology Center, Columbia University, Biological Sciences, 901 NWC Building, 550 West 120th Street, New York, N.Y., 10027, United States

ARTICLE INFO

Keywords:
Calcium imaging
Oxytocin
Antinociceptive
Dorsal horn

ABSTRACT

Recently, oxytocin (OT) has been studied as a potential modulator of endogenous analgesia by acting upon pain circuits at the spinal cord and supraspinal levels. Yet the detailed action mechanisms of OT are still undetermined. The present study aimed to evaluate the action of OT in the spinal cord dorsal horn network under nociceptive-like conditions induced by the activation of the *N*-methyl-D-aspartate (NMDA) receptor and formalin injection, using calcium imaging techniques. Results demonstrate that the spontaneous Ca^{2+}-dependent activity of the dorsal horn cells was scarce, and the coactivity of cells was mainly absent. When NMDA was applied, high rates of activity and coactivity occurred in the dorsal horn cells; these rates of high activity mimicked the activity dynamics evoked by a neuropathic pain condition. In addition, although OT treatment increased activity rates, it was also capable of disrupting the conformation of coordinated activity previously consolidated by NMDA treatment, without showing any effect by itself. Altogether, our results suggest that OT globally prevents the formation of coordinated patterns previously generated by nociceptive-like conditions on dorsal horn cells by NMDA application, which supports previous evidence showing that OT represents a potential therapeutic alternative for the treatment of chronic neuropathic pain.

1. Introduction

Recent evidence has described oxytocin (OT) as an inhibitor of nociceptive activity in either the central nervous system [1–5] or peripheral nerve terminals [6]. OT has also been reported as a successful alternative for pain management in humans [7,8]. OT administration demonstrated a striking antinociceptive effect by reducing the pain-related signals and perception. Particularly, evidence shows that OT is capable of diminishing the pain-related electrical activity of spinal cord dorsal horn neurons and therefore inhibiting the transmission of antinociceptive information [1]. However, the intrinsic participation of OT and its effect on inhibiting the transmission of nociceptive information in the functional networks of sensory processing of the dorsal horn circuitry has remained elusive.

On the other hand, most works done on the spinal cord have pursued a better and more profound understanding of the histological aspects of this region. For several years' electrophysiology has been the standard technique used to study the physiology of the neuronal components of the dorsal horn because of its excellent temporal resolution and sensitivity. Nevertheless, the functional networks of sensory processing were not completely accessible with the main techniques used in the last century. Calcium imaging techniques with epifluorescent or two-photon microscopy allow the observation and analysis of large areas with several neurons. Some studies done in intact [9–16] or *in vitro* spinal cord tissue have been beneficial in understanding how cells function and respond to different stimuli [17,18].

To address the changes produced by OT in the neuronal network circuits of the dorsal horn, we used calcium imaging analysis on spinal cord slices to describe overall neuronal activity in spinal cord dorsal horn slices *in vitro* on a circuit that had not been altered by any stimulus. Afterward, we challenged the system with the application of N-methyl-D-aspartate (NMDA) to simulate the nociceptive-related

Abbreviations: OT, oxytocin; NMDA, *N*-methyl-D-aspartate; NMDAr, *N*-methyl-D-aspartate receptors

* Corresponding author at: Departamento de Neurobiología del Desarrollo y Neurofisiología, Instituto de Neurobiología, Universidad Nacional Autónoma de México, Campus Juriquilla, Lab B-16. Boulevard Juriquilla, No. 3001, C.P. 76230, Querétaro, Mexico.
E-mail address: condes@unam.mx (M. Condés-Lara).
[1] http://132.248.142.23/web_site/home_pages/35.

https://doi.org/10.1016/j.ceca.2020.102246
Received 23 April 2020; Received in revised form 2 June 2020; Accepted 16 June 2020
Available online 18 June 2020

activation of dorsal horn neurons [17,19]. Finally, we show that OT application inhibits the pain-related changes in neuronal circuit dynamics produced by NMDA.

2. Experimental Procedures

2.1. Experimental animals and ethical standards

A total of 35 both sex neonatal rats of 8–12 days old (P8-P12) were used in the present experiments. The animals were housed in clear plastic cages and maintained on a 12:12 h light–dark cycle (lights on at 07:00 h) at room temperature (22 °C ± 2 °C), with food and water *ad libitum*. All experiments followed the National Institutes of Health Guide for the Care and Use of Laboratory Animals (NIH publication no. 80-23, revised 1996) and the International Association for the Study of Pain (IASP) Guidelines for the Use of Animals in Research [20], and were conducted with the approval of the Bioethics Committee at the Instituto de Neurobiología (Bioethical protocols numbers 008 − 010). All efforts were made to limit distress and use only the number of animals necessary to produce reliable scientific data.

2.2. General methods

2.2.1. Slice preparation

Rats were anesthetized with pentobarbital (50 mg/ kg) and perfused transcardially with ice-cold (~4 °C) saline-sucrose solution (sucrose, 238 mM; glucose, 30 mM; $NaHCO_3$, 25 mM; KCl, 3 mM; $MgCl_2$, 2.5 mM; oxygenated with 95 % O_2, 5% CO_2; pH = 7.4). Then, the lumbosacral section of the spinal cord was extracted and mounted on an NVSL Vibroslice™ (World Precision Instruments Inc., Sarasota, FL, USA), and 500 − 550 μm thick transverse slices were obtained. Slices remained for at least 1 h before experiments at room temperature (20 − 24 °C) in saline solution containing (in mM): 119 NaCl, 30 Glucose, 25 $NaHCO_3$, 6 KCl, 2.5 $MgCl_2$, 1.5 $CaCl_2$, oxygenated with 95 % O_2, 5% CO_2, pH = 7.4.

2.2.2. Calcium imaging and treatments

Slices were incubated in dark conditions for 30 − 60 min at room temperature in a solution with 1 mL of saline plus 1.8 % D-mannitol (Sigma-Aldrich Co., St. Louis, MO, USA; CAS No. 69-65-8) and 20 μL of a solution containing 5 μg of Fluo-8® AM (AAT Bioquest Inc., Sunnyvale, CA, USA; CAS No. 1345980-40-6) diluted in 50 μl dimethylsulphoxide (DMSO), and equilibrated with 95 % O_2 and 5 % CO_2. To obtain the Ca^{2+} fluorescence signals, a motorized inverted Olympus IX81 fluorescence microscope equipped with a UPlanSApo 10x/0.40na objective was used (Olympus Latin America, Inc, Florida, FL, USA). To record the Ca^{2+} fluorescence transient signals, light pulses at 488 nm (35–100 msec exposure) were delivered to the spinal cord slice using a xenon lamp (cell-R DSU module, Olympus) connected to the microscope with an optical fiber. Changes in Ca^{2+} fluorescence signals were recorded with an ORCA®-R^2 digital CCD camera (Hamamatsu Photonics K.K. Japan) that gives an image field of 866 × 660 μm (see Fig. 1A, B). Short videos (~240 s = epoch; 4–5 fps) were acquired with the xCellence-RT imaging software, v1.2 (Olympus Soft Imaging Solution GmbH, Germany) at 200–250 msec time intervals.

At the end of the experiment, potassium chloride solution (300 μl of KCl at 500 mM in 3 mL of the recording chamber solution, giving a concentration of 50 mM) was applied to the recording chamber as a positive control. Neurons active (15–124 depending on each experimental condition) during the experiment were identified due to their Ca^{2+} transients and recorded in the following groups:

- Control group: no treatment was added to the slice. We made recordings of basal activity of dorsal horn cells, in order to observe how the spontaneous Ca^{2+} activity is at the dorsal horn.
- NMDA group: 8 μM NMDA [24–26] was added to the sliced preparation and preincubated for 5 min before recordings to evaluate the possible changes in the calcium-dependent activity of spinal dorsal horn cells under excitatory input.
- NMDA + OT group: 8 μM NMDA + 5 μM OT. OT was added after NMDA preincubation in order to evaluate if OT would have an effect on the activity first promoted by NMDA pretreatment. Experiments for NMDA + OT were preincubated for 5 min with NMDA, after which OT was added. Five minutes later, the recordings were carried out (10 min total).
- OT group: 5 μM OT [4–6,35,40] was added to the slice in order to evaluate the effect of OT on spontaneous activity. OT experiments were preincubated 5 min before recordings; no NMDA was added to the preparation.
- Formalin 5% group: injection of formalin 5% was done 48 h before calcium imaging recordings, in order to evaluate the calcium-dependent activity of dorsal horn cells under a neuropathic pain-like condition and compare if the application of NMDA could reproduce this activity patron as a neuropathic pain model for calcium imaging of spinal cord slices.

2.3. Image analysis

Initial image processing was carried out using Im-Patch© (http://impatch.ifc.unam.mx/), an open-source software to analyze changes in fluorescence Ca^{2+} signals. This program was written in LabVIEW programming environment (National Instruments™, USA) by one of the co-authors of this paper and has been extensively validated in several reports analyzing Ca^{2+} fluorescent signals [21–23]. In brief, this program allowed us to extract a summary image, which was obtained from the standard deviation from each video; then, localization coordinates of neurons active during the experiment were automatically detected by pattern recognition using circular templates with a 3-pixel diameter (~4 μm) (Fig. 1C). Calcium transients, represented as changes in fluorescence $(F_i\text{-}F_o)/F_o$ (where F_i is the fluorescence intensity and F_0 the basal fluorescence of each neuron), from each region of interest were extracted over time (Fig. 1D). Photobleaching, noise, and airy disk phenomena were corrected as previously described [23–25].

2.3.1. Detection of neuronal activity

It has been reported that the first-time derivative of the Ca^{2+} transient reflects the electrical discharge of neurons; specifically, the positive time derivative of a Ca^{2+} transient is similar to the duration of the firing trains in neurons [23–25]. Therefore, frames with active neurons (seen with its derivative) were taken as an indirect measure of the electrical activity of neurons over time (global activity); in all cases, only amplitudes 2.5 times above the standard deviation of the noise value were considered for analysis. All recordings were examined manually to remove Ca^{2+} transients attributed to glial cells, which have been described as slower than neuron Ca^{2+} signals (minutes long) [23–25]. Detection of neuronal activity was driven as previously described [23–25]. Briefly, a binary matrix (N x F) that represents the activity of neurons recorded simultaneously over time was constructed with the data (one matrix per epoch), where 1 represents an active and 0 an inactive neuron (plotted as Fig. 1E). This binary matrix was called experimental matrix, where every row corresponds to an active neuron (N), while columns represent the number of frames (F) on the video, as follows: 1 column is equal to 1 frame. The sum of every column is a coactivity vector (1xF) that represents the coactivity of several neurons over time (plotted as Fig. 1F).

2.3.2. Coactivity analysis

After the experimental matrix was constructed, coactivity analysis was performed on a custom-made program, written in MATLAB (MathWorks, Inc. MA, USA) by a co-author of this paper, that also includes some algorithms from the Brain Connectivity Toolbox (https://

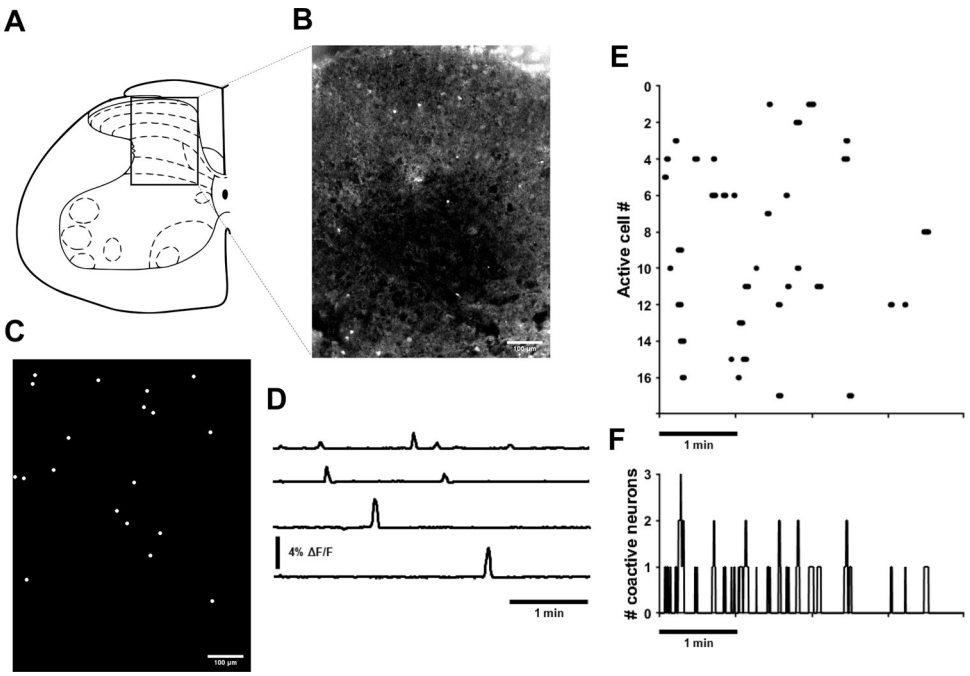

Fig. 1. Calcium imaging in spinal cord slice. (A) Scheme of the spinal cord area where calcium imaging was performed. the area corresponds to Rexed dorsal horn laminae I-V (866 × 660 μm). (B) Image of spinal cord tissue area recorded for 4 min. The spinal cord slice was loaded with Fluo-8 AM; spontaneous activity was recorded (scale bar = 100 μm). (C) Automatic selection of active neurons and their coordinates on the tissue area recorded during the experiment. (D) Examples of transient increases of calcium of 4 neurons during recordings (ΔF/F). (E) Raster plot showing the spontaneous activity of > 15 neurons in the dorsal horn of the spinal cord. Each row represents the activity of a single neuron across the series of images; cells are ordered and numbered from superficial to deep one (top to bottom, y-axis), and columns are movie frames converted to minute scale (x-axis, scale bar = 1 min). (F) The activity histogram shows the summed neuronal activity from the raster plot frame by frame and represents the number of coactive neurons along with the recordings (scale bar = 1 min).

sites.google.com/site/bctnet/). In this program, coactivity vectors from every experimental matrix were obtained, and the probability that a given peak appeared by chance was assessed by determining a significance threshold using Monte Carlo permutations (1000 times) as previously described [23–25]. The significance threshold was established as $p < 0.05$, and is marked as a dashed line on every coactivity histogram [23–25]; also, all the peaks that surpassed the significance level are denoted in red (Fig. 3B). For analysis, significant peaks of neuronal coactivity were stored in a matrix of coactivity peaks (A x P), where A is the number of active cells in every peak, and P is the number of coactivity peaks. The Jaccard similarity coefficient was measured to evaluate if coactivity vectors were different from one another [23–25]. Additionally, to evaluate an increase or decrease in synchronization of activity, coactivity vectors were counted in each epoch.

2.4. Drugs

Apart from the anesthetic (pentobarbital sodium; PiSA®, Mexico), and other reagents mentioned above, this study also used the following compounds (obtained from the sources indicated): *N*-methyl-D-aspartic acid (NMDA; CAS No. 6384-92-5) and oxytocin acetate salt hydrate (OT; CAS No. 50-56-6) purchased from Sigma-Aldrich Co. (St. Louis, MO, USA). OT and NMDA stock solutions were prepared before experiments and added to the recording chamber at the final concentration of 5 μM OT and 8 μM NMDA. For some experiments, formalin 5% (15 μL, diluted in saline) was injected subcutaneously (s.c.) into the dorsal surface of the hind paw 48 h prior to spinal cord extraction. NMDA and OT were dissolved in isotonic saline solution (0.9 % NaCl).

2.5. Data and statistical analysis

Most statistical methods used have been previously described [23–25]. Briefly, the number of cells was analyzed and the total activity during the epoch and number of coactivity peaks were considered for each experimental acute *in vitro* condition and plotted as the mean ± standard error of the mean (SEM). A non-matched Kruskal-Wallis with Dunn's *post hoc* test was used to analyze the differences between each group compared to the control condition and within groups.

We plotted the total activity against the coactivity peaks to compare the relation between both variables and performed a linear regression analysis to obtain the slope values and significance of the correlation of the variables. In addition, the global activity of every condition over time was represented by cumulative activity distributions, and the rates of accumulation were approximated with *ad hoc* linear regressions [23–26]. We considered statistical difference values as $p < 0.05$.

3. Results

We recorded an area of 866 × 660 μm of the spinal dorsal horn. This area covers the Rexed lamina I to V of the spinal dorsal horn (see Fig. 1A and a representative image of the tissue from the slice analyzed in Fig. 1B). The video recordings of the area visualized were further analyzed as previously described in the *Image analysis* section, and a summary image was obtained; from this summary image, an automatic localization of active neurons was performed. The coordinates of each neuron were used to identify every cell in the slice analyzed, as shown in Fig. 1C. Fig. 1D exemplifies representative Ca^{2+} transients from four spontaneous active neurons of the dorsal horn during 4 min of recording (epoch). Every epoch was plotted in a raster plot to visualize activity from several active neurons, where dots represent neuronal activity, the number of every active cell on the y-axis (organized from superficial to deeper lamina, I to V, in ascending order), and the temporal line of the experiment on the x-axis (Fig. 1E). An activity histogram is shown below every raster plot, and this represents the coactivity of the neurons over time; in this case, each peak is a coactivity vector extracted from the raster plot (Fig. 1F). In general terms, as validated in striatal neuronal tissues [23–26], the sequence of coactivity peaks could denote the activity sequence of different groups of several neurons alternating their activity during the recordings. In this sense, to analyze the role of OT in the spinal neuronal pain network, we analyzed the Ca^{2+} transients under different conditions.

3.1. NMDA increases the Ca^{2+}-dependent activity of cells in the dorsal horn circuit

First, we characterize the spontaneous Ca^{2+}-dependent activity in dorsal horn cells in Control situation (Fig. 2A). Our results revealed a scarce Ca^{2+} activity in Control situation. In Fig. 2B and C, the Ca^{2+} dependent activity in Control situation shows that the number of cells involved was low (28.71 ± 5.56, n = 7 slices) and the activity of these

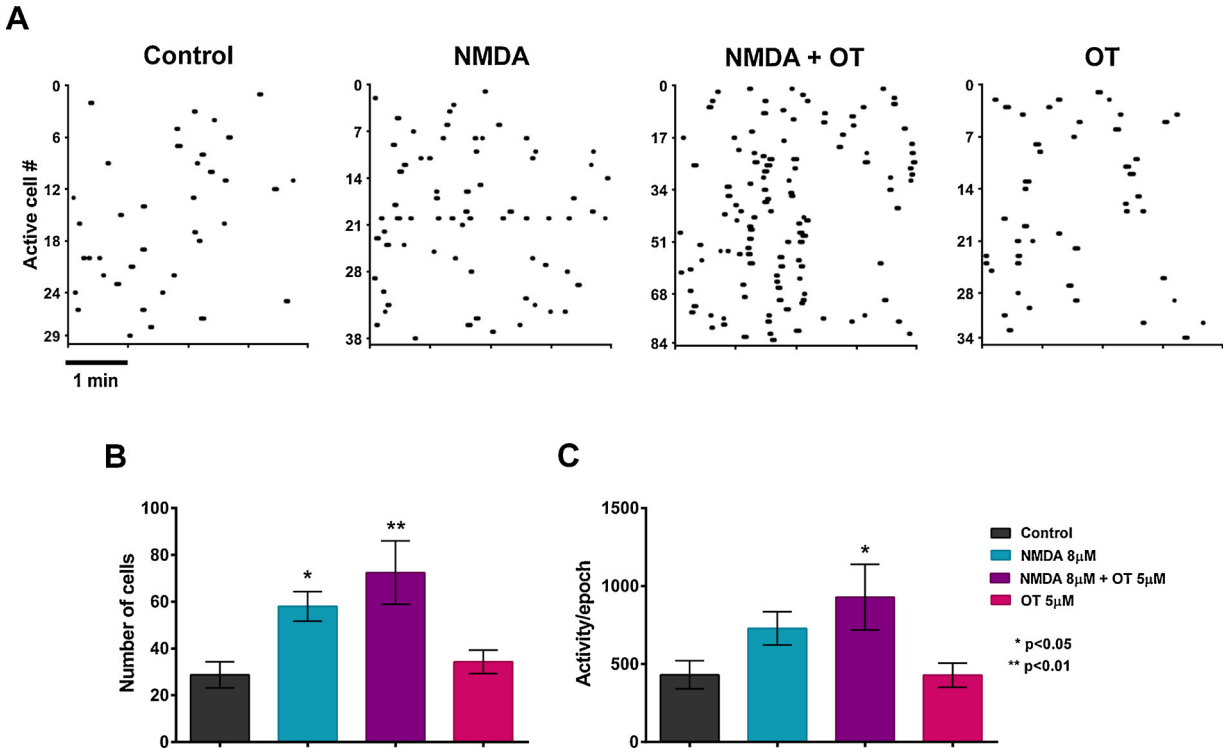

Fig. 2. NMDA increases the activity of spinal cord dorsal horn neurons.
(A) Representative raster plot of the different groups: control, 8 μM NMDA, 8 μM NMDA + 5 μM OT, and 5 μM OT; every epoch shows 4 min of activity of dorsal horn neurons. Note scarce control activity and an increase under NMDA and MNDA + OT. (B) Active cell number. The graph compares the number of active cells during epoch for each group; clearly, NMDA and NMDA + OT treatments increase the number of active cells. (C) Global activity. The graph compares the total activity for epoch under different treatments. NMDA increases the number of active cells and partially increases global activity compared with the control condition. In addition, NMDA + OT co-application increased significantly not only the number of cells but also the global activity compared with the control condition, indicating that OT recruits extracellular elements in addition to those recruited by NMDA by itself. Data are represented as mean ± SEM, n = 7, $p < 0.05$(*), or $p < 0.01$(**) compared to control, Kruskal-Wallis with Dunn's *post hoc* test. For treatments, NMDA experiments were preincubated for 5 min; NMDA + OT experiments were preincubated for 5 min with NMDA and then OT was added for another 5 min of preincubation (10 min total); finally, OT experiments were preincubated for 5 min; no NMDA was added to the preparation.

cells (*i.e.*, frames with active neurons) was scarce (431.30 ± 89.68, n = 7 slices) during the 4-minute recordings. This scarcity of spontaneous Ca^{2+}-dependent activity in dorsal horn cells agreed with previous reports [17,18].

Since we were interested in analyzing the effect of OT under an excitatory input, we used NMDA as an excitatory driver to increase the activity of the dorsal horn circuit; certainly, NMDA-sensitive receptors are known as the primary mediators of changes in neuronal activity in spinal Ca^{2+} mobilization related to nociceptive stimuli [17,18]. Similar approach has been used and validated in the spinal cord [24–26].

Under these considerations, we evaluated the action of NMDA application in spinal cord slices upon the Ca^{2+} transient events. Results showed that application of NMDA (8 μM) in spinal cord slices significantly increases the number of active cells (Fig. 2B, 58.00 ± 6.32, n = 7 slices, $p < 0.05$, Kruskal-Wallis, Dunn's post-test) and produces a partial increase in the global activity without being statistically significant when compared with the control group (Fig. 2C, 729.00 ± 106.80, n = 7 slices).

Considering that OT at spinal cord levels could act as an inhibitor of nociceptive activity in animals [4–6,35,36,40] and humans [7,8], we applied NMDA (8 μM) + OT (5 μM) to evaluate if OT modifies the Ca^{2+} activity evoked by NMDA (as nociceptive-like stimuli). For treatment co-application details, see section 2.2.2 Calcium imaging and treatments). We found that after the co-application of NMDA + OT, the number of active cells increases similarly to the NMDA group, when compared with the control group (Fig. 2B, 72.43 ± 13.56, n = 7 slices, $p < 0.01$, Kruskal-Wallis, Dunn's post-test). Besides, the co-application of NMDA + OT increases not only the number of active cells but also the overall activity (Fig. 2C, 928.70 ± 210.40, n = 7 slices, Kruskal-Wallis, Dunn's post-test) when compared with the control group.

Finally, the analysis of OT (5 μM) effects shows that the number of active cells and the global activity were similar to those of the control group (Fig. 2B, C, 34.29 ± 5.02 active cells, 428.70 ± 77.49 global activity, n = 7 slices). In brief, control Ca^{2+} activity and the cells number was scarce, NMDA increased the Ca^{2+} activity and the active cells number, NMDA + OT presented more Ca^{2+} activity and cells number participating and finally, OT along present an Ca^{2+} activity and cells number like in control situation.

3.2. Oxytocin prevents neuronal network dynamic changes produced by NMDA in dorsal horn cells

Afterward, we characterize if the increase in the number of active cells induced by NMDA produces changes in the activity dynamics of the dorsal horn circuit. Based on similar studies from striatal structures, where NMDA produces changes in activity dynamics of cells [23–25], we analyzed the coactivation of cells in the spinal cord as previously described [25].

Again, raster plots show the activity of dorsal horn cells over time under different conditions (Fig. 3A); colored dots represent the activity of neurons with statistical significance for coactivity. Coactivity histograms, below raster plots, represent the summed neural activity of every epoch (Fig. 3B). Every coactivity peak represents a group of active cells at the same time. After Monte Carlo permutations (see *2.3.2 Coactivity analysis*), all the synchronization peaks denoted in red surpassed the significance threshold represented in coactivity histograms

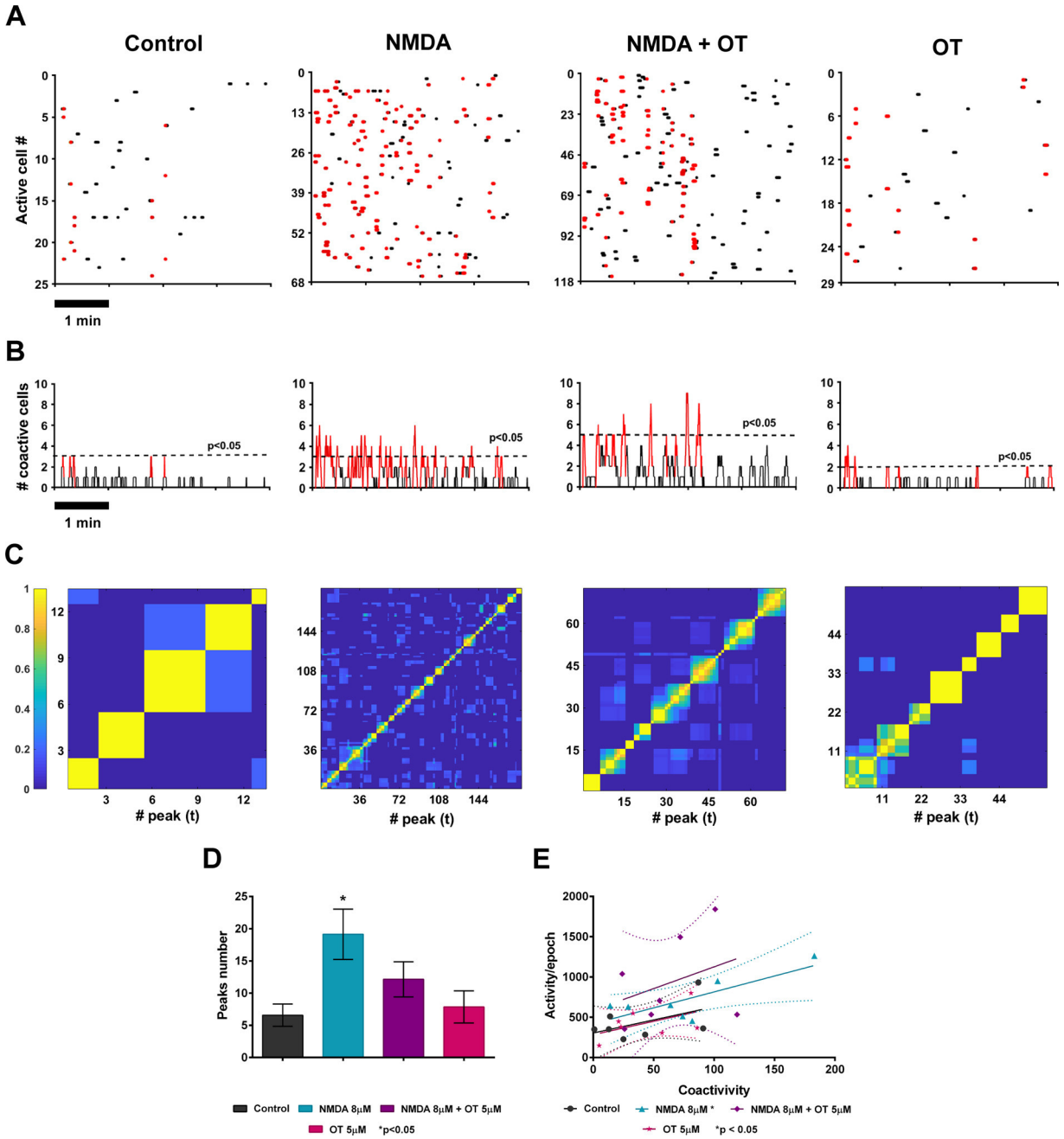

Fig. 3. Oxytocin treatment reduces the coordination of neuronal network circuits produced by NMDA in the spinal cord dorsal horn.
(A) Representative raster plots of the different groups; red dots represent the activity of sets of neurons with simultaneous recurrent activity, $p < 0.05$. (B) Coactivity histograms represent the number of coactive cells for each condition; peaks of synchronization denoted in red surpassed the significance threshold (represented as a dashed horizontal line). (C) Cross-correlation matrix of similarity index; compares all possible coactivity vectors paired over time for every treatment. (D) Number of coactivation peaks; the graph represents the appearance of synchronization peaks for each group. Note that OT treatment reduces the number of coactivity peaks produced by NMDA application to levels similar to those of the control condition. (E) Correlation between the global activity of epochs (Y-axis) *vs.* coactivity (X-axis) for each condition. When comparing the number of active frames (global activity) *versus* the relative coactivity, linear regression analysis indicated that only NMDA groups showed a correlation between the two variables, $p < 0.05$. Results suggest that OT treatment reduces the coordination of the activity produced by NMDA. The color scale bar in C represents the correlation between the coactivity vectors presented on every representative correlation matrix. Data are presented as mean ± SEM in D, solid lines represent the linear regression, and dotted lines represent the 95 % of the confidence interval, $n = 7$, $p < 0.05$(*) compared to control in D (Kruskal-Wallis with Dunn's *post hoc* test) or different than slope zero in E.

as a dashed horizontal line (Fig. 3B). We found few significant spontaneous peaks of coactivity in the control group (Fig. 3D, 6.57 ± 1.73, n = 7 slices). In contrast, NMDA (8 μM) application promotes changes in the activity dynamics of spinal cord circuitry characterized by an increase in the number of coactive cells, counted as the number of coactivity peaks (Fig. 3D,19.14 ± 3.91, n = 7, $p < 0.05$, Kruskal-Wallis, Dunn's post-test), indicating that pools of neurons synchronize their activity and alternate with other pools of neurons over time. Interestingly, the co-application of NMDA (8 μM) + OT (5 μM) prevents changes in coactivity dynamics, reducing the number of coactive peaks to non-statistically significant levels when compared with the control group (Fig. 3D, 12.14 ± 2.72, n = 7). Also, OT (5 μM) application does not produce any significant change in the coactive peak number compared to the control group (Fig. 3D, 7.85 ± 2.49, n = 7).

We also measured the Jaccard similarity index of all significant coactivity vectors, and we compared whether two vectors have the same components (neurons) or not from all possible pairs of vectors. Then, we plotted as a cross-correlation matrix in a pseudo-color scale (Fig. 3C); in this representation, a patchy appearance denotes that similar and several pools of neurons were in charge of activity synchronization over time [23–26]. As seen in Fig. 3C, NMDA produces a high level of synchronization marked as a patchy appearance on the plot.

To evaluate whether the global activity and coactivity of cells were correlated or not, we performed a linear regression analysis comparing the total activity of each experiment with the coactivity peak number. We found that only the NMDA group showed a significant correlation between global activity and coactivity that is not present under any other condition (Fig. 3E, $p < 0.05$, $n = 7$ slices, linear regression). These results suggest that NMDA induces synchronization in the Ca^{2+}-dependent activity of spinal dorsal horn neurons and that OT acts by disrupting this level of synchronization.

3.3. *In vivo formalin injection emulates increasing activity produced by NMDA in spinal cord slices in vitro*

Evidence shows that hind paw formalin injection in rats produces long-term pain-related changes in the spinal cord dorsal horn [17,18]. To evaluate if changes in neuronal activity dynamics produced by NMDA *in vitro* application are similar to changes produced by a central sensibilization developed by an inflammatory chronic pain model, we injected formalin 5% into the hind paw of the rats, and 48 h later we evaluated if the injection produced ex vivo changes in spinal cord neuronal activity. An example of activity evoked by formalin 5% injection is represented as a raster plot in Fig. 4A. By summating the activity over time, a graph of cumulative activity was obtained (Fig. 4B); this graph shows total global activity under different conditions over time (Ad hoc fitting of straight lines, where slopes become the rate of accumulation over time) [14]. An average of experiments of the control group shows 103.50 ± 0.31 (act/min), which increases to 189.07 ± 1.07 (act/min) for the NMDA group and 177.62 ± 0.69 (act/min) for the formalin group. OT shows a rate of accumulation of 113.925 ± 0.362 (act/min) that is similar to the control group, suggesting that OT does not have an effect on the calcium-dependent activity of the intact spinal cord dorsal horn cells along time. Finally, we did not find any statistical differences when comparing NMDA and formalin groups in i) number of cells (54.00 ± 8.28, $n = 7$ slices, Kruskal-Wallis, Dunn's post-test, data not shown), ii) global activity (shown as cumulative activity on Fig. 4B), and iii) number of coactivity peaks (8.7 ± 2.35, $n = 7$ slices, Kruskal-Wallis, Dunn's post-test, data not shown). Therefore, results exhibited that the injection of formalin 5% increases Ca^{2+} -dependent activity in dorsal horn cells in a similar way as the NMDA group."

4. Discussion and conclusions

Taken together, these results showed the following: (i) The silent nature of the dorsal horn circuit under control conditions. (ii) The dorsal horn circuit can be activated with NMDA application, which increases the number of active cells and the global activity of the circuit; also, NMDA treatment enhances the rates of coordinated activity of the dorsal horn network, regarding neuropathic pain plasticity evoked by the activation of NMDA receptors (NMDAr). (iii) OT can disrupt the coordinated activity patterns of ensembles of neurons in the dorsal horn of the spinal cord, and (iv) formalin injection produces changes in calcium-dependent activity similar to those evoked by NMDA treatment.

In normal conditions, dorsal horn circuitry has been described as silent, both in spinal cord slices [17,18] and in *in vivo* preparations [14]. This correlates with our results that although spontaneous calcium transients occur in dorsal horn neurons under control conditions, scarce synchronous activity is present but only in a few neurons (Figs. 1B and 2 D).

Because of the silent nature of the spinal dorsal horn circuit, we used NMDA as an excitatory drive of neuronal activity, in accordance with previous reports showing that NMDA application can induce an increase of calcium-dependent activity in silent networks as striatal structures [23–25]. Additionally, it has been largely documented that NMDAr activation is a crucial mediator of the amplification of nociceptive-related signaling in the spinal cord leading to plasticity mechanisms like central sensitization, which is the major component of inflammatory and neuropathic pain [19,30–33]. Also, activation of the glutamatergic system, and particularly activation of NMDAr, has been implicated in mechanisms of nociceptive related signaling facilitation in the spinal cord like allodynia and hyperalgesia.

We report that NMDA application in spinal cord slices can promote the activity of a silent circuit by increasing the overall calcium-dependent activity and the number of active cells. This is the first study to report the effects of NMDAr activation in a large number of cells (by slice 38–84) covering laminae I-V of the dorsal horn (Fig. 2). Also, our findings correlate with complementary evidence describing that nociceptive peripheral stimuli and electrical stimulation of dorsal roots increase the number and amplitude of calcium transients of neurons on superficial lamina (I-II) of the dorsal horn and that these changes are mediated by the activation of NMDAr [14,16,17,33].

Besides, NMDA also demonstrated to produce changes in the calcium-dependent activity dynamics of the spinal dorsal horn by enhancing the coordinated activity of neurons (Fig. 3). Consistent with this finding, previous data indicated that NMDA application in cultured spinal cord cells could generate coordinated activity that lasting for up to several hours [30]. Also, when imaging the neuronal network activity in the spinal cord during a nociceptive-like *in vivo* condition, the results show evidence of coordinated activity in the spinal cord (for a review see [34]). This synchronous calcium-dependent activity mediated by NMDAr activation was previously reported in spinal cord slices,

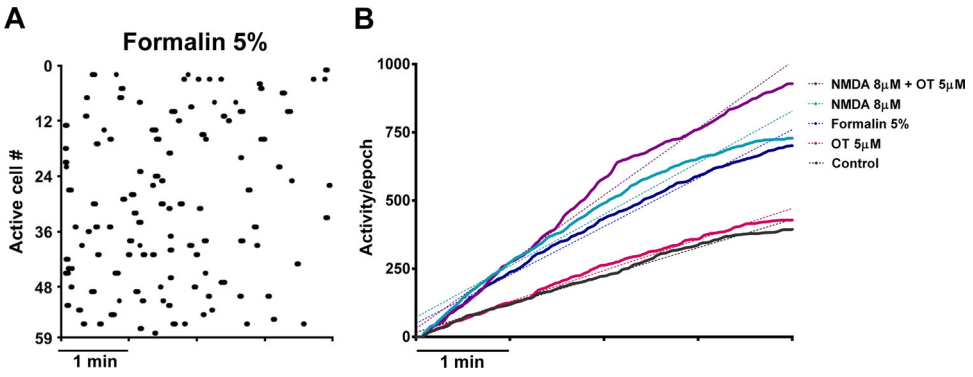

Fig. 4. NMDA activates neuronal network dynamics of the spinal cord dorsal horn similarly to a neuropathic pain condition.
(A) Representative raster plot shows the activity of dorsal horn neurons under formalin 5 % injection and (B) Cumulative activity of different conditions during 4-minute recordings. Note that the formalin *in vivo* injection 48 h prior to the *ex vivo* calcium imaging experiment produces changes in the neuronal network dynamics of spinal cord dorsal horn neurons that are mimicked by NMDA application.

specifically in the superficial laminae (I-III) of the dorsal horn, but only under the condition of a synaptic inhibition removal by blocking $GABA_A$ and glycine receptors [18]. Here, we demonstrated that the application of NMDA alone could evoke high rates of coordinated activity on assemblies of dorsal horn neurons (laminae I-V) even when synaptic inhibition remained intact.

To elucidate whether the facilitation of coordinated activity produced by NMDAr activation on dorsal horn neurons could be modified by OT treatment, we applied OT to the slices previously activated with NMDA. We found that the application of OT does not reduce the overall activity produced by NMDA on the contrary partially increases the activity (Fig. 2). However, OT is capable of reducing the coordinated activity associated with nociceptive-related calcium signaling (Fig. 3). Evidence indicates that OT can modulate the glutamatergic excitatory response in the spinal cord by reducing the increased firing rate produced by nociceptive-related signaling [1,2,35,36]. Although the reduction of NMDAr activity by OT has been described in neuronal cultures [37], evidence shows that the primary source of inhibitory action by OT on the spinal cord dorsal horn neuronal network is due to the overall increase in GABAergic transmission by direct and indirect means [38–40]. First, data indicates that OT directly increases the basal levels of extracellular GABAergic transmission [3,41,42]. Second, OT simultaneously decreases the glutamatergic activity by regulating the expression of the NR1 subunit of glutamatergic receptors and the levels of glutamate in the extracellular space by regulating glutamatergic transporter 1 [42]. Besides, indirect inhibition of the spinal cord dorsal horn circuit by OT action arises from the activation of a subpopulation of glutamatergic neurons that promotes local inhibition by recruiting GABAergic interneurons [43]. However, what we aimed to test in the present work by NMDA application is not an acute pain signaling but a pathological condition at the spinal cord as neuropathic pain condition. Taking that into account, we applied NMDA in order to mimics the phasic tone of NMDA that leads to the consolidation of central sensitization at the spinal dorsal horn that occurs under neuropathic pain-like conditions.

Interestingly, evidence suggested that the inhibitory effect of OT on the spinal cord dorsal horn is effective only upon previous activation of the glutamatergic nociceptive-related signaling. For example, OT counteracts the enhancement of excitatory activity characterized as an increase in frequency and amplitude of excitatory postsynaptic currents produced by activation of TRPV1 by capsaicin in a pain-related model without showing any effect by itself on the intact system [44]. And not only at spinal level but also at peripheral level, where evidence suggests that OT interacts directly or indirectly with TRPV1 receptor and attenuates capsaicin-induced nociception *via* TRPV1 desensitization without affecting intact cells [45]. This evidence correlates with our results, which showed that OT treatment reduces the coactivation of neuronal activity after NMDA application and that OT applied to control condition slices does not have any significant effects (Fig. 3).

One limitation of the previous evidence regarding OT inhibitory action on nociceptive-related models is the use of single-cell approaches, due to the effects that OT can have on different cell populations depending on the context, denoting the importance of studying the global actions of OT in the microcircuit as a whole. Our data complements these single-cell data measuring the spinal cord as a complete circuit, showing that despite the increase in global calcium-dependent activity and the recruitment of active cells, OT leads to a disruption of the coordination of neuronal network activity, therefore inhibiting nociceptive-related calcium signaling (Fig. 3), promoting an antinociceptive action.

In order to elucidate if this NMDAr activation in the spinal cord dorsal horn neurons is related to nociceptive-like signaling, we injected formalin 5% subcutaneously into the dorsal surface of the hind paw 48 h before calcium imaging recordings. We found that formalin injection produces long-lasting changes in calcium mobilization in dorsal horn neurons; these changes were similar to those observed in slices pre-treated with NMDA (Fig. 4). Our results correlate with evidence showing that, after 24 h, peripheral injury can trigger long-lasting changes in calcium signaling patterns in the dorsal horn neurons [17], therefore supporting the idea that the coordinated activity produced by NMDAr activation enhances nociceptive-related changes in the activity dynamics of the spinal cord dorsal horn, similar to a neuropathic pain model. It has been studied that formalin 5% injection on the hind paw of the rat can produce i) long-lasting secondary thermal and mechanical allodynia and hyperalgesia enhanced for 1–3 days after injection and lasted 3–4 weeks [27,28]. ii) hypersensitivity as well as molecular changes at dorsal root ganglion and spinal dorsal horn that resemble those induced by nerve injury, reaching its maximal effects between 1–3 days after injection, these effects remained for at least 14 days [28]. Based on this evidence we used Formalin 5% to induce neuropathic pain-like changes on the activity of the spinal dorsal horn cells. As the maximal effects were seen between 1–3 day after injection in previous reports [27–29], we tested calcium-dependent activity at 24 h and also at 48 h after formalin injection and changes in calcium-dependent activity were mainly observed after 48 h of formalin injection.

To summarize, the results presented here, combined with previous evidence from our group and others, indicate that OT application could represent a potential treatment to prevent the long-lasting changes in calcium mobilization in the dorsal horn regarding central sensitization under neuropathic pain conditions. The dorsal horn of the spinal cord is the site of the first synapse in the pain pathway and is crucial to study the plasticity mechanisms leading to chronic pain. Studying the global changes in network activity dynamics underlying central sensitization and how OT treatment counteracts these changes will prove useful to understand the development and possible treatment of chronic pain.

CRediT authorship contribution statement

Irma A. Tello-García: Conceptualization, Methodology, Validation, Formal analysis, Investigation, Visualization, Writing - original draft. **Jesús Pérez-Ortega:** Software, Validation. **Guadalupe Martínez-Lorenzana:** Methodology, Resources, Supervision. **Abimael González-Hernández:** Supervision, Writing - review & editing. **Miguel Condés-Lara:** Conceptualization, Methodology, Supervision, Resources, Funding acquisition, Writing - review & editing, Supervision.

Declaration of Competing Interest

The authors declare no conflicts of interest.

Acknowledgments

Irma A. Tello-García is a doctoral student from the Programa de Doctorado en Ciencias Biomédicas, Universidad Nacional Autónoma de México (UNAM) and has received CONACyT fellowship (no. 582491). This study was supported by grant no. IN200415 from PAPIIT-UNAM to MCL. The authors thank to Dr. Michael C. Jeziorski and Dr. Arturo G. Isla for their aid during the drafting of this article and to Jessica González Norris for reviewing the grammatical aspects of this paper.

References

[1] Y. Miranda-Cardenas, G. Rojas-Piloni, G. Martínez-Lorenzana, J. Rodríguez-Jiménez, M. López-Hidalgo, M.J. Freund-Mercier, M. Condés-Lara, Oxytocin and electrical stimulation of the paraventricular hypothalamic nucleus produce antinociceptive effects that are reversed by an oxytocin antagonist, Pain 122 (2006) 182–189, https://doi.org/10.1016/j.pain.2006.01.029.

[2] D. a Robinson, F. Wei, G.D. Wang, P. Li, S.J. Kim, S.K. Vogt, L.J. Muglia, M. Zhuo, Oxytocin mediates stress-induced analgesia in adult mice, J. Physiol. 540 (2002) 593–606, https://doi.org/10.1113/jphysiol.2001.013492.

[3] P. Juif, P. Poisbeau, Neurohormonal effects of oxytocin and vasopressin receptor agonists on spinal pain processing in male rats, Pain 154 (2013) 1449–1456, https://doi.org/10.1016/j.pain.2013.05.003.

[4] A. González-Hernández, A. Espinosa De Los Monteros-Zuñiga, G. Martínez-

Lorenzana, M. Condés-Lara, Recurrent antinociception induced by intrathecal or peripheral oxytocin in a neuropathic pain rat model, Exp. Brain Res. 237 (2019) 2995–3010, https://doi.org/10.1007/s00221-019-05651-7.
[5] E. García-Boll, G. Martínez-Lorenzana, M. Condés-Lara, A. González-Hernández, Oxytocin inhibits the rat medullary dorsal horn Sp5c/C1 nociceptive transmission through OT but not V1A receptors, Neuropharmacology 129 (2018) 109–117, https://doi.org/10.1016/j.neuropharm.2017.11.031.
[6] A. González-Hernández, A. Manzano-García, G. Martínez-Lorenzana, I.A. Tello-García, M. Carranza, C. Arámburo, M. Condés-Lara, Peripheral oxytocin receptors inhibit the nociceptive input signal to spinal dorsal horn wide-dynamic-range neurons, Pain 158 (2017) 2117–2128, https://doi.org/10.1097/j.pain.0000000000001024.
[7] H. Zayas-González, A. González-Hernández, A. Manzano-García, D. Hernández-Rivero, M.A. García-Cuevas, J.C. Granados-Mortera, L. Vaca-Aguirre, S. Flores-Fierro, G. Martínez-Lorenzana, M. Condés-Lara, Effect of local infiltration with oxytocin on hemodynamic response to surgical incision and postoperative pain in patients having open laparoscopic surgery under general anesthesia, Eur. J. Pain 23 (2019) 1519–1526, https://doi.org/10.1002/ejp.1427.
[8] M. Condés-Lara, H. Zayas-González, A. Manzano-García, E. Córdova-Quiroz, J. Granados-Mortera, M. García-Cuevas, J. Morales-Gómez, A. González-Hernández, Successful pain management with epidural oxytocin, CNS Neurosci. Ther. 22 (2016) 532–534, https://doi.org/10.1111/cns.12551.
[9] G. Cirillo, D. de Luca, M. Papa, Calcium imaging of living astrocytes in the mouse spinal cord following sensory stimulation, Neural Plast. 2012 (2012) 1–7, https://doi.org/10.1155/2012/425818.
[10] D. Davalos, J.K. Lee, W.B. Smith, B. Brinkman, M.H. Ellisman, B. Zheng, K. Akassoglou, Stable in vivo imaging of densely populated glia, axons and blood vessels in the mouse spinal cord using two-photon microscopy, J. Neurosci. Methods 169 (2008) 1–7, https://doi.org/10.1016/j.jneumeth.2007.11.011.
[11] E.C. Emery, A.P. Luiz, S. Sikandar, R. Magnúsdóttir, X. Dong, J.N. Wood, In vivo characterization of distinct modality-specific subsets of somatosensory neurons using GCaMP, Sci. Adv. 2 (2016) e1600990, , https://doi.org/10.1126/sciadv.1600990.
[12] M.J. Farrar, I.M. Bernstein, D.H. Schlafer, T.A. Cleland, J.R. Fetcho, C.B. Schaffer, Chronic in vivo imaging in the mouse spinal cord using an implanted chamber, Nat. Methods 9 (2012) 297–302, https://doi.org/10.1038/nmeth.1856.
[13] K.K. Fenrich, P. Weber, M. Hocine, M. Zalc, G. Rougon, F. Debarbieux, Long-term in vivo imaging of normal and pathological mouse spinal cord with subcellular resolution using implanted glass windows, J. Physiol. 590 (2012) 3665–3675, https://doi.org/10.1113/jphysiol.2012.230532.
[14] H.C. Johannssen, F. Helmchen, Two-photon imaging of spinal cord cellular networks, Exp. Neurol. 242 (2013) 18–26, https://doi.org/10.1016/j.expneurol.2012.07.014.
[15] K.J. Sekiguchi, P. Shekhtmeyster, K. Merten, A. Arena, D. Cook, E. Hoffman, A. Ngo, A. Nimmerjahn, Imaging large-scale cellular activity in spinal cord of freely behaving mice, Nat. Commun. 7 (2016) 11450, https://doi.org/10.1038/ncomms11450.
[16] S. Vrontou, A.M. Wong, K.K. Rau, H.R. Koerber, D.J. Anderson, Genetic identification of C fibres that detect massage-like stroking of hairy skin in vivo, Nature 493 (2013) 669–673, https://doi.org/10.1038/nature11810.
[17] C. Luo, P.H. Seeburg, R. Sprengel, R. Kuner, Activity-dependent potentiation of calcium signals in spinal sensory networks in inflammatory pain states, Pain 140 (2008) 358–367, https://doi.org/10.1016/j.pain.2008.09.008.
[18] R. Ruscheweyh, J. Sandkühler, Long-range oscillatory Ca2+ waves in rat spinal dorsal horn, Eur. J. Neurosci. 22 (2005) 1967–1976, https://doi.org/10.1111/j.1460-9568.2005.04393.x.
[19] C.J. Woolf, M.W. Salter, Neuronal plasticity: increasing the gain in pain, Science 288 (2000) 1765–1768, https://doi.org/10.1126/science.288.5472.1765.
[20] M. Zimmermann, Ethical guidelines for investigations of experimental pain in conscious animals, Pain 16 (1983) 109–110, https://doi.org/10.1016/0304-3959(83)90201-4.
[21] E.A. Rendón-Ochoa, T. Hernández-Flores, V.H. Avilés-Rosas, V.A. Cáceres-Chávez, M. Duhne, A. Laville, D. Tapia, E. Galarraga, J. Bargas, Calcium currents in striatal fast-spiking interneurons: dopaminergic modulation of Ca V 1 channels, BMC Neurosci. 19 (2018) 42, https://doi.org/10.1186/s12868-018-0441-0.
[22] A. Aparicio-Juárez, M. Duhne, E. Lara-González, F. Ávila-Cascajares, V. Calderón, E. Galarraga, J. Bargas, Cortical stimulation relieves parkinsonian pathological activity *in vitro*, Eur. J. Neurosci. 49 (2019) 834–848, https://doi.org/10.1111/ejn.13806.
[23] J. Pérez-Ortega, M. Duhne, E. Lara-González, V. Plata, D. Gasca, E. Galarraga, A. Hernández-Cruz, J. Bargas, Pathophysiological signatures of functional connectomics in parkinsonian and dyskinetic striatal microcircuits, Neurobiol. Dis. 91 (2016) 347–361, https://doi.org/10.1016/J.NBD.2016.02.023.
[24] L. Carrillo-Reid, F. Tecuapetla, D. Tapia, A. Hernández-Cruz, E. Galarraga, R. Drucker-Colin, J. Bargas, Encoding network states by striatal cell assemblies, J. Neurophysiol. 99 (2008) 1435–1450, https://doi.org/10.1152/jn.01131.2007.
[25] V. Plata, M. Duhne, J. Pérez-Ortega, R. Hernández-Martinez, P. Rueda-Orozco, E. Galarraga, R. Drucker-Colín, J. Bargas, Global actions of nicotine on the striatal microcircuit, Front. Syst. Neurosci. 7 (2013) 78, https://doi.org/10.3389/fnsys.2013.00078.
[26] O. Jáidar, L. Carrillo-Reid, A. Hernández, R. Drucker-Colín, J. Bargas, A. Hernández-Cruz, Dynamics of the Parkinsonian striatal microcircuit: entrainment into a dominant network state, J. Neurosci. 30 (2010) 11326–11336, https://doi.org/10.1523/JNEUROSCI.1380-10.2010.
[27] A.B. Salinas-Abarca, S.H. Avila-Rojas, P. Barragán-Iglesias, J.B. Pineda-Farias, V. Granados-Soto, Formalin injection produces long-lasting hypersensitivity with characteristics of neuropathic pain, Eur. J. Pharmacol. 797 (2017) 83–93, https://doi.org/10.1016/j.ejphar.2017.01.018.
[28] F.Y. Zhang, Y. Wan, Z.K. Zhang, A.R. Light, K.Y. Fu, Peripheral formalin injection induces long-lasting increases in cyclooxygenase 1 expression by microglia in the spinal cord, J. Pain 8 (2007) 110–117, https://doi.org/10.1016/j.jpain.2006.06.006.
[29] K.Y. Fu, A.R. Light, W. Maixner, Long-lasting inflammation and long-term hyperalgesia after subcutaneous formalin injection into the rat hindpaw, J. Pain 2 (2001) 2–11, https://doi.org/10.1054/jpai.2001.9804.
[30] E.W. Keefer, A. Gramowski, G.W. Gross, NMDA receptor-dependent periodic oscillations in cultured spinal cord networks, J. Neurophysiol. 86 (2001) 3030–3042, https://doi.org/10.1152/jn.2001.86.6.3030.
[31] J.D. Xie, S.R. Chen, H. Chen, W.A. Zeng, H.L. Pan, Presynaptic N-methyl-D-aspartate (NMDA) receptor activity is increased through protein kinase C in paclitaxel-induced neuropathic pain, J. Biol. Chem. 291 (2016) 19364–19373, https://doi.org/10.1074/jbc.M116.732347.
[32] Z. Hong-mei, Z. Li-jun, H.U. Xiao-dong, H.U. Neng-wei, Z. Tong, L.I.U. Xian-guo, H.-M. Zhang, L.-J. Zhou, X.-D. Hu, N.-W. Hu, T. Zhang, X.-G. Liu, Acute nerve injury induces long-term potentiation of C-fiber evoked field potentials in spinal dorsal horn of intact rat, Sheng Li Xue Bao: [Acta Physiol. Sin.] 56 (2004) 591–596 (Accessed 5 March 2020), http://www.ncbi.nlm.nih.gov/pubmed/15497039.
[33] H. Ikeda, J. Stark, H. Fischer, M. Wagner, R. Drdla, T. Jäger, J. Sandkühler, Synaptic amplifier of inflammatory pain in the spinal dorsal horn, Science 312 (2006) 1659–1662, https://doi.org/10.1126/science.1127233.
[34] N.A. Nelson, X. Wang, D. Cook, E.M. Carey, A. Nimmerjahn, Imaging spinal cord activity in behaving animals, Exp. Neurol. 320 (2019) 112974, , https://doi.org/10.1016/j.expneurol.2019.112974.
[35] M. Condés-Lara, I.A.S. Maie, A.H. Dickenson, Oxytocin actions on afferent evoked spinal cord neuronal activities in neuropathic but not in normal rats, Brain Res. 1045 (2005) 124–133, https://doi.org/10.1016/j.brainres.2005.03.020.
[36] Y.H. Jo, M.E. Stoeckel, M.J. Freund-Mercier, R. Schlichter, Oxytocin modulates glutamatergic synaptic transmission between cultured neonatal spinal cord dorsal horn neurons, J. Neurosci. 18 (1998) 2377–2386 http://www.ncbi.nlm.nih.gov/pubmed/9502799.
[37] S. Caruso, C. Agnello, M.G. Campo, F. Nicoletti, Oxytocin reduces the activity of N-methyl — D — aspartate receptors in cultured neurons, J. Endocrinol. Invest. 16 (1993) 921–924, https://doi.org/10.1007/BF03348959.
[38] M. Mazzuca, M. Minlebaev, A. Shakirzyanova, R. Tyzio, G. Taccola, S. Janackova, S. Gataullina, Y. Ben-Ari, R. Giniatullin, R. Khazipov, Newborn analgesia mediated by oxytocin during delivery, Front. Cell. Neurosci. 5 (2011) 1–9, https://doi.org/10.3389/fncel.2011.00003.
[39] C.-Y. Jiang, T. Fujita, E. Kumamoto, Synaptic modulation and inward current produced by oxytocin in substantia gelatinosa neurons of adult rat spinal cord slices, J. Neurophysiol. 111 (2014) 991–1007, https://doi.org/10.1152/jn.00609.2013.
[40] G. Rojas-Piloni, M. López-Hidalgo, G. Martínez-Lorenzana, J. Rodríguez-Jiménez, M. Condés-Lara, GABA-mediated oxytocinergic inhibition in dorsal horn neurons by hypothalamic paraventricular nucleus stimulation, Brain Res. 1137 (2007) 69–77, https://doi.org/10.1016/j.brainres.2006.12.045.
[41] A. González-Hernández, G. Rojas-Piloni, M. Condés-Lara, Oxytocin and analgesia: Future trends, Trends Pharmacol. Sci. 35 (2014) 549–551, https://doi.org/10.1016/j.tips.2014.09.004.
[42] J. Qi, W.Y. Han, J.Y. Yang, L.H. Wang, Y.X. Dong, F. Wang, M. Song, C.F. Wu, Oxytocin regulates changes of extracellular glutamate and GABA levels induced by methamphetamine in the mouse brain, Addict. Biol. 17 (2012) 758–769, https://doi.org/10.1111/j.1369-1600.2012.00439.x.
[43] J.D. Breton, P. Veinante, S. Uhl-Bronner, A.M. Vergnano, M.J. Freund-Mercier, R. Schlichter, P. Poisbeau, Oxytocin-induced antinociception in the spinal cord is mediated by a subpopulation of glutamatergic neurons in lamina I-II which amplify GABAergic inhibition, Mol. Pain 4 (2008), https://doi.org/10.1186/1744-8069-4-19 1744-8069-4–19.
[44] W. Sun, Q. Zhou, X. Ba, X. Feng, X. Hu, X. Cheng, T. Liu, J. Guo, L. Xiao, J. Jiang, D. Xiong, Y. Hao, Z. Chen, C. Jiang, Oxytocin relieves neuropathic pain through GABA release and presynaptic TRPV1 inhibition in spinal cord, Front. Mol. Neurosci. 11 (2018) 248, https://doi.org/10.3389/fnmol.2018.00248.
[45] Y. Nersesyan, L. Demirkhanyan, D. Cabezas-Bratesco, V. Oakes, R. Kusuda, T. Dawson, X. Sun, C. Cao, A.M. Cohen, B. Chelluboina, K.K. Veeravalli, K. Zimmermann, C. Domene, S. Brauchi, E. Zakharian, Oxytocin modulates nociception as an agonist of pain-sensing TRPV1, Cell Rep. 21 (2017) 1681–1691, https://doi.org/10.1016/j.celrep.2017.10.063.

Journal of Neuroscience Methods 350 (2021) 109048

Contents lists available at ScienceDirect

Journal of Neuroscience Methods

journal homepage: www.elsevier.com/locate/jneumeth

CLARITY with neuronal tracing and immunofluorescence to study the somatosensory system in rats

Guadalupe Martínez-Lorenzana, Mohammed Gamal-Eltrabily, Irma Alejandra Tello-García, Ataulfo Martínez-Torres, Marymar Becerra-González, Abimael González-Hernández, Miguel Condés-Lara *

Departamento de Neurobiología del Desarrollo y Neurofisiología, Instituto de Neurobiología, Universidad Nacional Autónoma de México, Campus Juriquilla, Boulevard Juriquilla, No. 3001, C.P. 76230, Querétaro, Mexico

ARTICLE INFO

Keywords:
Neuronal tracers
Immunofluorescence
CLARITY

ABSTRACT

Background: The CLARITY technique enables researchers to visualize different neuronal connections along the nervous system including the somatosensory system.
New method: The present work describes the antero-lateral and dorsal column pathways until the thalamic and cortical stations, as well as descending oxytocinergic and vasopressinergic innervations by means of combined CLARITY, neuronal tracing, and immunofluorescence techniques. We used male Sprague-Dawley rats of 13, 30, and 60 days.
Results: The main results are as follows: A) CLARITY is a reliable technique that can be combined with fluorescent neuronal tracers and immunofluorescence techniques without major procedure modifications; B) at spinal level, some primary afferent fibers were labeled by CGRP, as well as the presence of neuronal populations that simultaneously project to the gracile and ventral posterolateral thalamic nuclei; C) corticothalamic connections were visible when retrograde tracers were injected at thalamic level; D) oxytocin receptors were expressed in the spinal dorsal horn by GABAergic-positive neurons, reinforcing previous outcomes about the possible mechanism for oxytocin blocking the primary afferent sensory input.
Comparison with existing methods and Conclusions: The CLARITY technique lets us observe in a transparent way the entire processed tissue compared with classical histological methods. CLARITY is a potentially useful tool to describe neuroanatomical structures and their neurochemical stratus.

1. Introduction

Many studies have aimed at describing the fine structure of the central nervous system (CNS) and its relationship with specific motor, sensory or affective functions, among others. The beginning of this field was highlighted by the emergence of staining techniques, neuronal tracers (Mesulam, 1982) and immunohistochemical procedures to describe the biochemical nature of the CNS. In this context, techniques that make the brain transparent (e.g., CLARITY and CUBIC) have been to applied to understand the organization of the CNS or even whole organisms (for reviews, see Aswendt et al., 2017; Richardson and Lichtman, 2015; Silvestri et al., 2016).

Recently, Wang et al. (2020) described that both FG and FR, unlike viral tracers, were compatible with some other tissue clearing techniques e.g. FRUIT and 3DISCO which were implicated to successfully visualize primary motor cortex descending projections to the spinal cord. They could visualize the entire cortico spinal pathway using a two-photon microscope.

Specifically, CLARITY has been successfully applied in mouse brain immunestained against tyrosine hydroxylase, choline acetyltransferase parvalbumin glial fibrillary acidic protein, and DAPI (Chung and Deisseroth, 2013a,b; Chung et al., 2013a,b). The CLARITY technique has also been used in immunofluorescence procedures in rat brains for neuropeptide Y, and anti-pro-oxyphysin (Zheng and Rinaman, 2016). The combination between fluorescent dyes and tissue clearing technique may result challenging, since the latter can induce some tissue changes that diminish fluorescent proteins affinity, as well as, issues related to autofluorescence (Lai et al., 2017). However, Chung et al. (2013a),b

* Corresponding author.
E-mail address: condes@unam.mx (M. Condés-Lara).

https://doi.org/10.1016/j.jneumeth.2020.109048
Received 7 September 2020; Received in revised form 15 December 2020; Accepted 18 December 2020
Available online 24 December 2020

discussed the efficiency of CLARITY technique use in obtaining 3D fluorescence images of adult mouse brain.

From our perspective, CLARITY procedure can be important in visualizing numerous elements in CNS including the ascending and descending nociception-related structures involving the neurochemical factors related.

In this sense, the somatosensory system includes two independent systems that transmit the incoming sensory information from specific peripheral receptors to the supraspinal structures. The two systems are: 1) the anterior lateral (AL) and 2) the dorsal column–medial lemniscus (DC). Recent evidence suggests that some spinal neuronal populations project simultaneously within both systems (Condés-Lara et al., 2018), adding more complexity to their organization. Calcitonin gene-related peptide (CGRP) is another important peptide related to the somatosensory process at the level of primary afferent fibers (Cameron et al., 1988; Hökfelt et al., 1992). Moreover, descending oxytocinergic projections at spinal have been related to nociception modulation through local GABAergic mechanisms (Rojas-Piloni et al., 2007; Breton et al., 2008).

These observations demand further analysis to reinforce the structural organization of the CNS and provide the basis for functional approaches (i.e., electrophysiology); thus, a reliable, clear microscopic view of the nervous system, maintaining the integrity of the tissue and its neuronal connections instead of reconstructing the nervous system from sections, is required.

Afterward, the structure, organization, and function of brain cells has been a big challenge for neuroscientists and CLARITY could become a solution to the problem.

Indeed, combining neuroimaging techniques with ex vivo brain cleaning and light-sheet imaging, described as incompatible by Aswendt et al. (2017), at present, they could provide a new entry for studying the CNS organization, as well as function-structure relations by their possible combination with electrophysiological approaches.

In this study, we describe the performance of CLARITY in rats within different age groups and its successful combination with fluorescent neuronal tracers and immunofluorescence techniques to study elements of the somatosensory system, including the ascending AL and DC systems, the participation of CGRP in primary afferent fibers, and the descending oxytocinergic innervations and their local relation to local spinal GABAergic neurons.

2. Materials and methods

The experiments were carried out in accordance with the animal procedures and protocols approved by the Institutional Ethics Committee and following the ethical guidelines of the IASP (Zimmermann, 1983) and the Guide for the Care and Use of Laboratory Animals established by the NIH (2011). Also, ARRIVE guidelines was taken into account. *Male Sprague-Dawley rats divided into 3 groups: 1) group 1 (n = 2) of 13 days of birth; 2) group 2 (n = 2) of 30 days of birth and group 3 (n = 3) of adult rats of 60 days of age (with an average weight of 280–310 g) (see Table 1).*

The rats were individually housed in a temperature-controlled environment (23 ± 3 °C) and under a 12 h/12 h light/dark cycle with food and water *ad libitum*.

Table 1
Experimental conditions and tracer or immunofluorescent type used in each experimental group.

Groups	Experimental conditions	
Group 1: animals of 13 days of birth	Neuronal tracer TB, NB, TMR (n = 2)	
Group 2: rats of 30 days of birth	Neuronal tracer TMR (n = 1)	Immunofluorescent CGRP staining (n = 1)
Group 3: adult rats of 60 days of age	Neuronal tracer FG, TMR (n = 1)	Immunofluorescent GABA/OTR, OT/AVP staining (n = 2)

2.1. Injection of neural tracers

The animals were anesthetized by intraperitoneal injection of a mixture of ketamine and xylazine (70/6 mg/kg) and mounted in a stereotaxic apparatus. Then, 100 nl tetramethylrhodamine-labeled dextran (TMR, 3000 MW, lysine fixable from Invitrogen™) were injected in the left ventral posterolateral nucleus (VPL) of the thalamus, whereas 100 nl Fluoro-Gold™ (FG, Fluorochrome LLC, USA) or Neurobiotin® 488 (NB, Vector, laboratories) were injected into the right VPL with a Hamilton syringe coupled to a vernier. *In the case of animals with >30 days of age the following interaural stereotaxic coordinates were used: AP 5.4; L 3.2; H 3.5 mm (Paxinos and Watson, 1998). In the case of rats with 13 days-old rats we used external coordinates, from lambda (4.2 ± 0.2 mm anterior; from the medial line 2.8 ± 0.3 mm; and from the skull 4 ± 0.2 mm in deep).*

Furthermore, two granules of True Blue (TB, Sigma) were administered to the left side of the gracile nucleus (GRA). The rats were left for 4 or 13 days of survival depending on their age. Subsequently, the animals were deeply anesthetized with sodium pentobarbital (45 mg/kg; i.p.), and the extracted tissue was processed through CLARITY, a passive tissue clearing technique described by Zheng and Rinaman (2016).

2.2. CLARITY technique

Transcardiac perfusion was performed using 20 mL of cold 1X phosphate-buffered saline (PBS, pH 7.4) (Invitrogen, GIBCO 10,010) for rats of 13 days of birth and 40 mL for animals of 30 or 60 days of age, followed by hydrogel solution (150 mL for rats of 13 days of birth and 200 mL for animals 30 or 60 days of age) which contains 4% paraformaldehyde (Electron Microscopy Sciences, 15,710-S), 4% acrylamide (Bio-Rad, 161−0140) and 0.25 ٪ VA-044 initiator (Wako, 27776−21-2) in 50 mL a conical falcon tube with hydrogel solution for post-fixation and stored overnight in the same solution at 4 °C. The next procedure followed was to fill the Falcon tube with hydrogel solution and carefully seal it with parafilm, to avoid the eventual hydrogel immersed brain hybrids to oxygen in the air. We did not use of mineral oil nor nitrogen degassing described in other studies as a necessity for subsequent polymerization of acrylamide monomers (Chung et al., 2013a,b; Yang et al., 2014; Zheng and Rinaman, 2016). On the next day, polymerization was carried out for 3 h in a 37 °C water bath without shaking. The brain and spinal cord were placed in 40 mL of tissue clearing solution (0.2 M boric acid, pH 8.5 (Sigma-Aldrich, 339,067) containing 4.0 % sodium dodecyl sulphate (SDS) (Promega, H5114) in 50-ml falcon tubes. Later, the samples were placed in a rotating shaker incubator at 100 rotations/ minutes at 37 °C. The tissue clearing solution was replaced daily during the first week and then every 3 days. The samples were cleared for 14 days in case of animals of 13 and 30 days and for 30 days in case of adult animals.

Some tissues were analyzed only for neuronal tracers and others underwent an immunofluorescence procedure (see Table 1).

3. Immunofluorescence

For immunofluorescence procedures, the cleared tissue was transferred to 15 mL Falcon tubes to be washed in a 0.5 M boric acid (pH 8.5) solution containing 0.1 % Triton X-100 (rinsing buffer) to remove SDS residues. The following primary antibodies were used: anti-neurophysin (PS60, mouse, monoclonal, diluted 1: 250; a gift from Dr. H. Gainer from the National Institute of Neurological Disorders and Stroke, NIH, Bethesda MD); anti-AVP (polyclonal, rabbit, diluted 1: 500; Cat.no. AB1565, Millipore, Chemicon International, Temecula CA), anti-GABA (polyclonal, rabbit, diluted 1: 1500; Cat. No. A2052, SIGMA, USA), anti-CGRP (polyclonal, rabbit, diluted 1: 2000; Cat. No. AB15360 Chemicon International, Temecula CA), anti-OTR (polyclonal, goat, diluted 1: 400, Cat.no. sc-8103; Santa Cruz Biotechnology Inc, Santa

Cruz, CA, USA). A cocktail of two primary antibodies (2.5 mL) raised from different species were used in a 15 mL falcon tube and placed in a rotating shaker incubator for 72 h at 37 °C. Then, a 24 h wash was performed with a rinsing buffer, and the following secondary antibodies were added, diluted 1:300, depending on the characteristics of the primary antibody: donkey anti-goat IgG (Alexa Fluor 647 conjugate, Cat. no. A-21,447 or Alexa Fluor 488 conjugate, Cat.no. A11055); donkey anti-Rabbit IgG (Alexa Fluor 647 conjugate, Cat.no.A-31573, Alexa Fluor 555 conjugate, Cat.no A31572); donkey anti-mouse IgG (Alexa Fluor 488 conjugate, Cat.no. A21202). All secondary antibodies were obtained from Invitrogen, USA. Samples were incubated for 48 h at 37 °C in a rotating shaker in a 2.5 mL volume in a 15 mL falcon tube. Finally, the unbound antibodies were removed by washing in the rinsing solution.

Before imaging, the tissue was equilibrated in 1X PBS overnight at room temperature, then placed in 2,2′thiodiethanol (TDE, Sigma-Aldrich, 166,782) at serial concentrations of 20 %, 40 % and 60 % consecutively for 4–12 hours in each of them at room temperature without shaking. The tissue was kept in 60 % TDE for observation. Image acquisition was performed using a Zeiss 780 DUO confocal microscope with an Argon Multiline laser (emission 458-488−514 nm), DPSS laser emission at 561 nm and HeNe laser emission at 633 nm; as well as a multiphotonic system, the range of wavelength used to detect the different tracer and fluorophore are plotted in Table 2, with objectives of EC Plan-Neofluar 10x / 0.30 M27 lens with working distance of 5.2 mm – cover glass 0.17 mm and LD LCI Plan-Apochromat 25X / 0.8 lmm Korr DIC M27 (multi-immersion) with working distance of 0.57 mm – cover glass 0.17 mm, motorized stage and Zen by Zeiss software.

Depending on the thickness of the sample, 23.5–1025 Z-plane optical sections were obtained in steps of 0.5 or 5.00 µm. Images were rendered from the lumbar and thoracic segments of the spinal cord, as well as from complete brain tissue. Depending on the size of the sample, optical sections were acquired at a resolution of 1024 × 1024 or 512 × 512 pixels and scanned 4 times to reduce noise. In all cases, the images were enhanced (brightness and gamma) and analyzed with the ZEN 2 Blue Edition software (Carl Zeiss Microscopy GmbH, Göttingen, Germany). A two-dimensional projection, a single optical section or a 3D projection of the image (see supplementary video) was performed as applicable; the images were imported in file format (TIFF).

4. Results

Cleared CNS tissue was analyzed under a multiphotonic microscope to simultaneously detect neuronal fluorescent tracers and selective fluorescent antibodies. This tissue preparation allowed optimal observation of the tissue under light, fluorescence or confocal microscopes, thus providing a range of potential applications. Here we show the utility of the CLARITY and histological techniques in different areas of the CNS related to the somatosensory system.

Our first approach was to study the primary afferent fibers arriving at the spinal cord. The lumbar segment of the spinal cord of a 30-day-old animal was cut cross-sectionally into 4-mm blocks and processed for anti-CGRP immunofluorescence, and a confocal image projection was obtained from this region. In Fig. 1, the CGRP-labeled fibers noticeably arrive at the dorsal horn layers of the L4 segment of the spinal cord.

Furthermore, we continued with the histological analysis of cleared lumbar segments with different fluorescent neuronal tracers (see Fig. 2A) under confocal microscopy. This tissue presented labeled neurons on both sides of the dorsal horn of the spinal cord in 13-day-old animals. In the 13-day-old group, animals were injected with TB in the left GRA, TMR in the left VPL and NB in the right VPL. Fig. 2B shows a Z-stack projection of confocal mosaic images of this area. Upon analyzing ventrodorsally the spinal dorsal horn of the lumbar segment, and taking the midline as a reference, the TB-labeled neuronal groups were observed at the depth between 25−95 µm and 145−235 µm on both sides of the lumbar segment, in the middle and lateral parts of the Y axis. An example of TB-labeled cells is shown in Fig. 2D. TMR-labeled neurons were found at a depth between 80−125 µm and 165−340 µm on both sides and well distributed in both the middle and lateral parts of the horn (Fig. 2C). Regarding the NB tracer, the highest portion of labeled neurons was found at a depth of 200−235 µm, also distributed from the middle to lateral part of the spinal horn with respect to the midline and Y axis; an example of these cells is shown in Fig. 2E. Furthermore, we observed double- and triple-labeled neurons along the spinal horn; examples of these cells are shown in Fig. 2 F1−5.

The neural tracers are retained in cells after CLARITY technique, as well as their rostro-caudal distribution along the entire X axis of the lumbar segment of the spinal cord. In addition, it is worth mentioning that after CLARITY procedures, the TMR was preserved in magnificent conditions. Independently of animal age, TMR was successfully detected, without apparent alterations, in 30-day-old animals. In these animals, the TMR was injected unilaterally into the right VPL and many neurons were observed throughout the lumbar segment of the spinal cord from the rostral to the caudal part (Fig. 3A). These neurons are widely distributed on both sides of the horn, from the mid-region to its lateral part; an example of a group of TMR-labeled neurons is shown in Fig. 3B.

Further analysis was done regarding the distribution of neuronal tracer labeling in the spinal cord at L5 level. In this condition, the tissue portion in Fig. 2B was transversally analyzed. TMR injected into the left VPL (Fig. 4A), NB into the right VPL (Fig. 4B), and TB into the left GRA (Fig. 4C) labeled neurons bilaterally at L5 level. Fig. 4D shows a merged image of the same region in the different channels, and white spots depict triple-labeled cells. In Fig. 4E, a superimposition of this image with a scheme of the spinal cord at L5 presents the bilateral and deep distribution of spinal cord cells projecting to supraspinal levels.

Furthermore, we analyzed the corticothalamic projections of the somatosensory system. The ipsilateral VPL projections towards the cerebral cortex (Cx) were analyzed in two animals, one with TMR injected into the right VPL and the other with FG injected into the left VPL. The brain of the first animal was cleared, and a coronal block from interaural 6.88 mm to 1.20 mm, examined under the confocal microscope in a single field rostro-caudal extension, was obtained (see Fig. 5A). In this field, at S1HL level, a characteristic and stratified neuronal group was detected along layer VI of the Cx (Fig. 5A). The brain of the second animal was cleared, and a sagittal block from the lateral 1.90 mm–3.90

Table 2
Characteristics used in confocal microscopy for the use and detection of different neuronal tracers and fluorophores. The parameters used as Laser type, intensity, excitation and emission wavelengths, and the range of wavelength used for True blue (TB), Neurobiotin® 488 (NB), tetramethylrhodamine-labeled dextran (TMR), Fluoro-Gold™ (FG) and Alexa Fluor-488, -555, -647 detection are plotted. Excitation and Emission fluorescence values are approximate.

Tracer or Fluorophores	Lasers nm	Laser power %	Excitation Wavelength nm.	Emission Wavelength nm.	Range of wavelength used nm.
TB	750 multiphotonic system	8.0	365	425	371−451
NB	488	2.6	493	517	492−540
TMR	561	2.6	555	580	560−581
FG	730 multiphotonic system	6.5	373	565	498−594
Alexa Fluor-488	488	3.5	495	519	495−519
Alexa Fluor-555	561	1.2	555	565	556−579
Alexa Fluor-647	633	5.0	650	668	638−671

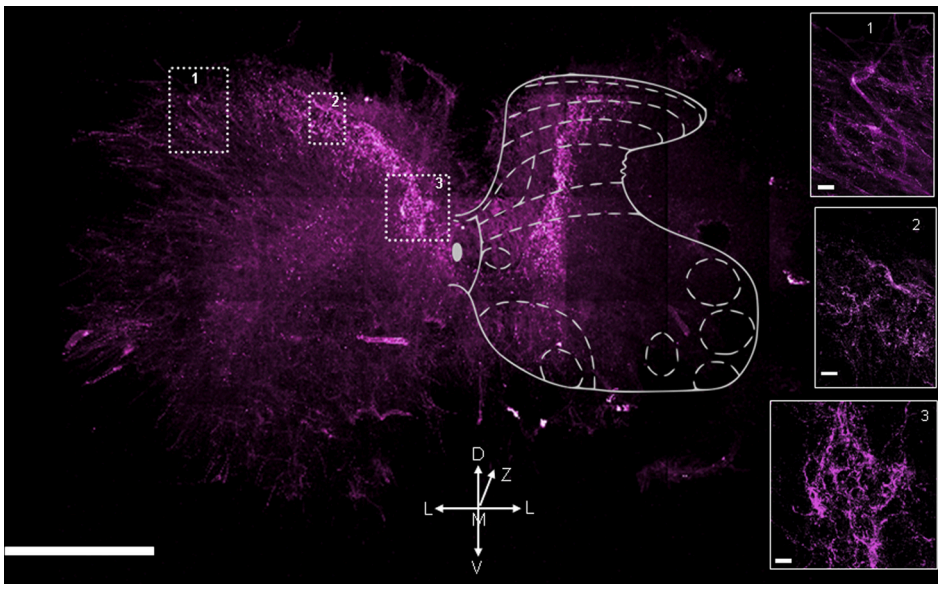

Fig. 1. Image from a cleared block of the lumbar segment (L4) of a 30-day-old animal's spinal cord. Transverse section from a block of 4 mm thyck showing peripheral CGRP-labeled fibers coming into the dorsal horn. Image obtained with an objective LD LCI Plan-Apochromat 25x/0.8 lmm Korr DIC M27, stack size; X=2720.62 μm, Y=2040.46 μm and Z=115 μm at a step size of 1.00 μm, scale bar=500 μm. The scale bar in 1, 2, and 3 are 20 μm.

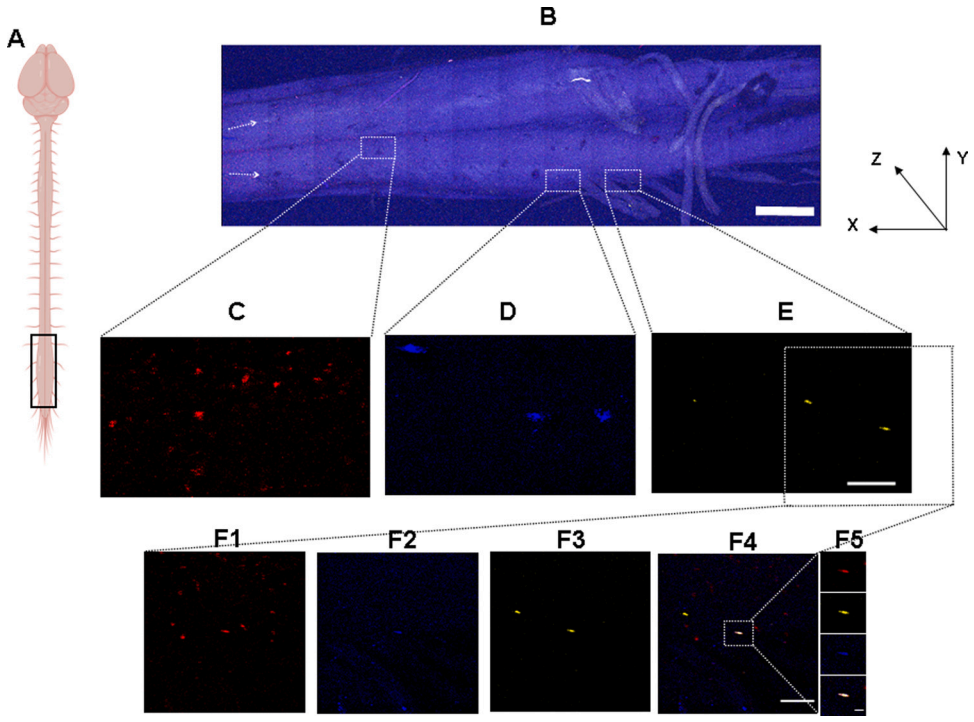

Fig. 2. Retrograde tracer preserved after CLARITY in the 13-day-old rat spinal cord. (A) A diagram of the spinal L1-S1 segment chosen for the analysis. **(B)** A projection of confocal images of the lumbar segment with neural tracers; the midline is clearly visible X = anteroposterior plane; Y = mediolateral plane; Z = dorsoventral plane (stack size; X=11052.50 μm, Y=3400.77 μm and Z=1100.00 μm. Notice that the clearest portion of the dorsal horn shows the stained cells (by transparency; see the arrow). For the mosaic, we used a step size of 5.00 μm (scale bar = 1 mm). **(C)** TMR-labeled neurons, injected in the left VPL, **(D)** TB-labeled neurons, injected in the left GRA, and **(E)** NB-labeled neurons, injected in the right VPL, scale bar=100 μm. **(F)** Multiple labeling in a neuronal group: **(F1)** TMR-labeled cells, **(F2)** TB-labeled cells, **(F3)** NB-labeled cells, **(F4)** the merge (**F1**+**F2**+**F3**) depicting a triple-labeled neuron (scale bar=100 μm), and **(F5)** a crop of the triple-labeled neuron obtained with all the neuronal tracers, scale bar=20 μm. Images obtained with a Zeiss 780 confocal microscope with an EC Plan Neofluar 10x/0.30 M27 lens. Image in B is illustrated in 3-D in SUPPLEMENTARY MATERIAL Fig. 1.

mm was analyzed under the confocal microscope in a medio-lateral extension, and a group of FG-labeled neurons was found in the same S1HL region (Fig. 5B).

In these same animals, the lumbar segment of the spinal cord was cleared and processed for anti-GABA or anti-OTR immunofluorescence in a 4 mm block from L5 to S2 segments to observe descending pathways. A Z-series of images revealed a large population of GABA-and OTR-labeled cells, which resulted in double-labeled neurons (Fig. 6 B1-B3). Fig. 6C1-C3 depicts GABAergic interneurons expressing OTR with 3.0x confocal zoom magnification.

Finally, the thoracic spinal segment obtained from adult animals was also cleared and observed under a confocal microscope. Dorsoventral images were acquired at the level of T8 segment, where OT and AVP-labeled fibers were observed on both sides of the spinal cord along its rostro-caudal extension. This suggests that these fibers pass through the lateral intermediate nucleus (IML) of the spinal cord since they are observed approximately 300 μm lateral to the midline (Fig. 7B). In addition, single optical sections from this area showed the presence of double-labeled fibers (OT/AVP) (Fig. 7B1 and B2).

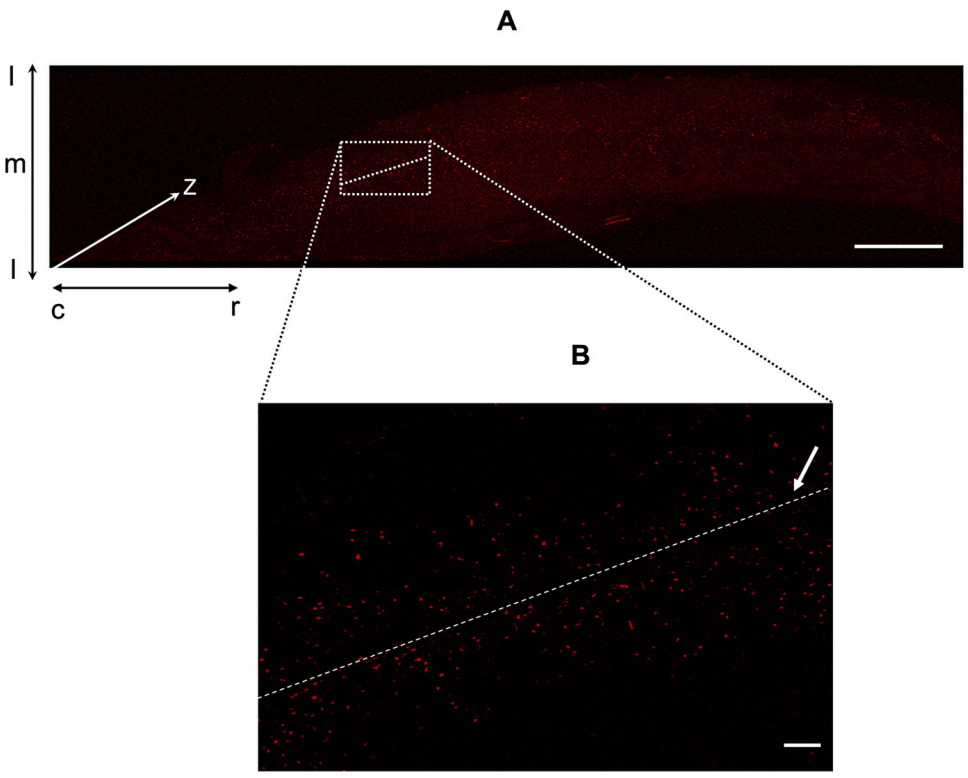

Fig. 3. CLARITY technique with TMR neuronal tracer applied in the spinal cord lumbar segment of a 30-day-old animal. (A) Confocal imaging of the lumbar enlargement (10x objective, stack size; X caudal (c) to rostral (r)= 11902.69 μm; Y medium (m) - lateral (l)= 2550.58 μm and Z=1025.00 μm at step size of 5.00 μm, scale bar = 1 mm). **(B)** A single optical section of TMR-labeled neurons on both sides of the dorsal horn; the arrow indicates the dotted line that demarcates the midline, scale bar=100 μm. Z: Dorso-Ventral Y: Medio-Lateral X: Caudal-Rostral.

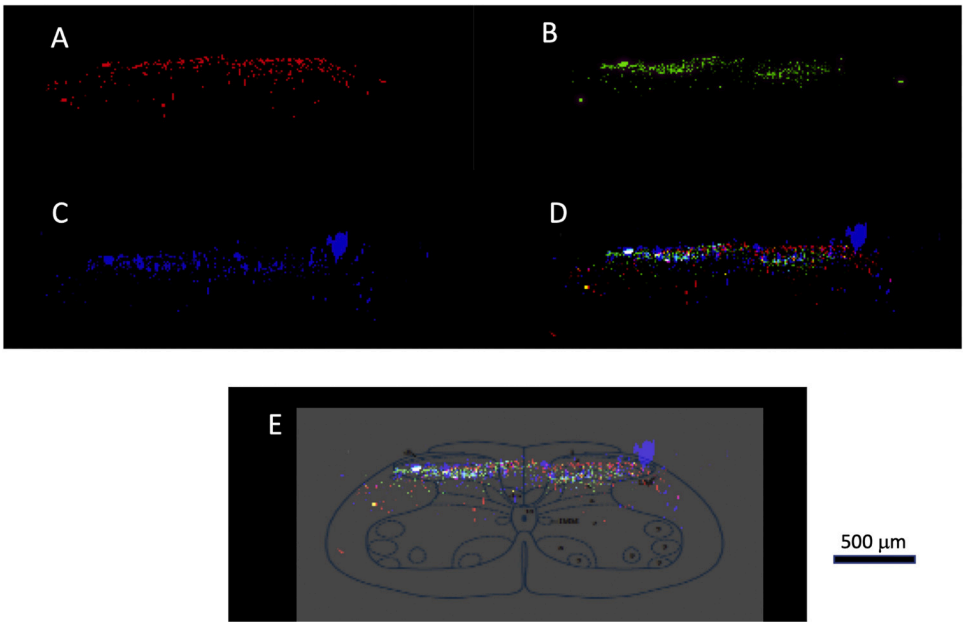

Fig. 4. Supraspinal retrograde transport to the spinal dorsal horn in CLARITY tissue. Using the confocal projection from Fig. 1, we observed L5 segment in a transversal section. **(A)** TMR-labeled neurons after injection into the left VPL. **(B)** NB-labeled neurons after injection into the right VPL. **(C)** right TB-labeled neurons after being injected into the GRA. **(D)** A merged image is depicting triple-labeled neurons in white. **(E)** Merged image is superimposed to an L5 spinal cord diagram to illustrate the neuronal distribution. Notice that positive cells are present on both sides of the spinal dorsal horn, nevertheless the injected side.

5. Discussion

Here, we demonstrate that the CLARITY technique could be successfully performed in young animals (13 and 30 days of age) and adult animals (60 days of age). Besides, our results show that neuronal tracing or immunofluorescence techniques can be combined with the CLARITY technique and adequately conserved after tissue clearing.

The CLARITY technique has been performed in young animals of up to 24days of age (Zheng and Rinaman, 2016). Many concerns were postulated about the possibility of applying this procedure in nervous tissue obtained from adult animals. Our results show that the CLARITY technique can be successfully performed in 60-day-old animals, suggesting that it could be valuable tool for studying morphological aspects of the nervous system in both young and adult animals.

As a first approach, we studied the first afferent coming from the skin receptors with the CLARITY technique combined with an immunofluorescent procedure to notice the CGRP (see Fig. 1). The CGRP neuropeptide was selected for its involvement in somatosensory and nociception processing and has been reported mainly in the dorsal root ganglion neuron somas (Cameron et al., 1988; Hökfelt et al., 1992; McNeill et al., 1988). Additionally, CGRP was detected in unmyelinated C and finely myelinated A fibers within laminae I, II outer (IIo) and V of

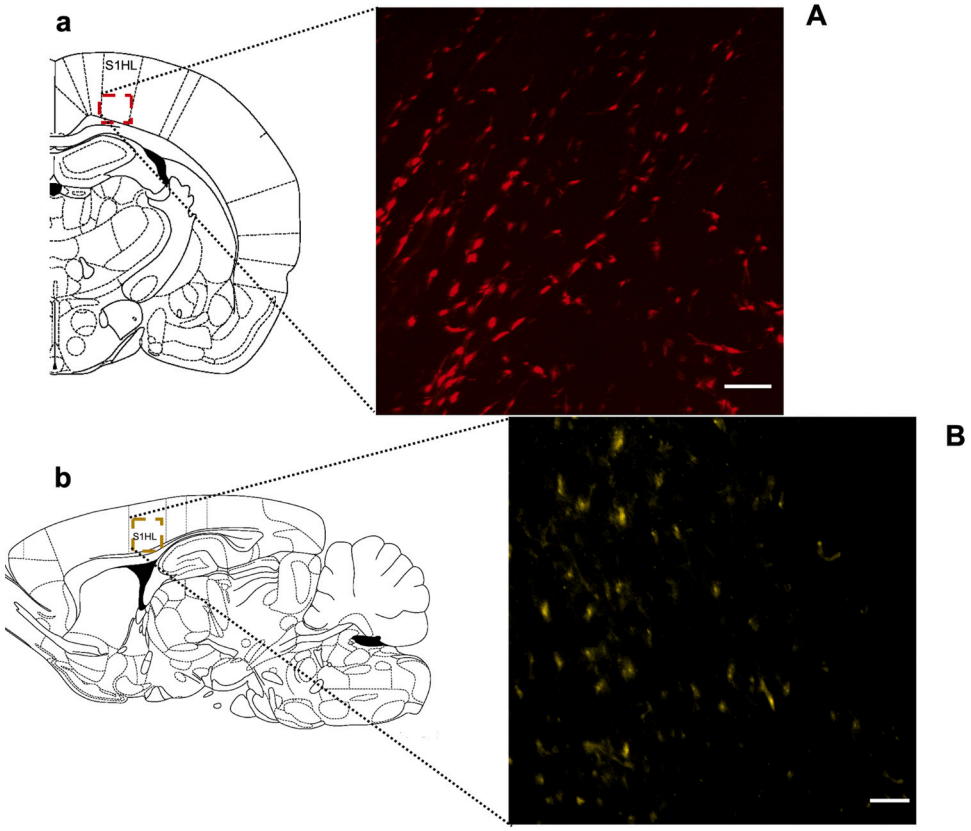

Fig. 5. TMR labeling cerebral cortex cells after neuronal tracers injected into the VPL of an adult animal. **(A)** Confocal image (10x objective, stack size; X=850.19 μm, Y=850.19 μm and Z=712.00 μm at a step size of 1.00 μm, scale bar=100 μm) of TMR-labeled neurons in cortex obtained from coronal block at AP 6.88 mm interaural **(a)**. **(B)** Confocal image of FG-labeled cortical neurons (25x objective; stack size X=340.08 μm, Y=340.08 μm and Z=25.00 μm at step size of 1.00 μm, scale bar=100 μm) of a sagittal block at L: 1.90 mm (Paxinos and Watson, 1998) **(b)**.

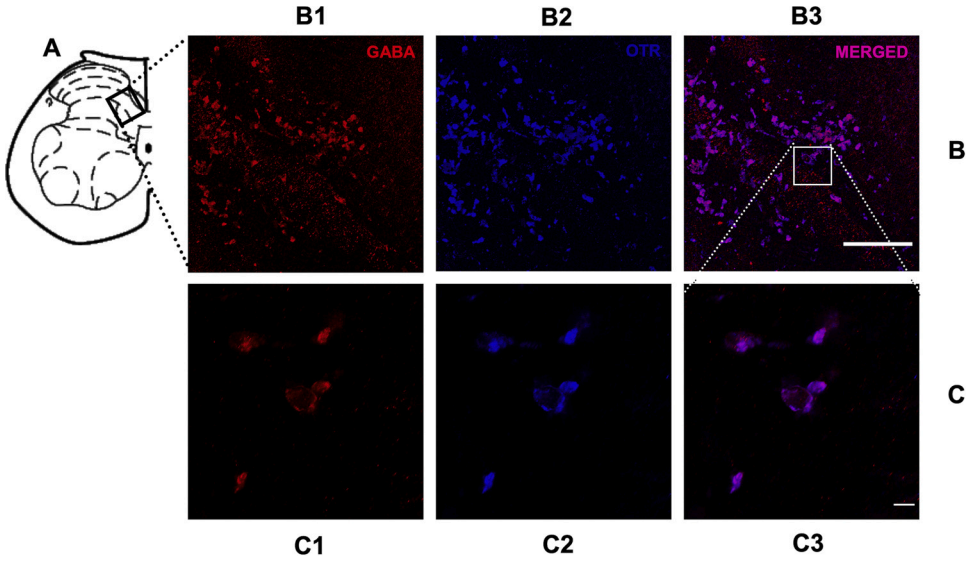

Fig. 6. GABA and OTR immunofluorescence in CLARITY tissue at L5 to S2 region of an adult rat. (A) A L5 segment with a box in the spinal cord's dorsal horn obtained from (Paxinos and Watson, 1998). **(B)** The images show the colocalization of GABAergic interneurons (RED) with OTR (BLUE) (25x objective, stack size; X=340.08 μm, Y=340.08 μm and Z=133.00 μm at step size of 0.50 μm, scale bar=100 μm). **(B1)** GABA-labeled neurons **(B2)** OTR-labeled cells and **(B3)** double-labeled cells coming from the merge of (B1) and (B2). **(C)** The image shows a crop from (B) obtained in all the channels (25x objective, 3.0x confocal zoom, stack size; X=112.34 μm, Y=112.34 μm and Z=23.50 μm at step size of 0.50 μm, scale bar=10 μm). **(C1)** GABA-labeled neurons **(C2)** OTR-labeled cells and **(C3)** the merge of (C1) and (C2) showing double-labeled cells.

the spinal dorsal horn and, to a lesser extent, in sympathetic and motor neurons in the intermediolateral and ventral horns (Gibson et al., 1984; Hökfelt et al., 1992; Ishida-Yamamoto and Tohyama, 1989; Marti et al., 1987; Senba and Tohyama, 1988; Willis and Coggeshall, 2004; Woolf and Wiesenfeld-Hallin, 1986). Interestingly, spinal cord injury (a chronic pain model) increased CGRP labeling, identified by means of immunocytochemistry techniques, in laminae III and IV bilaterally at the level of the hemisection, as well as in the two rostral and caudal segments close to the lesion site (Christensen and Hulsebosch, 1997; Sliwinski et al., 2018). In this study, we observed the presence of CGRP-labeled fibers (see Fig. 1 ()) in laminae I–V and the contour of the ventral horn on both sides of the spinal cord at L4 level detected by combined CLARITY and immunofluorescence techniques without any peripheral or spinal cord lesions. We believe that the CLARITY technique, when combined with immunofluorescence tools, can be useful for the detection of peptides or receptor expression in the spinal cord of adult rats.

In this context, neuronal tracers of the carbocyanine family (lipophilic neuronal tracers like DiI,) were cleared using the CLARITY technique (Jensen and Berg, 2016). However, modifications in the compound's molecular structure were required to avoid neuronal tracer clearance from the tissue during the rinsing process (Jensen and Berg,

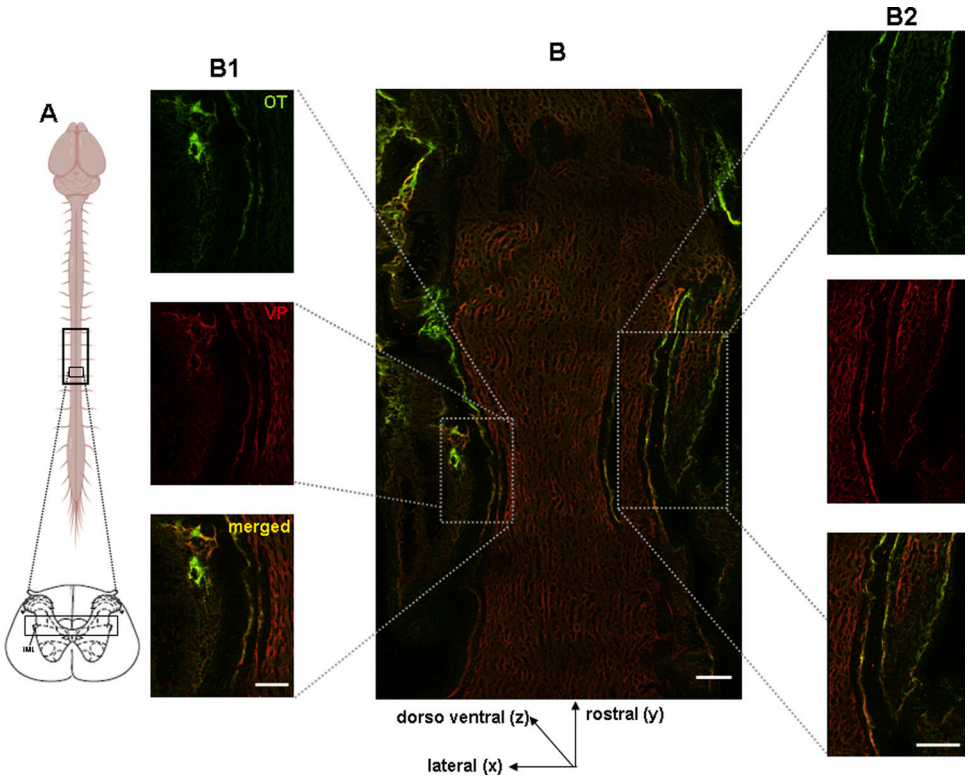

Fig. 7. Combined CLARITY and immunofluorescence (anti-OT and anti-VP) techniques in the spinal thoracic segment of an adult animal. (A) A diagram of the spinal cord showing the area analyzed in CLARITY. **(B)** Dorsomedial projection of confocal images obtained from the thoracic region at T8 level, where oxytocinergic fibers are labeled in green and vasopressinergic fibers labeled in red present at both lateral ends of the spinal cord running along the rostro-caudal axis (25x objective, stack size; X=1020.23 μm, Y=1700.38 μm and Z=295.00 μm at step size of 1.00 μm, scale bar=100 μm). **(B1)** An example of double-labeled fibers (OT/AVP fibers) obtained from a single optical section on the left side and **(B2)** on the right side of the spinal segment. In (B1) and (B2), OT-labeled fibers are in green, VP-labeled fibers in red and the double-labeled fibers are in yellow, scale bar=100 μm.

2016). We show that fluorescent dextran tracers with fixable lysin sidechains (i.e. TMR), biotin-based tracers (i.e. neurobiotin), and other small tracers i.e. FG and TB (Köbbert et al., 2000; Vercelli et al., 2000), were successfully conserved during the passive CLARITY process.

An important thing to consider when using the FG is the range of wavelength as well as with all other tracers, but in the case, it is an easy tracer but with a broad wavelength. See Table 2. Moreover, FG is a retrograde tracer, and it is no so god as a pathway's tracer at least in our case, we use FG to stain cellular corps of projecting neurons. Moreover, As FG is an inherently fluorescing compound, the only procedure necessary to study transport is sectioning and fluorescence microscopy. No histology other than fixation is required. Even in fresh tissue, fluorescence is intense. The addition of an anti-fading agent to the mounting medium is not necessary since FG has a remarkable photobleaching-resistance capacity.

Our results show the presence of spinal neurons that project towards the ipsilateral GRA (TB-labeled) and bilaterally to the VPL (NB-labeled and TMR-labeled) (Fig. 2C-D-E). These projections have been previously described as part of the AL and DC systems involved in transmitting somatosensory and pain information, respectively (Condés-Lara et al., 2018). The presence of triple-labeled neurons (TMR-TB-NB positive) (Fig. 2F) suggests the existence of certain neuronal populations in the spinal cord dorsal horn that participate in both pathways. A previous study in our laboratory described the presence of bifurcated spinal neurons in 60-day-old rats (Condés-Lara et al., 2018). Here, using a combined neuronal tracer and CLARITY technique, we show this neuronal population (Fig. 4) in both 13-day-old and 30-day-old animals.

Regarding the corticothalamic pathways, reciprocal interconnections between somatosensory cortices (SI and SII) and the thalamic VPL have been documented (Jones, 1985). Cappe et al. (2007) described a dual pattern of the cortical projections towards the VPL in rodents; numerous innervations arising from cortical layer VI end in small terminations within the VPL and, unlikely, fewer projections from layer V that form giant terminations in this thalamic nucleus. Monconduit et al. (2006) studied the SI–VPL interconnections in the somatosensory process and demonstrated, by means of neuronal tracer and histochemical techniques, the presence of retrogradely labeled neurons with apical dendrites in layer VI of the SI, being denser between bregma −1.3 and 0.8 mm (Paxinos and Watson, 2007) and progressively decreasing in both caudal and rostral directions. These studies support our results regarding the characteristic and stratified neuronal group detected along layer VI of the SI (TMR- and FG-labeled neurons) (Fig. 5) upon injection of these tracers in the VPL followed by brain tissue clearance.

In rats, immunofluorescence techniques were used alone for OT detection in the hypothalamic paraventricular nucleus (PVN) (Gamal-Eltrabily et al., 2018) or combined with the CLARITY technique (Zheng and Rinaman, 2016). Oxytocinergic innervations from the PVN towards the spinal cord have been previously described using neuronal tracing and immunohistochemistry (Condés-Lara et al., 2007; Saper et al., 1976; Sawchenko and Swanson, 1982; Swanson, 1977; Swanson and McKellar, 1979). In this context, PVN projections destinate the IML (Hosoya, 1980) and send collaterals to the dorsal horn at cervical and lumbar levels (Condés-Lara et al., 2003). Here, through combined CLARITY and immunofluorescence techniques, we describe the presence of oxytocinergic and vasopressinergic fibers throughout the thoracic segment of the spinal cord in adult rats. These fibers are clearly identified at the dorsal and ventral depth of the T8 segment and bilaterally reaching the IML. Interestingly, some fibers were double-labeled (OT-AVP positive), which is consistent with previous findings on the peptidergic nature of PVN projections to the spinal dorsal horn at lumbar level (Gamal-Eltrabily et al., 2018). These results potentiate the described role of PVN descending modulatory role in pain, as well as autonomic system modulation (Christensen and Hulsebosch, 1997; Sliwinski et al., 2018)

Our group has reported that PVN stimulation decreases the activity of spinal wide dynamic range neurons upon peripheral noxious stimulation. This effect is mediated by a descending oxytocinergic mechanism and could involve local GABAergic interneuron activity (Rojas-Piloni et al., 2007). The distribution of OT binding sites coincides with the innervations of OT, suggesting a modulating role for this peptide in sensory and autonomic functions (Reiter et al., 1994). Furthermore, immunocytochemical and immunofluorescence studies have shown that

GABA is predominantly found in interneurons in laminae I-III in the lumbar segment of the spinal dorsal horn (Moreno-López et al., 2013; Todd and McKenzie, 1989). A similar distribution of GABA has been described in the cervical, thoracic, lumbar and sacrum segments of the spinal cord, mainly laminae I-III; as well as immunoreactive fibers and small neurons in lamina X (Magoul et al., 1987). However, GABAergic neurons have also been described between layers I–V of the spinal cord at lumbosacral level (Zou et al., 2002). In this work, using CLARITY and immunofluorescence techniques, we identified GABA-labeled neurons within laminae IV and V at L5 level. Also, we analyzed OTR expression in the same region where we observed the presence of GABAergic neurons that express OTR (Fig. 6 B3 and C3). These findings support the possible involvement of GABAergic neurons in the OT-induced suppression of afferent activity (Condés-Lara et al., 2003; Miranda-Cárdenas et al., 2006; Rojas-Piloni et al., 2007) at this level. However, contrasting results regarding OTR expression in the spinal cord have been described. In rats, OTR-expressing neurons were identified in laminae I-III in the spinal dorsal horn, but no OTR expression by GABAergic neurons was documented (Moreno-López et al., 2013).I In mouse, OTR was mainly expressed in laminae I—II of the spinal dorsal horn and lamina X (Wrobel et al., 2011). This suggests that the detection of OTR and/or its colocalization with GABA could vary depending on the depth of the spinal cord laminae. In this context, the CLARITY technique amplifies OTR and GABA labeling detection (see Fig. 6), which makes it better than immunofluorescence alone, as also observed with CGRP labeling. Finally, considering the size of GABA-OTR labeled neurons, we believe they are interneurons that express OTR; however, further studies using electron microscopy techniques are required to demonstrate the nature of these cells. In fact, the expression of OTR by GABAergic neurons could prove that OT inhibitory action is mediated by GABA interneurons. Nevertheless, the OT inhibitory action mechanism could be direct at the presynaptic level of primary sensory afferents.

In conclusion, our results show that the CLARITY technique can be performed in nervous tissue obtained from young (13- and 30-day-old) and adult (60-day-old) rats. Fixable fluorescent neuronal tracers can be combined with CLARITY, but the degree of dye loss has not been estimated. The quantity of tracers lost by the CLARITY procedure was not estimated and we only could give a qualitative result regarding the positive cells ant fibers. CLARITY was used to identify central pathways of both AL and DL systems, which are involved in somatosensory and nociception processes. Additionally, combined CLARITY and immunofluorescence techniques were successful, and we identified descending oxytocinergic and vasopressinergic fibers in the spinal thoracic system, as well as OTR expression and GABAergic interneuron distribution at lumbar level, which could be the core mechanism for OT descending inhibition. Finally, CGRP labeling detection was notably improved when CLARITY was used in the absence of nervous lesions. Together, these data point out the potential use of CLARITY to study neuromorphological data in physiological and pathological conditions at different ages.

CRediT authorship contribution statement

Guadalupe Martínez-Lorenzana: Investigation, Software, Formal analysis, Methodology, Writing - review & editing, Data curation, Project administration. **Mohammed Gamal-Eltrabily:** Investigation, Software, Formal analysis, Methodology, Writing - review & editing, Data curation, Project administration. **Irma Alejandra Tello-García:** Investigation, Software, Formal analysis, Methodology. **Ataulfo Martínez-Torres:** Conceptualization, Resources, Supervision. **Marymar Becerra-González:** Investigation, Software, Formal analysis, Methodology. **Abimael González-Hernández:** Conceptualization, Resources, Supervision. **Miguel Condés-Lara:** Conceptualization, Resources, Supervision, Formal analysis, Writing - review & editing, Data curation, Project administration.

Declaration of Competing Interest

The authors declare that the research was conducted in the absence of any commercial or financial relationships that could be construed as a potential conflict of interest.

Acknowledgements

We acknowledge Elsa Nydia Hernández Ríos for her technical assistance with the confocal microscope and Jessica González Norris for proofreading the manuscript. This research was financially supported by the Programa de Apoyo a Proyectos de Investigación e Innovación Tecnológica (PAPIIT-UNAM Mexico) under Grant agreement no. IN200415 to MCL and Grant no. IA203119 to AGH.

Appendix A. Supplementary data

Supplementary data associated with this article can be found, in the online version, at https://doi.org/10.1016/j.jneumeth.2020.109048.

References

Aswendt, M., Schwarz, M., Abdelmoula, W.M., Dijkstra, J., Dedeurwaerdere, S., 2017. Whole-brain microscopy meets in vivo neuroimaging: techniques, benefits, and limitations. Mol. Imaging Biol. 19, 1–9.
Breton, J.D., Veinante, P., Uhl-Bronner, S., Vergnano, A.M., Freund-Mercier, M.J., Schlichter, R., Poisbeau, P., 2008. Oxytocin-induced antinociception in the spinal cord is mediated by a subpopulation of glutamatergic neurons in lamina I-II which amplify GABAergic inhibition. Mol. Pain 29, 4–19.
Cameron, A.A., Leah, J.D., Snow, P.J., 1988. The coexistence of neuropeptides in feline sensory neurons. Neuroscience 27, 969–979.
Cappe, C., Morel, A., Rouiller, E.M., 2007. Thalamocortical and the dual pattern of corticothalamic projections of the posterior parietal cortex in macaque monkeys. Neuroscience 146, 1371–1387.
Christensen, M.D., Hulsebosch, C.E., 1997. Spinal cord injury and anti-NGF treatment results in changes in CGRP density and distribution in the dorsal horn in the rat. Exp. Neurol. 147, 463–475.
Chung, K., Deisseroth, K., 2013a. CLARITY for mapping the nervous system. Nat. Methods 10, 508–513.
Chung, K., Deisseroth, K., 2013b. CLARITY for mapping the nervous system. Nat. Methods 10, 508–513.
Chung, K., Wallace, J., Kim, S.Y., Kalyanasundaram, S., Andalman, A.S., Davidson, T.J., Deisseroth, K., et al., 2013a. Structural and molecular interrogation of intact biological systems. Nature 497 (7449), 332–337.
Chung, K., Wallace, J., Kim, S.-Y., Kalyanasundaram, S., Andalman, A.S., Davidson, T.J., Deisseroth, K., et al., 2013b. Structural and molecular interrogation of intact biological systems. Nature 497, 332–337.
Condés-Lara, M., González, N.M., Martínez-Lorenzana, G., Delgado, O.L., Freund-Mercier, M.J., 2003. Actions of oxytocin and interactions with glutamate on spontaneous and evoked dorsal spinal cord neuronal activities. Brain Res. 976, 75–81.
Condés-Lara, M., Martínez-Lorenzana, G., Rojas-Piloni, G., Rodríguez-Jiménez, J., 2007. Branched oxytocinergic innervations from the paraventricular hypothalamic nuclei to superficial layers in the spinal cord. Brain Res. 1160, 20–29.
Condés-Lara, M., Martínez-Lorenzana, G., Rojas-Piloni, G., Tello-García, I.A., Manzano-García, A., Rubio-Beltran, E., González-Hernández, A., 2018. Axons of individual dorsal horn neurons bifurcated to project in both the anterolateral and the postsynaptic dorsal column systems. Neuroscience 371, 178–190.
Gamal-Eltrabily, M., Márquez-Morales, C., Martínez-Lorenzana, G., González-Hernández, A., Condés-Lara, M., 2018. Peptidergic nature of nociception-related projections from the hypothalamic paraventricular nucleus to the dorsal horn of the spinal cord. Neurosci. Lett. 685, 124–130.
Gibson, S.J., Polak, J.M., Bloom, S.R., Sabate, I.M., Mulderry, P.M., Ghatei, M.A., McGregor, G.P., Morrison, J.F., Kelly, J.S., Evans, R.M., 1984. Calcitonin gene-related peptide immunoreactivity in the spinal cord of man and of eight other species. J. Neurosci. 4, 3101–3111.
Hökfelt, T., Arvidsson, U., Ceccatelli, S., Cortes, R., Cullheim, S., Dagerlind, A., Johnson, H., Orazzo, C., Piehl, F., Pieribone, V., Schalling, M., Terenius, L., Ulfhake, B., Verge, V.M., Villar, M.Z., Wiesenfeld-Hallin, Z., Xu, X.J., Xu, Z., 1992. Calcitonin gene-related peptide in the brain, spinal cord, and some peripheral systems. Ann. N. Y. Acad. Sci. 657, 119–134.
Hosoya, Y., 1980. The distribution of spinal projection neurons in the hypothalamus of the rat, studied with the HRP method. Exp. Brain Res. 40, 79–87.
Ishida-Yamamoto, A., Tohyama, M., 1989. Calcitonin gene-related peptide in the nervous tissue. Prog. Neurobiol. 33, 335–386.
Jensen, K.H.R., Berg, R.W., 2016. CLARITY-compatible lipophilic dyes for electrode marking and neuronal tracing. Sci. Rep. 6.
Jones, E.G., 1985. The Thalamus. Springer US, New York.

Köbbert, C., Apps, R., Bechmann, I., Lanciego, J.L., Mey, J., Thanos, S., 2000. Current concepts in neuroanatomical tracing. Prog. Neurobiol. 62, 327–351.
Lai, H.M., Ng, W.L., Gentleman, S.M., Wu, W., 2017. Chemical probes for visualizing intact animal and human brain tissue. Cell Chem. Biol. 24 (6), 659–672.
Magoul, R., Onteniente, B., Geffard, M., Calas, A., 1987. Anatomical distribution and ultrastructural organization of the gabaergic system in the rat spinal cord. An immunocytochemical study using anti-GABA antibodies. Neuroscience 20, 1001–1009.
Marti, E., Gibson, S.J., Polak, J.M., Facer, P., Springall, D.R., van Aswegen, G., Aitchison, M., Koltzenburg, M., 1987. Ontogeny of peptide- and amine-containing neurones in motor, sensory, and autonomic regions of rat and human spinal cord, dorsal root ganglia, and rat skin. J. Comp. Neurol. 266, 332–359.
McNeill, D.L., Chung, K., Carlton, S.M., Coggeshall, R.E., 1988. Calcitonin gene-related peptide immunostained axons provide evidence for fine primary afferent fibers in the dorsal and dorsolateral funiculi of the rat spinal cord. J. Comp. Neurol. 272, 303–308.
Mesulam, M., 1982. Tracing Neuronal Connections with Horseradish Peroxidase. Wiley, New York, p. 251.
Miranda-Cárdenas, Y., Rojas-Piloni, G., Martínez-Lorenzana, M., Rodríguez-Jiménez, J., López-Hidalgo, M., Freund-Mercier, M.J., Condés-Lara, M., 2006. Oxytocin and electrical stimulation of the paraventricular hypothalamic nucleus produce antinociceptive effects that are reversed by an oxytocin antagonist. Pain 122, 182–189.
Monconduit, L., Lopez-Avila, A., Molat, J.L., Chalus, M., Villanueva, L., 2006. Corticofugal output from the primary somatosensory cortex selectively modulates innocuous and noxious inputs in the rat spinothalamic system. J. Neurosci. 26, 8441–8450.
Moreno-López, Y., Martínez-Lorenzana, G., Condés-Lara, M., Rojas-Piloni, G., 2013. Identification of oxytocin receptor in the dorsal horn and nociceptive dorsal root ganglion neurons. Neuropeptides 47, 117–123.
Paxinos, G., Watson, C., 2007. The Rat Brain in Stereotaxic Coordinates. Academic Press.
Reiter, M.K., Kremarik, P., Freund-Mercier, M.J., Stoeckel, M.E., Desaulles, E., Feltz, P., 1994. Localization of oxytocin binding sites in the thoracic and upper lumbar spinal cord of the adult and postnatal rat: a histoautoradiographic study. Eur. J. Neurosci. 6, 98–104.
Richardson, D.S., Lichtman, J.W., 2015. Clarifying tissue clearing. Cell 162, 246–257.
Rojas-Piloni, G., López-Hidalgo, M., Martínez-Lorenzana, G., Rodríguez-Jiménez, J., Condés-Lara, M., 2007. GABA-mediated oxytocinergic inhibition in dorsal horn neurons by hypothalamic paraventricular nucleus stimulation. Brain Res. 1137, 69–77.
Saper, C.B., Loewy, A.D., Swanson, L.W., Cowan, W.M., 1976. Direct hypothalamo-autonomic connections. Brain Res. 117, 305–312.
Sawchenko, P.E., Swanson, L.W., 1982. Immunohistochemical identification of neurons in the paraventricular nucleus of the hypothalamus that project to the medulla or to the spinal cord in the rat. J. Comp. Neurol. 205, 260–272.
Senba, E., Tohyama, M., 1988. Calcitonin gene-related peptide containing autonomic efferent pathways to the pelvic ganglia of the rat. Brain Res. 449, 386–390.
Silvestri, L., Costantini, I., Sacconi, L., Pavone, F.S., 2016. Clearing of fixed tissue: a review from a microscopist's perspective. J. Biomed. Opt. 21, 081205.
Sliwinski, C., Nees, T.A., Puttagunta, R., Weidner, N., Blesch, A., 2018. Sensorimotor activity partially ameliorates pain and reduces nociceptive fiber density in the chronically injured spinal cord. J. Neurotrauma 35, 2222–2238.
Swanson, L.W., 1977. Immunohistochemical evidence for a neurophysin-containing autonomic pathway arising in the paraventricular nucleus of the hypothalamus. Brain Res. 128, 346–353.
Swanson, L.W., McKellar, S., 1979. The distribution of oxytocin- and neurophysin-stained fibers in the spinal cord of the rat and monkey. J. Comp. Neurol. 188, 87–106.
Todd, A.J., McKenzie, J., 1989. GABA-immunoreactive neurons in the dorsal horn of the rat spinal cord. Neuroscience 31, 799–806.
Vercelli, A., Repici, M., Garbossa, D., Grimaldi, A., 2000. Recent techniques for tracing pathways in the central nervous system of developing and adult mammals. Brain Res. Bull. 51, 11–28.
Wang, P., Zhang, D., Bai, S., Tao, B., Li, S., Wang, T., Shang, A., 2020. Feasibility of commonly used fluorescent dyes and viral tracers in aqueous and solvent-based tissue clearing. Neurosci. Lett. 737, 135301.
Willis, W.D., Coggeshall, R.E., 2004. Sensory Mechanisms of the Spinal Cord. Springer US, New York.
Woolf, C., Wiesenfeld-Hallin, Z., 1986. Substance P and calcitonin gene-related peptide synergistically modulate the gain of the nociceptive flexor withdrawal reflex in the rat. Neurosci. Lett. 66, 226–230.
Wrobel, L., Schorscher-Petcu, A., Dupré, A., Yoshida, M., Nishimori, K., Tribollet, E., 2011. Distribution and identity of neurons expressing the oxytocin receptor in the mouse spinal cord. Neurosci. Lett. 495, 49–54.
Yang, B., Treweek, J.B., Kulkarni, R.P., Deverman, B.E., Chen, C.K., Lubeck, E., Shah, S., Cai, L., Gradinaru, V., 2014. Single-cell phenotyping within transparent intact tissue through whole-body clearing. Cell 158 (4), 945–958.
Zheng, H., Rinaman, L., 2016. Simplified CLARITY for visualizing immunofluorescence labeling in the developing rat brain. Brain Struct. Funct. 221, 2375–2383.
Zimmermann, M., 1983. Ethical guidelines for investigations of experimental pain in conscious animals. Pain 16, 109–110.
Zou, X., Lin, Q., Willis, W.D., 2002. The effects of sympathectomy on capsaicin-evoked fos expression of spinal dorsal horn GABAergic neurons. Brain Res. 958, 322–329.

NEUROSCIENCE
RESEARCH ARTICLE

M. Condés-Lara et al. / Neuroscience 371 (2018) 178–190

Axons of Individual Dorsal Horn Neurons Bifurcated to Project in Both the Anterolateral and the Postsynaptic Dorsal Column Systems

M. Condés-Lara,[a]* G. Martínez-Lorenzana,[a] G. Rojas-Piloni,[a] I. A. Tello-García,[a] A. Manzano-García,[a] E. Rubio-Beltran[b] and A. González-Hernández[a]

[a] *Departamento de Neurobiología del Desarrollo y Neurofisiología, Instituto de Neurobiología, Universidad Nacional Autónoma de México, Campus UNAM Juriquilla, Querétaro, Mexico*

[b] *Div. of Pharmacology and Vascular Medicine, Department of Internal Medicine, Erasmus University Medical Centre. 3000 CA Rotterdam, The Netherlands*

Abstract—Sensory information stimulates receptors of somatosensory system neurons generating a signal that codifies the characteristics of peripheral stimulation. This information reaches the spinal cord and is relayed to supra-spinal structures through two main systems: the postsynaptic dorsal column-medial lemniscal (DC-ML) and the anterolateral (AL) systems. From the classical point of view, the DC-ML has an ipsilateral ascending pathway to the Gracilis (GRA) or Cuneate (CUN) nuclei and the AL has a contralateral ascending pathway to the ventral posterolateral (VPL) thalamic nucleus. These two systems have been the subject of multiple studies that established their independence and interactions. To analyze the ascending projections of L1–L5 spinal dorsal horn neurons in the rat, two retrograde neuronal tracers were injected into the GRA and the VPL. Additionally, an electrophysiological study was performed by applying electrical stimulation at the GRA or VPL and recording antidromic evoked activity in single unit spinal cord cells. Importantly, a subset of spinal dorsal horn neurons exhibited double staining, indicating that these neurons projected to both the GRA and the VPL. These double-stained neurons were located on both sides of the dorsal horn of the spinal cord. The spinal dorsal horn neurons exhibited antidromic and collision activities in response to both GRA and VPL electrical activation. These results show spinal cord neurons with bifurcated bilateral projections to both the DC-ML and AL systems. Based on these results, we named these neurons bilateral and bifurcated cells.

Key words: retrograde tracers, collision test, bilateral and bifurcated cells, spinal projecting cells, anatomical and electrophysiological study.

INTRODUCTION

Skin receptors are specialized to detect particularities in skin stimulation and transmit this coded information to spinal dorsal horn neurons. These neurons, also called second order neurons, send the information to the supra-spinal structures by two main pathways: the ipsilateral dorsal column-medial lemniscal (DC-ML) and the contralateral anterolateral (AL) systems.

The DC-ML system senses primary afferents concerning tactile and proprioceptive information arriving at the spinal cord and forms the ipsilateral dorsal column pathway to reach the Gracile (GRA) or the Cuneate (CUN) nuclei. Then, neurons at the GRA and CUN reach the contralateral ventral-postero-lateral (VPL) and ventral-postero-medial thalamic nucleus via the medial lemniscus pathway. Also, primary afferents reach another cluster of spinal neurons called postsynaptic dorsal column, that send their axons to the ipsilateral GRA or CUN nucleus and then by the medial lemniscus reach the contralateral thalamus (Angaut-Petit, 1975a,b).

The AL system receives primary afferent information concerning pain, temperature and crude touch, and dorsal spinal cord projection neurons extend their axons contralaterally to reach the brain stem reticular formation, midbrain, tectal region and several thalamic

*Corresponding author. Fax: +52-(442)-2381042.
E-mail address: condes@unam.mx (M. Condés-Lara).
URL: http://132.248.142.23/web_site/home_pages/35?locale=en (M. Condés-Lara).

Abbreviations: AL, anterolateral system; anti-anti, double antidromic activated cell; Anti, antidromic activated cell; AV, anterior ventral thalamic nucleus; CUN, Cuneate nuclei; DC-ML, postsynaptic dorsal column-medial lemniscal system; EEG, electroencephalographic activity; FG, Fluoro Gold retrograde tracer; FR, Fluoro Rubi retrograde tracer; GRA, Gracilis nuclei; LDV, lateral dorsal ventral thalamic nucleus; Po, posterior thalamic nucleus; RT, reticular thalamic nucleus; STT, spinothalamic tract; TB, True Blue retrograde tracer; VL, ventral lateral thalamic nucleus; VPL, ventral posterolateral thalamic nucleus; WDR, wide dynamic range neurons; ZI, zona incerta.

https://doi.org/10.1016/j.neuroscience.2017.11.050
0306-4522/

structures (Martin and Jessell, 1991; Guilbaud et al., 1993; Gardner and Johnson, 2013). Hence, the AI system is formed by the spinoreticular, spinomesencephalic and the spinothalamic (STT) tracts. Two reviews on pain and the somatic and visceral pathways by Almeida et al. (2004) and Millan (1999) summarize the classical view of these tracts.

The DC-ML and the STT systems have been described as independent and separate pathways until they reach the thalamus, and little is known about their interconnections, which are the main focus of the present study. In pioneer studies, Kevetter and Willis (1984) described the 2% of spinothalamic cells projecting to both sides of the thalamus. Also, these authors described that the 38% of spinothalamic cells project to the ipsilateral medial thalamus and the 19% of cells project to the ipsilateral lateral thalamus. Lu and Willis (1999) reviewed this work with the same precision. Also, Apkarian and Hodge (1989) and Hodge and Apkarian (1990) described that 17% of the spinal projecting cells reach the ipsilateral thalamus.

As well as the DC-ML and AL systems (Hendry et al., 1999), yet we found no reports concerning their interactions or interconnections. Therefore, the present study describes a particular set of spinal cord dorsal horn neurons projecting to both ipsilateral GRA and contralateral VPL. To the best of our knowledge, this is the first description of interconnections between the DC-ML and AL systems.

Retrograde fluorescent tracers were injected into the left GRA and the right VPL thalamic nuclei. The results show that both fluorescent tracers labeled individual neurons on both sides of the spinal cord (L1–L5). To confirm our results, we performed the electrophysiological collision test using electrical stimulation at the GRA and/or VPL to produce antidromic responses in neurons of the spinal cord identified as wide dynamic range (WDR).

Preliminary results were presented in an IASP congress (Condés-Lara et al., 2016).

EXPERIMENTAL PROCEDURES

The experiments were carried out in accordance with the National Institute of Health Guide for the Care and Use of Laboratory Animals (NIH Publications No. 80-23) revised 1996, as well as the European Communities Council Directive of 24 November 1986 (86/609/EEC). Also, the recommendations of the IASP Ethical Guidelines (Zimmermann, 1983) and the recommendations of the Instituto de Neurobiología Ethical Commission. The Animal House of our institute provided male Sprague–Dawley rats weighing an average of 280–310 g. They were individually housed in a temperature-controlled (23 ± 3 °C) environment and subjected to a 12 h/12 h light/dark cycle with food and water available *ad libitum*. Two sets of experimental approaches were used: Retrograde fluorescent tracers, with three tracers' combinations: True Blue (TB) in the GRA and Fluoro Gold (FG) in the VPL; TB in the GRA and Fluoro Rubi (FR) in the VPL; and TB in the GRA and FG in the VPL with immunofluorescence. The second experimental approach used Electrophysiology techniques.

Note that while describing results, observations of the left side were considered ipsilateral (left GRA) and observations on the right are considered contralateral (right VPL). The reason was that our electrophysiological recording sites in the spinal cord of the rat were the left side (ipsilateral) and the receptive field evoking responses were also the left side (ipsilateral).

Injection of fluorescence retrograde tracers in the GRA and VPL

Injection of Fluoro Gold (FG) and True blue (TB). Fifteen rats were anesthetized with a ketamine/xylazine mixture (70/6 mg/kg, i.p.) and placed in a stereotaxic frame. The animals head was initially secured in ventroflex position. A skin incision was made and then the muscles of the back of the neck were dissected laterally from the midline. The atlanto-occipital membrane and underlying meninges were opened, exposing the cisterna magna and the dorsum of the lower medulla. A stainless-steel microelectrode carrying a small pellet (400–500 μm) of True Blue (TB) (True Blue Chloride, No. Cat T-0695 Sigma, St. Louis, MO USA) attached to the tip was inserted into the left GRA at 0.5 mm lateral to the middle of the caudal region of the nucleus (between 0.5 and 1.0 mm caudal to the obex) under a microscope. Then, with the head in a stereotaxic position (Paxinos and Watson, 1998), a trephine hole was drilled into the skull to pressure inject 60–90 nl of a Fluoro Gold (FG) (Fluoro-Gold, Fluorochrome, LLC. Denver, CO, USA) solution (2.5% in distilled water) into the right VPL. The glass micropipettes were prepared under a microscope such that they had a 4–10 μm tip; the pipettes were attached to a 1 μl Hamilton syringe mounted in a microdriver system. The pipettes and syringe were filled with glycerin and only the pipette tip was charged with the tracer. This procedure allowed us to perform injections of 20–30 nl ± 10 nl.

The FG injections were performed at three depths for each experimental animal with the purpose of making an extended dorsal ventral VPL injection (interaural stereotaxic coordinates: AP 6.1; L 2.8; H 3.3, 3.5 and 3.7 mm) (Paxinos and Watson, 1998).

The animals were allowed to recover for 13 days. Then, an overdose of anesthesia (50 mg/kg of pentobarbital) was delivered, and the animals were perfused through the heart using a peristaltic pump with a brief rinse of saline (200 ml), followed by 4% paraformaldehyde (300 ml) in 0.1 M phosphate buffer (pH 7.4). The brains and spinal cords were removed, postfixed for an additional 2 h, and cryoprotected in a 30% sucrose solution 0.1 M phosphate buffer (pH 7.4) for two days. The brains and spinal cords were cut (40 μm) in a freezing microtome. Spinal cord sections were collected in 5 serialized series of 50 to 65 sections each one. The first series was used to observe the spinal cord location, the second and third were used for fluorescence process and the other two stored for

further verifications. Each section had 40 μm and the distance between section was 200 μm giving us about 64 spinal cord sections per series in each rat. All sections were then mounted on gelatinized slides, dehydrated, cleaned, and cover slipped for the subsequent microscopic analysis. The brain and spinal cord sections were observed under an Olympus IX81 microscope equipped with an OH-ORCA-FLASH40 digital camera and fluorescence illumination system or with a confocal microscope (Zeiss Axiovert LSM 500 meta) with a multiphotonic laser (Chameleon ultra) and the proper specific filter for each fluorescence wavelength spectrum, and digital images of the labeled neurons were obtained.

Labeled cells count. One of the above described serial sections was used to count the number of stained cells. With a total of 320 spinal cord sections between L1 and L6 taken from 6 rats (64 per animal) we counted the stained dorsal spinal cord cells located in both the ipsilateral and contralateral sides. These counts were used to construct Table 1. The profiles of selected sections and the location of labeled neurons were analyzed and quantified using the Data Image Tracer (version 1.2) software, as well as a semi-automatic Image Processing System MD3 (Minnesota Datametrics). Computer-assisted images from adjacent Nissl and immunofluorescence sections were generated using a Leica DMLB. Digital higher-power images (100× and 200×) of labeled neurons were also obtained with this same device. Plots of labeled neurons were placed on the immunofluorescence sections and on spinal cord diagrams from Paxinos and Watson (1998) atlas.

Fluoro Ruby (FR) and True blue (TB). Five rats were prepared to compare the results obtained using the FG and TB injections. The purpose of this maneuver was to confirm that neurons were double marked. The tissue sections, sites of injections and spinal cord samples were similar to those described previously. Briefly, small pellets of TB were inserted into the left GRA nucleus under a microscope, and 60 to 90 nl of a 10% solution of FR (Fluoro-Ruby No. Cat. AG335, Millipore, Temecula, California, USA) in saline was injected at three different depths in the right VPL at the same coordinates described above. The animals were allowed to recover for 10–13 days; then they were deeply anesthetized and perfused as described in the previous section. The tissue sectioning, mounting and analysis were similar to the previous section.

Immunofluorescence for FG. To ensure that the FG-stained cells did indeed co-localize with TB, other sections of the same rats were preincubated with blocking serum for 20 min at room temperature and then incubated overnight at 4 °C with rabbit anti-FG (Fluorochrome, LLC) diluted 1:500 in 0.1 M phosphate-buffered saline (PBS) (pH 7.4) containing 0.5% Triton X-100 (Triton X-100, No. de cat. X100, Sigma–Aldrich, St. Louis, MO USA) and 5% normal goat serum (Goat serum, No. de cat. 16,210, Gibco, Invitrogen, Auckland, New Zeeland). After rinsing in PBS, the sections were incubated with a secondary antibody, AlexaFluor 555-conjugated goat anti-rabbit diluted 1:300 (AlexaFluor 555-conjugated goat anti-rabbit, No. de cat. A21428, Molecular Probes by Life technologies, Eugene, OR, USA), for 24 h. After rinsing, the sections were mounted on gelatin-coated, dehydrated, cleared, and cover slipped with DPX. The sections were examined under a confocal microscope (Zeiss Axiovert LSM 500 meta) with a multiphotonic laser (Chameleon ultra). Specific filters were used for each fluorescence wavelength, and digital images of the labeled neurons were obtained.

Electrophysiological recordings of the spinal cord cells activated by electrical stimulation of the GRA and VPL

Twenty-five male Wistar rats (280–310 g) were housed individually under 12-h:12-h light/dark conditions, with food and water available *ad libitum*. The rats were anesthetized with 3% sevoflurane in an atmosphere of 1/3 oxygen and 2/3 nitric oxide. The rats were placed in a hermetically sealed box with the anesthesia and when a loss of reflexes was confirmed, they were tracheotomized to provide artificial ventilation and placed in a stereotaxic frame to fix their heads and spinal cords.

Concentric bipolar electrodes were placed in the right VPL at AP 6.1 ± 0.5; L 2.8; and H 3.5 ± 0.3 mm using the interaural point according to the Paxinos stereotaxic atlas (Paxinos and Watson, 1998), and the atlanto-occipital foramen was exposed to allow access to the left GRA nucleus. The spinal cords were exposed at the L3–L5 level to record the neuronal activity on the left side.

The dorsal spinal cord cells were recorded using glass micropipettes filled with 4% pontamine sky blue in 1 M KCl (impedance of 8–10 M ohms). At the end of the recordings or in the recording sites of interest, pontamine blue was injected iontophoretically using a cathodic current (15–20 μA) for 25 min. The cells were

Table 1. Single and double stained dorsal horn cells number. The Table shows the number of spinal cord cells stained with only TB or FG and with both TB and FG. The data were obtained from 6 rats. The mean of ipsilateral and contralateral cells is also shown. Note the differences between the mean number of TB/FG labeled ipsilateral (2.6) and contralateral cells (0.58). Ipsilateral refers to the left side and contralateral refers to the right side because we recorded the spinal cord cells on the left side

	Ipsilateral		Contralateral	
	Number	Mean	Number	Mean
TB (only)	2302	1.429	1264	0.776
FG (only)	1352	0.839	913	0.556
TB/FG	4365	2.684	954	0.585

recorded using a Dual Microprobe Amplifier WPI without filters at an amplification of X10 and then the signals were amplified (X100) in a Grass P511 (the bandpass filters were set between 300 and 3000 Hz). Another Grass P511 was used to amplify the electroencephalographic (EEG) activity from two electrodes placed at the cortex. The EEG was used to indicate the level of anesthesia and was characterized by the presence of slow waves sleep (2–6 Hz); in this case, the bandpass filters were fixed at 3–300 Hz. The activities were digitalized using a Spike 2 and the appropriate software (Cambridge Electronic Device, CED).

We recorded 225 cells at the L3–L4 segments of the spinal dorsal horn that have a receptive field on the left hind foot. Only the wide dynamic range cells that responded to tactile and nociceptive stimulation were tested. Under these conditions, 172 cells were tested by electrically stimulating the GRA or VPL. The response latencies were used to calculate the conduction velocities. In addition, for the recorded spinal cord cells we considered a distance of 85 mm from the GRA and 100 mm from the VPL.

The recorded cells were found during the microelectrode displacement into the spinal cord and were activated by gently taping into the receptive field (RF). When a neuron was found in order to characterized the cell responses, mechanical and nociceptive stimulus (taping the receptive field with different intensities and hand squeezing) was delivered. Finally, a pair of electrodes (fine needles 27 G) attached to a stimulus isolator unit were inserted into the RF to deliver electric stimulation into the receptive field of the recorded neuron. We constructed peri-stimulus time histograms after triggering the activity by analyzing the RF signal artifact. We also used the spontaneous or evoked action potentials to trigger the GRA or VPL electrical stimulation with variable delays. These delays in the GRA or VPL stimulation allowed us to measure the collision time between the spontaneous and evoked action potentials in response to GRA or VPL stimulation in the recorded spinal cord cells and to describe their antidromic characteristics. The antidromic spike responses, evoked by stimulating the contralateral VPL or ipsilateral GRA, were provoked by single 1-ms square-wave pulses with intensities starting at 100 μA and increasing until a threshold was reached for each cell, but never exceeding 300 μA. When a stable cell recording was obtained, the following criteria were used to establish the antidromic characteristic of the cell responses: a constant latency, the ability to follow a stimulus train of 333 Hz, and a collision of the orthodromic spikes with the antidromically evoked spikes. The collision test was performed by first testing the GRA or VPL stimulation. If we observed a spike response, we used the spontaneous activity or spikes evoked by the RF stimulation to trigger the GRA or VPL stimulation with variable delays to observe the collision between the triggering spike and the antidromic GRA- or VPL-evoked response. The collision time was calculated as the sum of the latency of the antidromic response plus the refractory period. The latencies and conduction speeds were expressed as the means ± the standard error of the mean (SEM). At the end of the experiments, the recording sites were marked by electrophoretic deposition of pontamine sky blue (20 min 15 μA cathodic current) and electrolytic lesions were made at the stimulating points, then an overdose of anesthesia was delivered. The lumbar spinal cords and the brains were removed and fixed by immersion in a 10% formaldehyde solution for 72 h. Samples were frozen, cut in serial 40-μm sections, and Nissl-stained with cresyl violet. GRA and VPL electrolytic lesions were confirmed by localizing the stimulating electrode tips.

RESULTS

We will first describe our histological results and then our electrophysiological results. We only analyzed the animals in which the FG injection into the VPL thalamic nucleus and the TB injection into the GRA nucleus were located in the appropriate sites, as well as the cases in which we switched FG for FR to corroborate our results. We also used the FG antibody and an AlexaFluor 555-conjugated secondary antibody to verify our results. In Fig. 1, we can observe the histological location of the TB dye in the GRA, as well as the retrograde staining of the cells in the CUN after the FG injection into the VPL.

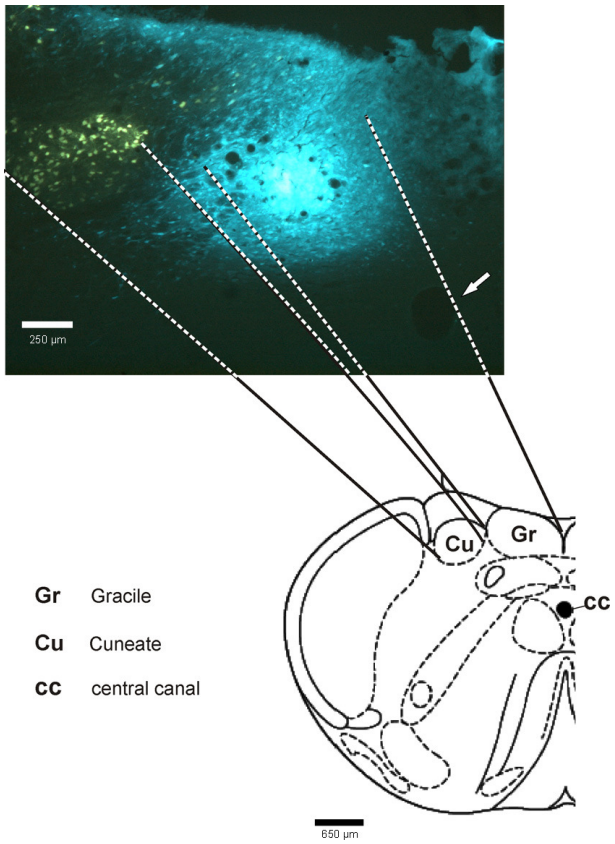

Fig. 1. Histological section showing the TB deposit site in the GRA. Observe the retrograde labeling of cells in the CUN nucleus after the FG injection in the VPL. The lower schema locates the structures corresponding to the section.

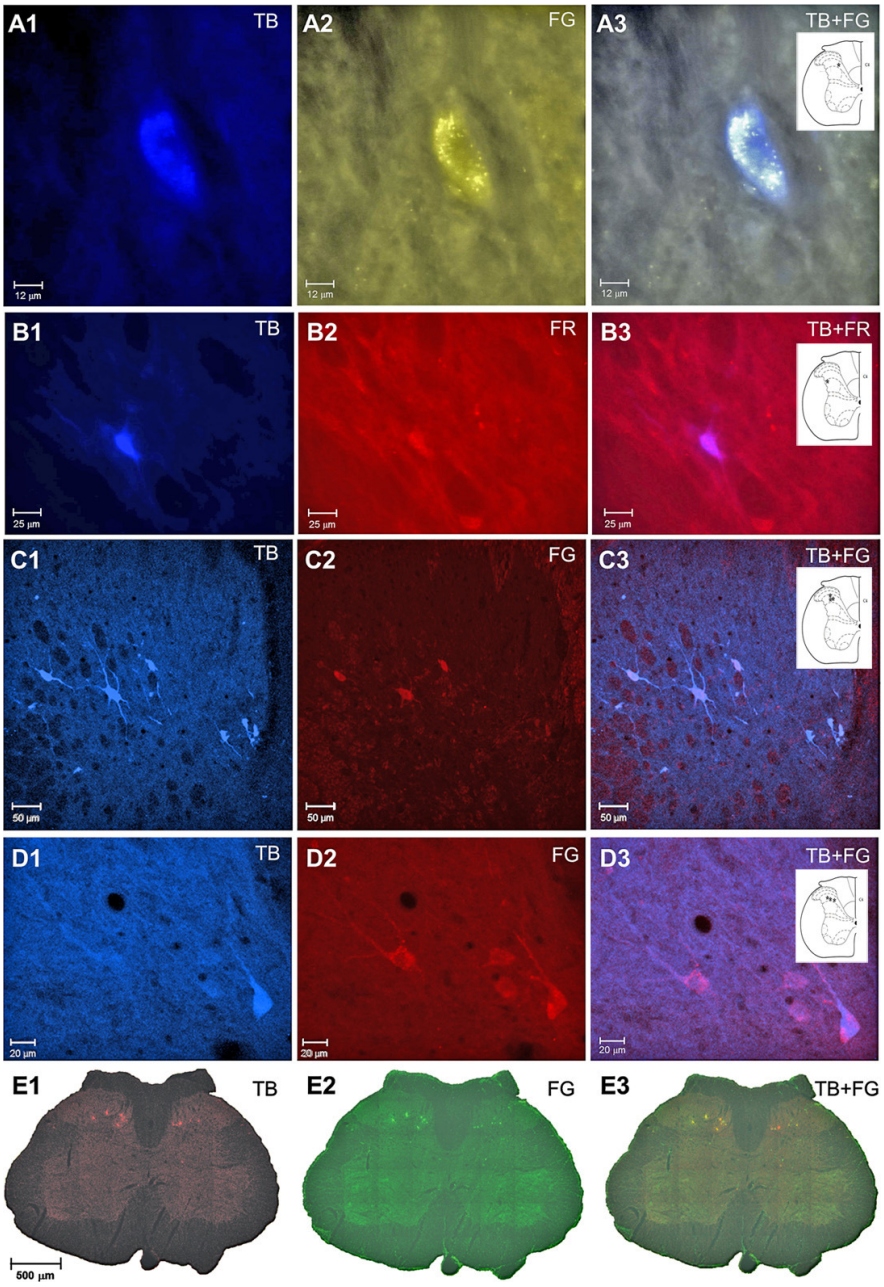

Fig. 2. Labeled spinal dorsal horn cell. The first column shows images of the labeled cells after the TB injection in the GRA, the middle column shows images of the cells projecting to the VPL, and the right column shows the merged images of the cells projecting to both the GRA and VPL. TB was inserted into the GRA nucleus, and FG or FR B2 was injected into the VPL. The first line A1, 2 and 3 shows a cell labeled with TB, FG and TB/FG located in the medial portion of the Rexed layer 4. The second line shows an example of a cell labeled with TB showed in B1, FR in B2 and both TB and FR in B3. The TB- and FR-positive cells were located in the lateral portion of layer 5; note the change in the location of the FR tracer. Lines C1, 2 and 3 illustrate the confocal microscopy images of spinal cord cells at layer 4 using the FG antibody. The image in C1 illustrates the TB-labeled cells, and the image in C2 shows the FG antibody-positive cells. The single and double TB and FG antibody-labeled cells are displayed in lines D1, 2 and 3. The images were obtained from the medial portion of spinal cord layer 4 using a confocal microscope. The E1, 2 and 3 images were obtained from a spinal cord mosaic using a confocal microscope. The images show the TB-labeled E1, FG-labeled cells E2 and FG/TB double-labeled cells E3 in layer 4 of the dorsal horn on both sides of the spinal cord. Note that the color of the TB-labeled cells was changed to red for better contrast. The spinal cord scheme insertions in A3, B3, C3 and D3 indicate the cell's locations. (For interpretation of the references to color in this figure legend, the reader is referred to the web version of this article.)

Due to the high levels of TB staining, we could not observe the FG retrograde staining of the cells in the GRA. Nevertheless, the image in Fig. 1 confirms that TB was present in the GRA and that the FG-stained cells in the CUN indicate retrograde FG transport from the VPL.

We selected TB and the FG or FR retrograde tracers' due to their different excitation wavelengths, which allows selective and unambiguous identification.

TB- and FG-positive neurons in the spinal cord

The TB and FG applications stained the spinal dorsal horn cells between L1 and L6 with a variable distribution. At L1 and L6, the stained cells were very scarce; in contrast, at L3 and L4 we found a peak in the cell density. In fact, we observed cells that were stained with TB, FG and TB/FG, as illustrated in Fig. 2A1, A2 and A3. The cells were bilaterally distributed, but there were fewer cells on the right side of the spinal cord, even though FG was injected into the right VPL and TB into the left GRA. From sections between L1 and L6 taken from 6 rats, the mean number of stained cells per section was 1.42 ipsilateral TB- (only) positive cells vs 0.77 contralateral TB-(only) positive cells, and 0.83 ipsilateral FG-(only) positive cells vs 0.55 contralateral FG-(only) positive cells. We observed 2.68 double-stained cells (TB/FG) on the ipsilateral side and 0.58 on the contralateral side (a mean rate of 4.62 cell ipsilateral by 1 cell contralateral). Subsequently, we plotted the number of cells on each side (Table 1) and observed differences between sides using the mean number of cells/side.

TB- and FR (Fluoro Ruby)-labeled neurons in the spinal cord

Injecting FR instead of FG into the VPL confirmed the previous results. Fig. 2B1, B2 and B3 shows the single- and double-labeled cells that were positive for TB and/or FR.

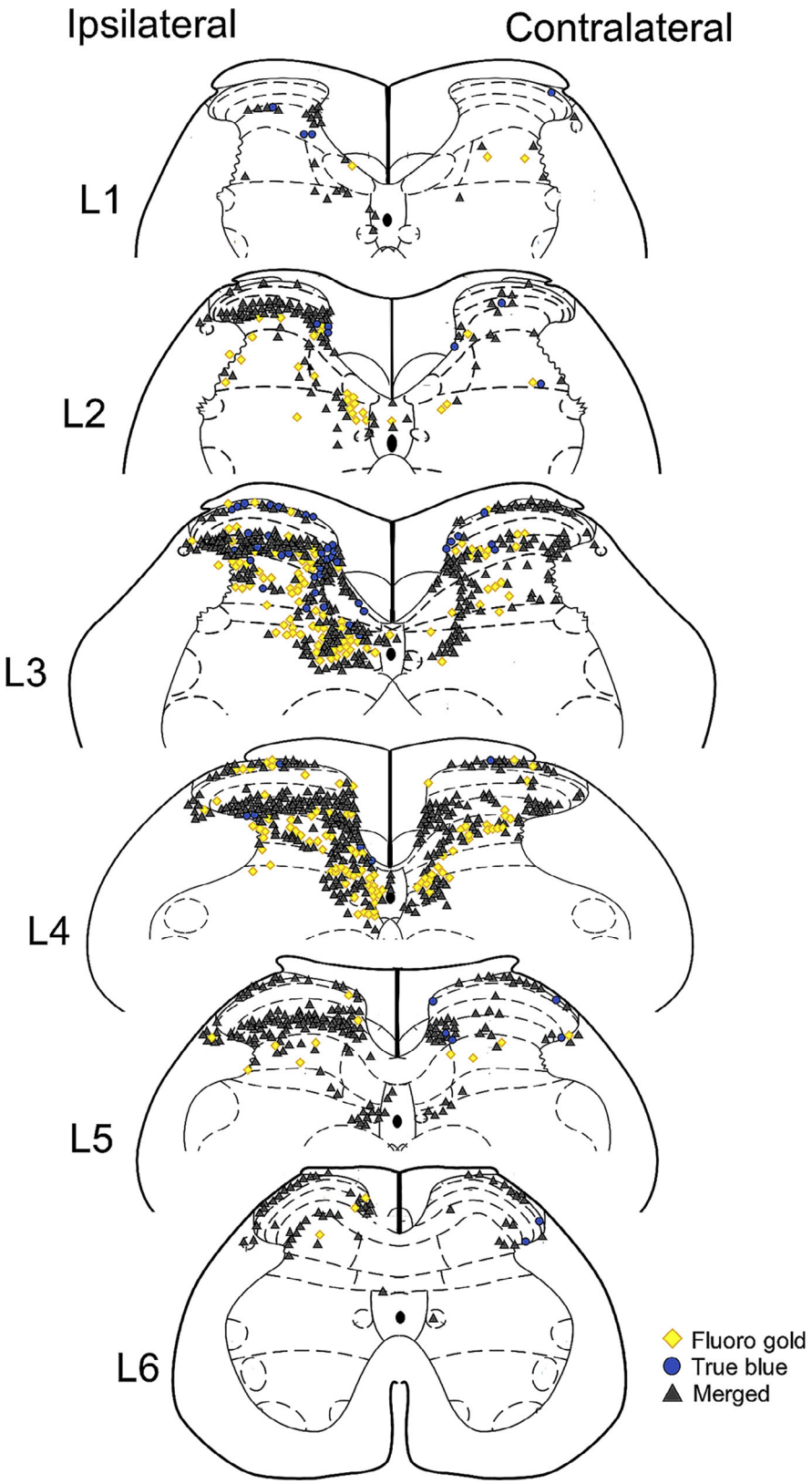

Fig. 3. Schematic illustration of the TB-, FG- and TB/FG-stained cells at spinal cord levels L1-L6. The plotted results were obtained from two representative rats. The blue circles represent the TB-positive cells, the yellow circles represent the FG-positive cells, and the black triangles represent the TB/FG-positive cells. Note the reduced number of labeled cells at L1 and L6. (For interpretation of the references to color in this figure legend, the reader is referred to the web version of this article.)

TB and FG antibody-labeled neurons in the spinal cord

After confirming that the spinal cord cells project to the GRA and the VPL using two different retrograde tracers, we decided to use the FG antibody to label the spinal cord sections that were injected with FG into the VPL for immunofluorescence staining. Fig. 2C1, C2 and C3 shows examples of the TB-, FG- and TB/FG-positive spinal cord cells, respectively. The images of the cells that were stained with the FG antibody and an AlexaFluor 555-conjugated secondary antibody were observed through confocal microscopy. Briefly, the confocal microscopy results using the FG antibody also confirmed the presence of double-labeled and bilateral stained cells, as illustrated in Fig. 2D1, D2 and D3 in a mosaic composition of a lumbar spinal section. Fig. 2 also illustrates the location of the stained cells in the spinal cord.

Bilateral and bifurcated spinal cord cells

Using the confocal microscope (Zeiss Axiovert LSM 500 meta) with a multiphotonic laser (Chameleon ultra) and the appropriate filters, we captured mosaic images of the FG-, TB- and FG/TB-labeled cells in the spinal cord. These images are presented in Fig. 2E1, E2 and E3. It is important to note that TB- or FG-stained cells are present in both sides of the spinal cord; thus, we termed them bilateral and bifurcated cells because they send projections to the GRA and VPL. However, the number and distribution of these cells were not uniform along the lumbar segments, with the highest number of them in the L4 and L5 segments of the spinal cord. Six hundred sections from two rats were used to show the distribution and location of the bilateral and bifurcated spinal cord neurons along lumbar segments. This distribution is plotted in Fig. 3 using the drawings of the spinal cord provided by the 1998 Paxinos and Watson atlas. We observed the highest number of cells in layers 1 and 4, and in the lateral and medial portions of layers 5, 6 and 7.

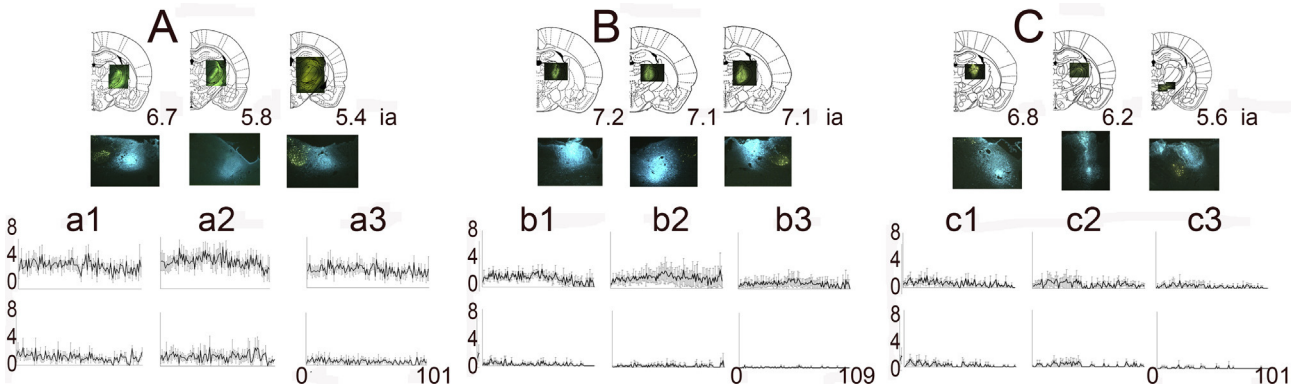

Fig. 4. Histological location of the thalamic FG injection and GRA-FG deposit. A: shows three anteroposterior schemas with large FG injections, giving the average amount (three rats) for a1 FG, a2 TB and a3 FG/TB-stained cells ipsilateral (upper graph) and contralateral (lower graph) to the GRA injection side. B: four schemas of thalamic medium injections and in the lower graphs the mean number of ipsilateral (upper graph) and contralateral (lower graph) b1 FG-, b2 TB- and b3 FG/TB-stained cells in the spinal cord. C: A histological example of smaller tracer deposits. Notice that the injection sites (the brightest) are surrounded by a local transport, giving the impression of larger injection sites. ia: distance from interaural plane.

Relationship between double-stained cells and tracer size and location of tracers

Three groups of three rats each were selected according to the size of injections in the thalamus and GRA regions.

The largest FG thalamic injection reached the rostral portion of the VPL from 6.70 to 5.40 anteroposterior plane, and the TB injection into the GRA included the ventral and the dorsal parts of the nucleus tractus solitarius (Sol). With these sizes of tracer deposits, FG- and TB-positive cells and double-stained FG/TB cells were found in superficial 1, 2; intermediate 4, 5; and deep 6, 7 spinal cord layers (Fig. 4A, a1, a2, a3). The superficial FG-positive cells seem related to the posterior thalamic nuclei (Po), while the intermediate cells seem related to the lateral dorsal ventral (LDV), medial (LDDM), anterior ventral (AV) and ventral lateral (VL) thalamic nucleus. The deeper FG cells were related to the VL, zona incerta (ZI) and reticular (RT) thalamic nucleus. The relationships between structures and stained spinal cord cells were corroborated with smaller tracer injections (Fig. 4B, C). The quantity of superficial TB-stained cells was related to the GRA and Sol participation and cells were less numerous in deeper laminas.

Smaller FG and TB injections let us to confirm the involvement of the above-described nuclei because less cells were stained in the spinal cord (Fig. 4B, b1, b2, b3 illustrates these results). The smaller deposits of tracers confirm the results but with less quantity of spinal cord stained cells (Fig. 4C, c1, c2 c3). Moreover, we observed that Sol involvement is related to the superficial spinal cord cells. In the three groups of rats, we observed stained cells with TB, FG and TB/FG in both sides of the spinal cord. Smaller and more anterior FG and TB deposits generated stained cells in both sides of spinal cord, thus we decided to confirm the presence of the bilateral and bifurcated spinal cord cells using another methodological approach.

Characteristics of cells recorded and antidromic or orthodromic cell responses to GRA or VPL electrical stimulation

We focused our experimental interest on wide dynamic range cells (WDR) due to their participation in nociception. In Fig. 5 an example of a WDR cell is plotted during electrical stimulation of its receptive field. The peri stimulus time histograms allowed us to specify the amount of A-beta-fiber (0–20 ms), A-delta-fiber (20–90 ms), and C-fiber (90–300 ms) action potentials produced by each train of 20 stimuli. The latencies and the estimated type of activated fiber were in agreement with previous reports (Urch and Dickenson, 2003).

Twenty-seven cells responded antidromically (Fig. 6) and 78 cells responded orthodromically (Fig. 7) to the electrical stimulation of the GRA. Seventeen cells responded antidromically and 43 responded orthodromically to the electrical stimulation of the VPL.

The antidromic spinal cord cells that were activated by the GRA stimulation had a mean latency of 9.85 ± 1.001 ms, which corresponded to a conduction speed of 10.96 ± 0.989 m/s. The antidromic cells that were activated by the VPL stimulation had a mean latency of 10.82 ± 1.2 55, which corresponded to a conduction speed of 11.36 ± 1.239 m/s. Table 2 A shows the mean latency and estimated conduction speed for the antidromic cells responding only to GRA(-anti) or VPL(-anti) stimulation. Because different pathways, including cortical relays could mediate the orthodromic responses, the conduction speeds and latencies of these cells were not included in Table 2.

Antidromic branched cells respond to GRA and VPL electrical stimulation

Seven cells were antidromically activated by the electrical stimulation of both GRA and VPL (in Table 2 A GRA-anti-anti and VPL-anti-anti). The mean latency for GRA-activated cells and VPL-activated cells was 7.28 ± 1.39 2 ms and 13.71 ± 2.417 ms, respectively. Fig. 6 shows

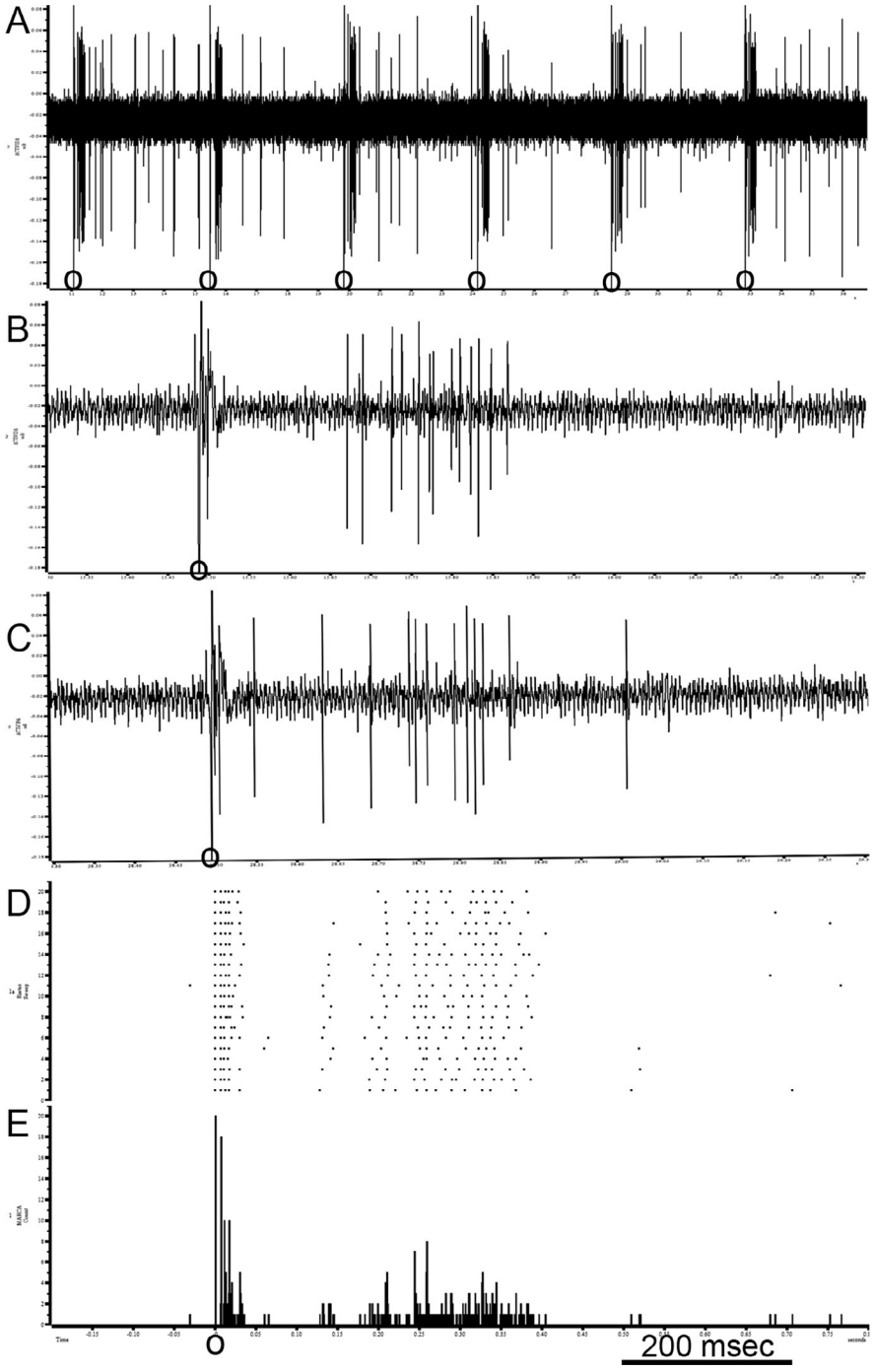

Fig. 5. WDR neuron responding to electrical stimulation of receptive field. In (A) six consecutive responses to electric stimulation are shown. In (B and C) single responses are plotted. In (D) raster display showing the consistence of the responses and in E the peristimulus time histogram of the digitalized cell action potentials. Notice that between 200 and 300 ms the C fibers were activated. Bin time 1 ms. 0 designates the stimulus artifact.

an example of an antidromic cell responding to electrical stimulation of both the GRA (Fig. 6A) and the VPL (Fig. 6B). It is important to notice that the cell activity illustrated in Fig. 6 is from a cell with the shortest latency and it was found in the superficial layers of the dorsal horn.

The mean conduction velocity was 13.689 ± 1.937 m/s for the cells projecting to the GRA and 9.629 ± 2 .324 m/s for the cells projecting to the VPL. It is interesting to notice that the GRA and VPL latencies were significantly different (t = 3.198; gl = 6; $P < 0.01$), but the conduction velocities were not (t = 2.27; gl = 6; $P < 0.6$). These values are listed in Table 2B. Another characteristic of spinal cord cells that respond to the antidromic stimulation was that they can follow high frequencies of stimulation, which is described as a characteristic (Fuller and Schlag, 1976) of the antidromic cells responses as it is illustrated in Fig. 6C, D.

Location of the recorded cells. After the recording and collision test, neurons that exhibited antidromic responses to GRA or VPL electrical stimulation were marked by an iontophoretic pontamine blue injection. The mean depth of 17 localized recorded cells was 748.9 ± 307.7 μm; two examples of histological spinal cord sections showing the recording sites are provided in Fig. 8.

DISCUSSION

General remarks

Our results show a higher proportion of ipsilateral bifurcated projecting cells (4.6 cells) when compared to the contralateral side (1 cell), however further studies are needed to see if this result can be replicated while using the right side as a reference.

The application of retrograde tracers in the GRA and VPL and the use of three different approaches TB (GRA)/FG(VPL) and TB(GRA)/FR (VPL) with direct fluorescence or immunofluorescence procedures, let us to detect labeled neurons on both sides of the lumbar segments of the spinal cord. This result was confirmed using the electrophysiological technique of antidromic activation, demonstrating that the ipsilateral GRA and the contralateral VPL electrical stimulations produced antidromic activities in the same spinal-cord cell. In brief, these results indicate a subset of L1-L6 spinal cord cells that project directly and bilaterally to the GRA and VPL.

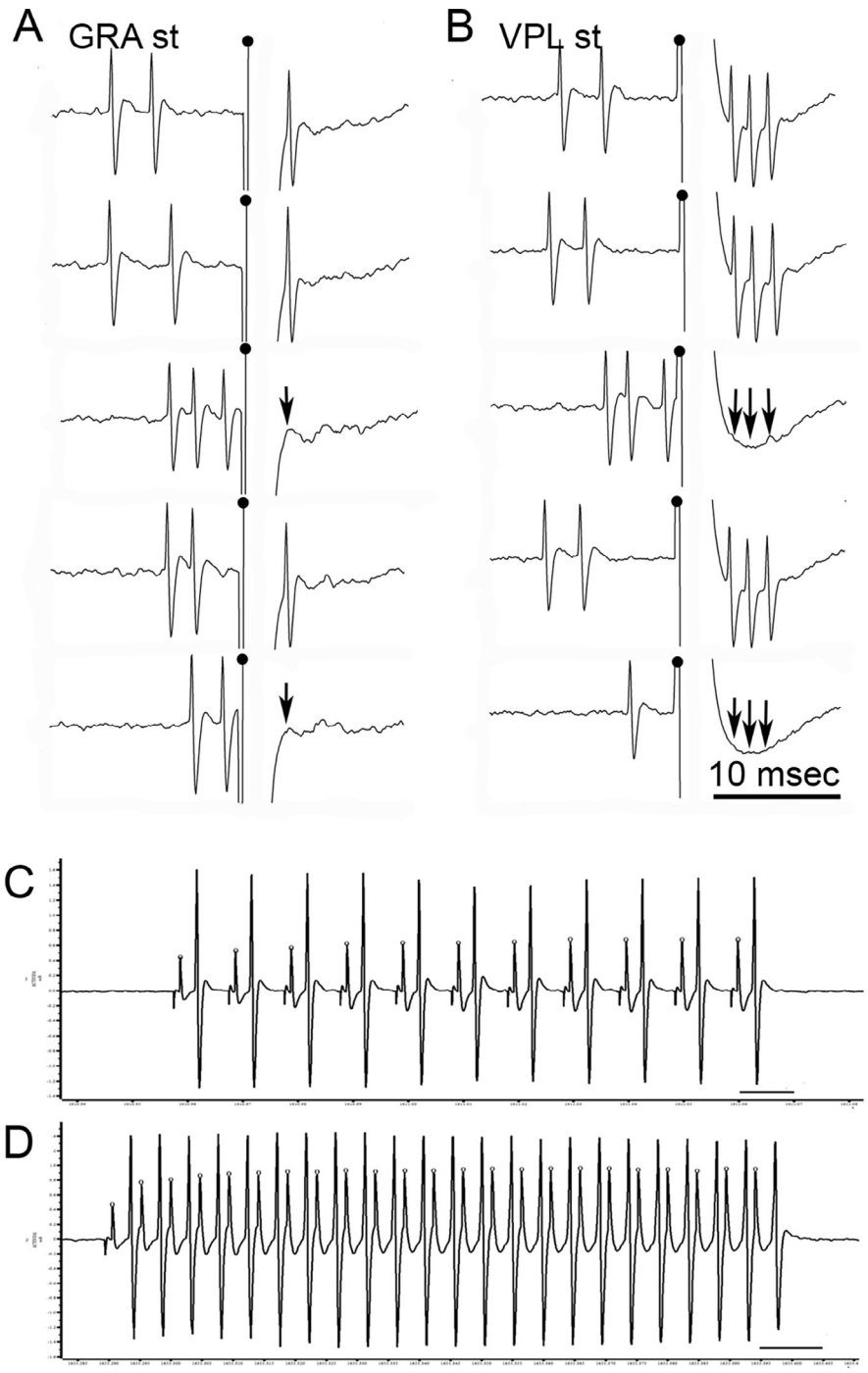

Fig. 6. Electrophysiological collision test. A single unit electrophysiological recording of a neuron responding to antidromic electrical stimulation of the GRA in (A) and VPL in (B) is illustrated. The arrows show the absence of an antidromic response due to the collision between the spontaneous and the antidromic action potential. In traces 1, 2 and 4, we can observe the fixed latency as a characteristic of the antidromic responses. Another characteristic of the antidromic-activated cells is their ability to follow high frequencies of stimulation. The recordings of spinal dorsal horn cells following 120 or 240 Hz stimulations are shown in (C and D) respectively.

Histological results

Extensive documentation has shown that the spinothalamic and dorsal column pathways are independent; however, the studies of Apkarian and Hodge (1989) and Hodge and Apkarian (1990) show a bilateral spinal cell projection to the posterior ventral posterolateral thalamic complex. Using the retrograde tracer with HRP, these authors reported that at least 17% of the spinothalamic cells in the spinal cord were found ipsilateral to the thalamic injections. Also, Kevetter and Willis (1984) previously reported that the 19% of the lateral thalamus and the 38% of the medial thalamus received an ipsilateral spinal projection. These authors also reported that the 2% of spinothalamic cells project to both sides of the thalamus. Our findings confirm the ipsilateral and the contralateral spinal cord projection to the VPL and furthermore for the first time demonstrate that these spinal neurons have a bifurcated projection to the GRA. This bilateral and bifurcated projection involves the postsynaptic DC-ML and the spino thalamic pathway for the AL systems.

Importantly, when the VPL injection site was changed in the antero-posterior or in the medial–lateral plane, the number of double-labeled spinal cord projection cells changed possibly due to the topographical representation of the body in the VPL (Mountcastle and Henneman, 1952). However, in the current version only the lumbar segments of the spinal cord were analyzed.

In fact, the spinal cord projection neurons have been extensively studied, particularly the lamina I projections to the caudal ventrolateral medulla, lateral parabrachial area and periaqueductal gray matter. Most of the lamina I projection neurons have been identified when the TB deposits located in the deeper part of the GRA nuclei and reached the solitarius tract, as has been suggested in previous descriptions (Bester et al., 1997, 2000; Gauriau and Bernard, 2002). This lamina I projection has also shown to have bilateral projections (Spike et al., 2003). In another study, the ascending spinohypothalamic projections through the contralateral side, also have a component along the ipsilateral side (Burstein et al., 1996). In a previous study (Rojas-Piloni et al., 2008), we used Diamidino Yellow (DY) and TB injections into the ipsilateral GRA and contralateral VPL, respectively, and we did not observe double-stained cells in the dorsal horn of

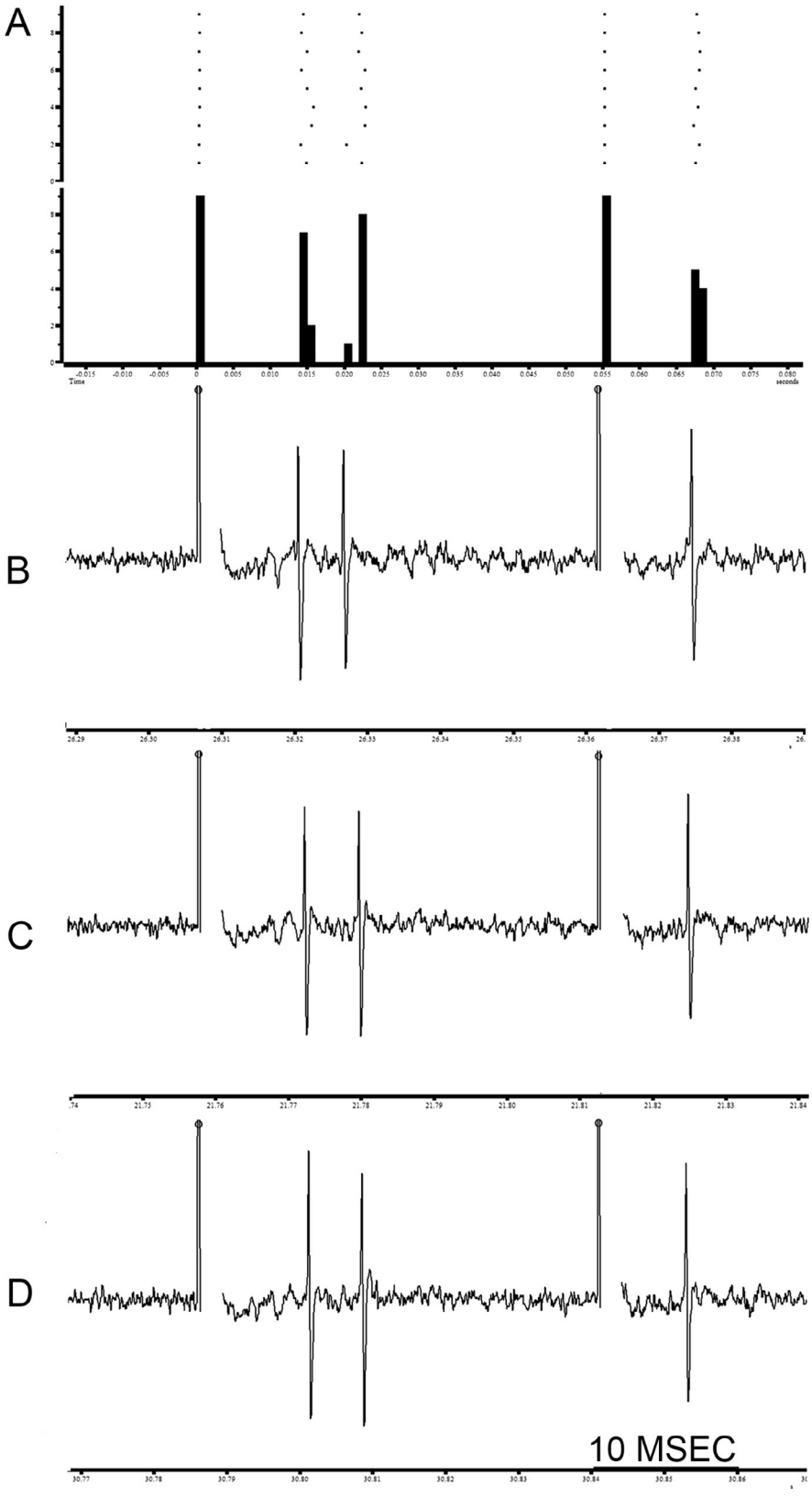

Fig. 7. Orthodromic responses to GRA and VPL electrical stimulation. In A, shows the raster display implemented with the digitalized signals for an orthodromic spinal cord cell responding to electrical stimulation of both GRA and VPL. In B, peri-stimulus time histogram of the stimulus artifact and the spike responses, the bin time was 1 ms. C, D and E individual recorded traces of the cell responses. The first responses on the left correspond to the GRA stimulation and the responses on the right correspond to the VPL stimulation. Notice the latencies variations in the responses, which allowed us to classify them as orthodromic.

the spinal cord. The main difference with our current results, is in the VPL injection sites, since the VPL tracer injection was more caudal (Ap 5.4 mm) and lateral (L 3.2 mm) compared to that in the present paper (Ap 6.1 and L 2.8 mm). This apparent discrepancy in the results due to the injection site locations only indicates the somatotopic and functional organization of the thalamus. Another interesting difference is that a particular cell population appears in the superficial layers of the spinal cord if the GRA injection involves the solitary tract, as described in the previous paragraphs. An important conclusion is that the neuroanatomical connections between the AL and DC-ML systems need to be conceptually restructured based on their functional interactions. Further studies need to address this subject.

Electrophysiological results

The recorded cells were characterized as wide dynamic range (WDR) cells due to their responses to different kinds of somatic stimulation intensities including noxious stimulation (see Fig. 5). Notice that between the antidromic activated cells by GRA and VPL we found one that was located in the superficial layers of the spinal cord. This cell displayed a characteristic double spike studied by Dickenson's works (Seagrove et al., 2004; Rojas-Piloni et al., 2007). This type of cells with double spontaneous and evoked spike activity is related with nociception and an enhanced response to noxious stimulation as wind-up (Dickenson, 1990). In fact, we focused our attention on WDR neurons because of their electrophysiological characteristics (e.g., they are projecting cells and are involved in nociception). It is interesting that Apkarian and Hodge (1989) proposed an ipsilateral spinal cord projection to the VPL that could be related to pain transmission in primates, but they did not provide any experimental support. Nevertheless, our present electrophysiological results support this hypothesis, namely that specific RF electrical stimulation activates the A delta and C fibers in the recorded spinal cord neurons.

Our present cell responses were orthodromic and antidromic to the stimulation of GRA or VPL, but the

Table 2. Latencies and conductions speeds values of antidromic activated cells. A, shows the mean and standard error values for the latencies (msec) and conduction speeds (m/s) for the antidromic (anti) responses produced by the GRA or VPL stimulation (as an example, GRA-anti-msec means that GRA stimulation produces an antidromic response and the value corresponds to the latency in msec. GRA-anti-m/s means that GRA stimulation produces an antidromic response and the value corresponds to the conduction speeds in m/s). The comparisons between the GRA and VPL latencies (msec) and conduction speeds (m/s) for the cells responding antidromically to GRA and VPL shown in B. The minimum value for significance was $P < 0.05$. Note that although the GRA vs. VPL anti-anti latency differences (msec) were significant, the differences in conduction speeds were not significant. These data are important for assuming that the axons that project to the VPL and the GRA have the same type of fiber. gl: liberty degrees; t: T value; NS: nonsignificant; **: $P < 0.05$; GRA: Gracilis nucleus; VPL: ventral posterolateral thalamic nucleus; anti: antidromic responses; anti-anti: antidromic responses for both GRA and VPL stimulation; msec: latency response in milliseconds; m/s: conduction speed

	N	Latency	m/s	
A				
GRA-anti	27	9.86 ± 1.00	10.96 ± 0.98	
VPL-anti	17	10.82 ± 1.25	11.36 ± 1.23	
GRA-anti-anti	7	7.28 ± 1.39	13.68 ± 1.93	
VPL-anti-anti	7	13.71 ± 2.41	9.62 ± 2.32	
		gl	*t*	*P* <
B				
GRAvsVPL-anti-anti-msec		6	3.198	0.019 **
GRAvsVPL-anti-anti-m/s		6	2.272	0.063 NS

most important finding was that some cells responded antidromically to both GRA and VPL electrical stimulation. This result confirms the existence of bifurcated spinal dorsal horn cells that project to the GRA and VPL. The antidromic activation technique has been widely used to demonstrate direct pathways, as well as cells with collaterals to different structures. The results shown in Table 2B demonstrate that the comparison between the conduction speeds of the antidromic spinal cord cells that responded to both GRA and VPL electrical stimulation were not significant, but the latencies were different, indicating that the spinal cord cells used the same size and type of bifurcated axons. Of course, the latencies were different because the distances were different.

Finally, the electrophysiological recordings using the collision test of spinal dorsal horn neurons during GRA and VPL electrical stimulation confirm our neuroanatomical results.

Functional considerations

Until now, it has been thought that the DC-ML system is related to the tactile and proprioceptive modalities, while the AL system is related to pain, temperature and crude touch. Moreover, the postsynaptic DC-ML system seems to be ipsilateral to the GRA or CUN nuclei at the medulla level, and the AL system is composed of several pathways, including the spino-thalamic, spino-mesencephalic and spinoreticular tracts. Strictly, our results only involved the spino-thalamic tract.

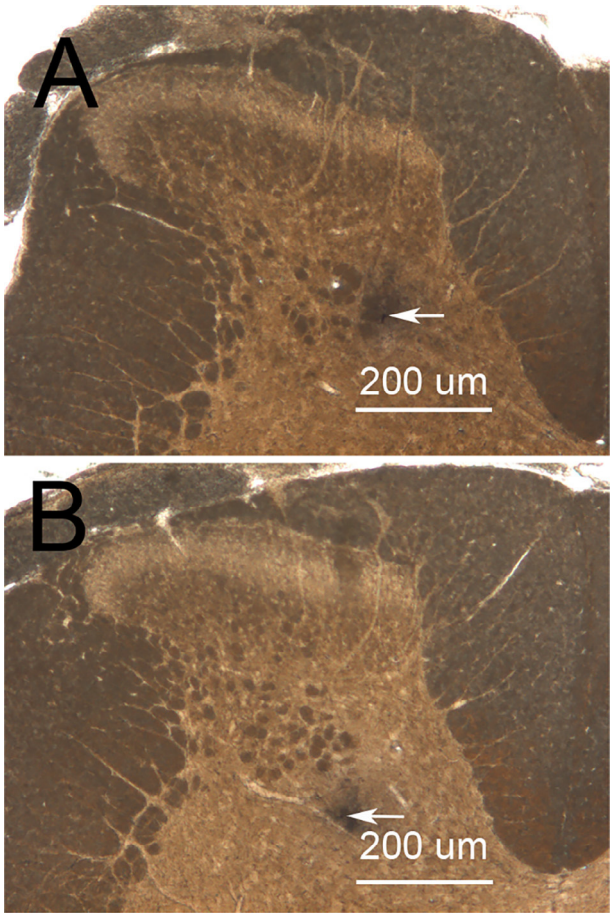

Fig. 8. Histological control of the recorded antidromic spinal cord cells. A section of the dorsal horn spinal cord at L4 is shown in (A) the white arrow points to the site of a recorded antidromic cell that responded to GRA and VPL electrical stimulation. The depth of the microdrive tip was 700 μm. Panel (B) shows another pontamine blue injection indicating the location of a recorded cell at a depth of 830 μm.

The present data show that single WDR spinal cord cells project bilaterally to the GRA and VPL, and it is possible that this neuronal arrangement serves to ensure that the alarm system of nociception generates a descending diffuse response. This last conclusion is supported by the finding that when the inhibitory paraventricular nucleus of the hypothalamus was stimulated, c-Fos activation was observed in the spinal cord, and the double and bifurcated cells were also c-Fos positive (Condés-Lara et al., 2015), providing negative feedback to reach a homeostatic state (Condés-Lara et al., 2009). This particular situation can explain the result showing that the threshold for nociceptive stimulation decreases on both sides of the body in neuropathic (Guilbaud et al., 1986; Desmeules et al., 1995) or carrageenan-induced (Guilbaud et al., 1986) pain models. In studies of human pain, the thalamic response has bilateral representation, likely reflecting generalized arousal in response to pain (Peyron et al., 2000). Additionally, a less common phenomenon reported in literature is the tactile hypersensitivity in the contralateral hind paw in experimental neuropathy. Some studies show contralateral tac-

tile allodynia from 10 to 120 days (Seltzer et al., 1990; Shir and Seltzer, 1990; Takaishi et al., 1996; Sinnott et al., 1999; Tabo et al., 1999). A 2-mm polyethylene cuff implanted around the sciatic nerve (Mosconi and Kruger, 1996) produces a decrease in the withdrawal threshold of both the ipsilateral and contralateral hind paws to normally innocuous tactile stimulation with von Frey hairs (Pitcher et al., 1999a,b). This evidence is of interest not only with respect to spinal cord pain representation, but also with respect to at least some forms of clinical chronic neuropathic pain (Kozin et al., 1976; Oaklander et al., 1998); it also suggests that altered sensory information processing may be established and maintained by bilateral peripheral nerve injury or inflammation (Bennett, 1999). Similarly, an increase in the contralateral neuronal firing rate was demonstrated in neuropathic rats (Pitcher and Henry, 2000).

Based on studies showing that tactile allodynia in experimental neuropathy is substantially decreased or abolished following spinal cord transection (Bian et al., 1998; Sung et al., 1998) or by an injection of lidocaine into the brain stem (Pertovaara et al., 1996). It has been argued that the greater tactile sensitivity of the nerve-injured hind paw is sustained via a supraspinal loop with tonic descending facilitating properties. In fact, the bilateral and bifurcated spinal cord projection neurons described in the present study could be responsible for this complex loop. But we don't know if this loop facilitates or inhibits the incoming afferent nociceptive and tactile information.

CONCLUSIONS

The results of the present study show that; (1) A sub-set of spinal dorsal horn cells is bifurcated and bilateral since they have projections to both main systems, the anterolateral and dorsal columns systems. (2) The unequal proportion of bifurcated cells regarding the body sides could be involved with the location of the stimulation source as a comparator. (3) The bilateral actions could interact with the diffuse endogenous inhibitory descending systems. (4) Further studies will be required to discern the real function of these novel interactions of the spinal cord projection cells.

CONFLICT OF INTEREST STATEMENT

The authors have no conflicts of interest to declare.

Acknowledgments—We acknowledge Jessica González Norris for proofreading the manuscript, Ing. Nydia Hernández Rios of the Microscopy Unit at the Neurobiology Institute for her technical assistance in the use of the confocal microscope. We are also indebted to UNAM (México) (PAPIIT-DGAPA Grant RN200415-2 to MCL) and the National Council of Science and Technology (CONACyT, Mexico) for financial support (Grant No. 164536 to MCL and Grant 176782 to GRP). AGH is a Postdoctoral CONACyT Fellow. ITG and AMG were also supported by CONACYT (México).

REFERENCES

Almeida TF, Roizenblatt S, Tufik S (2004) Afferent pain pathways: a neuroanatomical review. Brain Res 1000:40–56.

Angaut-Petit D (1975a) The dorsal column system: I. Existence of long ascending postsynaptic fibers in the cat's fasciculus Gracilis. Exp Brain Res 22:457–470.

Angaut-Petit D (1975b) The dorsal column system: II. Functional properties and bulbar relay of the postsynaptic fibres of the cat's fasciculus Gracilis. Exp Brain Res 22:471–493.

Apkarian AV, Hodge Ch (1989) Primate spinothalamic pathways: I. A quantitative study of the cells of origin of the spinothalamic pathway. J Comp Neurol 288:447–473.

Bennett GJ (1999) New frontiers in mechanisms and therapy of painful peripheral neuropathies. Acta Anaesthesiol Sin 37:197–203.

Bester H, Chapman V, Besson JM (2000) Physiological properties of the lamina I spinoparabrachial neurons in the rat. J Neurophysiol 83:2239–2259.

Bester H, Matsumoto N, Besson JM, Bernard JF (1997) Further evidence for the involvement of the spinoparabrachial pathway in nociceptive processes: a c-Fos study in the rat. J Comp Neurol 383:439–458.

Bian D, Ossipov MH, Zhong C, Malan Jr TP, Porreca F (1998) Tactile allodynia, but not thermal hyperalgesia, of the hind limbs is blocked by spinal transection in rats with nerve injury. Neurosci Lett 1241:79–82.

Burstein R, Falkowsky O, Borsook D, Strassman A (1996) Distinct lateral and medial projections of the spinohypothalamic tract of the rat. J Comp Neurol 373:549–574.

Condés-Lara M, Martínez-Lorenzana G, Rubio-Beltrán E, Rodríguez-Jiménez J, Rojas-Piloni G, González-Hernández A (2015) Hypothalamic paraventricular nucleus stimulation enhances c-Fos expression in spinal and supraspinal structures related to pain modulation. Neurosci Res 98:59–63.

Condés-Lara M, Martínez-Lorenzana G, Rojas-Piloni G, Tello-García I, Rubio-Beltrán E, González-Hernández A (2016) Bilateral dorsal horn neurons projecting throughout the dorsal column and the antero lateral system. A neuroanatomical and electrophysiological study, in rats. 16th World Congress on Pain 2016 International Association for the Study of Pain YOKOHAMA, JAPAN Septiembre 26–30.

Condés-Lara M, Rojas-Piloni G, Martínez-Lorenzana G, Rodríguez-Jiménez J (2009) Paraventricular hypothalamic oxytocinergic cells responding to noxious stimulation and projecting to the spinal dorsal horn represent a homeostatic analgesic mechanism. Eur J Neurosci 30:1056–1063.

Desmeules JA, Kayser V, Weil-Fuggaza J, Bertrand A, Guilbaud G (1995) Influence of the sympathetic nervous system in the development of abnormal pain-related behaviours in a rat model of neuropathic pain. Neuroscience 67:941–951.

Dickenson AH (1990) A cure for wind-up: NMDA receptor antagonists as potential analgesics. Trends Pharmacol Sci 11:307–309.

Fuller JH, Schlag JS (1976) Determination of antidromic excitation by the collision test: problems of interpretation. Brain Res 112:283–298.

Gardner EP, Johnson K (2013) The somatosensory system: receptors and central pathways. In: Kandel ER, Schwartz JH, Jessell TM, Siegelbaum SA, Hudspeth AJ, editors. Principles of neural science. New York: Mc Graw Hill. p. 475–497.

Gauriau C, Bernard JF (2002) Pain pathways and parabrachial circuits in the rat. Exp Physiol 87:251–258.

Guilbaud G, Benoist JM, Condés-Lara M, Gautron M (1993) Further evidence for the involvement of SmI cortical neurons in nociception: their responsiveness at 24 hr after carrageenin-induced hyperalgesic inflammation in the rat. Somatosens Mot Res 10:229–244.

Guilbaud G, Peschanski M, Briand A, Gautron M (1986) The organization of spinal pathways to ventrobasal thalamus in an experimental model of pain (the arthritic rat). An electrophysiological study. Pain 26:301–312.

Hendry SHC, Hsiao SS, Bushnell C (1999) Somatic sensation. In: Zigmond MJ, Bloom FE, Landis SC, Roberts JL, Squire LR, editors. Fundamental neuroscience. San Diego: Academic Press. p. 761–790.
Hodge CJ, Apkarian AV (1990) The spinothalamic tract. Crit Rev Neurobiol 5:363–398.
Kevetter OA, Willis WD (1984) Collateralization in the spinothalamic tract: new methodology to support or deny phylogenetic theories. Brain Res Rev 7:1–14.
Kozin F, McCarty DJ, Sims J, Genant H (1976) The reflex sympathetic dystrophy syndrome. I. Clinical and histologic studies: evidence for bilaterality, response to corticosteroids and articular involvement. Am J Med 60:321–331.
Lu G-W, Willis WD (1999) Branching and/or collateral projections of spinal dorsal horn neurons. Brain Res Rev 29:50–82.
Martin JH, Jessell TM (1991) Modality coding in the somatic sensory system. In: Kandel ER, Schwartz JH, Jessell TM, Siegelbaum SA, Hudspet AJ, editors. Principles of neural science. New York: Mc Graw Hill. p. 341–352.
Millan J (1999) The induction of pain: an integrative review. Prog Neurobiol 57:1–164.
Mosconi T, Kruger L (1996) Fixed-diameter polyethylene cuffs applied to the rat sciatic nerve induce a painful neuropathy: ultrastructural morphometric analysis of axonal alterations. Pain 64:37–57.
Mountcastle VB, Henneman E (1952) The representation of tactile sensibility in the thalamus of the monkey. J Comp Neurol 97:409–439.
Oaklander AL, Romans K, Horasek S, Stocks A, Hauer P, Meyer RA (1998) Unilateral postherpetic neuralgia is associated with bilateral sensory neuron damage. Ann Neurol 44:789–795.
Paxinos G, Watson C (1998) The rat brain in stereotaxic coordinates, 6th. San Diego: Elsevier Academic.
Pertovaara A, Wei H, Hämäläinen MM (1996) Lidocaine in the rostroventromedial medulla and the periaqueductal gray attenuates allodynia in neuropathic rats. Neurosci Lett 218:127–130.
Peyron R, Laurent B, García-Larrea L (2000) Functional imaging of brain responses to pain. A review and meta-analysis. Neurophysiology 5:263–288.
Pitcher GM, Ritchie J, Henry JL (1999) Paw withdrawal threshold in the von Frey hair test is influenced by the surface on which the rat stands. J Neurosci Meth 87:185–193.
Pitcher GM, Ritchie J, Henry JL (1999) Nerve constriction in the rat: model of neuropathic, surgical and central pain. Pain 83:37–46.
Pitcher GM, Henry JL (2000) Cellular mechanisms of hyperalgesia and spontaneous pain in a spinalized rat model of peripheral neuropathy: changes in myelinated afferent inputs implicated. Eur J Neurosci 12:2006–2020.
Rojas-Piloni G, Dickenson AH, Condés-Lara M (2007) Superficial dorsal horn neurons with double spike activity in the rat. Neurosci Lett 419:147–152.
Rojas-Piloni G, Martínez-Lorenzana G, DelaTorre S, Condés-Lara M (2008) Nociceptive spinothalamic tract and postsynaptic dorsal column neurons are modulated by paraventricular hypothalamic activation. Eur J Neurosci 28:546–558.
Seagrove LC, Suzuki R, Dickenson AH (2004) Electrophysiological characterization of rat lamina I dorsal horn neurons and the involvement of excitatory amino acid receptors. Pain 108:76–87.
Seltzer Z, Dubner R, Shir Y (1990) A novel behavioral model of neuropathic pain disorders produced in rats by partial sciatic nerve injury. Pain 43:205–218.
Shir Y, Seltzer Z (1990) A-fibers mediate mechanical hyperesthesia and allodynia and C-fibers mediate thermal hyperalgesia in a new model of causalgiform pain disorders in rats. Neurosci Lett 115:62–67.
Sinnott CJ, Garfield JM, Strichartz GR (1999) Differential efficacy of intravenous lidocaine in alleviating ipsilateral versus contralateral neuropathic pain in the rat. Pain 80:521–531.
Spike RC, Puskár Z, Andrew D, Todd AJ (2003) A quantitative and morphological study of projection neurons in lamina I of the rat lumbar spinal cord. Eur J Neurosci 18:2433–2448.
Sung B, Na HS, Kim YI, Yoon YW, Han HC, Nahm SH, Hong SK (1998) Supraspinal involvement in the production of mechanical allodynia by spinal nerve injury in rats. Neurosci Lett 246:117–119.
Tabo E, Jinks SL, Eisele Jr JH, Carstens E (1999) Behavioral manifestations of neuropathic pain and mechanical allodynia, and changes in spinal dorsal horn neurons, following L4–L6 dorsal root constriction in rats. Pain 180:503–520.
Takaishi K, Eisele Jr JH, Carstens E (1996) Behavioral and electrophysiological assessment of hyperalgesia and changes in dorsal horn responses following partial sciatic nerve ligation in rats. Pain 66:297–306.
Urch CE, Dickenson AH (2003) In vivo single unit extracellular recordings from spinal cord neurons of rats. Brain Res Protoc 12:26–34.
Zimmermann M (1983) Ethical guidelines for investigations of experimental pain in conscious animals. Pain 16:109–110.

(Received 19 October 2017, Accepted 30 November 2017)
(Available online 9 December 2017)

EJP
European Journal of Pain

ORIGINAL ARTICLE

The role of peripheral vasopressin 1A and oxytocin receptors on the subcutaneous vasopressin antinociceptive effects

A. Manzano-García, A. González-Hernández, I.A. Tello-García, G. Martínez-Lorenzana, M. Condés-Lara

Departamento de Neurobiología del Desarrollo y Neurofisiología, Instituto de Neurobiología, Universidad Nacional Autónoma de México, Querétaro, México

Correspondence
Miguel Condés-Lara
E-mail: condes@unam.mx

Funding sources and conflict of interest disclosure
This work was sponsored by grant (to M. Condés-Lara) PAPIIT-UNAM (Grant No. IN200415) and (to A. González-Hernández) PAPIIT-UNAM (Grant No. IA203117). A. Manzano-García is a doctoral student from Programa de Doctorado en Ciencias Biomédicas, Universidad Nacional Autónoma de México (UNAM) and received fellowship (597467) from CONACYT. I.A. Tello-García also is a doctoral student form Programa de Doctorado en Ciencias Biomédicas, UNAM and received fellowship (414165) from CONACYT.

Conflicts of interest disclosures
The authors have no conflicts of interest to declare

Accepted for publication
23 September 2017

doi:10.1002/ejp.1134

Abstract

Background: Vasopressin (AVP) seems to play a role as an antinociceptive neurohormone, but little is known about the peripheral site of action of its antinociceptive effects. Moreover, AVP can produce motor impairment that could be confused with behavioural antinociception. Finally, it is not clear which receptor is involved in the peripheral antinociceptive AVP effects.
Methods: In anaesthetized rats with end-tidal CO_2 monitoring, extracellular unitary recordings were performed, measuring the evoked activity mediated by Aβ-, Aδ-, C-fibres and post-discharge. Behavioural nociception and motor impairment were evaluated under subcutaneous AVP (0.1–10 μg) using formalin and rotarod tests. Selective antagonists to vasopressin ($V_{1A}R$) or oxytocin receptors (OTR) were used. Additionally, vasopressin and oxytocin receptors were explored immunohistochemically in skin tissues.
Results: Subcutaneous AVP (1 and 10 μg/paw) induced antinociception and a transitory reduction of the end-tidal CO_2. The neuronal activity associated with Aδ- and C-fibre activation was diminished, but no effect was observed on Aβ-fibres. AVP also reduced paw flinches in the formalin test and a transitory locomotor impairment was also found. The AVP-induced antinociception was blocked by the selective antagonist to $V_{1A}R$ (SR49059) or OTR (L368,899). Immunohistochemical evidence of skin VP and OT receptors is given.
Conclusions: Subcutaneous AVP produces antinociception and behavioural analgesia. Both V1a and OTR participate in those effects. Our findings suggest that antinociception could be produced in a local manner using a novel vasopressin receptor located in cutaneous sensorial fibres. Additionally, subcutaneous AVP also produces important systemic effects such as respiratory and locomotor impairment.
Significance: Our findings support that AVP produces peripheral antinociception and behavioural analgesia in a local manner; nevertheless, systemic effects are also presented. Additionally, this is the first detailed electrophysiological analysis of AVP antinociceptive action after subcutaneous administration. The results are reasonably explained by the demonstration of $V_{1A}R$ and OTR in cutaneous fibres.

1. Introduction

Arginine-vasopressin (AVP), a neurohypophysial hormone well known for its effects on water homeostasis and blood pressure regulation, has been implied as a potential peptide modulating nociception. In rodents, intracerebroventricular (Kordower

and Bodnar, 1984) and intrathecal (Thurston et al., 1988, 1992; Peng et al., 2015) AVP administration produces behavioural analgesia. Furthermore, a physiological antinociceptive participation of AVP has been suggested by the facts that the AVP-deficient Brattleboro rat strain has hyperalgesia and diminished stress-induced analgesia (Bodnar et al., 1982), and that the systemic hyperosmotic challenge, a model of physiological release of AVP, produces antinociception (Schorscher-Petcu et al., 2010). In this sense, normal AVP plasma concentrations in humans increase from ≈ 4 pg/mL to >13 pg/mL after hypertonic saline infusion (Baylis and Robertson, 1980). Importantly, painful stimuli produce an increment in plasma AVP in rodents (Suzuki et al., 2009) and humans (Kendler et al., 1977; Auböck and Konzett, 1983; Yang et al., 2012), reaching concentrations >25 pg/mL in the latter (Yang et al., 2012).

Systemic AVP (or analogue) administration produces antinociception in chemical, thermal, inflammatory and mechanical nociceptive tests (Berkowitz and Sherman, 1982; Berson et al., 1983; Schorscher-Petcu et al., 2010; Mogil et al., 2011). However, the site of the AVP antinociceptive action after its peripheral administration had not been explored. It has been suggested that AVP could act at dorsal root ganglion (DRG) neurons enhancing $GABA_A$ currents (Qiu et al., 2014a). Recently, Qiu et al. (2014b) showed that subcutaneous AVP diminished the number of flinches induced by acetic acid, suggesting a peripheral local effect. Nevertheless, peripheral AVP administration produces motor impairment (Andrews et al., 1983; Ettenberg et al., 1983), but no information about locomotor effects in behavioural models of pain is available. Furthermore, considering that AVP can cross the blood–brain barrier (Zlokovic et al., 1990), the action site (peripheral vs. central) preceding systemic AVP administration remains ambiguous.

Although the consensus about the receptor involved in AVP-induced antinociception is related to activation of the vasopressin 1a receptor ($V_{1A}R$) (Schorscher-Petcu et al., 2010; Mogil et al., 2011; Qiu et al., 2014a,b), the role of cutaneous oxytocin receptors (OTR) (González-Hernández et al., 2017) cannot be excluded considering their similitudes (Chini and Manning, 2007). Therefore, the aim of this study was to (1) evaluate the existence of local antinociceptive effects induced by subcutaneous (s.c.) AVP administration, (2) evaluate the participation of $V_{1A}R$ and OTR and (3) differentiate between antinociception and motor impairment. Consequently, we performed electrophysiological recordings of wide dynamic range (WDR) neurons and used behavioural models of acute pain and locomotor function as well as selective high-affinity $V_{1A}R$ (SR49059) (Serradeil-Le Gal et al., 1993) and OTR (L-368,899) (Williams et al., 1994) antagonists. Using these methods, we found that the s.c. administration of AVP has a local antinociceptive effect that is mainly mediated by $V_{1A}R$, but we also found OTR participation. In fact, we found $V_{1A}R$ and OTR immunohistochemically positive cutaneous sensorial fibres that could explain our results. Furthermore, AVP produces an important respiratory and motor impairment.

2. Materials and methods

2.1 Experimental animals

Experiments were performed using male Wistar rats (n = 105 rats, 280–320 g). Animals were housed in individual cages in a climate-controlled room, with water and food *ad libitum* and a 12-hour light-dark cycle. All experiments were carried out in accordance with the International Association for the Study of Pain (IASP) Guidelines for the Use of Animals in Research (Zimmermann, 1983) and with the approval of the Bioethical Committee at the Instituto de Neurobiología (Bioethical Committee protocols numbers 008, 009 and 010).

2.2 Electrophysiological approach

2.2.1 Surgical procedure

The rats were anaesthetized with urethane (1.2 g/kg; intraperitoneal, i.p.). A tracheotomy was performed to provide artificial ventilation (55 strokes/min, containing two-thirds N_2O and one-third O_2) and to monitor end-tidal CO_2 (Capstar-100 CO_2 analyzer; CWI Inc., Ardmore PA, USA) during the experiment (depicted in Fig. 1A,B,F). The temperature was maintained at 38 °C using a circulating water pad system. The rats were secured in a stereotaxic frame and the lumbar vertebrae were fixed to a spinal frame to improve the stability of the preparation. A laminectomy was performed to expose L4–L6 spinal cord segments, and the dura was carefully removed.

2.2.2 Electrophysiological recordings

Extracellular single unit recordings from deep dorsal horn segments (depth 500–1000 μm) were made using quartz platinum/tungsten microelectrodes

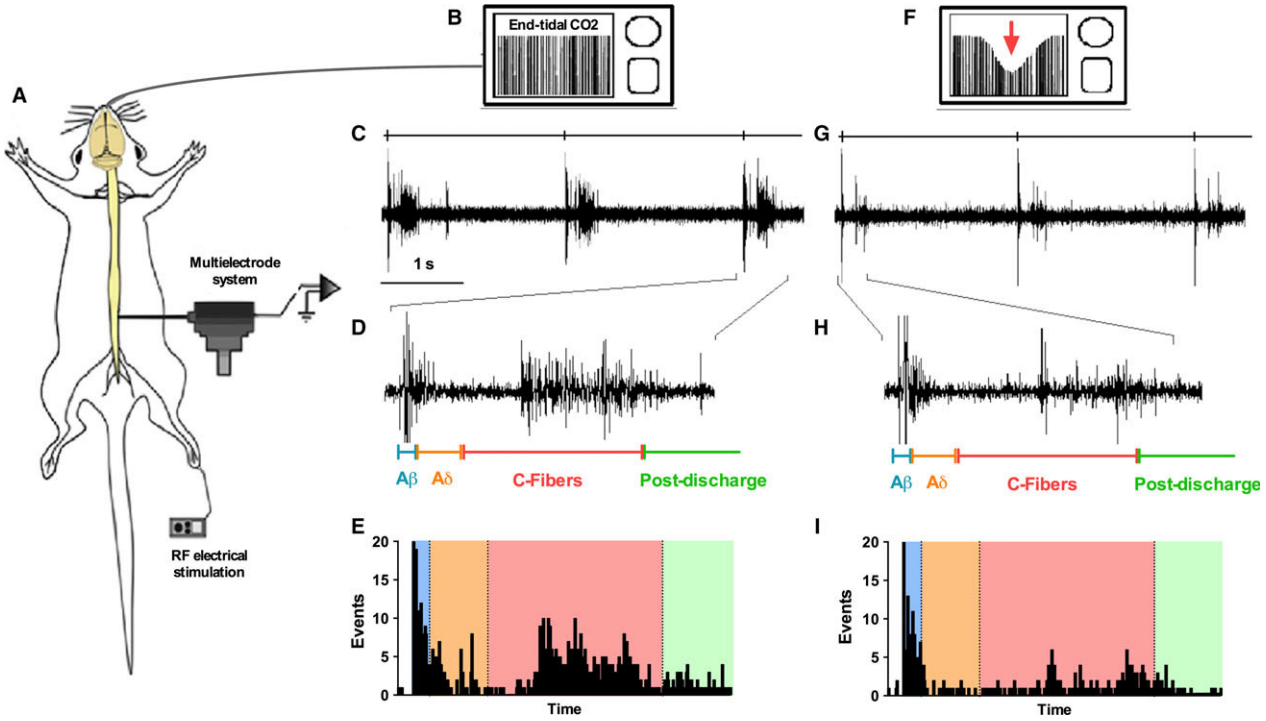

Figure 1 Spinal cord neuronal responses to the receptive field (rf) electrical stimulation. (A) Experimental set-up depicting the recording site at the spinal cord and the rf area of stimulation. (B) Represents the measurement of end-tidal CO_2 with a capnography monitor during the electrophysiological experiments. (C) Stimulus artefact and three responses of WDR spinal neurons after rf electrical stimulation. (D) Single response induced by rf electrical stimulation, and time latencies depicting the different fibre components. (E) Peristimulus time histogram obtained from 20 responses to rf electrical stimulation. (F) Depicts the acute reduction of end-tidal CO_2 10 min after AVP (10 μg/50 μL) s.c. administration. (F, G, H, I) show the effect 40 min after AVP (10 μg/50 μL) s.c. administration in the rf. Notice the reduction of activity mediated by Aδ- and C-fibres, and post-discharge.

(≈3–9 MΩ). Neuronal activity was recorded, amplified (×1000), filtered (300 Hz-3 KHz), digitalized and analysed using the Spike 2 system (CED, Cambridge, UK) (Fig. 1A,C,D,G,H). Recorded neurons received afferent input from the ipsilateral hind paw region, and the receptive field (RF) was found with non-noxious tactile stimulation (gentle tapping of the hind paw). Once a single-cell signal responsive to RF stimulation was located, two stainless stimulation electrodes (27 G) were inserted subcutaneously into the RF (Fig. 1A). Stimuli (1-ms pulses at 0.5 Hz; Grass S11 Stimulator) with increasing intensities were given to determine the threshold for activating Aδ- and C-fibres (high threshold stimulation). Only cells that responded to both low and high threshold stimulation were used in this study; these cells are classified as wide dynamic range (WDR) neurons. Peristimulus time histograms (PSTH) were used to classify and quantify the evoked WDR neuronal responses according to the following stimulated fibre latencies: Aβ (0–20 ms), Aδ (20–90 ms), C-fibres (90–300 ms) and post-discharge (300–800 ms) (Fig. 1E,I) (Urch and Dickenson, 2003).

2.2.3 Experimental design

Each peristimulus histogram was constructed with a series of 20 electrical pulses (1 ms, 0.5 Hz) at an intensity adjusted to 3 times the threshold required to evoke a C-fibre response. After 4 control series, each one separated by a 5-min interval, AVP (0.1, 1 or 10 μg/50 μL) was administered s.c. into the RF; then, stimulation was given at minutes 0, 5, 10, 20, 30, 40, 50 and 60 after AVP administration. To evaluate whether the pharmacological effect of AVP was local or systemic, AVP (10 μg/50 μL) was administered s.c. into the paw contralateral to the electrical stimulation in one group of rats. To test $V_{1A}R$ or OTR participation in AVP effects, the specific antagonists SR49059 (10 μg/50 μL; $V_{1A}R$ antagonist) or L-368,899 (10 μg/50 μL; OTR antagonist) were given s.c. in the RF 5 min prior to AVP, and then the aforementioned protocol was followed. As the doses used for the agonist and antagonist could change in their bioavailability and pharmacodynamics due to the subcutaneous administration, the selection followed literature references points (Serradeil-Le Gal

et al., 1993; Williams et al., 1994; Alexander et al., 2015). However, the AVP doses were 0.1, 1 and 10 to have a curve dose response.

2.3 Behavioural tests

2.3.1 Formalin-induced pain behaviour

Animals were habituated to the observation chamber for 30 min for 3 consecutive days prior to the experimental day. On the day of the test, the animals were placed in the observation chamber for 30 min, then AVP (0.1, 1 or 10 μg/50 μL) was injected s.c. into the dorsal surface of the right hind paw; 5 min later, formalin (50 μL of 1% formalin, diluted in saline) was injected s.c. into the same site as the AVP. The nociceptive behaviour (number of paw flinches or shakes) was quantified for 1 min every 5 min over the 60 min following formalin administration; this period was chosen to evaluate the three phases of the formalin test defined as follows: phase 1 (0:10 min), interphase (10:20 min) and phase 2 (20:60 min). To evaluate whether the pharmacological effect of AVP was local or systemic, AVP (10 μg/50 μL) was administered s.c. into the left hind paw (contralateral to the formalin administration) in one group of rats. In the groups with antagonists L-368,899 (100 μg/50 μL) or SR49059 (10 μg/50 μL), the antagonists were given s.c. injections 5 min prior to the AVP at the same site in the hind paw, and then the aforementioned protocol was followed.

2.3.2 Rotarod

A rotarod apparatus (IITC Inc. Life Science, CA, USA) was used to study the administration effects of AVP on locomotor function. The rotarod's velocity was set at 15 revolutions per minute (rpm) with a cut-off time of 180 s (drum diameter 9.52 cm). The rats were trained for 3 consecutive days (2 trainings per day). Training and experimental sessions consisted of 3 consecutive cycles of locomotion. In each cycle, the latency to fall from the rotarod was recorded and then averaged. After the training days, the same group of 9 rats was used for 21 days to evaluate the locomotor effect without treatment (control) and after the administration of saline (vehicle group), AVP (10 μg/50 μL) or OT (100 μg/50 μL). The drugs were injected s.c. into the dorsal surface of the hind paw 10 min prior to the rotarod test, with 24 h between the administration of each treatment.

2.4 Compounds

Apart from the anaesthetic (urethane), the drugs used were [Arg^8]-vasopressin acetate salt (AVP); oxytocin (OT); (2*S*)-1-[[(2*R*,3*S*)-5-Chloro-3-(2-chlorophenyl)-1-[(3,4-dimethoxyphenyl)sulfonyl]-2,3-dihydro-3-hydroxy-1*H*-indol-2-yl]carbonyl]-2-pyrrolidinecarboxamide (SR49059) and (2*S*)-2-Amino-*N*-[(1*S*,2*S*,4*R*)-7,7-dimethyl-1-[[[4-(2-methylphenyl)-1-piperazinyl]sulfonyl]methyl]bicyclo[2.2.1]hept-2-yl]-4-(methylsulfonyl)butanamide (L-368,899). All compounds were obtained from Sigma-Aldrich. AVP, OT and L-368,899 were dissolved in saline, whereas SR49059 was dissolved in DMSO (10%).

2.5 Data analysis

2.5.1 Electrophysiology

The mean number of action potentials evoked by peripheral stimuli in the four control series was set as 100% (we only used cells with less than a 10% variation in their activity during the control series). After drug administration, the number of action potentials was quantified in each series (from 0 to 60 min) and normalized compared to the control value. Throughout the experiment, the effect of AVP was evaluated globally as area under the curve (AUC, calculated with the trapezoid method) to unfold the time with the maximum response to AVP. Separate and global statistical comparisons were made between the effect of the different doses of AVP and the reversion by the antagonists. Only one unit was recorded for each animal. *Formalin test.* AUC constructed with the behavioural nociceptive response during phase 1, interphase and phase 2 was calculated. The statistical comparison between the effect of the different doses of AVP and the reversion by antagonists was done separately for each phase. *Rotarod.* The statistical comparison between the mean latencies to fall in each treatment and the control situation was conducted.

Figure data are presented as mean ± SEM (standard error of the mean). In all cases, statistical analysis was performed using GraphPad Prism® V6.01 software (La Jolla, CA, USA). Normal distribution was tested. In the electrophysiological experiments, a two-way repeated measures ANOVA was performed to analyse the effect of the treatments across the course of the experiment. One-way ANOVA was used to compare the global effect of different AVP doses and the participation of V_{1A}R and OTR in peripheral vasopressin effects in the electrophysiological and behavioural

models. Dunnett's post-hoc test was used to compare the treated groups versus the control groups. Tukey's post-hoc test was used when multiple comparisons were assessed. A probability value of $p < 0.05$ was considered statistically significant. The number of animals used in each experiment is reported in the results section.

2.6 Immunofluorescence for OTR and $V_{1A}R$

Three male Wistar rats (280–310 g) were prepared for an immunofluorescence of skin.

The animals were decapitated and immediately after, the lateral hairy skin areas were excised with a scalpel, snap-frozen in Tissue-Tek O.C.T. Compound (Sakura Finetek USA, Inc, Torrance, CA, USA), placed in liquid nitrogen-chilled isopentane and stored at −80 °C before sectioning. A double immunofluorescence for OTR and $V_{1A}R$ was performed on slide-mounted samples of 20-μm thick cryostat sections after fixation in 4% phosphate-buffered paraformaldehyde for 10 min at room temperature. The sections were stored in four consecutive series. The first was used for immunofluorescence as follows: a primary antibody cocktail was used for 24 h at 4 °C; it included polyclonal antibodies against OTR (raised in goat, diluted 1:400, Cat.no. sc-8103; Santa Cruz Biotechnology Inc, SantaCruz, CA, USA) and $V_{1A}R$ (raised in rabbit, diluted 1:300, Cat.no. A53272; Epigentek Group Inc, USA). The sections were washed for 5 min with 0.1M PBS and then incubated with the appropriate secondary antibody for 24 h at 4 °C. The secondary antibodies used were donkey anti-Goat IgG (Alexa Fluor 488 conjugate, Cat.no. A-11055; Invitrogen, USA) and donkey anti-Rabbit IgG (Alexa Fluor 555 conjugate, Cat.no. A-31572; Invitrogen). The second series of sections was treated without the primary antibody as a negative control to avoid a possible false-positive staining. The two remaining series were stored for further analysis.

2.7 Confocal microscopy and image analysis

Confocal images of the lateral hairy skin were acquired using the LSM510 or LSM780 confocal microscope system (Zeiss, Mexico) with 25 × /0.8, 40 × /1.3 and 63 × /1.32 NA oil immersion objective, using the 488-nm argon laser to excite Alexa Fluor 488, and 561-nm diode laser for Alexa Fluor 555. The pinhole, Z-sectioning intervals were kept constant for all images. About 15–30 optical Z-sections of 0.5–1 μm thickness were obtained from the 20-μm thick tissue for each skin image stack.

Optical sections were acquired at a digital size of 1024 × 1024 pixels and averaged three times to reduce noise. In all cases, the image obtained was improved (brightness and gamma) and analysed using the ZEN 2 Blue Edition Software (Carl Zeiss Microscopy GmbH, Göttingen, Germany). In addition, the colour for each channel was selected as follows: green for OTR and red for $V_{1A}R$. In all cases, a 2-dimensional projection image and a single optical section image (where the $V_{1A}R$ and OTR signal were strong) were imported in Tag Image File Format (TIFF) and were used to compose the multi-panel figures. In addition, an orthogonal projection using four optical sections was performed.

3. Results

3.1 Electrophysiological approach

3.1.1 Effect of peripheral AVP administration on the afferent spinal cord activity

The electrophysiological recordings of spinal cord neuronal activity showed that the lowest dose of AVP (0.1 μg/50 μL, $n = 6$ cells) did not change the neuronal activation evoked by Aβ-, Aδ- and C-fibres nor did it change the post-discharge (Fig. 2). The intermediate AVP dose, 1 μg/50 μL ($n = 5$ cells), did not affect the activity mediated by Aβ-fibres (Fig. 2A,E,I). Nevertheless, this dose produced a statistically significant reduction in the neuronal activity mediated by Aδ-fibres globally (Fig. 2F,J) and a non-significant reduction in the activity mediated by C-fibres (Fig. 2G,K). The peripheral administration of the highest dose of AVP (10 μg/50 μL, $n = 6$ cells) did not affect the activity mediated by Aβ-fibres (Fig. 2A,E,I), but it provoked a reduction in the activity evoked by Aδ- (Fig. 2B,F,J) and C-fibres (Fig. 2C,G,K) throughout the experiment. A two-way ANOVA showed a significant reduction of Aδ-mediated activity throughout the experiment, except 20 min after AVP administration, and a significant reduction of C-mediated activity starting on minute 20 (Fig. 2B,C) with the highest dose of AVP. In addition, this dose produced a global decrease in post-discharge (Fig. 2H,L) with a maximum effect 30 and 40 min after AVP administration (Fig. 2D). On the other hand, the administration of AVP (10 μg/50 μL, $n = 5$ cells) in the paw contralateral to the stimulated paw did not change the neuronal activation evoked by Aβ-, Aδ- and C-fibres (Fig. 2E,F,G,H,I,J,K, L), but a non-significant reduction in post-discharge was observed.

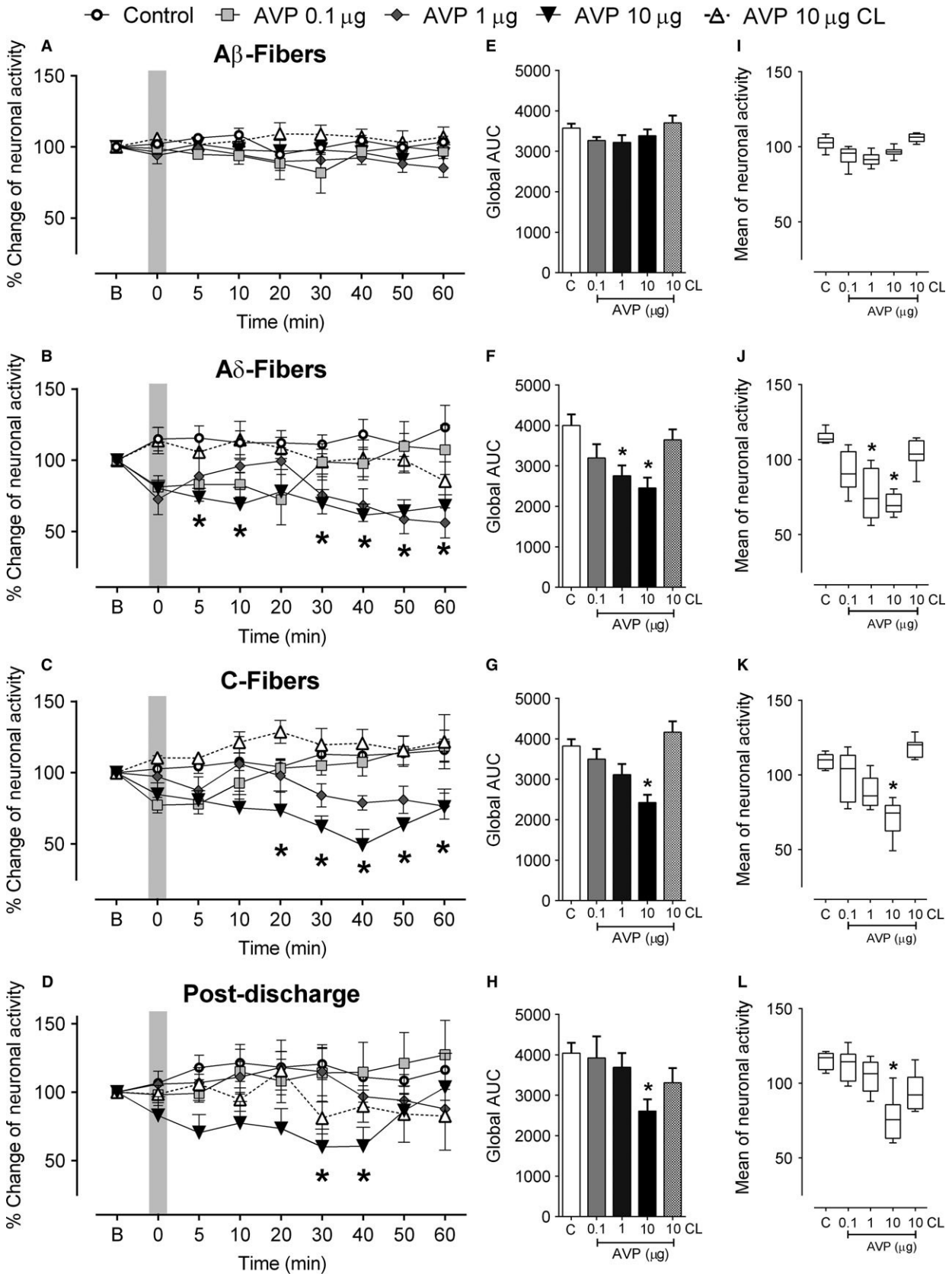

Figure 2 Effect of peripheral AVP administration on the afferent spinal cord activity. (A, B, C, D) graphs show the temporal course of the effects of peripheral AVP administration (dashed line) on the activity of spinal WDR neurons evoked by each type of fibre. *$p < 0.05$ represents the statistical difference between AVP (10 μg) and the control value at the same time (two-way ANOVA, Tukey's post-hoc test); for the sake of clarity, only the comparison of the maximum AVP dose is presented. (E, F, G, H) show the area under the curve (AUC) of the entire experiment for each treatment. (I, J, K, L) show the global data distribution for each dose. The boxes show the 95th and 5th percentiles, mean, and minimum and maximum values. Notice the inhibition of activity mediated by Aδ- and C-fibres, and post-discharge by AVP (10 μg). *$p < 0.05$, one-way ANOVA, Dunnett's post-hoc test. It is important to notice that AVP in doses of 10 μg applied in the contralateral (CL) paw produced no significant changes over the afferent activation.

3.1.2 Participation of V_{1A}R and OTR in the effect of peripheral AVP administration on the afferent spinal cord activity

In this set of experiments, we only used the AVP dose, which showed a significant reduction in the activity evoked by Aδ- and C-fibres, and the post-discharge from the prior experiments (AVP 10 μg/50 μL). Local pretreatment with the specific V_{1A}R antagonist SR49059 (10 μg/50 μL, $n = 5$ cells) completely abolished the AVP-induced antinociception throughout the experiment (Figs. 3 and 4). A comparison between the effects of AVP and AVP plus SR groups revealed a significant difference for Aδ, C and post-discharge global activity (Fig. 4F,G,H). Additionally, a two-way ANOVA analysis showed that pretreatment with the V_{1A}R antagonist reverted the effect of AVP in every measurement during the experiment (Fig. 4A,B,C,D). On the other hand, local pretreatment with the specific OTR antagonist, L-368,899 (10 μg/50 μL, $n = 5$ cells), produced a partial reversion of the global AVP-induced antinociception. Statistical comparison did not show differences between the AVP plus L3 and control groups nor between the AVP plus L3 and AVP groups when global activity was compared (Fig. 5F,G,H).

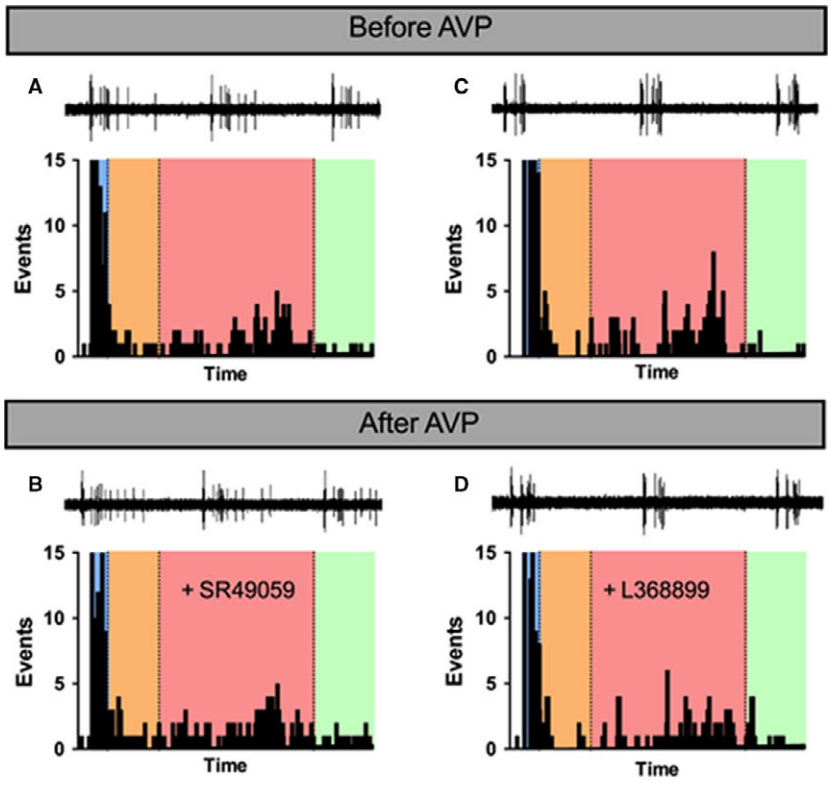

Figure 3 Effect of pretreatment with specific V_{1A}R and OTR antagonists on the AVP actions. (A, B) correspond to the same experiment. (A) Depicts three control responses of a WDR spinal neuron after receptive field (rf) electrical stimulation and a control peristimulus time histogram. (B) Represents the responses after 30 min of AVP administration and pretreatment with V_{1A}R antagonist SR49059. Notice the absence of AVP-induced reduction in Aδ- and C-fibre-evoked activity. (C, D) correspond to the same experiment. (C) Depicts control responses and peristimulus time histogram. (D) Represents the responses after 30 min of AVP administration and pretreatment with OTR antagonist L368899. Notice the blockade of AVP reduction in Aδ- and C-fibre-evoked activity.

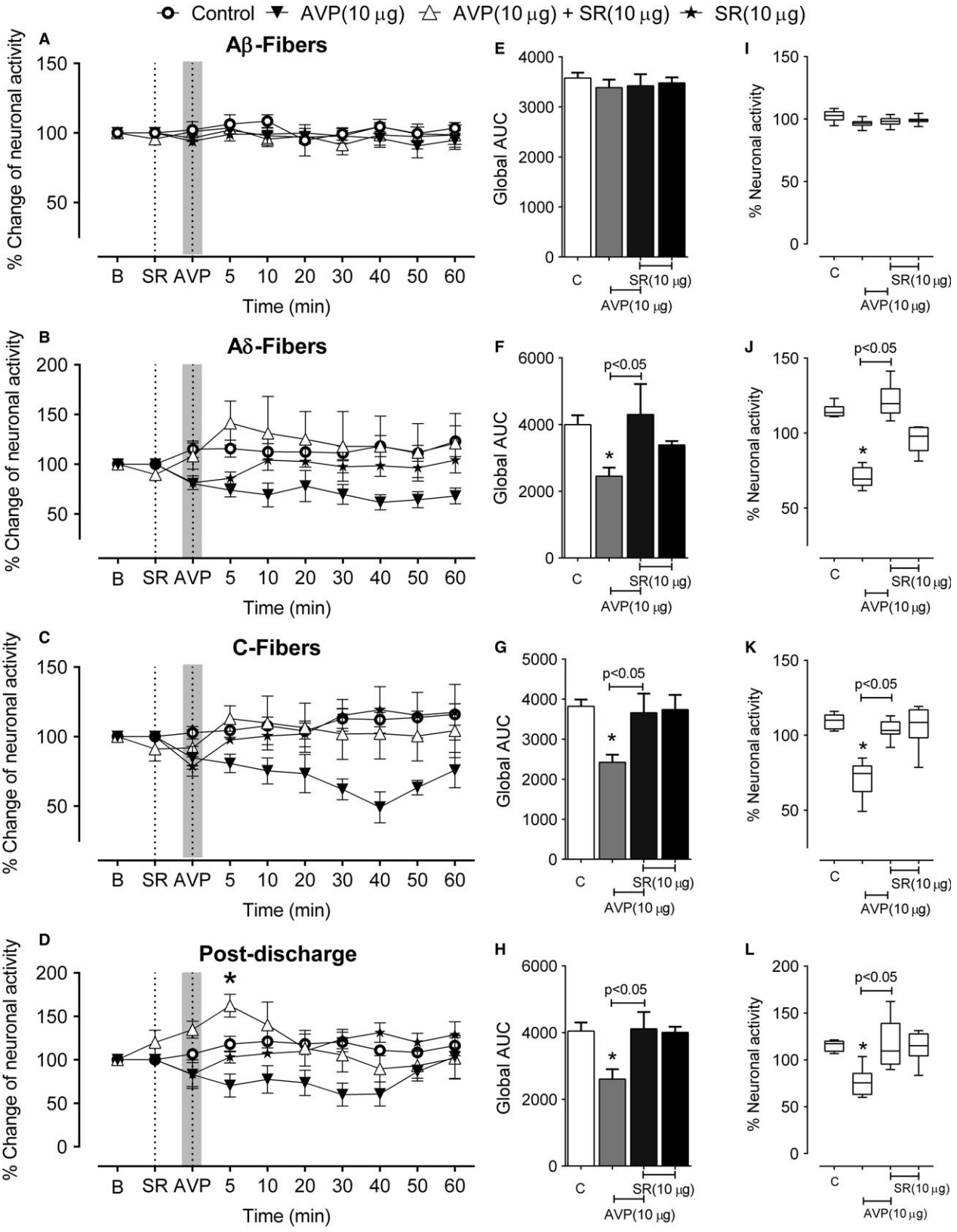

Figure 4 V1a receptor participation in the effects of peripheral AVP administration. (A, B, C, D) graphs show the temporal course of the effects of peripheral AVP (dashed line in darkened area) in animals pretreated with the $V_{1A}R$ antagonist (SR49059) (dashed line). *$p < 0.05$ represents the statistical difference between AVP (10 μg) + $V_{1A}R$ antagonist (10 μg) compared with the control value at the same time (two-way ANOVA, Tukey's post-hoc test); for the sake of clarity, only the comparison of the AV*P* + $V_{1A}R$ antagonist is presented. (E, F, G, H) show the area under the curve (AUC) of the entire experiment for each treatment. (I, J, K, L) show the global data distribution for each dose. The boxes show the 95th and 5th percentiles, mean, and minimum and maximum values. Notice the blockade produced by $V_{1A}R$ antagonist over the response produced by peripheral AVP (10 μg). *$p < 0.05$, one-way ANOVA, Tukey's post-hoc test.

Nevertheless, a two-way ANOVA analysis showed that pretreatment with OTR antagonist prevented the effect of AVP throughout the experiment, except for Aδ activity 60 min after AVP administration (Fig. 5A,B,C,D). Neither $V_{1A}R$ antagonist nor OTR antagonist administration produced an effect per se on Aβ-, Aδ-, and C-fibres, and post-discharge evoked responses ($n = 5$, $n = 6$ cells per group, respectively) (Figs. 4 and 5).

3.2 Effect of peripheral AVP administration on end-tidal CO_2

As described in the Surgical Procedure section, end-tidal CO_2 was recorded during the electrophysiological experiments. After s.c. administration of AVP (1 and 10 μg/50 μL, $n = 6$ rats per group), we found a reduction in end-tidal CO_2 between minutes 5 and 20. This effect was not present after OT administration (31 μg/50 μL, $n = 6$ rats) (Fig. 6). S.c. preadministration of $V_{1A}R$ (10 μg/50 μL, $n = 5$) and OTR (10 μg/50 μL, $n = 6$) antagonists did not prevent the end-tidal CO_2 reduction produced by AVP (data not shown).

3.3 Behavioural approach

3.3.1 Effect of peripheral AVP administration on formalin-induced pain behaviour

Peripheral administration of AVP (0.1 μg/50 μL, $n = 6$) failed to modify any of the three formalin test phases (Fig. 7A,B). AVP (1 μg/50 μL, $n = 6$) reduced the behavioural nociceptive response in phases 1 and 2 of the formalin test (Fig. 7A,B). AVP (10 μg/50 μL, $n = 6$) diminished the behavioural nociceptive response in all phases of the formalin test (phase 1, interphase and phase 2) (Fig. 7A,B). In contrast, the contralateral administration of AVP (10 μg/50 μL, $n = 5$) only diminished the behavioural nociceptive response in phase 1 and the interphase (Fig. 7A,B).

3.3.2 Participation of $V_{1A}R$ and OTR in the effect of AVP in the formalin test

Local pretreatment with either the $V_{1A}R$ antagonist SR49059 (10 μg/50 μL) or the OTR antagonist L-368,899 (100 μg/50 μL) failed to modify the effect of AVP (10 μg/50 μL) in phase 1 and the interphase; however, both antagonists partially reverted phase 2 of the formalin test ($n = 6$ per group) (Fig. 7C,D). The sole administration of SR49059 (10 μg/50 μL, $n = 7$) provoked a statistically significant increment in the behavioural nociceptive responses during the interphase and phase 2 of the formalin test (Fig. 7C). The antagonist L-368,899 had no significant effects (Fig. 7D).

3.3.3 Effect of peripheral AVP and OT administration on locomotor function

The s.c. administration of AVP (10 μg/50 μL, $n = 10$ rats) produced locomotor impairment as shown by the decrease in latency to fall. Locomotor impairment was totally absent 1 h after AVP administration. In contrast, the administration of OT (100 μg/50 μL) did not produce motor impairment (Fig. 8).

3.4 $V_{1A}R$ and OTR immunofluorescence

A double immunofluorescence technique against $V_{1A}R$ and OTR was accomplished in the lateral hairy skin tissues. This technique allowed us to observe in the same tissue of both types of receptors. The presence of $V_{1A}R$ was clearly detected in thin cutaneous fibres, and we confirmed the previous results of OTR fibres in the skin (González-Hernández et al., 2017). We tried to verify $V_{1A}R$ and OTR co-localization using the orthogonal view tool since both receptors were very close to each other in several regions and samples of both receptors. However, we did not have any evidence of co-localization between the two receptors. Figure 9 illustrates an example of at least two parallel fibres, one with $V_{1A}R$ and another with OTR.

4. Discussion

Taken together, these results show that s.c. AVP administration produces two discernible effects: (1) antinociception and behavioural analgesia; and (2) systemic responses (respiratory and locomotor impairment) that seem unrelated to antinociception but could temporarily predominate over the former.

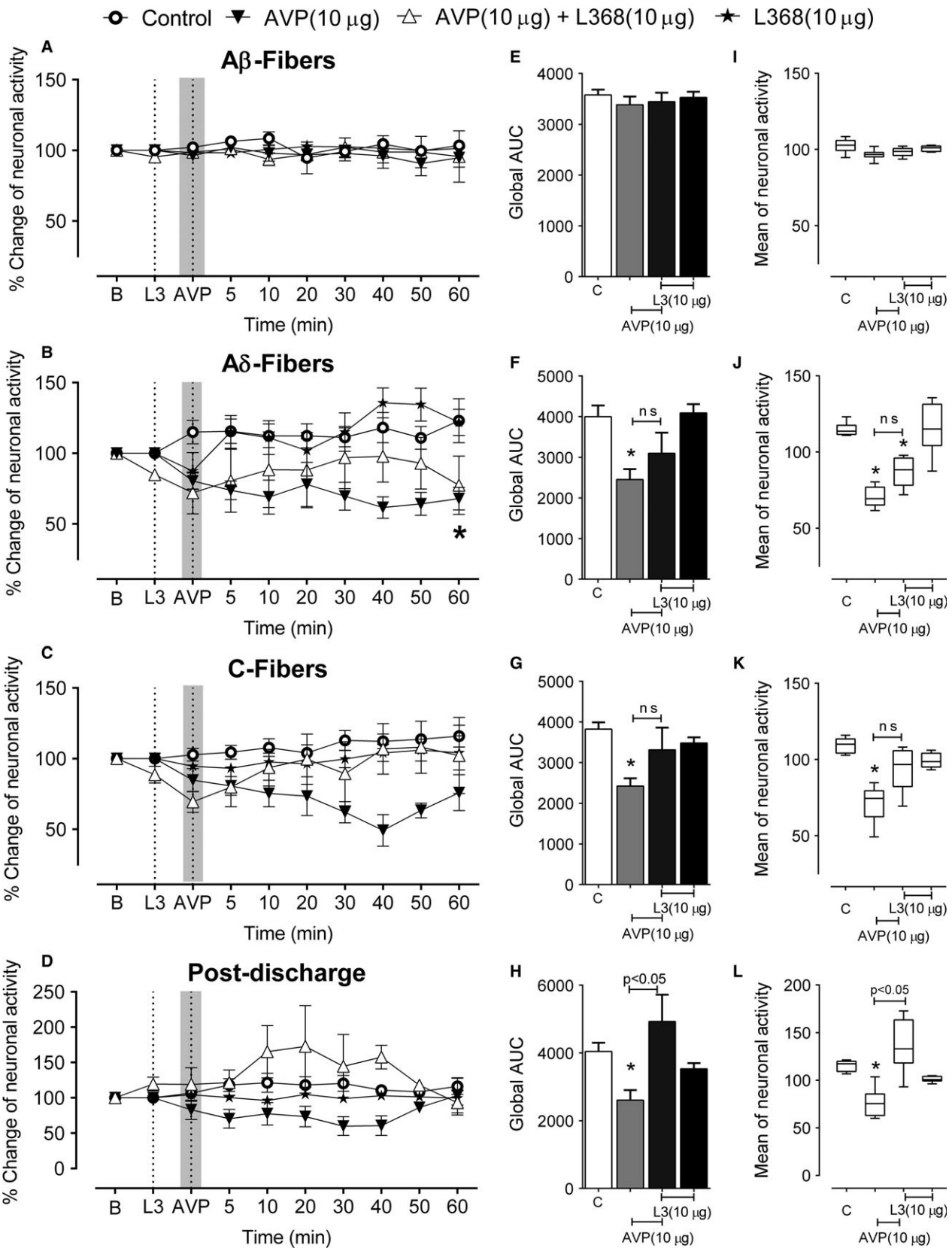

Figure 5 OT receptor participation in the effects of peripheral AVP administration. (A, B, C, D) Graphs showing the temporal course of the effects of peripheral AVP (dashed line in darkened area) in animals pretreated with the OTR antagonist (L368,899) (dashed line). Statistical difference between AVP (10 μg) + OTR antagonist (10 μg) compared with the control value at the same time (two-way ANOVA, Tukey's post-hoc test) was assessed. (E, F, G, H) show the area under the curve (AUC) of the entire experiment for each treatment. (I, J, K, L) show the global data distribution for each dose. The boxes show the 95th and 5th percentiles, mean, and minimum and maximum values. Notice the partial blockade produced by OTR antagonist over the response produced by peripheral AVP (10 μg) (F, J, G, K). *$p < 0.05$, one-way ANOVA, Tukey's post-hoc test.

Finally, our findings could be mediated by the presence of $V_{1A}R$ and OTR in cutaneous fibres.

4.1 Antinociception induced by peripheral AVP administration

AVP as an antinociceptive molecule has been previously addressed (Berkowitz and Sherman, 1982; Berson et al., 1983; Schorscher-Petcu et al., 2010; Mogil et al., 2011; Qiu et al., 2014a,b). It was hypothesized that systemic AVP could produce peripheral antinociception by up-regulating the function of the $GABA_A$ receptor (Qiu et al., 2014a) or inhibiting acid-sensing ion channels in the DRG (Qiu et al., 2014b). To our knowledge, only one work previously addressed the possible peripheral local effect of AVP administration (Qiu et al., 2014b). Qiu et al. (2014b) described that OT and AVP produced local antinociception after intraplantar injection of acetic acid. In fact, using electrophysiological and behavioural approaches, our results show that sub-cutaneous AVP produces antinociception.

It is well accepted that Aδ- and C-fibres of primary afferent carry the nociceptive information to the spinal cord, whereas Aβ-fibres preferentially transmit non-nociceptive information (Basbaum et al., 2009). Thus, the finding that s.c. AVP in the receptive field reduces the activity mediated by Aδ- and C-fibres, but not by Aβ-fibres, is interpreted as a specific antinociceptive effect. However, it is important to remark that only the s.c. administration in the receptive field had this effect, whereas the s.c. administration in the paw contralateral to the stimulated paw did not diminish the activity evoked by Aδ- and C-fibres.

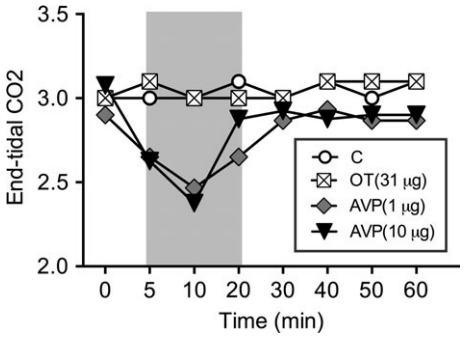

Figure 6 Effect of peripheral AVP administration on the end-tidal CO_2. The graph shows the time course of end-tidal CO_2 after peripheral AVP administration. The grey area indicates the maximum decrease in end-tidal CO_2 after 1 and 10 μg AVP administration. Notice that OT does not produce this effect.

Subsequently, we studied whether this antinociceptive effect could transform into behavioural analgesia using the formalin test. Formalin administration produces paw shakes with three distinguishable phases (Barrot, 2012). Phase 1 (0–10 min), characterized by intense paw shakes, is possibly mediated by the activation of TRP channels (McNamara et al.,2007). The nociceptive behaviour diminishes during the interphase (10–20 min), but it is not known if this decrease is mediated by central modulation or by the absence of formalin activity (Matthies and Franklin, 1992; Fischer et al., 2014). Finally, phase 2 (20–60 min), characterized by the reappearance of nociceptive behaviour, is probably induced by peripheral inflammation and central sensitization (Hunskaar and Hole, 1987). Considering that both ipsilateral (to the site of formalin application) and contralateral AVP administration (10 μg/50 μL) diminished the response in phase 1 and interphase, this effect could be correlated with the locomotor impairment observed and described elsewhere (Andrews et al., 1983; Ettenberg et al., 1983). However, only ipsilateral AVP administration produced an important reduction in nociceptive behaviour during phase 2 of the formalin test. In fact, our electrophysiological data show an early reduction of activity evoked by Aδ-fibres starting 5 min after AVP administration followed by a reduction in C-fibres and post-discharge when applied only in the same paw where formalin was administered, so it is possible that an early local effect could be masked by the systemic response.

Additionally, it remains to be addressed whether AVP could participate in other mechanisms related to nociception. AVP has multiple anti-inflammatory effects (Russel and Walley, 2010) that could contribute to the reduction in the phase 2 of the formalin test described in this study. It is interesting to notice that $V_{1A}R$ knockout mice present an increased response in phase 2 of the formalin test (Schorscher-Petcu et al., 2010), which is consistent with our data when the V1aR antagonist alone incremented this phase.

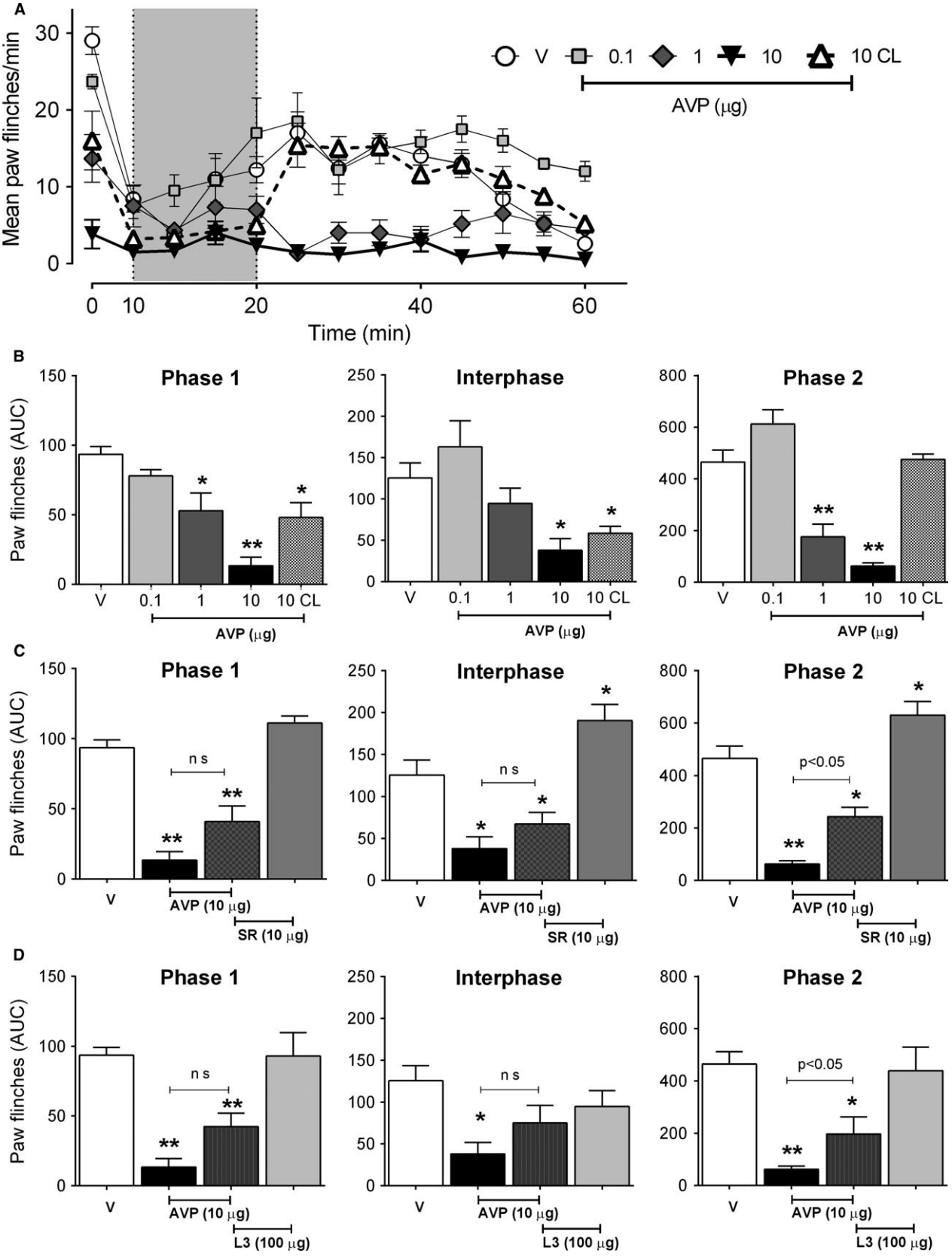

Figure 7 Effect of peripheral AVP on the formalin nociceptive-evoked response. (A) Time course of formalin paw flinches after the administration of AVP at different doses. The grey area represents the interphase between the two formalin-evoked responses. Notice the absence of flinch responses produced by ipsilateral 10 μg compared with the contralateral 10 μg of AVP during phase 2 of the formalin test. (B) Area under the curve (AUC) quantification of AVP effect on the formalin response throughout the different phases: phase 1 (0–10 min), interphase (10–20 min) and phase 2 (20–60 min). (C) AUC analysis showed the participation of V1a receptor in the effect of peripheral AVP in the formalin test. (D) Shows the participation of OT receptor in the effect of peripheral AVP in the formalin test. *$p < 0.05$, **$p < 0.01$ one-way ANOVA, Dunnett's post-hoc test for B, Tukey's post-hoc test for C and D.

4.2 Participation and location of $V_{1A}R$ and OTR in the antinociceptive effects of peripheral AVP

AVP (Peng et al., 2015) and OT produce central (Condés-Lara et al., 2008; DeLaTorre et al., 2009) and peripheral (Hobo et al., 2012; Qiu et al., 2014b) antinociception; however, the receptor involved in those effects is still a matter of debate (González-Hernández et al., 2014). In this regard, administration of AVP or OT in $V_{1A}R$ knockout mice failed to evoke behavioural analgesia (Schorscher-Petcu et al., 2010; Mogil et al., 2011; Qiu et al., 2014b). Nevertheless, there is evidence of OTR participation in central (Miranda-Cardenas et al., 2006) and peripheral (Juif and Poisbeau, 2013; Gong et al., 2015) antinociception. We found that both receptors seem to be implicated in peripheral AVP antinociception. Owing to the highly similar structure of AVP and OT, the former could bind with similar affinity to V1a and OT receptors in *in vitro* experiments (Manning et al., 2008). Consequently, we used two high-affinity, non-peptide antagonists to study the participation of both receptors (Serradeil-Le Gal et al., 1993; Williams et al., 1994). In our electrophysiological approach, the AVP-induced antinociception appears to be preferentially mediated by $V_{1A}R$ although OTR also participates. Similarly, both antagonists partially blockade the antinociceptive effect of AVP in phase 2 of the formalin test. It is possible that a complete reversion did not occur with either antagonist because of the multiple nociceptive factors involved in this behavioural test; for example, the numerous peripheral inflammatory mediators (Shibata et al., 1989) and central sensitization mechanisms (Tjølsen et al., 1992). Our immunohistochemical results demonstrated that peripheral OTR and $V_{1A}R$ are present and that AVP could participate using both receptors due to the lack of total reversion with the specific antagonists. Nevertheless, we never used both antagonists simultaneously.

In DRG, $V_{1A}R$ mRNA is markedly expressed in small and medium-diameter cells (Schorscher-Petcu et al., 2010), whereas OTR has been found co-localizing with both IB4 and CGRP (Moreno-López et al., 2013; Gong et al., 2015). OTR and $V_{1A}R$ seem to be located in very close proximity, but we could not specify if they co-localized or only co-existed. Our results confirmed the existence of OTR in peptidergic peripheral nerve terminals (González-Hernández et al., 2017) and revealed the presence of $V_{1A}R$ in peripheral fibres.

4.3 Systemic versus local AVP effects

Systemic effects of AVP considered the transitory diminution of end-tidal CO_2 and the locomotor impairment.

4.3.1 End-tidal CO_2

Systemic AVP produces vasoconstriction, preferentially in non-vital organs (László et al., 1991). Our

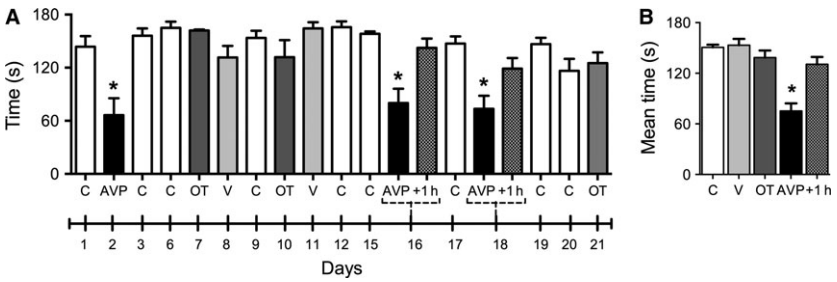

Figure 8 Locomotor effects induced by peripheral AVP administration. (A, B) Shows the effects on a motor function studied with the rotarod test. (A) Course over 21 days of the motor effects induced by AVP administration (10 μg), OT (100 μg), vehicle (V-saline) or control (C) measurements. AVP+1 h represents the effect on motor function 1 h after AVP administration. In (B), the mean time of the different treatments along the days is presented. *$p < 0.05$, one-way ANOVA, Dunnett's post-hoc test.

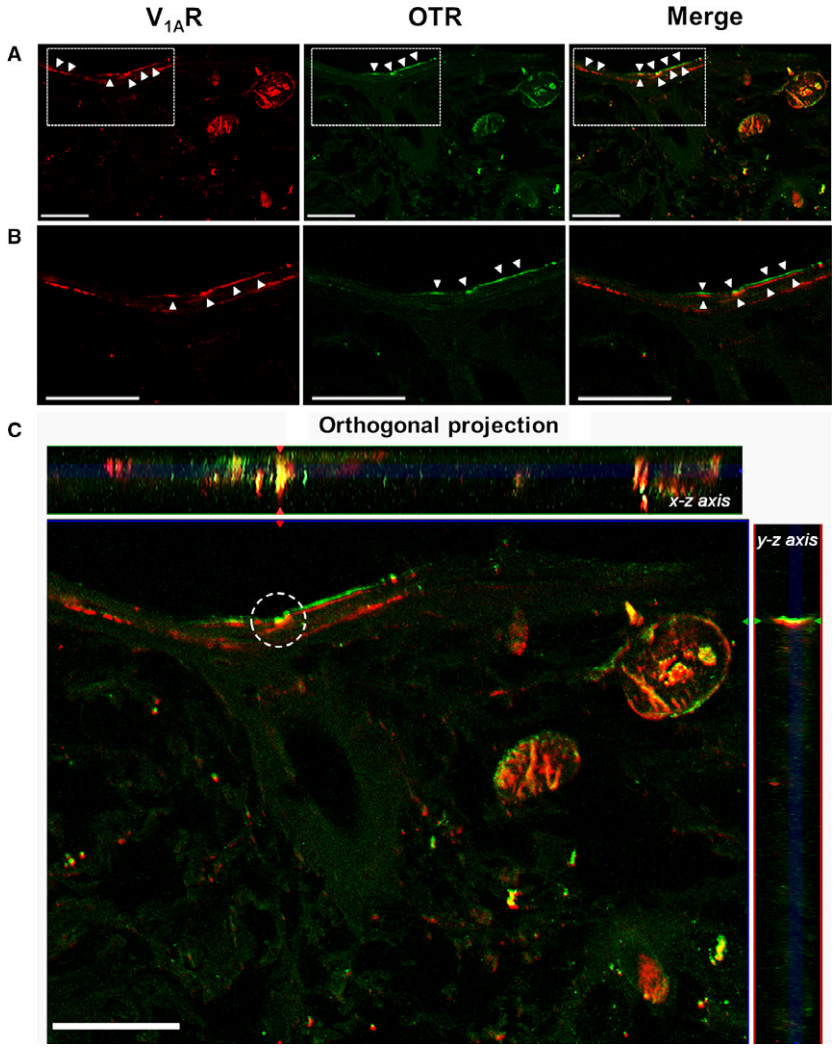

Figure 9 Representative confocal image of a skin (dermis and epidermis) section for $V_{1A}R$ and OTR immunofluorescence. The images are double-labelled sections of dermis and epidermis with antibodies against $V_{1A}R$ (red) and OTR (green) in the lateral hairy skin paw. The arrows show the site where $V_{1A}R$ and OTR are preferentially present in the dermis/epidermis. Panels in A are the *z*-stack projection from 4 optical sections (25×/0.8 NA objectives). Panels in B are a single optical section cropped from panels A (from the box) showing that $V_{1A}R$ and OTR signals are near but not co-localized; the optical section was selected at the point with the best signal for $V_{1A}R$ and OTR. Panel C shows an orthogonal view displaying four optical sections at 25×/1.3 NA; y-z plane and x-z plane show no co-localization between $V_{1A}R$ and OTR. Scale bars: 50 μm.

finding of end-tidal CO_2 reduction could be explained by a transitory hypoperfusion in non-vital vascular beds and a subsequent diminished transport of CO_2 from the periphery to the lungs (Anderson and Breen, 2000). On this subject, although the relation of a hypertensive response to AVP and antinociception was not approached in the current study, previous studies have explored this possibility and have not found a correlation between pressor and analgesic effects of AVP (Berkowitz and Sherman, 1982; Berson et al., 1983).

4.3.2 Locomotor impairment

It has been reported that the systemic AVP can produce locomotor impairment (Andrews et al., 1983; Ettenberg et al., 1983) and this effect can be confused with antinociception, when nociceptive behaviour is estimated as motor responses (Cartmell et al., 1991). We confirmed the AVP induced locomotor impairment with the rotarod test. This transitory effect could have a role in the diminish of phase 1 and interphase of the formalin test by both ipsi and contralateral AVP administration. Nonetheless,

during phase 2 only ipsilateral AVP produced behavioural antinociception, suggesting that this is a local effect unrelated to locomotor function.

4.3.3 Central versus peripheral AVP antinociceptive effects

AVP has multiple antinociceptive actions in the central nervous system. Microinjection of AVP in the nucleus raphe magnus (Yang et al., 2006b), caudate nucleus (Yang et al., 2006a) and spinal cord (Peng et al., 2015) produces antinociception. The participation of opiate and serotonin systems in AVP central antinociception has also been reported (Yang et al., 2009). Additionally, it is possible that circulating AVP could cross the blood–brain barrier (Zlokovic et al., 1990). Although the participation of central effects after peripheral AVP administration could not be explored in this study, it is unlikely that they play a major role in our results on the antinociceptive effect. Indeed, Rojas-Piloni et al. (2010) used a similar electrophysiological model and reported that spinal AVP microinjection did not diminish the responses evoked by Aδ- and C-fibres. On the other hand, in the current study, the contralateral (to electrical stimuli and to formalin) administration of AVP neither diminished the activity mediated by Aδ- and C-fibres nor produced the behavioural antinociceptive effect during phase 2 of the formalin test. Consequently, the presence of a $V_{1A}R$ in the periphery seems to be responsible for the AVP action.

5. Conclusion

Subcutaneous AVP diminished the evoked activity mediated by Aδ- and C- fibres and produced behavioural antinociception with $V_{1A}R$ and OTR implications. The immunohistochemical location of $V_{1A}R$ and OTR in cutaneous fibres suggests their mediation in the local effects. However, subcutaneous AVP administration produces respiratory CO_2 decrement and locomotor impairment that could be confused with antinociception.

Acknowledgements

Thanks are due to Jessica González Norris for reviewing the grammatical aspects of this paper, to Dr. Daisy Gasca-Martínez for her technical assistance with the rotarod test, to Elsa Nydia Hernández Ríos for her technical assistance in confocal microscopy and to Dr. Michael C. Jeziorski for his aid during the drafting.

Author contributions

A.M.G. contributed to the acquisition, analysis and interpretation of data and participated in drafting the manuscript. A.G.H. contributed to the conception and design of the study; to the acquisition, analysis and interpretation of data; and participated in drafting the manuscript. I.A.T.G contributed to the acquisition, analysis and interpretation of data. G.M.L contributed to the design of the study and to the analysis and interpretation of data. M.C.L. guided the research group, contributed to both the conception and the design of the study; to the analysis and interpretation of data; and participated in drafting and finalizing the manuscript. All authors participated in a critical review of the final manuscript.

References

Alexander, S.P.H., Davenport, A.P., Kelly, E., Marrion, N., Peters, J.A. et al. (2015). The concise guide to PHARMACOLOGY 2015/16: G protein-coupled receptors. *Br J Pharmacol* 172, 5744–5869.

Anderson, C.T., Breen, P.H. (2000). Carbon dioxide kinetics and capnography during critical care. *Crit Care* 4, 207–215.

Andrews, J.S., Newton, B.A., Sahgal, A. (1983). The effects of vasopressin on positively rewarded responding and on locomotor activity in rats. *Neuropeptides* 4, 17–29.

Auböck, J., Konzett, H. (1983). Ischemic pain versus mental task: Effect on plasma arginine vasopressin in man. *Pain* 15, 93–99.

Barrot, M. (2012). Tests and models of nociception and pain in rodents. *Neuroscience* 211, 39–50.

Basbaum, A.I., Bautista, D.M., Scherrer, G., Julius, D. (2009). Cellular and molecular mechanisms of pain. *Cell* 139, 267–284.

Baylis, P.H., Robertson, G.L. (1980). Plasma vasopressin response to hypertonic saline infusion to assess posterior pituitary function. *J R Soc Med* 73, 255–260.

Berkowitz, B.A., Sherman, S. (1982). Characterization of vasopressin analgesia. *J Pharmacol Exp Ther* 220, 329–334.

Berson, B.S., Berntson, G.G., Zipf, W., Torello, M.W., Kirk, W.T. (1983). Vasopressin-induced antinociception: An investigation into its physiological and hormonal basis. *Endocrinology* 113, 337–343.

Bodnar, R.J., Wallace, M.M., Kordower, J.H., Nilaver, G., Cort, J., Zimmerman, E.A. (1982). Modulation of nociceptive thresholds by vasopressin in the Brattleboro and normal rat. *Ann N Y Acad Sci* 394, 735–739.

Cartmell, S.M., Gelgor, L., Mitchell, D. (1991). A revised rotarod procedure for measuring the effect of antinociceptive drugs on motor function in the rat. *J Pharmacol Meth* 26, 149–159.

Chini, B., Manning, M. (2007). Agonist selectivity in the oxytocin/vasopressin receptor family: New insights and challenges. *Biochem Soc Trans* 35, 737–741.

Condés-Lara, M., Martínez-Lorenzana, G., Rodríguez-Jiménez, J., Rojas-Piloni, G. (2008). Paraventricular hypothalamic nucleus stimulation modulates nociceptive responses in dorsal horn wide dynamic range neurons. *Neurosci Lett* 444, 199–202.

DeLaTorre, S., Rojas-Piloni, G., Martínez-Lorenzana, G., Rodríguez-Jiménez, J., Villanueva, L., Condés-Lara, M. (2009). Paraventricular oxytocinergic hypothalamic prevention or interruption of long-term potentiation in dorsal horn nociceptive neurons: Electrophysiological and behavioral evidence. *Pain* 144, 320–328.

Ettenberg, A., van der Kooy, D., Le Moal, M., Koob, G.F., Bloom, F.E. (1983). Can aversive properties of (peripherally-injected) vasopressin account for its putative role in memory? *Behav Brain Res* 7, 331–350.

Fischer, M., Carli, G., Raboisson, P., Reeh, P. (2014). The interphase of the formalin test. *Pain* 155, 511–521.

Gong, L., Gao, F., Li, J., Li, J., Yu, X. et al. (2015). Oxytocin-induced membrane hyperpolarization in pain-sensitive dorsal root ganglia

neurons mediated by Ca(2+)/nNOS/NO/KATP pathway. *Neuroscience* 289, 417–428.

González-Hernández, A., Rojas-Piloni, G., Condés-Lara, M. (2014). Oxytocin and analgesia: Future trends. *Trends Pharmacol Sci* 35, 549–551.

González-Hernández, A., Manzano-García, A., Martínez-Lorenzana, G., Tello-García, I.A., Carranza, M., Arámburo, C. and Condés-Lara, M. (2017). Peripheral oxytocin receptors inhibit the nociceptive input signal to spinal dorsal horn wide-dynamic-range neurons. *Pain* 158, 2117–2128.

Hobo, S., Hayashida, K., Eisenach, J.C. (2012). Oxytocin inhibits the membrane depolarization-induced increase in intracellular calcium in capsaicin sensitive sensory neurons: A peripheral mechanism of analgesic action. *Anesth Analg* 114, 442–449.

Hunskaar, S., Hole, K. (1987). The formalin test in mice: Dissociation between inflammatory and non-inflammatory pain. *Pain* 30, 103–114.

Juif, P.E., Poisbeau, P. (2013). Neurohormonal effects of oxytocin and vasopressin receptor agonists on spinal pain processing in male rats. *Pain* 154, 1449–1456.

Kendler, K.S., Weitzman, R.E., Fisher, D.A. (1977). The effect of pain on plasma arginine vasopressin concentrations in man. *Clin Endocrinol (Oxf)* 8, 89–124.

Kordower, J.H., Bodnar, R.J. (1984). Vasopressin analgesia: Specificity of action and non-opioid effects. *Peptides* 5, 747–756.

László, F.A., László, F. Jr, De Wied, D. (1991). Pharmacology and clinical perspectives of vasopressin antagonists. *Pharmacol Rev* 43, 73–108.

Manning, M., Stoev, S., Chini, B., Durroux, T., Mouillac, B., Guillon, G. (2008). Peptide and non-peptide agonists and antagonists for the vasopressin and oxytocin V1a, V1b, V2 and OT receptors: Research tools and potential therapeutic agents. *Prog Brain Res* 170, 473–512.

Matthies, B.K., Franklin, K.B. (1992). Formalin pain is expressed in decerebrate rats but not attenuated by morphine. *Pain* 51, 199–206.

McNamara, C.R., Mandel-Brehm, J., Bautista, D.M., Siemens, J., Deranian, K.L. et al. (2007). TRPA1 mediates formalin-induced pain. *Proc Natl Acad Sci U S A* 104, 13525–13530.

Miranda-Cardenas, Y., Rojas-Piloni, G., Martínez-Lorenzana, G., Rodríguez-Jiménez, J., López-Hidalgo, M., Freund-Mercier, M.J., Condés-Lara, M. (2006). Oxytocin and electrical stimulation of the paraventricular hypothalamic nucleus produce antinociceptive effects that are reversed by an oxytocin antagonist. *Pain* 122, 182–189.

Mogil, J.S., Sorge, R.E., LaCroix-Fralish, M.L., Smith, S.B., Fortin, A. et al. (2011). Pain sensitivity and vasopressin analgesia are mediated by a gene-sex-environment interaction. *Nat Neurosci* 14, 1569–1573.

Moreno-López, Y., Martínez-Lorenzana, G., Condés-Lara, M., Rojas-Piloni, G. (2013). Identification of oxytocin receptor in the dorsal horn and nociceptive dorsal root ganglion neurons. *Neuropeptides* 47, 117–123.

Peng, F., Qu, Z.W., Qiu, C.Y., Liao, M., Hu, W.P. (2015). Spinal vasopressin alleviates formalin-induced nociception by enhancing GABAA receptor function in mice. *Neurosci Lett* 593, 61–65.

Qiu, F., Hu, W.P., Yang, Z.F. (2014a). Enhancement of GABA-activated currents by arginine vasopressin in rat dorsal root ganglion neurons. *Sheng Li Xue Bao* 66, 647–657.

Qiu, F., Qiu, C.Y., Cai, H., Liu, T.T., Qu, Z.W. et al. (2014b). Oxytocin inhibits the activity of acid-sensing ion channels through the vasopressin, V1A receptor in primary sensory neurons. *Br J Pharmacol* 171, 3065–3076.

Rojas-Piloni, G., Mejía-Rodríguez, R., Martínez-Lorenzana, G., Condés-Lara, M. (2010). Oxytocin, but not vassopressin, modulates nociceptive responses in dorsal horn neurons. *Neurosci Lett* 476, 32–35.

Russell, J.A., Walley, K.R. (2010). Vasopressin and its immune effects in septic shock. *J Innate Immun* 5, 446–460.

Schorscher-Petcu, A., Sotocinal, S., Ciura, S., Dupré, A., Ritchie, J. et al. (2010). Oxytocin-induced analgesia and scratching are mediated by the vasopressin-1A receptor in the mouse. *J Neurosci* 30, 8274–8284.

Serradeil-Le Gal, C., Wagnon, J., Garcia, C., Lacour, C., Guiraudou, P. et al. (1993). Biochemical and pharmacological properties of SR 49059, a new, potent, nonpeptide antagonist of rat and human vasopressin V1a receptors. *J Clin Invest* 92, 224–231.

Shibata, M., Ohkubo, T., Takahashi, H., Inoki, R. (1989). Modified formalin test: Characteristic biphasic pain response. *Pain* 38, 347–352.

Suzuki, H., Kawasaki, M., Ohnishi, H., Otsubo, H., Ohbuchi, T. et al. (2009). Exaggerated response of a vasopressin-enhanced green fluorescent protein transgene to nociceptive stimulation in the rat. *J Neurosci* 29, 13182–13189.

Thurston, C.L., Culhane, E.S., Suberg, S.N., Carstens, E., Watkins, L.R. (1988). Antinociception vs motor effects of intrathecal vasopressin as measured by four pain tests. *Brain Res* 463, 1–11.

Thurston, C.L., Campbell, I.A., Culhane, E.S., Carstens, E., Watkins, L.R. (1992). Characterization of intrathecal vasopressin-induced antinociception, scratching behavior, and motor suppression. *Peptides* 13, 17–25.

Tjølsen, A., Berge, O.G., Hunskaar, S., Rosland, J.H., Hole, K. (1992). The formalin test: An evaluation of the method. *Pain* 51, 5–17.

Urch, C.E., Dickenson, A.H. (2003). In vivo single unit extracellular recordings from spinal cord neurones of rats. *Brain Res Brain Res Protoc* 12, 26–34.

Williams, P.D., Anderson, P.S., Ball, R.G., Bock, M.G., Carroll, L. et al. (1994). 1-(((7, 7-Dimethyl-2 (S)-(2 (S)-amino-4-(methylsulfonyl) butyramido) bicyclo [2.2. 1] heptan-1 (S)-yl) methyl) sulfonyl)-4-(2-methylphenyl) piperazine (L-368,899): An orally bioavailable, non-peptide oxytocin antagonist with potential utility for managing preterm labor. *J Med Chem* 37, 565–571.

Yang, J., Chen, J.M., Liu, W.Y., Song, C.Y., Wang, C.H., Lin, B.C. (2006a). Arginine vasopressin in the caudate nucleus plays an antinociceptive role in the rat. *Life Sci* 79, 2086–2090.

Yang, J., Chen, J.M., Liu, W.Y., Song, C.Y., Wang, C.H., Lin, B.C. (2006b). Effect of arginine vasopressin in the nucleus raphe magnus on antinociception in the rat. *Peptides* 27, 2224–2229.

Yang, J., Yuan, H., Chu, J., Yang, Y., Xu, H., Wang, G., Liu, W.Y., Lin, B.C. (2009). Arginine vasopressin antinociception in the rat nucleus raphe magnus is involved in the endogenous opiate peptide and serotonin system. *Peptides* 30, 1355–1361.

Yang, J., Lu, L., Wang, H.C., Zhan, H.Q., Hai, G.F. et al. (2012). Effect of intranasal arginine vasopressin on human headache. *Peptides* 38, 100–104.

Zimmermann, M. (1983). Ethical guidelines for investigation of experimental pain in conscious animals. *Pain* 16, 109–110.

Zlokovic, B.V., Hyman, S., McComb, J.G., Lipovac, M.N., Tang, G., Davson, H. (1990). Kinetics of arginine-vasopressin uptake at the blood-brain barrier. *Biochim Biophys Acta* 27, 191–198.

Research Paper

PAIN®

Peripheral oxytocin receptors inhibit the nociceptive input signal to spinal dorsal horn wide-dynamic-range neurons

Abimael González-Hernández[a], Alfredo Manzano-García[a], Guadalupe Martínez-Lorenzana[a], Irma A. Tello-García[a], Martha Carranza[b], Carlos Arámburo[b], Miguel Condés-Lara[a,*]

Abstract

Oxytocin (OT) has emerged as a mediator of endogenous analgesia in behavioral and electrophysiological experiments. In fact, OT receptors (OTRs) in the spinal dorsal horn participate in a selective inhibition of the neuronal activity mediated by Aδ and C fibers but not Aβ fibers. This study shows that OTRs are expressed in the terminal nerve endings and are able to inhibit nociceptive neuronal firing. Indeed, local peripheral OT blocked the first sensorial activity of Aδ and C fibers recorded in the spinal cord neurons. Furthermore, using the formalin behavioral nociceptive test, we demonstrated that only ipsilateral OTR activation inhibits pain behavior. Our data are reinforced by the fact that the OTR protein is expressed in the sciatic nerve. Consistent with this, immunofluorescence of primary afferent fibers suggest that OTRs could be located in nociceptive-specific terminals of the skin. Taken together, our results suggest that OTRs could be found in nociceptive terminals and that on activation they are able to inhibit nociceptive input.

Keywords: Analgesia, C fibers, Oxytocin receptor, Pain, WDR cells

1. Introduction

Oxytocin (OT) is a nonapeptide that is released mainly into the central nervous system by the hypothalamic paraventricular and supraoptic nuclei.[46] Oxytocin binding sites and receptors are widely extended.[18] This peptide is involved in different physiological functions such as: (1) cardiovascular activity; (2) breathing; (3) feeding; (4) social interactions; and more recently, (5) nociception.[2,7,33,41] Regarding nociception, OT has emerged as an interesting molecule to induce analgesia at the spinal cord level, not only in animal pain models[12,16,37,42] but also in humans.[9,10] More recently, it was described[16] as a particular cell population in the parvocellular part of the paraventricular nuclei that controls magnocellular OT activity and suppress nociception under activation. In fact, Juif and Poisbeau[26] demonstrated that intravenous OT administration diminishes the evoked neuronal activity associated with C-fiber activation in wide-dynamic-range (WDR) cells pointing out that this effect is at the dorsal root ganglionDRG level. More recently, it has been suggested that OT released from the supraoptic nuclei modulates nociception by activating oxytocin receptors (OTRs) located in DRG nociceptive neurons through a similar mechanism.[16] Furthermore, experiments using whole-cell patch clamps and voltage clamps on isolated DGR neurons have found that OT inhibits the acid-sensing ion channel currents induced by acidification,[43] and there are similar results from studies using capsaicin.[22] Certainly, OT does not cross the blood–brain barrier,[17] and the current consensus about the peripheral antinociceptive properties of OT is restricted at the DRG level. Because OTRs are expressed in DRG cells[40,55] and in the trigeminal ganglia,[49] no study has yet reported on its role in the peripheral terminal nociceptive nerve endings. However, these studies have failed to extend its potential role of peripheral action of OT on terminal nerve endings (ie, on superficial skin layer) as observed for other antinociceptive systems.[3]

In this context, the present study was designed to describe and test not only the potential peripheral local antinociceptive action of OT, but also the functional role of OTR in peripheral nociceptive skin terminals. To conduct this study, we used electrophysiological (extracellular unitary recordings of spinal dorsal horn WDR cells), a behavioral nociceptive test (formalin test), and molecular and pharmacological tools to reveal a new mechanism at the periphery modulating nociception. We present evidence for a specific role of OT in OTR modulating the nociceptive input at the terminal nerve endings.

2. Experimental procedures

2.1. Animals

A total of 121 male Wistar rats (220-280 g) from the Neurobiology Institute Animal House were used in the experiments. Animals

Sponsorships or competing interests that may be relevant to content are disclosed at the end of this article.

Departamento de [a] Neurobiología del Desarrollo y Neurofisiología y, [b] Neurobiología Celular y Molecular, Instituto de Neurobiología, Universidad Nacional Autónoma de México, Campus UNAM-Juriquilla, Querétaro, México

**Corresponding author. Address: Departamento de Neurobiología del Desarrollo y Neurofisiología, Instituto de Neurobiología, Universidad Nacional Autónoma de México, Campus UNAM-Juriquilla, 76230 Querétaro, México. Tel./fax: +(52)(442)-238-1042. E-mail address: condes@unam.mx (M. Condés-Lara).*

Supplemental digital content is available for this article. Direct URL citations appear in the printed text and are provided in the HTML and PDF versions of this article on the journal's Web site (www.painjournalonline.com).

PAIN 158 (2017) 2117–2128

http://dx.doi.org/10.1097/j.pain.0000000000001024

were maintained on a 12:12 hours light and dark cycle (light beginning at 07:00 hours) and housed in a special room at constant temperature (22°C ± 2°C) and humidity (50%) with food and water ad libitum. Our Institutional Ethics Committee approved all animal procedures and protocols, and they followed the IASP ethical guidelines,[58] a Guide for the Care and Use of Laboratory Animals established by the NIH, and ARRIVE guidelines for reporting experiments involving animals.[35] All efforts were made to limit distress and use only the number of animals necessary to produce reliable scientific data.

2.2. General methods

2.2.1. Surgical procedures for electrophysiological experiments

Animals were anesthetized with urethane (1-1.2 g/kg) and then an intratracheal cannula was inserted for artificial ventilation (55 strokes/min). Subsequently, animals were mounted onto a stereotaxic frame and secured in a spinal cord unit frame; the lumbar vertebrae were fixed to improve stability at the recording site to perform a laminectomy to expose the L2-L4 spinal cord segments. The dura was carefully removed, and to avoid desiccation, we covered the exposed spinal cord with mineral oil. The animals were not paralyzed, and we did not observe a withdrawal reaction during the experiments as previously reported.[36] End tidal CO_2 was monitored with a Capstar-100 CO_2 analyzer (CWI Inc, Ardmore, PA) and kept between 2.5% and 3.0% by adjusting the stroke volume to maintain a normal acid-base equilibrium. Core body temperature was maintained at 38°C using a circulating water pad.

2.2.2. Extracellular unitary recordings

Extracellular unitary recordings were made using 7 quartz-platinum/tungsten microelectrodes (impedance 4-7 MΩ) mounted in a multichannel microdrive "System Eckhorn." The multi-electrode system was manipulated with the 7-channel version of the fiber-electrode manipulator "System Eckhorn" using Eckhorn Matrix multiuser software (Thomas RECORDING GmbH, Giessen, Germany). The microelectrodes were lowered (400-900 μm from the surface) in small steps (2-5 μm) into the superficial laminae of the left dorsal horn segments to search for single-unit discharges. For each recorded cell, the specific somatic receptive field (RF) was located by tapping on the entire ipsilateral hind paw and toes; electrical stimulation was then applied by 2 electrodes inserted into the RF (see below). In this case, 2 fine needles (27 G) attached to a stimulus isolator unit were inserted subcutaneously (s.c.) into the RF of the recorded neuron. The electrical test stimulation was then conducted; this test consists of 20 stimuli at 0.5 Hz with 1-millisecond pulse duration at 1.5 times the threshold intensity (0.1-3 mA) required to evoke a C-fiber response.

The extracellular neuronal activity induced by electrical stimulation of the RF was recorded, amplified, digitalized, and discriminated using CED hardware and Spike 2 software (Version 5.20; Cambridge Electronic Design, Cambridge, United Kingdom). Raw and discriminated signals were fed through an audio monitor and displayed on an oscilloscope. Waveforms and recorded spike trains were stored on a hard drive for off-line analysis. Baselines and evoked activities of the spinal dorsal horn WDR neurons were recorded and analyzed as cumulative frequency and post-stimulus time histograms to detect the occurrence of statistically significant neuronal responses. All WDR cells recorded were found between 450 to 750 μm from the surface. On this basis, the stimulating threshold to evoke action potentials and their frequency of occurrence, resulting from the stimulation of the peripheral RF on the hind paw, were attributed to the recruitment of Aβ-, Aδ-, and C fibers. Considering the distance between the RF and the recording electrode, the peak latencies observed correspond to peripheral conduction velocities[50] within the Aβ- (0-20 milliseconds), Aδ- (21-90 milliseconds), and C fibers (90-350 milliseconds) (**Fig. 1A–D**). Thus, the number of action potentials that occurred in response to 20 RF stimuli was compared before (basal) and after vehicle/drug (50 μL; s.c., in the RF) treatment.

Accordingly, the neuronal-evoked responses were evaluated immediately after (t = 0) OT (1, 10 and 56 μg/paw; n = 6 cells, each dose) or vehicle (isotonic saline; n = 5 cells) administration at 5, 10, 20, 40, 60, 80, and 100 minutes. The role of OTR in the OT effect was also evaluated by s.c. administration of the potent (pK_i = 8.1)[25] and selective antagonist[50] L-368,899 (10 μg/paw; n = 4 cells). The antagonist was administered 5 minutes before OT or vehicle.

2.2.3. Formalin-induced acute nociception

Acute nociception was assessed using the 1% formalin test.[15] Rats were placed in open Plexiglass observation chambers for 1 hour during 3 consecutive days to allow them to become familiar with their surroundings. On the fourth day, and after 30 minutes in the Plexiglass chamber, they were removed for formalin administration. Formalin (1%) was injected s.c. (50 μL) into the dorsal surface of the right hind paw using a 30-gauge needle. Animals were then returned to the chambers and nocifensive behavior was observed immediately after formalin injection. Nocifensive behavior was quantified as the number of flinches of the injected paws during 1-minute periods every 5 minutes for up to 60 minutes after injection.[34,52] Flinching was characterized as a rapid and brief withdrawal or flexing of the injected paw. Formalin-induced flinching behavior was biphasic. The initial acute phase (0-10 minutes) was followed by a relatively short quiescent period, which was then followed by a prolonged persistent response (15-60 minutes). At the end of the experiments, the rats were killed in a CO_2 chamber. Oxytocin (0.1, 10, 31, and 100 μg/paw; n = 6 rats, each dose) or vehicle was administered 5 minutes before formalin. Furthermore, the L-368,899 was given (10 and 100 μg/paw; n = 5 rats each dose) 5 minutes before OT or vehicle.

2.2.4. Motor coordination test

A motor coordination test (rota-rod test) in an independent group of rats was performed in a treadmill apparatus (IITC Inc Life Science, Los Angelss, CA). Briefly, this test consists of placing the animals on a cylinder (diameter: 7 cm) rotating at a constant speed of 15 revolutions per minute (rpm). Animals were trained to walk on the cylinder (cutoff time: 180 seconds) in 5 previous consecutive sessions without any treatment, and in the sixth session they received 31 μg/paw of OT (n = 5) or vehicle (50 μL; n = 5). The time it took to fall was counted.

2.2.5. Immunofluorescence of primary afferent fibers

The left sciatic nerve was exposed in 6 male Wistar rats (280-310 g). Distal to the 3 peripheral branches (sural, common peroneal, and tibial nerves) of the sciatic nerve, the tracer True Blue (TB) was placed under microscopic control; in this case, we used a stainless steel wire charging tiny pellets of TB attached to

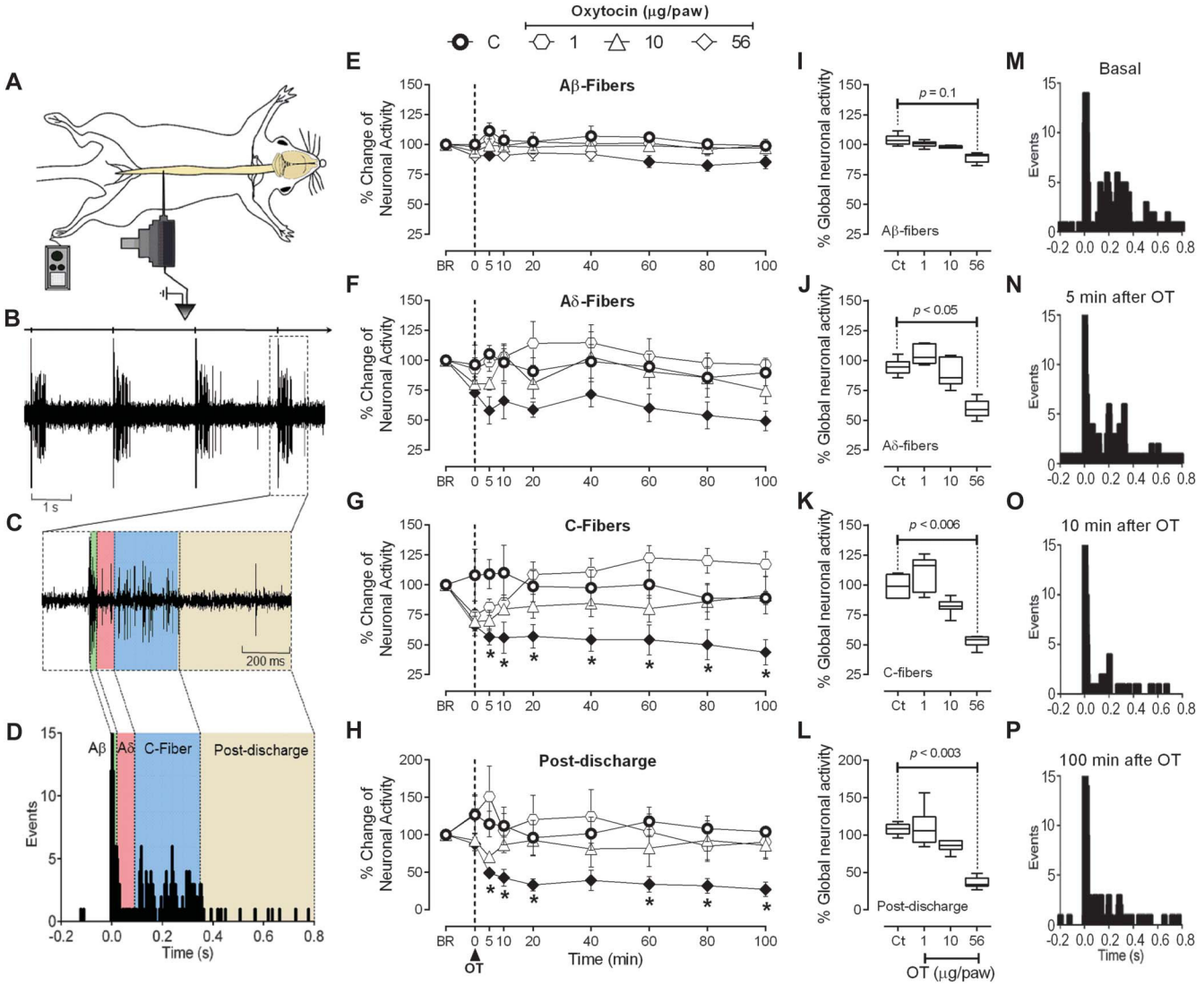

Figure 1. Peripheral oxytocin inhibits the nociceptive activation fibers arriving at second-order wide-dynamic-range (WDR) cells. (A) Experimental setup design illustrating the electrophysiological recording of lumbar spinal dorsal horn WDR cells and the location of the receptive field (RF) stimulation on the paw. (B) Raw data of 4 stimulus artifacts (upper line) and consecutive WDR responses to RF stimulation. (C) Raw tracing of a single response to RF stimulation. (D) Peri-stimulus time histograms (PSTHs) constructed from 20 WDR responses to RF stimulation depicting the different fiber components (Aβ fibers, Aδ fibers, C fibers, and postdischarge). (E, F, G, and H) Time course changes in the percentage average of the different fibers activating WDR cell responses induced by RF stimulation and the effects to subcutaneous (s.c.) oxytocin (OT) injection (1, 10, and 56 μg/paw; n = 6 each dose) at time 0. *$P < 0.05$, statistically significant difference compared at the same time with control (●; n = 5) responses. For the sake of clarity, solid symbols (⬣, ▲, ◆), instead of empty symbols, represent significant ($P < 0.05$) responses vs its respective (100%) initial basal response (BR). Notice that OT predominantly inhibits (compared with control curve, ●) the response of C fibers and postdischarge. Panels I, J, K, and L show global neuronal activity (obtained from the respective time course figures) of Aβ fibers, Aδ fibers, C fibers, and postdischarge in response to s.c. OT; this neuropeptide was able to preferentially block the neuronal activity associated to Aδ fibers, C fibers, and postdischarge but not Aβ fibers. This inhibition is clearly depicted in panels M, N, O, and P, where the PSTHs were obtained for 1 WDR neuron illustrating the effect of s.c. OT (56 μg/paw) at different times after OT administration. In this case, note that OT blocks the activity associated with the activation of nociceptive fibers (ie, Aδ fibers and C fibers).

its blunt tip. After 5 days, the animals were killed by decapitation and immediately after, the lateral hairy skin areas were excised with a scalpel, snap frozen in Tissue-Tek O.C.T. Compound (Sakura Finetek USA, Inc, Torrance, California), placed in liquid nitrogen–chilled isopentane, and stored at −80°C before sectioning.

Triple immunofluorescence for the OTR, IB4, and calcitonin gene–related peptide (CGRP) was performed on free-floating and slide-mounted samples of 50-μm thick cryostat sections after fixation in 4% phosphate-buffered paraformaldehyde for 10 minutes at room temperature. A primary antibody cocktail was used for 24 hours at 4°C; it included polyclonal antibodies against OTR (raised in goat, diluted 1:400, Cat.no. sc-8103; Santa Cruz Biotechnology Inc, Santa Cruz, CA) and the CGRP (raised in rabbit, diluted 1:2000, Cat.no. AB15360; Chemicon International, Temecula, CA). The sections were washed for 5 minutes with 0.1 M PBS and then incubated with the appropriate secondary antibody for 24 hours at 4°C. The secondary antibodies used were donkey anti-Goat IgG (Alexa Fluor 488 conjugate, Cat.no. A-11055; Invitrogen, Grand Island, NY) and donkey anti-Rabbit IgG (Alexa Fluor 647 conjugate, Cat.no. A-31573; Invitrogen). To detect isolectin B4 (IB4) binding, we included 1:400 *Griffonia simplicifolia* isolectin (GS-IB4) Alexa Fluor 568 (Cat.no. I21412; Invitrogen) during secondary antibody incubations.

An extra group of 3 rats was required during the submission process. This group had the same experimental protocol but

the tissue was cut serially in 20 μm-thick cryostat sections. One section was treated as previous experiments and the following sections without the primary antibody for each OTR (1:400), IB4 (1:400), or CGRP (1:2000). This maneuver allowed us to reveal the possible unspecific immunofluorescence for the OTR, IB4, and CGRP in order to avoid a possible false positive staining.

2.2.6. Confocal microscopy and image analysis

Confocal images of the peripheral terminal sensory in the lateral hairy skin were acquired using the LSM510 or LSM780 confocal microscope system (Zeiss, Mexico) with 25×/0.8, 40×/1.3, and 63×/1.32 NA oil immersion objective. Using the 488-nm argon laser to excite Alexa Fluor 488, 561-nm diode laser for Alexa Fluor 568, and 633-nm helium/neon laser to excite the Alexa Fluor 633 signal. The pinhole, Z-sectioning intervals were kept constant for all images. About 40 to 100 optical Z-sections of 1-μm thickness were obtained from the 50-μm thick tissue for each skin image stack.

Optical sections were acquired at a digital size of 1024 × 1024 pixels and averaged 3 times to reduce noise. In all cases, the image obtained was improved (brightness and gamma) and analyzed using the ZEN 2 Blue Edition Software (Carl Zeiss Microscopy GmbH, Göttingen, Germany). In addition, the color for each channel was selected as follows: green for OTR, red for IB4, and blue for CGRP. In all cases, a 2-dimensional projection image and a single-optical section image (where the OTR signal was strong) were imported in Tag Image File Format (TIFF) and were used to compose the multipanel figures. Furthermore, projection images were 3D rendered and a pseudo-3D (2.5D) graphic was made. In addition, an orthogonal projection using 6 to 8 optical sections was performed.

2.2.7. Sodium dodecyl sulfate polyacrylamide gel electrophoresis and Western blot

A group of 12 rats was subdivided into 3 groups (control; saline injection, 50 μL/paw, s.c.; and 1% formalin injection, 50 μL/paw, s.c.; n = 4 each) to determine the presence of OTR in the peripheral nerve. After 1 day postinjection, all animals were killed by decapitation and the left sciatic nerve (ipsilateral to s.c. injection) was exposed; the connective tissue was carefully removed and the nerve was cut above the trifurcation of the tibial, common peroneal, and sural rami nerves. Then, the fragments were frozen and stored at −70°C. In all cases, an ≈2-cm fragment of sciatic nerve was collected.

The tissue was homogenized and extracted for 2 hours by agitation in ice-cold hypotonic Tris-HCl buffer (Tris 50 mM, pH: 9) containing a protease inhibitor cocktail (Complete Mini; Roche, Mannheim, Germany) and 0.5 mM phenylmethylsulfonyl fluoride (PMSF; Sigma, St. Louis, MO). The homogenates were centrifuged at 10,000 rpm for 20 minutes at 4°C. The supernatants were collected and the protein content was quantified using the Bradford method.[5] Then 30-μg protein of each sample was resolved by 1-dimensional denaturing sodium dodecyl sulfate polyacrylamide gel electrophoresis in 1.0-mm thick, 6-cm long, 12% gel using the Laemmli[31] buffer system in a Mini-PROTEAN II cell (Bio-Rad, Hercules, CA). The samples were run under reducing conditions (in the presence of 5% [wt/vol] 2-mercaptoethanol) and constant voltage (100 V stacking gel; 150 V separating gel). Prestained molecular weight markers (Bio-Rad) were used to estimate the molecular weight.

After electrophoresis, the slabs were equilibrated in cold transfer buffer (25 Mm Tris-HCl, 192 mM glycine, 20% methanol vol/vol, pH 8.3) for 30 minutes and electrotransferred (at 200 mA for 1 hour)[47] to nitrocellulose membranes (Bio-Rad). After transfer, the membranes were washed with 30 mM Tris, 500 mM NaCl Tris Buffered Saline (TBS), at pH 7.5 for 10 minutes, then blocked with 5% (wt/vol) nonfat dry milk (Bio-Rad) in TBS for 2 hours. After washing the membranes 3 times with Tris Buffered saline with tween 20 TTBS (TBS containing 1% [wt/vol] non-fat dry milk, and 0.05% [wt/vol] Tween 20) for 10 minutes, they were incubated overnight at room temperature in TTBS with the OTR antibody (raised in goat, diluted 1:500, Cat.no. sc-8103, Santa Cruz Biotechnology Inc). After that, membranes were rinsed 3 times (10 minutes each) in TTBS and incubated during 2 hours at 4°C with a secondary antibody (rabbit anti-Goat IgG-HRP conjugate, diluted 1:3000, Cat.no. 81-1620; Invitrogen). Protein signal detection was achieved by incubating the membranes in Electrochemiluminiscence (ECL) reagent (Amersham-Pharmacia, Buckinghamshire, United Kingdom) for 5 minutes and exposed to Kodak BioMax ML film. The next day, blots were stripped and incubated overnight at room temperature with GAPDH antibody (raised in rabbit, diluted 1:1000, Cat.no. 2118; Cell Signaling Technology); membranes were then rinsed 3 times with TTBS and incubated for 2 hours at 4°C with a secondary antibody (goat anti-Rabbit IgG-HRP conjugate, diluted 1:3000, Cat.no. 65-6120; Invitrogen). The anti-GAPDH was used as internal control to normalize OTR's protein expression level. In both cases, immunoblots were scanned and bands were semiquantitatively analyzed using Image Lab Software (v5.2.1; Bio-Rad Laboratories).

2.2.8. Drugs

In addition to the anesthetic (urethane), this study used the following compounds (obtained from the sources indicated): OT acetate salt hydrate (Sigma Chemical Co, St Louis, MO) and the (*S*)-2-amino-*N*-((1*S*,2*S*,4*R*)-7,7-dimethyl-1-((4-*o*-tolylpiperazin-1-ylsulfonyl) methyl) bicycle [2.2.1] heptan-2-yl)-4-(methylsulfonyl) butanamide hydrochloride (L-368,899 hydrochloride; Tocris Bioscience, Northpoint, United Kingdom). The OT was dissolved in physiological saline, whereas L-368,899 was dissolved in 10% DMSO, and the resulting solution was gauged with saline. These vehicles had no effect on the baseline values of neuronal activity or on behavioral responses. The doses mentioned in this text refer to substance-free base.

2.2.9. Statistical analysis

All data, tables, and figures in the text are presented as mean ± SEM. The number of evoked potentials induced by electrical stimulation of the paw was normalized and expressed as percentage change from the respective baseline (100%). This baseline response was established after an identified neuron had a ≤10% variation in the neuronal responses induced by RF stimulation during 5 consecutive tests (10 minutes between each test). Furthermore, the baseline value refers to evoked neuronal response before peripheral treatment with OT or L-368,899 plus OT. The difference in neuronal activity evoked within 1 group of animals before and after treatment was compared using a 2-way repeated measures analysis of variance. In addition, temporal-course was adjusted to obtain global neuronal activity because of the treatment; in this case, a 1-way analysis of variance was performed. In the formalin test, curves were constructed by plotting the number of flinches as a function of time. The area under the number of flinches against

time curves, an expression of the duration and intensity of the effect, was calculated by the trapezoidal rule, and a 1-way analysis of variance was performed. In the motor coordination test, a Student *t* test was used to compare time to fall. The 1-way and 2-way analyses of variance were followed, if applicable, by the Student–Newman–Keuls post hoc test. In all cases, statistical significance was accepted at $P < 0.05$.

3. Results

3.1. Peripheral local administration of oxytocin inhibits the nociceptive activity of the second-order wide-dynamic-range neurons

Peripheral electrical stimulation of the RF elicited well-defined neuronal responses of the spinal dorsal horn WDR cells (**Fig. 1A–D**). Briefly, 1 pulse of stimuli in the RF elicited a classical neuronal response of a spinal second-order WDR neuron (**Fig. 1B–C**). This neuronal activity could be broken down according to the conduction velocities of primary afferent fibers (ie, Aβ-, Aδ-, C fibers, and postdischarge) (**Fig. 1D**). Interestingly, after a single subcutaneous administration of OT (s.c.; 1-56 μg/50 μL) (**Fig. 1E–H**), a dose-dependent decrease in the firing responses elicited by 20 electrical stimuli on the RF was observed (compared with its respective basal responses). These inhibitions (≈40%-60% of basal response) were particularly more pronounced in the Aδ fibers, C fibers, and postdischarge, starting 5 minutes after OT administration and lasting up to 100 minutes. When we analyzed these results as global neuronal activity (**Fig. 1I–L**), we found that OT mainly inhibits the neuronal firing associated with the activation of Aδ fibers, C fibers, and postdischarge (**Fig. 1J–L**). **Figure 1M–P** show peri-stimulus time histograms obtained from 1 WDR neuron before and after OT administration; these figures clearly depict the inhibition of C-fiber activity.

3.2. The antinociceptive effect of subcutaneous oxytocin has a local and specific effect

Because the electrophysiological experiments showed that OT selectively inhibits the activity of Aδ and C fibers, a set of experiments using the 1% formalin test (50 μL formalin injected s.c. into the dorsal surface of the hind paw) were performed to test the potential antinociceptive behavioral effects of peripheral local OT. Subcutaneous (s.c.) formalin produced a typical pattern of flinching behavior characterized by a biphasic time course (**Fig. 2A**). Phase 1 of the nociceptive response began immediately after formalin injection and then gradually declined (≈10 minutes). Phase II began about 15 minutes after formalin injection and lasted for 1 hour. Subcutaneous injection of OT (31 and 100 μg; ipsilateral to formalin injection) significantly prevented formalin-induced nociception in rats (**Fig. 2A**). Indeed, OT but not vehicle, prevented flinching behavior in phase I (100 μg/paw; **Fig. 2B**) and phase II (31 and 100 μg/paw; **Fig. 2C**) of the formalin test. In contrast, contralateral peripheral injection of a supramaximal dose of OT (100 μg/paw) failed to modify formalin-induced flinching behavior, thus indicating a local effect. This antinociceptive action is not only local but also specific, because the highest dose of OT did not produce any changes in the motor coordination test (**Fig. 2D**). We also used Western blotting and found that OTR is expressed in the sciatic nerve, which innervates the paw; moreover, the s.c.

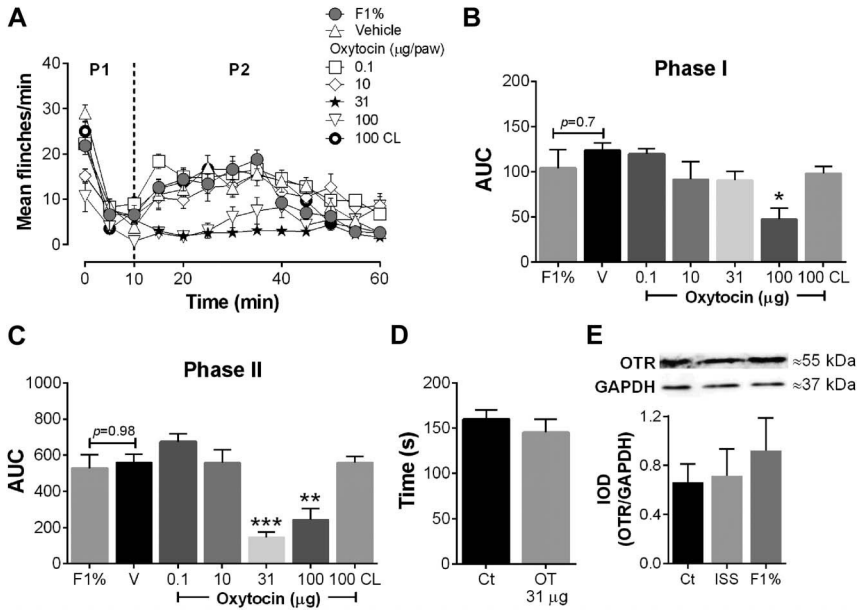

Figure 2. Subdermic oxytocin (OT) administration selectively inhibits behavioral nociception. (A) Time course during phase I (P1) and phase II (P2) of the mean number per minute of flinches observed after subcutaneous (s.c.) treatment with vehicle (V) (n = 6) or OT (0.1-100 μg/paw; n = 6 each dose) in rats submitted to the 1% formalin test. Note that although 31 and 100 μg/paw (administered ipsilaterally to formalin injection) diminish nociceptive behavior, 100 μg/paw (administered contralaterally [100 CL]; n = 6) follows the same pattern as the formalin curve (F1%; n = 6) and the control curve (vehicle). Panels B and C show the time course data expressed as area under the mean number of flinches against time curve (AUC). Oxytocin reduced AUC values during phase I (100 μg/paw) and phase II (31 and 100 μg/paw), indicating an antinociceptive effect; remarkably, 100 μg/paw of OT administered contralaterally has no effect on the flinching behavior induced by formalin. $^{*}P < 0.05$, $^{**}P < 0.01$ and $^{***}P < 0.001$, statistically significant difference compared to V. (D) Oxytocin (n = 5) has no effect (compared to control; n = 5) on the time spent (seconds) on the treadmill apparatus (rota-rod test) before falling, suggesting that OT-induced antinociception is specific. (E) Western blot analysis of the oxytocin receptor obtained from the sciatic nerve of naive rats (Ct; n = 4), or isotonic saline solution (ISS; n = 4) or formalin (F1%; n = 4) injected (50 μL/paw). The sciatic nerve tissue was collected 1 day after ISS or formalin injection. Data are expressed as the integrated optical intensity This Figure 2 in A the abscisa has not level and it is TIME. normalized against GAPDH, and they represent the mean ± SEM of 4 independent experiments.

formalin injection (**Fig. 2E**) did not seem to modify this expression.

3.3. Blocking the oxytocin receptors abolished the oxytocin-induced antinociception in behavioral and electrophysiological assays

Because OTRs seem to be expressed in the sciatic nerve (**Fig. 2E**), we examined their functional role in the electrophysiological and behavioral experiments. As shown in **Figure 3**, a subcutaneous injection of the potent and selective OTR antagonist L-368,899 (10 and 100 μg/paw) was able to block the 31 μg/paw OT-induced behavioral antinociception (**Fig. 3A–C**). This effect was clearly observed in phase II of the formalin test (**Fig. 3C**) and no changes were observed in animals pretreated with the vehicle. Interestingly, an increase in the nocifensive response was elicited in the 10 μg/paw L-368,899 during phase II (**Fig. 3C**). Furthermore, when we measured the neuronal activity of a group of WDR neurons (**Figs. 3D–H, 4**), we found that OT-induced Aδ fiber C fiber, and postdischarge inhibition were abolished by the 10 μg/paw L-368,899, and we observed no effect when we only administered the antagonist (**Fig. 4B–D**).

3.4. Oxytocin receptors are present in CGRPergic fibers but not in IB4 terminal sensory fibers

Figure 5 shows the immunofluorescence to OTR, IB4, and CGRP from 3 different experiments (A, B, and C); it is important to point out that in the absence of primary antibodies, no unspecific staining was observed (**Fig. 5Aiii–Ciii**). Furthermore, as shown in **Figure 6**, OTRs (Ai) do not colocalize with IB4 (Aii) but predominantly colocalizes with CGRPergic fibers (Aiii). In both cases (CGRP+ and IB4+ fibers), the sensory fibers were located between the epidermis and dermis, suggesting that OTR could be expressed in the terminal nerve fibers. It is interesting to note that although the projection image (*z*-stack projection) (**Fig. 6Ai–iv**) clearly depicts the presence of OTR, IB4, and CGRP in the tissue, OTRs were mainly colocalized with CGRP as it was observed in 1 representative orthogonal view section (see **Fig. 6B**). These results are clearly depicted in several representative single optical sections (**Fig. 6Ci–iv**). Similar results are shown in **Figure 7** (see also supplemental Figure 4, available online at http://links.lww.com/PAIN/A459), where OTRs (i) did not colocalize with IB4 fibers (ii) but it had a colocalization with CGRPergic fibers (iii).

Finally, although we did not find TB-positive fibers in the periphery, the tracer was successfully carried at the spinal cord (data not shown).

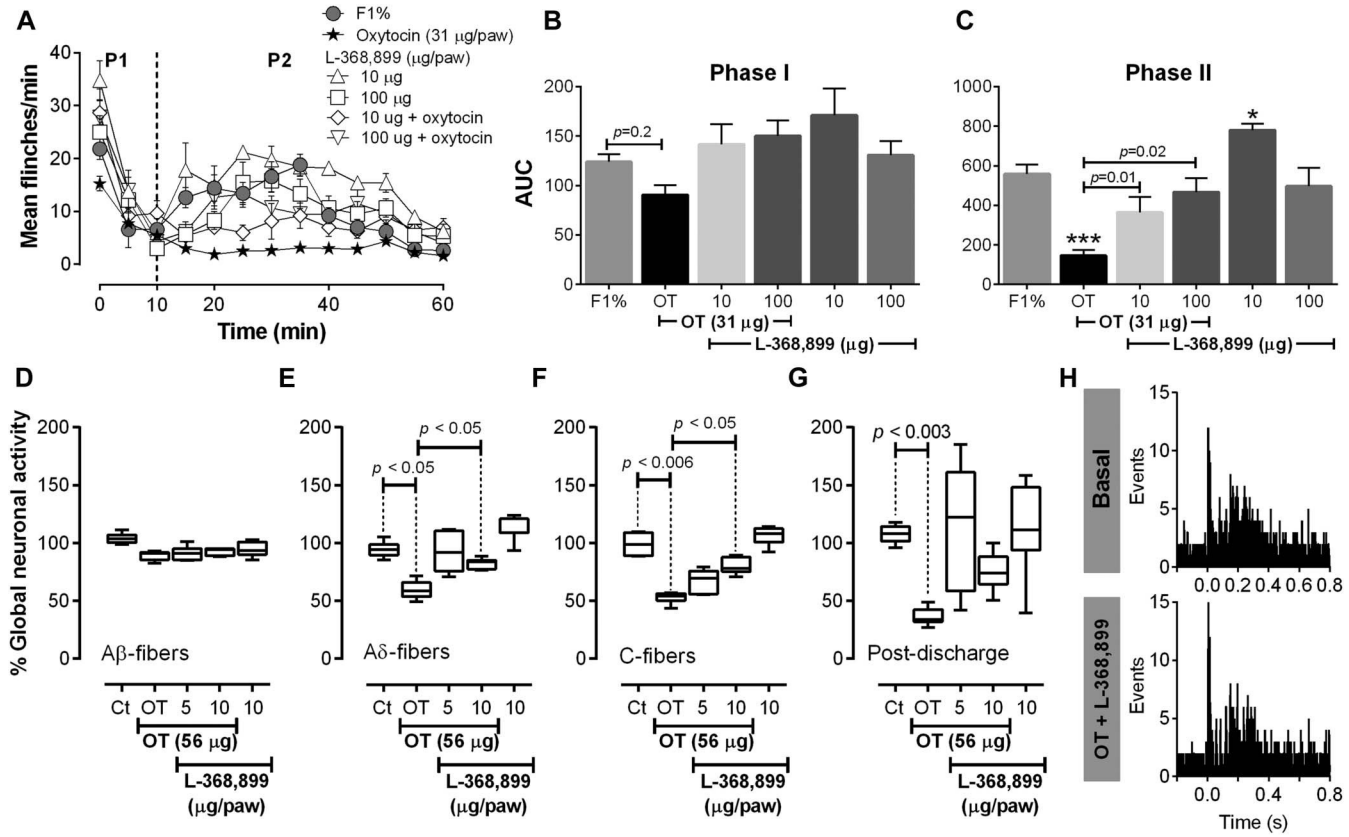

Figure 3. Role of oxytocin receptors (OTRs) in behavioral and electrophysiological oxytocin (OT)-induced antinociception. (A) Time course during phase I (P1) and phase II (P2) of the mean number of flinches observed after subcutaneous treatment with L-368,899 (10 or 100 μg/paw; OTR selective antagonist; n = 5 each dose) or L-368,899 plus OT (31 μg/paw; n = 5) in rats submitted to the 1% formalin test. Note that L-368,899 reverses the OT-induced antinociception. Panels B and C show the data from the time course expressed as area under the mean number of flinches against time curve. Blockade of OTR by L-368,899 inhibits the OT-induced antinociception in phase II; it is interesting to note that 10 μg/paw L-368,899 enhances the flinching (C) behavior induced by formalin. $^{*}P < 0.05$ and $^{***}P < 0.001$, statistically significant difference compared to formalin (F1%). (D, E, F, and G) Global neuronal activity (obtained from the respective time course figures, see supplemental digital content, available online at http://links.lww.com/PAIN/A459) of the wide dynamic-range (WDR) cells in response to 56 μg/paw OT (n = 6) or 5 and 10 μg/paw L-368,899 plus OT (n = 4 each dose). Pretreatment with L-368,899 was able to block the OT-induced inhibition of neuronal activity associated with Aδ-fiber and C-fiber activation. Note that 10 μg/paw L-368,899 alone (n = 4) has no significant effect on the neuronal-evoked responses. Panel H shows 2 PSTH obtained before (basal response) and after OT + L-368,899 (1 hours after oxytocin) for 1 WDR neuron, thus illustrating that L-368,899 (56 μg/paw) inhibits the OT-induced antinociception (compared with Fig. 1N–P).

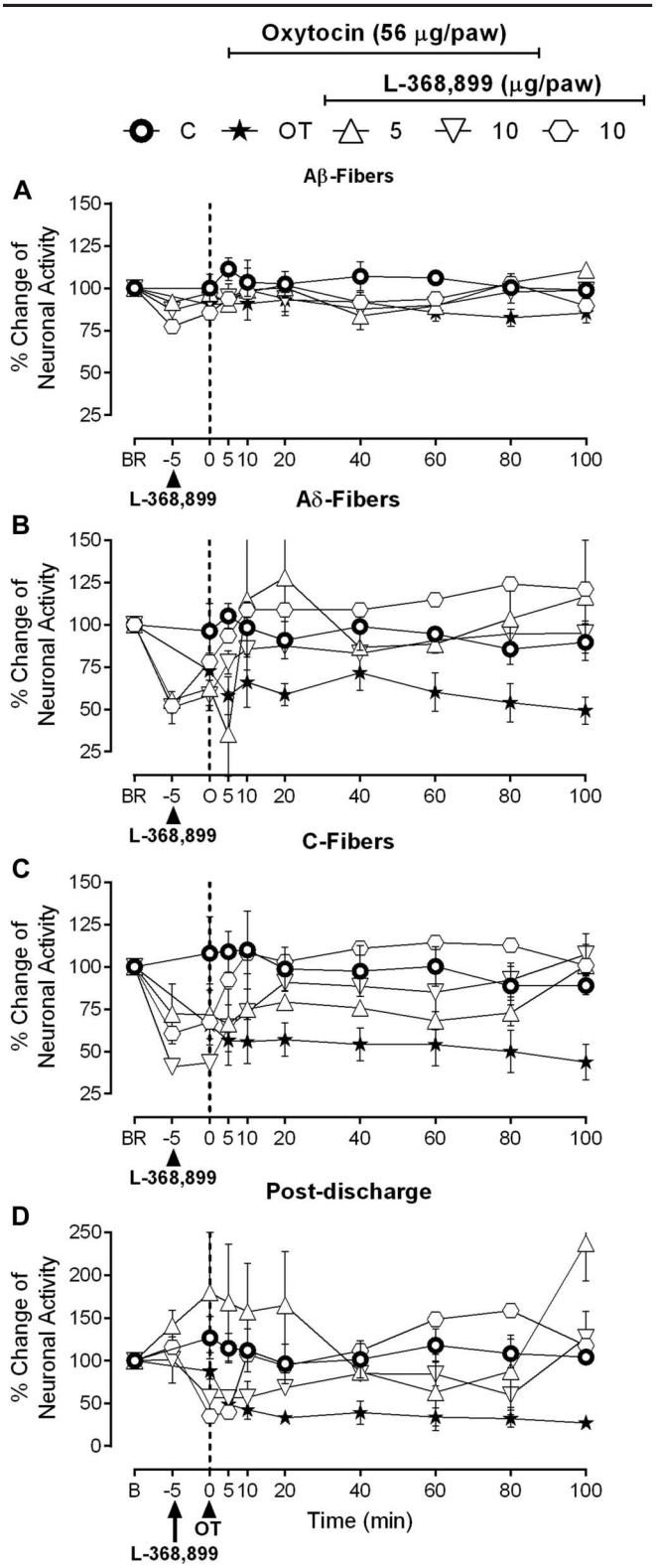

Figure 4. Blockade of oxytocin receptors (OTRs) inhibits the oxytocin (OT)-induced antinociception in the second-order wide-dynamic-range (WDR) cells mediated by (A) Aβ-, (B) Aδ-, (C) C fibers, and (D) postdischarge. Effect of subcutaneous bolus injection of L-368,899 per se or on the inhibition of nociceptive WDR responses induced by OT (56 μg/paw) of the receptive field electrical stimulation. *$P < 0.05$ vs the corresponding control response (●). BR, basal response, before any administration.

4. Discussion

4.1. General

Our findings show that peripheral activation of OTRs on the superficial skin layer is able to induce inhibition of the C-fiber discharge and suppress behavioral nociception. Oxytocin receptors could be expressed in CGRPergic terminal nerves innervating the superficial skin. The role of this receptor is supported considering that subcutaneous OT–induced antinociception was reverted by L-368,899 (a potent and selective OTR antagonist) in electrophysiological and behavioral experiments. This effect seems to be local, because OT ipsilateral (not contralateral) to formalin inhibited nociception in the formalin test.

4.2. Subcutaneous oxytocin blocks the nociceptive input to the spinal dorsal horn wide-dynamic-range cells

As previously reported,[50] electrical stimulation of the peripheral RF produces a typical well-defined triphasic neuronal–evoked response corresponding to Aβ-, Aδ-, and C-fiber activation. We found that OT administered s.c into the RF inhibits the evoked nociceptive (Aδ fiber and C fiber) neuronal responses (**Fig. 1**) and this effect lasts up to 100 minutes. Although at this point we cannot ascertain the specific location of OT effects (ie, peripheral vs central), some studies suggest that OT not only induces analgesia in the spinal cord of rodents[8,37,57] and humans,[9,10] but also inhibits nociception at the peripheral level by acting on OTRs located in the DRG,[16,26,30] as described in the Introduction section.

Indirect evidence for this hypothesis came from an early study in a mouse model of chronic abdominal pain where an in vivo intracolonic administration of a selenoether OT analog with similar biological activity in OTR than OT was able to inhibit chronic visceral hypersensitivity.[11] This suggestion gains weight when considering the pharmacokinetic properties of several neuropeptides, including OT (such as poor absorption and low metabolic stability).[29] Therefore, it is reasonable to suppose that the pharmacological effect observed after single s.c. OT administration is restricted to a local effect. To validate this hypothesis, we performed behavioral, molecular, and pharmacological tests.

4.3. Oxytocin inhibits the formalin-induced flinching behavior by a local and specific effect

Because s.c. OT inhibits the nociceptive-evoked activity of WDR cells, we hypothesized that this inhibition should be replicated in a pain behavior model. In accordance, flinching behavior induced by s.c. formalin is dose-dependent reduced by OT in both phases (**Fig. 2A–C**). Considering that 100 μg/paw OT in the contralateral paw was ineffective, this neuropeptide seems to be a local effect. Moreover, although 100 μg/paw OT inhibited the nocifensive behavior in both phases, it has been reported that 200 to 1000 μg/kg OT (50-250 μg for a 0.25 kg rat) administered s.c. inhibited the locomotor activity (ambulatory and nonambulatory) by activating peripheral V1a receptors.[54] To avoid possible bias because locomotor performance could influence the nociceptive tests,[27] we decided to use the dose of 31 μg/paw OT. In any case, the 31 μg/paw (that inhibited phase II of the formalin test) did not have any effect on the motor coordination test when using the rota-rod test (**Fig. 2D**). The notion that s.c. OT uses a local mechanism to exert its antinociceptive effect is strongly supported in conjunction with the fact that OTRs are expressed in the sciatic nerve (**Fig. 2E**).

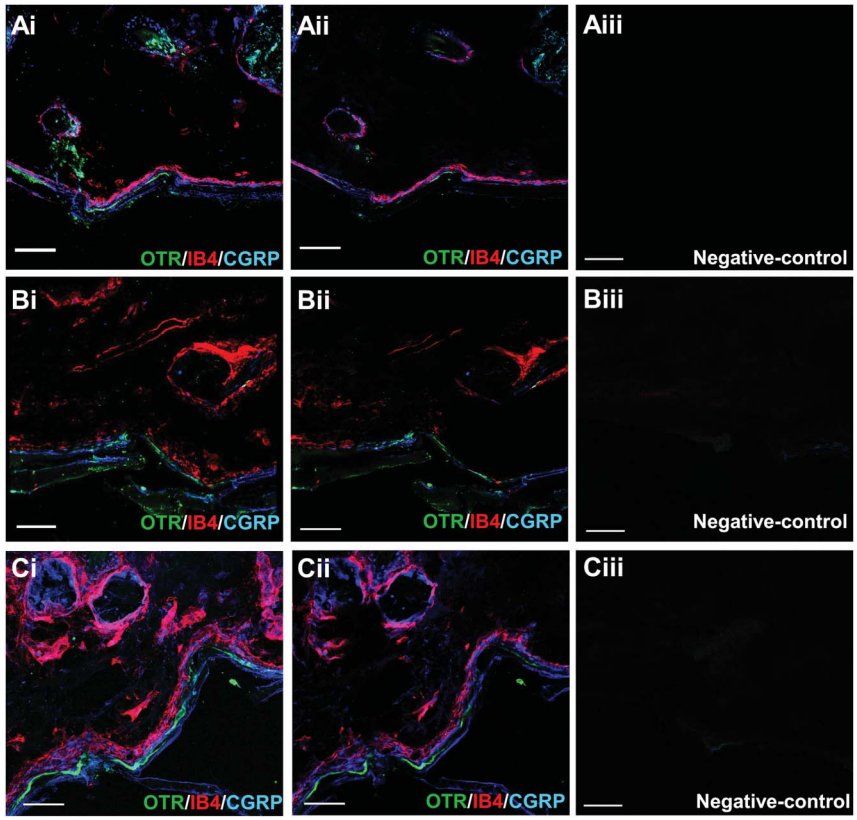

Figure 5. Confocal image of a skin section for oxytoxin receptor (OTR), IB4, and calcitonin gene–related peptide (CGRP) immunofluorescence. Panels Ai, Bi, and Ci are the *z*-stack projection from 40 optical sections (25×/0.8 NA objectives) from 3 different experiments. Panels Aii, Bii, and Cii are single optical sections from the *z*-stack projection; the optical section was selected at the point that signal for OTR was better (see supplemental Figures 1, 2, and 3 for details about the OTR colocalization with CGRP and IB4; available online at http://links.lww.com/PAIN/A459). The co-localization between OTR and CGRP is show in white-grey colors Panels Aiii, Biii, and Ciii are the negative controls showing no specific labeling in the absence of primary antibodies. It is important to point out that in this set of experiments the intensity color was adjusted at the maximum to appreciate possible unspecificity from the secondary antibodies used. Scale bars: 50 μm.

4.4. Defining the role of peripheral oxytocin receptors in peripheral oxytocin-induced antinociception

Direct evidence of the involvement of peripheral OTRs in OT-induced antinociception in behavioral (**Fig. 3A–C**) and electrophysiological (**Fig. 3D–H**) experiments originates from the fact that antinociception was clearly antagonized by L-368,899, a specific and potent OTR antagonist[53] (**Fig. 4**). Correspondingly, we found that OTRs could be localized in cutaneous nociceptive peptidergic terminals (**Figs. 5–7**). Previous reports have strongly supported the role of peripheral OTRs in nociception,[16,26] but the potential role in peripheral nociceptor endings remains obscure, as previously suggested.[19] In this context, a previous study using an isolated ex vivo preparation showed that OT could block the capsaicin-induced release of CGRP from dural nociceptors,[49] supporting the idea that OTRs could be present in terminal nerve endings. Certainly, apart from the spinal cord[40,48,55] DRG[40] and trigeminal ganglia,[49] OTR was found in mouse embryonic skin[21] supporting our hypothesis. In this context, our work is the first to show that OTRs can be found in nociceptive terminals and that on nociceptive stimulation they are able to inhibit the nociceptive input.

4.5. Considerations about the specificity of the antibody against oxytocin receptor

During the submission process of the present paper, the reviewers strongly suggested to perform an immunostaining control to avoid the possible false positive OTR in skin terminals. In **Figure 5**, the first antibody missing showed nonunspecific staining. In addition, during the submission, a new possibility of OT action was published in PAIN in which Kubo et al.[30] suggested that the OT effects suppressing orofacial hypersensitivity can be mediated by the vasopressin (VP)-1A receptor (V_1A-R). This assumption is based on the action of a selective V_1A-R antagonist over isolated trigeminal ganglia neurons. Considering the molecular structure similarity between OT and VP, this assumption is a possibility as was also suggested elsewhere[44] using OT knockout mice. However, the isolated trigeminal ganglia neurons[30] as well as the knockout OT mice[44] used could develop compensatory mechanisms to compensate the lack of OT regulations. Nevertheless, the question that remains is whether OT could have a cross-action with the V_1AR, although this question does not invalidate that our current description of peripheral OTR used OT to act. Considering the molecular, electrophysiological, pharmacological, and behavioral results and that the current OTR has a juxtaposition with peptidergic CGRP fibers, an important possibility is that OT uses the OT receptor.

A serious characteristic for using antibodies in research is their specificity, a property dependent on the species studied. In a recent study, using OTR knockout mice[56] has suggested that the antibody used in our study has a lack of specificity to detect adequately the presence of OTR. However, the large number of regulatory elements controlling transcription and tissue-specific localization of the OTR[17] and the fact that knockout mice could develop an array of compensatory

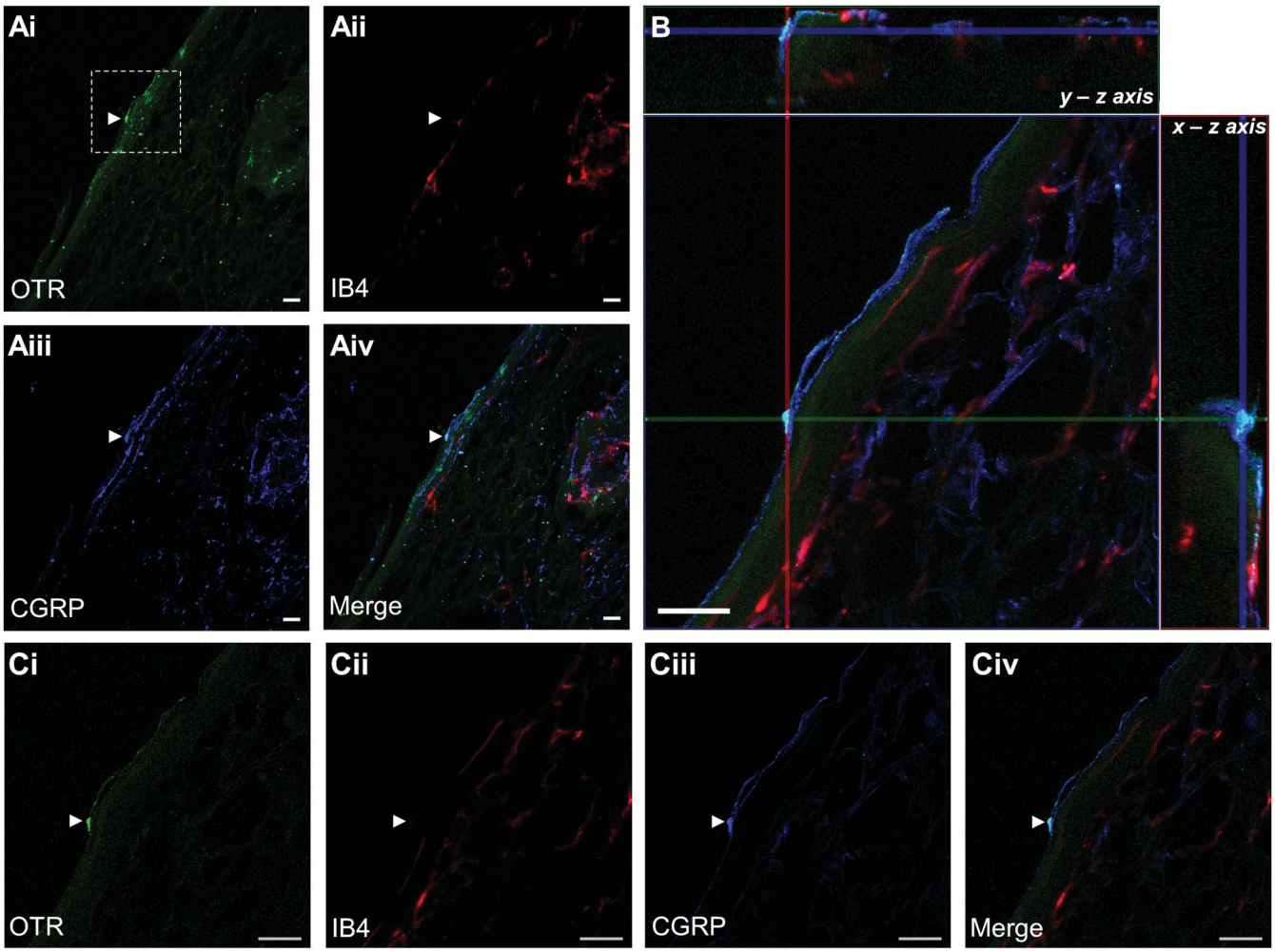

Figure 6. Triple labeling of terminal nerve endings in dermis and epidermis sections with antibodies against oxytoxin receptor (OTR), calcitonin gene–related peptide (CGRP), and IB4. Confocal microscopic images of OTR (green), IB4 (red), and CGRP (blue) immunofluorescence in the skin. Ai, ii, iii, and iv are *z*-stack projection from 8 optical sections; images were taken with 25×/0.8 NA objectives. The arrows show the free termination of OTR positive. Panel B shows an orthogonal view displaying 8 optical sections (1 μm each) at 40×/1.3 NA; y-z plane and x-z axis show colocalization between OTR (green) and CGRP (blue) but not with IB4 (red). The co-localization between OTR and CGRP is show in white colors. Ci-Civ show a focal plane of the *z*-stack; OTR and CGRP appear in the same plane and the arrow shows the free termination OTR and CGRP positive; this image was taken with 25×/0.8 NA objectives. Scale bars: 50 μm.

mechanisms to adjust the absence of deleted receptors (ie change the endogenous protein expression profile[23]), this transgenic approach could lead to a potential flaw in the immunodetection of this receptor. Admittedly, the evidence presented by Yoshida et al.[56] could undermine our findings using immunofluorescence, but we need to keep in mind that perhaps the knockout OTR model is not the best model to evaluate the antibody specificity for a key receptor involved in several significant physiological functions.[18] Thus, the physical presence of OTR at the periphery will be definitely established with the advent of more selective OTR antibodies, which to the best of our knowledge, are not currently available. In any case, our pharmacological experiments, (in electrophysiological and behavioral tests) using a highly potent and selective OTR antagonist, support the presence of this receptor at the peripheral level. Consequently, it is important to point out some key aspects to properly appreciate the results found: First, in our manuscript we discuss and present evidence of others research groups suggesting that OTR could be expressed in the peripheral nerves.[11,13,14,16,21,26,49]

Second, the antibody used is recommended for the detection of OTR by Western blotting, immunofluorescence, and enzyme-linked immunospecific assay. Apart from the use of mice, the work done by Yoshida et al.[56] was performed using immunohistochemistry. Although immunohistochemistry and immunofluorescence are similar techniques, a key information in the work of Yoshida et al.[56] is missing (the dilution used). Indeed, the antibody concentration used is critical to avoid false positive results when considering that VP AV1a receptors are similar to OTR and share a high degree of homology.[28,29] Furthermore, the "unspecific" antibody (LS-A246) tested by Yoshida et al.[56] (antibody to OTR) was primarily designed to react preferentially with the human OTR instead of the rodent OTR. Indeed, the LS-A246 was raised against synthetic 16 amino acids from the third cytoplasmatic domain of the human OTR. This is relevant considering that although a high degree of homology between rat and human OTR exists, the third intracellular loop are different between these 2 species,[1,28,39] and maybe the fact that the signal by LS-A246 was observed in knockout mice[56] reflects the complexity of compensatory mechanisms in these animals.

Subsequently, the specificity and sensitivity of the antibody that we used has been tested by several research groups analyzing not only the role of OTR in nociception[38] but also in autonomic and cardiovascular systems.[6,20,24,32,45,51] Hence, the interesting

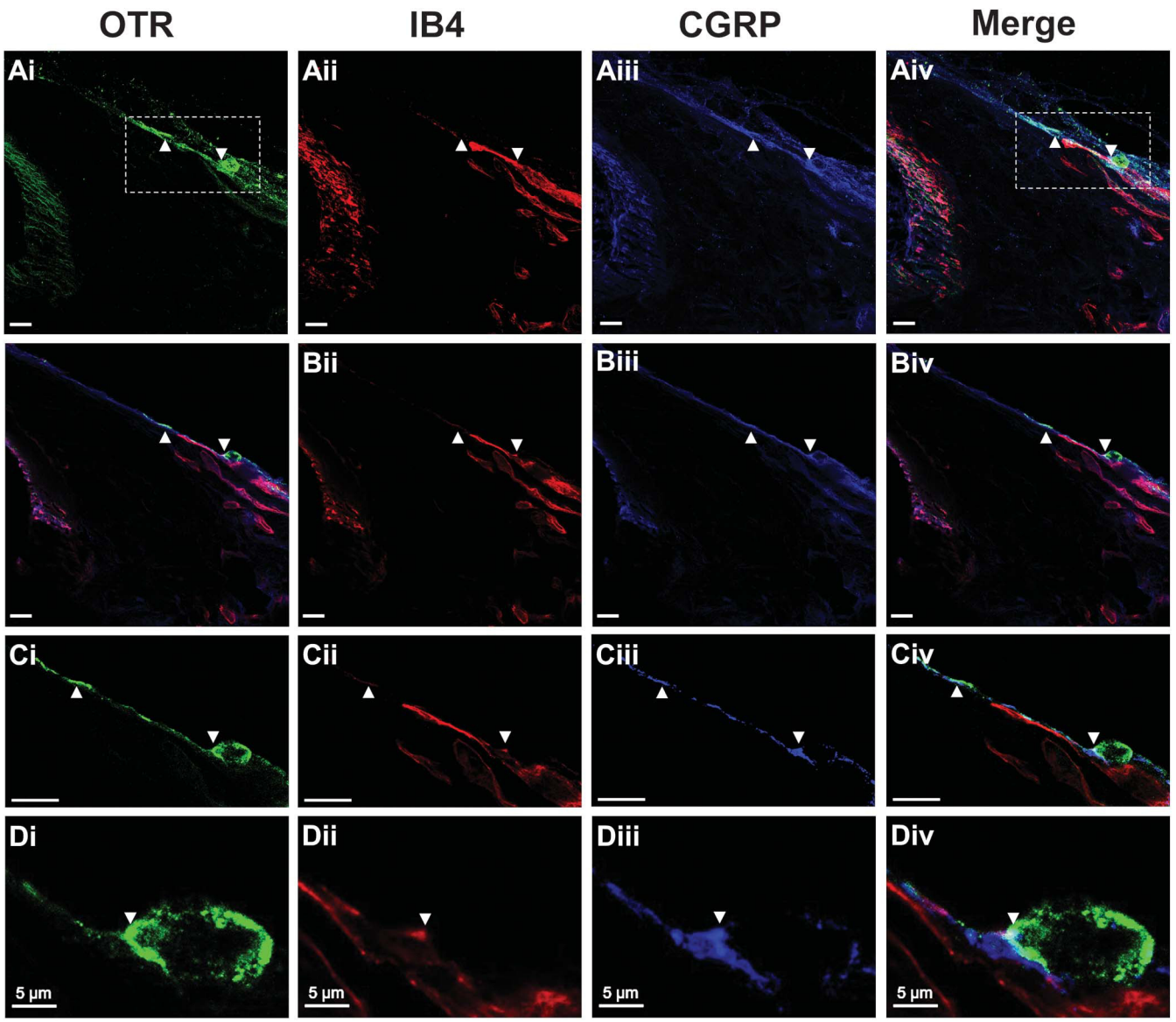

Figure 7. Triple-labeling of terminal nerve endings on dermis and epidermis sections with antibodies against oxytocin receptor (OTR), calcitonin gene–related peptide (CGRP), and IB4. Representative confocal images of immunofluorescent-labeled terminal sensory nerves in the lateral hairy skin paw (OTR in green, IB4 in red, and CGRP in blue). Panels in A are the *z*-stack projection from 40 optical sections; the images were taken with 25×/0.8 NA objectives. The arrows show the OTR-positive fiber and cellular body. Panels in B are single optical sections taken with 40× objective (section thickness 1 μm) from the *z*-stack projection in A. Panels in C are single optical sections (40×/1.3 NA) from the box in panel A. Panels in D are cropped images from panel C showing a terminal nerve ending. Although the *z*-stack projection (Ai, ii, iii, and iv) depicts the presence of OTR, IB4, and CGRP in the tissue, OTRs are predominantly colocalized with CGRP when we observe the 1 representative optical section (see B, C and D). The co-localization between OTR and CGRP is show in white colors (see merge). These results are clearly depicted in several representative optical sections (orthogonal view, supplemental Figure 4, available online at http://links.lww.com/PAIN/A459), and this suggestion is reinforced by similar data obtained from the 3D-rendered and 2.5D-reconstructed images (see supplemental Figures 5 and 6, available online at http://links.lww.com/PAIN/A460 and http://links.lww.com/PAIN/A461 respectively). Scale bar in panels A, B, and C: 20 μm.

findings by Yoshida et al.[56] suggesting that this antibody is unspecific need to be taken cautiously.

Finally, regarding the physiological function of OTRs on peripheral skin, OT is expressed in cultured human keratinocytes and is released in response to external stimuli (resembling injuries).[14] Skin keratinocytes responding to stimulation can indirectly modulate the activity of sensory fibers[13] and could modulate action potentials in primary afferent fibers.[4]

5. Conclusion

Our work suggests that the antinociception induced by subcutaneous OT is mediated by a peripheral mechanism (probably at the terminal nociceptive fiber endings by OTR activation), and it reveals a new potential role for OT in pain modulation.

Conflict of interest statement

The authors have no conflicts of interest to declare.

Acknowledgments

The authors thank Jessica González Norris for reviewing the grammatical aspects of this paper. In addition, the authors also acknowledge Elsa Nydia Hernández Ríos for her technical assistance in confocal microscopy. This work was sponsored by

grant (to MCL) PAPIIT-UNAM (Grant No. IN200415). IATG is a CONACyT Fellow. Alfredo Manzano García is a doctoral student from Programa de Doctorado en Ciencias Biomédicas, Universidad Nacional Autónoma de México (UNAM) and received fellowship 597467 from CONACYT.
A. González-Hernández and A. Manzano-García contributed equally to the work.

Appendix A. Supplemental digital content

Supplemental digital content associated with this article can be found online at http://links.lww.com/PAIN/A459.

Supplemental video content

Video content associated with this article can be found online at http://links.lww.com/PAIN/A460, http://links.lww.com/PAIN/A461, and http://links.lww.com/PAIN/A462.

Article history:
Received 2 December 2016
Received in revised form 4 May 2017
Accepted 30 May 2017
Available online 19 July 2017

References

[1] Adan RA, Van Leeuwen FW, Sonnemans MA, Brouns M, Hoffman G, Verbalis JG, Burbach JP. Rat oxytocin receptor in brain, pituitary, mammary gland, and uterus: partial sequence and immunocytochemical localization. Endocrinology 1995;136:4022–8.
[2] Atasoy D, Betley JN, Su HH, Sternson SM. Deconstruction of a neural circuit for hunger. Nature 2012;488:172–7.
[3] Bardoni R, Tawfik VL, Wang D, François A, Solorzano C, Shuster SA, Choudhury P, Betelli C, Cassidy C, Smith K, de Nooij JC. Delta opioid receptors presynaptically regulate cutaneous mechanosensory neuron input to the spinal cord dorsal horn. Neuron 2014;81:1312–27.
[4] Baumbauer KM, DeBerry JJ, Adelman PC, Miller RH, Hachisuka J, Lee KH, Ross SE, Koerber HR, Davis BM, Albers KM. Keratinocytes can modulate and directly initiate nociceptive responses. Elife 2015;4:e09674.
[5] Bradford MM. A rapid and sensitive method for the quantitation of microgram quantities of protein utilizing the principle of protein-dye binding. Anal Biochem 1976;72:248–54.
[6] Caligioni CS, Oliver C, Jamur MC, Franci CR. Presence of oxytocin receptors in the gonadotrophin-releasing hormone (GnRH) neurones in female rats: a possible direct action of oxytocin on GnRH neurones. J Neuroendocrinol 2007;19:439–48.
[7] Condés-Lara M, González NM, Martínez-Lorenzana G, Delgado OL, Freund-Mercier MJ. Actions of oxytocin and interactions with glutamate on spontaneous and evoked dorsal spinal cord neuronal activities. Brain Res 2003;976:75–81.
[8] Condés-Lara M, Maie IAS, Dickenson AH. Oxytocin actions on afferent evoked spinal cord neuronal activities in neuropathic but not in normal rats. Brain Res 2005;1045:124–33.
[9] Condés-Lara M, Zayas-González H, Manzano-García A, Córdova-Quiroz E, Granados-Mortera J, García-Cuevas M, Morales-Gómez J, González-Hernández A. Successful pain management with epidural oxytocin. CNS Neurosci Ther 2016;22:532–4.
[10] Condés-Lara M, Zayas-González H, Manzano-García A, González-Hernández A. Response to letter to the editor by eisenach and Yaksh on "successful pain management with epidural oxytocin". CNS Neurosci Ther 2016;22:867–8.
[11] de Araujo AD, Mobli M, Castro J, Harrington AM, Vetter I, Mettehnthaler M, Wan J, Lewis RJ, King GF, Brierley SM, Alewwod PF. Selenoether oxytocin analogues have analgesic properties in a mouse model of chronic abdominal pain. Nat Commun 2014;5:3165.
[12] DeLaTorre S, Rojas-Piloni G, Martínez-Lorenzana G, Rodríguez-Jiménez J, Villanueva L, Condés-Lara M. Paraventricular oxytocinergic hypothalamic prevention or interruption of long-term potentiation in dorsal horn nociceptive neurons: electrophysiological and behavioral evidence. PAIN 2009;144:320–8.
[13] Denda M, Nakatani M, Ikeyama K, Tsutsumi M, Denda S. Epidermal keratinocytes as the forefront of the sensory system. Exp Dermatol 2007; 16:157–61.
[14] Denda S, Takei K, Kumamoto J, Goto M, Tsutsumi M, Denda M. Oxytocin es expressed in epidermal keratinocytes and releases upon stimulation with adenosine 5′-[γ-thio]triphosphate in vitro. Exp Dermatol 2012;21: 535–61.
[15] Dubuisson D, Dennis SG. The formalin test: a quantitative study of the analgesic effects of morphine, meperidine, and brain stem stimulation in rats and cats. PAIN 1977;4:161–74.
[16] Eliava M, Melchior M, Knobloch-Bollmann HS, Wahis J, da Silva Gouveia M, Tang Y, Ciobanu AC, Triana del Rio R, Roth LC, Althammer F, Chavant V, Goumon Y, Gruber T, Petit-Demoulière N, Busnelli M, Chini B, Tan LL, Mitre M, Froemke RC, Chao MV, Giese G, Sprengel R, Kuner R, Poisbeau P, Seeburg PH, Stoop R, Charlet A, Grinevich V. A new population of parvocellular oxytocin neurons controlling magnocellular neuron. Activity and inflammatory pain processing. Neuron 2016;89:1291–304.
[17] Ermisch A, Ruhle HJ, Landgraf R, Hess J. Blood-brain barrier and peptides. J Cereb Blood Flow Metab 1985;5:350–7.
[18] Gimpl G, Fahrenholz F. The oxytocin receptor system: structure, function, and regulation. Physiol Rev 2001;81:629–83.
[19] González-Hernández A, Rojas-Piloni G, Condés-Lara M. Oxytocin and analgesia: future trends. Trends Pharmacol Sci 2014;35:549–51.
[20] Gutkowska J, Jankowski M. Oxytocin revisited: it is also a cardiovascular hormone. J Am Soc Hypertens 2008;2:318–25.
[21] Hammock EAD, Levitt P. Oxytocin receptor ligand binding in embryionic tissue and postnatal brain development of the C57BL/6J mouse. Behav Neurosci 2013;7:195.
[22] Hobo S, Hayashida K, Eisenach JC. Oxytocin inhibits the membrane depolarization-induced in intracellular calcium in capsaicin sensitive neurons: a peripheral mechanism of analgesic action. Anesth Analg 2012;114:442–9.
[23] Harris JA, Hirokawa KE, Sorensen SA, Gu H, Mills M, Ng LL, Bohn P, Mortrud M, Ouellette B, Kidney J, Smith KA, Dang C, Sunkin S, Bernard A, Oh SW, Madisen L, Zeng H. Anatomical characterization of Cre driver mice for neural Circuit mapping and manipulation. Front Neural Circuits 2014;8:76.
[24] Jankowski M, Bissonauth V, Gao L, Gangal M, Wang D, Danalache B, Wang Y, Stoyanova E, Cloutier G, Blaise G, Gutkowska J. Anti-inflammatory effect of oxytocin in rat myocardial infarction. Bas Res Cardiol 2010;105:205–18.
[25] Jasper JR, Harrell CM, O'Brien JA, Pettibone DJ. Characterization of the human oxytocin stably expressed in 293 human embryonic kidney cells. Life Sci 1995;57:2253–61.
[26] Juif PE, Poisbeau P. Neurohormonal effects of oxytocin and vasopressin receptor agonists on spinal pain processing in male rats. PAIN 2013;154: 1449–56.
[27] Kayser V, Elfassi IE, Aubel B, Melfort M, Julius D, Gingrich JA, Hamon M, Bourgoin S. Mechanical, thermal and formalin-induced nociception is differentially altered in 5-HT_{1A}−/−, 5-HT_{1B}−/−, 5-HT_{2A}−/−, 5-HT_{3A}−/− and 5-HTT−/− knock-out male mice. PAIN 2007;130:235–48.
[28] Kimura T, Tanizawa O, Mori K, Brownstein MJ, Okayama H. Structure and expression of a human oxytocin receptor. Nature 1992;356:526–9. Erratum in: Nature;357:176.
[29] Kompelia UB, Lee VHL. Pharmacokinetics of peptide and protein drugs. In: Lee VHL, editor. Peptide and protein drug delivery. Marcel Dekker, Inc, 1991. p. 391–484.
[30] Kubo A, Shinoda M, Katagiri A, Takeda M, Suzuki T, Asaka J, Yeomans D, Iwata K. Oxytocin alleviates orofacial mechanical hypersensitivity associated with infraorbital nerve injury through vasopressin-1A receptors of the rat trigeminal ganglia. PAIN 2017;158:649–59.
[31] Laemmli UK. Cleavage of structural proteins during the assembly of the head of bacteriophage T4. Nature 1970;227:680–5.
[32] Lozić M, Greenwood M, Šarenac O, Martin A, Hindmarch C, Tasić T, Paton J, Murphy D, Japundžić-Žigon N. Overexpression of oxytocin receptors in the hypothalamic PVN increases baroreceptor reflex sensitivity and buffers BP variability in conscious rats. Br J Pharmacol 2014;171:4385–98.
[33] Mack SO, Kc P, Wu M, Coleman BR, Tolentino-Silva FP, Haxhiu MA. Paraventricular oxytocin neurons are involved in neural modulation of breathing. J Appl Physiol 2002;92:826–34.
[34] Malmberg AB, Yaksh TL. Antinociceptive actions of spinal nonsteroidal anti-inflammatory agents on the formalin test in the rat. J Pharmacol Exp Ther 1992;263:136–46.
[35] McGrath JC, Drummond GB, McLachlan EM, Kilkenny C, Wainwright CL. Guidelines for reporting experiments involving animals: the ARRIVE guidelines. Br J Pharmacol 2010;160:1573–6.
[36] Mena F, González-Hernández A, Navarro N, Castilla A, Morales T, Rojas-Piloni G, Martínez-Lorenzana G, Condés-Lara M. Prolactin fractions from lactating rats elicit effects upon sensory spinal cord cells of male rats. Neuroscience 2013;248:552–61.

[37] Miranda-Cárdenas Y, Rojas-Piloni G, Martínez-Lorenzana M, Rodríguez-Jiménez J, López-Hidalgo M, Freund-Mercier MJ, Condes-Lara M. Oxytocin and electrical stimulation of the paraventricular hypothalamic nucleus produce antinociceptive effects that are reversed by an oxytocin antagonist. PAIN 2006;122:182–9.
[38] Modi ME, Majchrzak MJ, Fonseca KR, Doran A, Osgood S, Vanase-Frawley M, Feyfant E, McInnes H, Darvari R, Buhl DL, Kablaoui NM. Peripheral administration of a long-acting peptide OT receptor agonist inhibits fear induced freezing. J Pharm Exp Ther 2016;358:164–72.
[39] Morel A, O'Carroll AM, Brownstein MJ, Lolait SJ. Molecular cloning and expression of a rat V1a arginine vasopressin receptor. Nature 1992;356:523–6.
[40] Moreno-López Y, Martínez-Lorenzana G, Condés-Lara M, Rojas-Piloni G. Identification of oxytocin receptor in the dorsal horn and nociceptive dorsal root ganglion neurons. Neuropeptides 2013;47:117–23.
[41] Petersson M. Cardiovascular effects of oxytocin. Prog Brain Res 2002;139:281–8.
[42] Pinto-Ribeiro F, Ansah OB, Almeida A, Pertovaara A. Influence of arthritis on descending modulation of nociception from the paraventricular nucleus of the hypothalamus. Brain Res 2008;1197:63–75.
[43] Qiu F, Qiu C-Y, Cai H, Liu T-T, Qu Z-W, Yang Z, Li J-D, Zhou Q-Y, Hu W-P. Oxytocin inhibits the activity of acid-sensing ion channels through the vasopressin V1A receptor in primary sensory neurons. Br J Pharmacol 2014;171:3065–76.
[44] Schorscher-Petcu A, Sotocinal S, Ciura S, Dupré A, Ritchie J, Sorge RE, Crawley JN, Hu SB, Nishimori K, Young LJ, Tribollet E, Quirion R, Mogil JS. Oxytocin-induced analgesia and scratching are mediated by the vasopressin-1A receptor in the mouse. J Neurosci 2010;30:8274–84.
[45] Suzuki M, Honda Y, Li MZ, Masuko S, Murata Y. The localization of oxytocin receptors in the islets of Langerhans in the rat pancreas. Regul Peptides 2013;183:42–5.
[46] Swanson LW, Sawchenko PE. Hypothalamic integration: organization of the paraventricular and supraoptic nuclei. Annu Rev Neurosci 1983;6:269–324.
[47] Towbin H, Staehelin T, Gordon J. Electrophoretic transfer of proteins from polyacrylamide gels to nitrocellulose sheets: procedure and some applications. Proc Natl Acad Sci U S A 1979;76:4350–4.
[48] Tribollet E, Barberis C, Arsenijevic Y. Distribution of vasopressin and oxytocin receptors in the rat spinal cord: sex-related differences and effect of castration in pudendal motor nuclei. Neuroscience 1997;78:499–509.
[49] Tzabazis A, Mechanic J, Miller J, Klukinov M, Pascual C, Manering N, Carson DS, Jacobs A, Qiao Y, Cuellar J, Frey WH II, Jacobs D, Angst M, Yeomans DC. Oxytocin receptor: expression in the trigeminal nociceptive system and potential role in the treatment of headache disorders. Cephalalgia 2016;36:943–50.
[50] Urch CE, Dickenson AH. In vivo single unit extracellular recordings from spinal cord neurons of rats. Brain Res Protoc 2003;12:26–34.
[51] Weston GC, Cann L, Rogers PA. Myometrial microvascular endothelial cells express oxytocin receptor. Int J Obst Gynaecol 2003;110:149–56.
[52] Wheeler-Aceto H, Cowan A. Standardization of the rat paw formalin test for the evaluation of analgesics. Psychopharmacology (Berl) 1991;104:35–44.
[53] Williams PD, Anderson PS, Ball RG, Bock MG, Carroll L, Chiu SH, Clineschmidt BV, Culberson JC, Erb JM, Evans BE, Fitzpatrick SL, Freidinger RM, Kaufman MJ, Lundell GF, Murphy JS, Thompson KL, Veber DF. 1-((7,7-Dimethyl-2(S)-(2(S)-amino-4-(methylsulfonyl)butyramido) bicyclo [2.2.1]-heptan-1(S)-yl)methyl)sulfonyl)-4-(2-methylphenyl)piperazine (L-368,899): an orally bioavailable, non-peptide oxytocin antagonist with potential utility for managing preterm labor. J Med Chem 1994;37:565–71.
[54] Wolfe M, Wisniewski H, Ibañez G, Tariga H, Hargrove D, Lindstrom BF. Peripheral vasopressin type 1a receptors mediate locomotor inhibition following systemic oxytocin administration in rats. 323.12/M40. In: Neuroscience meeting planner. Chicago, IL: Society for Neuroscience, 2015. Online.
[55] Wrobel L, Schorcher-Petcu A, Dupré A, Yoshida M, Nishimori K, Tribollet E. Distribution and identity of neurons expressing the oxytocin receptor in the mouse spinal cord. Neurosci Lett 2011;495:49–54.
[56] Yoshida M, Takayanagi Y, Inoue K, Kimura T, Young LJ, Onaka T, Nishimori K. Evidence that oxytocin exerts anxiolytic effects via oxytocin receptor expressed in serotonergic neurons in mice. J Neurosci 2009;29:2259–71.
[57] Yu SQ, Lundeberg T, Yu LC. Involvement of oxytocin in spinal antinociception in rats with inflammation. Brain Res 2003;983:12–22.
[58] Zimmermann M. Ethical guidelines for investigations of experimental pain in conscious animals. PAIN 1983;16:109–10.